

ISSN 1881-7815    Online ISSN 1881-7823

# **BST**

## **BioScience Trends**

Volume 11, Number 3  
June, 2017



[www.biosciencetrends.com](http://www.biosciencetrends.com)



# BST

## BioScience Trends



ISSN: 1881-7815  
Online ISSN: 1881-7823

CODEN: BTIRCZ

Issues/Year: 6

Language: English

Publisher: IACMHR Co., Ltd.

**BioScience Trends** is one of a series of peer-reviewed journals of the International Research and Cooperation Association for Bio & Socio-Sciences Advancement (IRCA-BSSA) Group and is published bimonthly by the International Advancement Center for Medicine & Health Research Co., Ltd. (IACMHR Co., Ltd.) and supported by the IRCA-BSSA and Shandong University China-Japan Cooperation Center for Drug Discovery & Screening (SDU-DDSC).

**BioScience Trends** devotes to publishing the latest and most exciting advances in scientific research. Articles cover fields of life science such as biochemistry, molecular biology, clinical research, public health, medical care system, and social science in order to encourage cooperation and exchange among scientists and clinical researchers.

**BioScience Trends** publishes Original Articles, Brief Reports, Reviews, Policy Forum articles, Case Reports, News, and Letters on all aspects of the field of life science. All contributions should seek to promote international collaboration.

## Editorial Board

### Editor-in-Chief:

Norihiro KOKUDO  
*National Center for Global Health and Medicine, Tokyo, Japan*

### Co-Editors-in-Chief:

Xue-Tao CAO  
*Chinese Academy of Medical Sciences, Beijing, China*  
Rajendra PRASAD  
*University of Delhi, Delhi, India*  
Arthur D. RIGGS  
*Beckman Research Institute of the City of Hope, Duarte, CA, USA*

### Chief Director & Executive Editor:

Wei TANG  
*The University of Tokyo, Tokyo, Japan*

### Senior Editors:

Xunjia CHENG  
*Fudan University, Shanghai, China*  
Yoko FUJITA-YAMAGUCHI  
*Beckman Research Institute of the City of Hope, Duarte, CA, USA*  
Na HE  
*Fudan University, Shanghai, China*  
Kiyoshi KITAMURA  
*The University of Tokyo, Tokyo, Japan*  
Misao MATSUSHITA  
*Tokai University, Hiratsuka, Japan*  
Munehiro NAKATA  
*Tokai University, Hiratsuka, Japan*  
Takashi SEKINE

*Toho University, Tokyo, Japan*  
Ri SHO  
*Yamagata University, Yamagata, Japan*  
Yasuhiko SUGAWARA  
*Kumamoto University, Kumamoto, Japan*  
Ling WANG  
*Fudan University, Shanghai, China*

### Managing Editor:

Jianjun GAO  
*Qingdao University, Qingdao, China*

### Web Editor:

Yu CHEN  
*The University of Tokyo, Tokyo, Japan*

### Proofreaders:

Curtis BENTLEY  
*Roswell, GA, USA*  
Christopher HOLMES  
*The University of Tokyo, Tokyo, Japan*  
Thomas R. LEBON  
*Los Angeles Trade Technical College, Los Angeles, CA, USA*

### Editorial Office

Pearl City Koishikawa 603,  
2-4-5 Kasuga, Bunkyo-ku, Tokyo 112-0003, Japan  
Tel: +81-3-5840-8764 Fax: +81-3-5840-8765  
E-mail: office@biosciencetrends.com

# BioScience Trends

## Editorial and Head Office

Pearl City Koishikawa 603, 2-4-5 Kasuga, Bunkyo-ku,  
Tokyo 112-0003, Japan

Tel: +81-3-5840-8764, Fax: +81-3-5840-8765  
E-mail: office@biosciencetrends.com  
URL: www.biosciencetrends.com

## Editorial Board Members

Girdhar G. AGARWAL <i>(Lucknow, India)</i>	Takahiro HIGASHI <i>(Tokyo, Japan)</i>	Francesco MAROTTA <i>(Milano, Italy)</i>	Shin'ichi TAKEDA <i>(Tokyo, Japan)</i>
Hirotsugu AIGA <i>(Geneva, Switzerland)</i>	De-Fei HONG <i>(Hangzhou, China)</i>	Yutaka MATSUYAMA <i>(Tokyo, Japan)</i>	Sumihito TAMURA <i>(Tokyo, Japan)</i>
Hidechika AKASHI <i>(Tokyo, Japan)</i>	De-Xing HOU <i>(Kagoshima, Japan)</i>	Qingyue MENG <i>(Beijing, China)</i>	Puay Hoon TAN <i>(Singapore, Singapore)</i>
Moazzam ALI <i>(Geneva, Switzerland)</i>	Sheng-Tao HOU <i>(Ottawa, Canada)</i>	Mark MEUTH <i>(Sheffi eld, UK)</i>	Koji TANAKA <i>(Tsu, Japan)</i>
Ping AO <i>(Shanghai, China)</i>	Yong HUANG <i>(Ji'ning, China)</i>	Satoko NAGATA <i>(Tokyo, Japan)</i>	John TERMINI <i>(Duarte, CA, USA)</i>
Hisao ASAMURA <i>(Tokyo, Japan)</i>	Hirofumi INAGAKI <i>(Tokyo, Japan)</i>	Miho OBA <i>(Odawara, Japan)</i>	Usa C. THISYAKORN <i>(Bangkok, Thailand)</i>
Michael E. BARISH <i>(Duarte, CA, USA)</i>	Masamine JIMBA <i>(Tokyo, Japan)</i>	Fanghua QI <i>(Ji'nan, Shandong)</i>	Toshifumi TSUKAHARA <i>(Nomi, Japan)</i>
Boon-Huat BAY <i>(Singapore, Singapore)</i>	Kimitaka KAGA <i>(Tokyo, Japan)</i>	Xianjun QU <i>(Beijing, China)</i>	Kohjiro UEKI <i>(Tokyo, Japan)</i>
Yasumasa BESSHO <i>(Nara, Japan)</i>	Ichiro KAI <i>(Tokyo, Japan)</i>	John J. ROSSI <i>(Duarte, CA, USA)</i>	Masahiro UMEZAKI <i>(Tokyo, Japan)</i>
Generoso BEVILACQUA <i>(Pisa, Italy)</i>	Kazuhiro KAKIMOTO <i>(Osaka, Japan)</i>	Carlos SAINZ-FERNANDEZ <i>(Santander, Spain)</i>	Junming WANG <i>(Jackson, MS, USA)</i>
Shiuan CHEN <i>(Duarte, CA, USA)</i>	Kiyoko KAMIBEPPU <i>(Tokyo, Japan)</i>	Yoshihiro SAKAMOTO <i>(Tokyo, Japan)</i>	Xiang-Dong Wang <i>(Boston, MA, USA)</i>
Yuan CHEN <i>(Duarte, CA, USA)</i>	Haidong KAN <i>(Shanghai, China)</i>	Erin SATO <i>(Shizuoka, Japan)</i>	Hisashi WATANABE <i>(Tokyo, Japan)</i>
Naoshi DOHMAE <i>(Wako, Japan)</i>	Bok-Luel LEE <i>(Busan, Korea)</i>	Takehito SATO <i>(Isehara, Japan)</i>	Lingzhong XU <i>(Ji'nan, China)</i>
Zhen FAN <i>(Houston, TX, USA)</i>	Mingjie LI <i>(St. Louis, MO, USA)</i>	Akihito SHIMAZU <i>(Tokyo, Japan)</i>	Masatake YAMAUCHI <i>(Chiba, Japan)</i>
Ding-Zhi FANG <i>(Chengdu, China)</i>	Shixue LI <i>(Ji'nan, China)</i>	Zhifeng SHAO <i>(Shanghai, China)</i>	Aitian YIN <i>(Ji'nan, China)</i>
Xiaobin FENG <i>(Beijing, China)</i>	Ren-Jang LIN <i>(Duarte, CA, USA)</i>	Judith SINGER-SAM <i>(Duarte, CA, USA)</i>	George W-C. YIP <i>(Singapore, Singapore)</i>
Yoshiharu FUKUDA <i>(Ube, Japan)</i>	Lianxin LIU <i>(Harbin, China)</i>	Raj K. SINGH <i>(Dehradun, India)</i>	Xue-Jie YU <i>(Galveston, TX, USA)</i>
Rajiv GARG <i>(Lucknow, India)</i>	Xinqi LIU <i>(Tianjin, China)</i>	Peipei SONG <i>(Tokyo, Japan)</i>	Benny C-Y ZEE <i>(Hong Kong, China)</i>
Ravindra K. GARG <i>(Lucknow, India)</i>	Daru LU <i>(Shanghai, China)</i>	Junko SUGAMA <i>(Kanazawa, Japan)</i>	Yong ZENG <i>(Chengdu, China)</i>
Makoto GOTO <i>(Tokyo, Japan)</i>	Hongzhou LU <i>(Shanghai, China)</i>	Hiroshi TACHIBANA <i>(Isehara, Japan)</i>	Xiaomei ZHU <i>(Seattle, WA, USA)</i>
Demin HAN <i>(Beijing, China)</i>	Duan MA <i>(Shanghai, China)</i>	Tomoko TAKAMURA <i>(Tokyo, Japan)</i>	<i>(as of June 26, 2017)</i>
David M. HELFMAN <i>(Daejeon, Korea)</i>	Masatoshi MAKUUCHI <i>(Tokyo, Japan)</i>	Tadatoshi TAKAYAMA <i>(Tokyo, Japan)</i>	

**Reviews**

---

- 243 - 253      **C-to-U editing and site-directed RNA editing for the correction of genetic mutations.**  
*Luyen Thi Vu, Toshifumi Tsukahara*
- 254 - 266      **The T-Box transcription factor 3 in development and cancer.**  
*Tarryn Willmer, Aretha Cooper, Jade Peres, Rehana Omar, Sharon Prince*
- 267 - 273      **Traditional Chinese medicine for human papillomavirus (HPV) infections: A systematic review.**  
*Jing Lin, Lanting Chen, Xuemin Qiu, Na Zhang, Qiting Guo, Yan Wang, Mingyan Wang, Hans-Jürgen Goyer, Dajin Li, Ling Wang*

**Original Articles**

---

- 274 - 281      **Liver fibrosis after antiretroviral therapy in a longitudinal cohort of sexually infected HIV patients in eastern China.**  
*Qian Wei, Haijiang Lin, Yingying Ding, Xing Liu, Qionghai Wu, Weiwei Shen, Meiyang Gao, Na He*
- 282 - 291      **Re-entry and related predictors among HIV-infected clients receiving methadone maintenance treatment in Guangdong province, China.**  
*Xiaofeng Luo, Xiao Gong, Peizhen Zhao, Xia Zou, Wen Chen, Li Ling*
- 292 - 296      **Time series analysis of weekly influenza-like illness rate using a one-year period of factors in random forest regression.**  
*Hongyan Wu, Yunpeng Cai, Yongsheng Wu, Ren Zhong, Qi Li, Jing Zheng, Denan Lin, Ye Li*
- 297 - 302      **Posttraumatic stress disorder eliminates association of *TrkB* rs1187327 with HDL-C in Chinese Han adolescents.**  
*Ting Cao, Qiwei Guo, Mi Su, Yue Feng, Mei Fan, Yanjun Si, Nazakat H Memon, Jia Lin, Dingzhi Fang*
- 303 - 307      **Unique *Trichomonas vaginalis* gene sequences identified in multinational regions of Northwest China.**  
*Jun Liu, Meng Feng, Xiaolan Wang, Yongfeng Fu, Cailing Ma, Xunjia Cheng*
- 308 - 318      **Paeoniflorin prevents TLR2/4-mediated inflammation in type 2 diabetic nephropathy.**  
*Tingmin Zhang, Qijin Zhu, Yunxia Shao, Kun Wang, Yonggui Wu*
- 319 - 325      **Preoperative biliary drainage versus direct surgery for perihilar cholangiocarcinoma: A retrospective study at a single center.**  
*Yulong Cai, Qi Tang, Xianze Xiong, Fuyu Li, Hui Ye, Peipei Song, Nansheng Cheng*

- 
- 326 - 332      **Perfusion and drainage difference in the liver parenchyma: Regional plane in segment 6.**  
*Hayato Abe, Shintaro Yamazaki, Masamichi Moriguchi, Tokio Higaki, Tadatoshi Takayama*
- 333 - 339      **Index of convexity: A novel method for assessing liver functional reserve using technetium-99m-galactosyl human serum albumin liver scintigraphy.**  
*Takafumi Sato, Junichi Arita, Yosuke Inoue, Rintaro Koga, Yu Takahashi, Akio Saiura*
- 340 - 345      **Clinical correspondence to hepatocellular carcinoma-related lesions with atypical radiological pattern.**  
*Tokio Higaki, Yutaka Midorikawa, Yosuke Nakashima, Hisashi Nakayama, Shunichi Matsuoka, Mitsuhiko Moriyama, Masahiko Sugitani, Tadatoshi Takayama*
- 346 - 354      **Sustained release vancomycin-coated titanium alloy using a novel electrostatic dry powder coating technique may be a potential strategy to reduce implant-related infection.**  
*Jing Han, Yi Yang, Junren Lu, Chenzhong Wang, Youtao Xie, Xuebin Zheng, Zhenjun Yao, Chi Zhang*

### Brief Report

---

- 355 - 359      **Comparative transcriptomic analysis identifies reprogramming and differentiation genes differentially expressed in UiPSCs and ESCs.**  
*Liang Shi, Yazhou Cui, Xiaoyan Zhou, Jing Luan, Linli Wang, Jinxiang Han*

### Letters

---

- 360 - 362      **Once malaria is eliminated, more attention should be paid to imported malaria: Data from five years of surveillance in the City of Yiwu in eastern China.**  
*Xuanjun Dong, Jie Yang, Lianqin Lou, Liebo Zhu, Xiayan Feng, Linong Yao*
- 363 - 365      **Potential proteins targeted by let-7f-5p in HeLa cells.**  
*Yu Wang, Xiujuan Chen, Yi Zhang, Jiandong Song*

### Guide for Authors

---

### Copyright

---

# C-to-U editing and site-directed RNA editing for the correction of genetic mutations

Luyen Thi Vu, Toshifumi Tsukahara\*

School of Materials Science, Japan Advanced Institute of Science and Technology (JAIST), Nomi City, Ishikawa, Japan.

## Summary

Cytidine to uridine (C-to-U) editing is one type of substitutional RNA editing. It occurs in both mammals and plants. The molecular mechanism of C-to-U editing involves the hydrolytic deamination of a cytosine to a uracil base. C-to-U editing is mediated by RNA-specific cytidine deaminases and several complementation factors, which have not been completely identified. Here, we review recent findings related to the regulation and enzymatic basis of C-to-U RNA editing. More importantly, when C-to-U editing occurs in coding regions, it has the power to reprogram genetic information on the RNA level, therefore it has great potential for applications in transcript repair (diseases related to thymidine to cytidine (T>C) or adenosine to guanosine (A>G) point mutations). If it is possible to manipulate or mimic C-to-U editing, T>C or A>G genetic mutation-related diseases could be treated. Enzymatic and non-enzymatic site-directed RNA editing are two different approaches for mimicking C-to-U editing. For enzymatic site-directed RNA editing, C-to-U editing has not yet been successfully performed, and in theory, adenosine to inosine (A-to-I) editing involves the same strategy as C-to-U editing. Therefore, in this review, for applications in transcript repair, we will provide a detailed overview of enzymatic site-directed RNA editing, with a focus on A-to-I editing and non-enzymatic site-directed C-to-U editing.

**Keywords:** C-to-U editing, <sup>CV</sup>U-oligodeoxynucleotides, <sup>CNV</sup>K-oligodeoxynucleotides, APOBEC1, enzymatic site-directed RNA editing, non-enzymatic site-directed RNA editing

## 1. Introduction

Cytidine to uridine (C-to-U) RNA editing is a post-transcriptional process that modifies one or more cytidine (C) nucleotides to uridine (U) nucleotides in transcript sequences, without changing the corresponding genomic sequences. C-to-U RNA editing involves various mechanisms and functions; the process can create start or stop codon and can alter encoded amino acids and splice site choices (1). C-to-U RNA editing was first reported in vertebrates for the mRNA encoding apolipoprotein B (apoB). The mechanism

of apoB editing was later shown to involve hydrolytic deamination at the C4 position of the cytidine (2,3). This conversion requires cis-acting elements (tripartite regulatory sequences) surrounding the edited cytidine and trans-acting elements (a multiprotein complex known as the editosome), which includes a catalytic cytidine deaminase and multiple auxiliary proteins (1). C-to-U RNA editing has also been reported in mitochondria and chloroplasts in higher plants (4). C-to-U RNA editing is conserved among species of flowering plants and usually occurs within regions of highly conserved amino acid sequences of mitochondrial proteins (5).

C-to-U editing and adenosine to inosine (A-to-I) editing are two distinct types of substitutional RNA editing in mammals. Because substitutional RNA editing has powerful potential to recode point mutations, many studies have focused on manipulating and mimicking RNA editing; a therapeutic RNA editing approach was first proposed and applied in 1995. The goal of this

Released online in J-STAGE as advance publication May 8, 2017.

\*Address correspondence to:

Dr. Toshifumi Tsukahara, School Materials of Science, Japan Advanced Institute of Science and Technology (JAIST), 1-1 Asahidai, Nomi City, Ishikawa 923-1292, Japan.  
E-mail: tsukahara@jaist.ac.jp

approach is to correct mutated RNA sequences in order to treat genetic diseases caused by point mutations. Subsequently, several other studies have improved and developed this method, termed enzymatic site-directed RNA editing. This innovative approach could potentially be applied for treating human diseases such as some neurological disorders by repairing adenosine or cytidine mutations in mRNA without changing the endogenous level of the mRNA target. Enzymatic site-directed RNA editing includes not only C-to-U editing but also A-to-I editing. While enzymatic site-directed A-to-I RNA editing was successfully performed both *in vitro* and in cells, enzymatic site-directed C-to-U RNA editing has not yet been reported. Theoretically, both of these editing approaches employ the same strategy and the RNA editing machinery requires two main factors: complementary RNA sequences that can specifically bind to targeted sequences (guide RNA) and the editing enzyme that performs deamination. Moreover, non-enzymatic site-directed C-to-U editing was recently reported and has prompted great interest because it does not require the restrictive conditions dictated by site-directed enzymatic RNA editing. Therefore, the present review focuses on enzymatic site-directed A-to-I RNA editing and non-enzymatic site-directed C-to-U RNA editing for correcting genetic diseases.

## 2. C-to-U RNA editing in mammals

Although various types of RNA editing occur in mammalian cells, deamination of adenosine to inosine (A-to-I) or cytidine to uridine (C-to-U) are the two major types of RNA editing (6,7). A-to-I deamination has been observed at hundreds of thousands of sites and mostly occurs in non-coding and intronic regions, especially in targets containing Alu repeat sequences (8,9). When A-to-I editing occurs in coding regions, it has most commonly been associated with the recoding of brain proteins (10). C-to-U RNA editing is less prevalent than A-to-I RNA editing in humans (7). The few identified physiological C-to-U RNA editing targets include apolipoprotein B (apoB) pre-mRNA in intestinal cells and several recently validated, but uncharacterized mRNA targets; in an early study, 32 previously unknown APOBEC1 (apoB editing catalytic subunit 1) editing sites in the 3' untranslated regions (3' UTRs) of diverse mRNA transcripts were identified and validated (11). In addition, 56 novel editing sites in 54 intestinal mRNAs and 22 novel sites in 17 liver mRNAs in AU-rich segments of the 3' UTRs were also identified (12). Recently, 410 C-to-U RNA editing events across 275 transcripts were also found in bone marrow-derived macrophages, and nearly all (97%) of these C-to-U events were detected in the 3' UTRs (13). C-to-U RNA editing of apoB pre-mRNA occurs at nucleotides 6666 and 6802 in the nucleus (14,15). The C6666U editing event changes a glutamine codon

(CAA) to an in-frame translational stop codon (UAA). Thus, C6666-unedited apoB RNA generates a full-length ApoB100 protein, whereas C6666U-edited apoB RNA yields a truncated ApoB48 protein (48% of the full-length ApoB100 protein). ApoB100 is synthesized in the liver, whereas ApoB48 is generated in the small intestine. The tissue-specificity of apoB RNA editing in humans is due to the tissue-specific expression of apoB editing catalytic subunit 1 (APOBEC1), which is expressed solely in the small intestine. APOBEC-1 enzyme is a member of the cytidine deaminase (CDA) family that act on monomeric nucleoside and nucleotide substrates, and has ability to carry out the deamination from cytidine (C) to uridine (U) in pre-mRNA target. Both ApoB48 and ApoB100 proteins play important roles in regulation lipid metabolism (14). The C6802U editing event changes a threonine codon (ACA) to an isoleucine (AUA). The C6802U editing event occurs together with the C6666U editing event; therefore, C6802U is detected in the mRNA but is not expressed in the truncated ApoB48 protein (15).

C-to-U RNA editing is dependent on cis-acting elements, as well as on the stoichiometric regulation of trans-acting factors within the macromolecular enzyme complex (editosome) responsible for targeted deamination. The cis-acting elements consist of 50 nucleotides (nt) flanking the edited cytidine containing a tripartite regulatory motif (the mooring sequence), which includes an 11-nt motif (UGAUCAGUAUA) located in an AU-rich sequence downstream of the edited base; these cis-acting elements combining with trans-acting factors are necessary and sufficient to carry out C-to-U RNA editing *in vitro* (16-20). The mooring sequence located at the 3' of the edited cytidine is combined with a 5' efficiency sequence to adopt a stable secondary structure that enhances specificity (18,19). The core of the C-to-U editing editosome includes at least three proteins: APOBEC1 and two requisite cofactors, APOBEC1-complementation factor (ACF) and RNA-binding-motif-protein 47 (RBM47) (21). APOBEC1 is a member of the APOBEC family of RNA-specific cytidine deaminases. Similar to other members of the cytidine deaminase family, APOBEC1 contains a zinc-dependent deaminase domain important for cytidine deamination (22). APOBEC-1 forms homodimers in which specific amino acids within the APOBEC1 catalytic domain are bound to AU-rich sequences in the vicinity of the apoB pre-mRNA. This binding is weak and insufficient for mRNA association *in vitro* (23); therefore, the ACF cofactor (known as A1CF), a putative RNA-binding protein (RBP), is required. This cofactor binds the mooring sequence with high affinity and together with APOBEC1 forms the minimal editosome in *in vitro* experiments (21). ACF is a member of the Elav/HeIN1/HuR family and contains multiple repeats of a single-stranded RNA-recognition motif (RRM). N- and C-terminal sequences flanking the

multiple RRM in ACF are necessary for its interaction with the APOBEC1 enzyme (24). Interestingly, while ACF knockout mice (ACF<sup>-/-</sup> mutant mice) die early during gestation, editing efficiency is increased in ACF<sup>+/-</sup> mutant mice, which is inconsistent with the fact that ACF is required for editosome activity *in vitro*. Although there is much biological evidence for ACF and APOBEC1-mediated C-to-U deaminase activity *in vitro*, there is as of yet no clear evidence that ACF is genetically required for apoB RNA editing *in vivo*. Thus, the role of ACF in the complex *in vivo* remains to be elucidated (25). Recently, a novel RBP (RBM47) was identified as another cofactor that is essential for C-to-U RNA editing *in vivo* (26). RBM47 can interact with APOBEC1 and ACF in the holoenzyme of the editosome and function with APOBEC1 in editing apoB transcripts. However, the functional consequences of the interaction between ACF and RBM47 *in vivo* remain unclear. Moreover, RBM47 can also substitute for ACF in the enzyme complex performing C-to-U RNA editing *in vitro*. Rbm47<sup>gt/gt</sup> mutant mice, which harbor a gene-trap mutant allele expressing  $\beta$ -geo instead of *Rbm47*, does not have detectable Rbm47 mRNA or RBM47 protein expression or Rbm47 activity and in the small intestines of these mice, the C-to-U RNA editing of apoB and four other C-to-U RNA editing targets (*Sult1d1*- *Sulfotransferase 1 family member D1*, *Serinc1*- *Serine Incorporator 1*, *Casp6*- *Caspase 6* and *2010106E10Rik*- *RIKEN cDNA 2010106E10*) was significantly reduced even though their expression levels were not changed. Therefore, RBM47 plays a critical role in C-to-U RNA editing and is a component of the editosome (26).

Interestingly, APOBEC3A (A3A), another member of the cytidine deaminase family that is structurally related to APOBEC1 and is expressed primarily in myeloid cells, including monocytes and macrophages, has been identified as a novel C-to-U RNA editing enzyme (27,28). A3A functions in the inhibition of retrotransposons and several viruses including HIV-1 (human immunodeficiency virus type 1), HTLV1 (human T-cell lymphotropic virus type 1), HPV (human papillomavirus), parvovirus, and hepatitis B. The transcripts of hundreds of genes, including implicated viral pathogenesis, Alzheimer's disease, peripheral blood monocytes exposed to hypoxia and/or interferons, and M1 (proinflammatory) macrophage differentiation, undergo site-specific C-to-U RNA editing (27,28).

### 3. C-to-U RNA editing in plants

In addition to mammals, C-to-U RNA editing also takes place in plants. Although essential differences are known between C-to-U editing in mammals and C-to-U editing in plants, it may be technically possible to modify or combine components of the plant RNA-editing apparatus (especially the cytidine deaminase

of plants) with guide RNA (complementary RNA sequence that specifically binds to target sequences) to replace the mammalian APOBEC1 enzyme in applications for human therapy. This approach would open up numerous applications in C-to-U editing if it is successfully developed. We therefore discuss C-to-U editing in plants, not only as a comparison with the process occurring in mammals, but also as an expected correlation. There are two main types of RNA editing occurring in plants: C-to-U RNA editing and, less frequently, U-to-C RNA editing. C-to-U RNA editing takes place in plant plastids and mitochondria (29-32). Both organelles contain their own circular genomes, which encode genes responsible for photosynthesis and respiration, respectively.

The circular genomes of plastids in higher plants are 120-130 kb nucleotides in size; it is estimated that 20-30 cytidines are converted to uridines, suggesting that the average editing frequency is approximately 0.02% in the plastid genome (33). Few mRNAs in plastids do not contain either start or stop codons; therefore, C-to-U editing enables the expression of functional proteins by generating start or stop codons and modifying amino acid sequences (34-36). In plastids, C-to-U RNA editing occurs in mRNAs but not in other RNA types, including transfer RNA (tRNA) and ribosome RNA (rRNA).

The average editing frequency in plant mitochondria is much higher than in plastid C-to-U RNA editing; for example, the total size of the mitochondrial genome in *Arabidopsis thaliana* (*A. thaliana*) is approximately 367 kb, with only 30 kb consisting of genes encoding the subunits of respiratory chain complexes (37). However, 441 C-to-U RNA editing events have been identified in mitochondrial open reading frames (38). In contrast with plant plastids, C-to-U RNA editing of plant mitochondria occurs in both mRNA and tRNA, but not in rRNA. In mitochondria, C-to-U editing events occur in coding regions and less frequently in introns and other untranslated regions. These events restore and correct open reading frames to enable gene expression in plant mitochondria. Without C-to-U RNA editing, several respiratory chain proteins would not be produced and no functional mitochondria could be assembled and maintained in plant cells. In addition, C-to-U editing events in mitochondrial tRNAs are essential for restoring important base-pairings to correct the folding and processing of tRNA precursors (39,40).

C-to-U RNA editing in plants involves various corresponding editing machineries and mechanisms. Moreover, it is clear that cis-elements adjacent to the editing sites are necessary to ensure C-to-U editing specificity. Many studies have shown that, in contrast with mammalian cis-elements, the major cis-acting recognition elements in plants are located in the 5' flanking region upstream of the editing sites, while the 3' flanking region makes a relatively small contribution to C-to-U RNA editing efficiency. Cis-elements are

required for C-to-U RNA editing in both plastids and mitochondria (41-45). In general, an upstream sequence of <20 nucleotides, and in some cases a downstream sequence of <10 nucleotides, suffice as cis-elements for RNA editing (46). Some components of trans-acting factors bind to cis-elements at the essential 5' flanking upstream region and, subsequently, the specific downstream cytidine is recognized and targeted as an editing site. Next, the RNA editing machinery is recruited to the editing site and enzymatic modification occurs, changing the targeted C to U.

Several pentatricopeptide repeat (PPR) motif-containing proteins have been identified as one part of the trans-acting factors required for C-to-U RNA editing in both chloroplasts and mitochondria. These PPR proteins have been characterized as site-specific recognition factors for a number of targeted cytidines that bind directly to cis-elements. PPR proteins consist of tandem arrays of degenerate 35-amino-acid repeats (the PPR motifs), which can vary in number from 2 to 30 (47-49). The PPR family can be divided into the P and PLS subfamilies, based on the PPR motif structure (50). The PPR family includes many members; approximately 450 family members exist in *Arabidopsis* including approximately 250 and 200 P and PLS subfamily members, respectively (51). Members of the P subfamily contain a simple array of PPR motifs (P), whereas those of the PLS subfamily contain an array of triplets namely, long (L) and short (S) PPR-like motifs and canonical PPR motifs (P). Members of the PLS subfamily can be further divided into the PLS, E/E+ (Extended), and DYW (Aspartate-tyrosine-tryptophan) classes according to the different C-terminal domains (50,52). Members of the PLS subfamily has been reported as trans-acting RNA editing factors in plants, whereas P subfamily members are associated with the RNA maturation process including the translational machinery. The PPR motif contains two anti-parallel  $\alpha$ -helices that interact with each other to generate a helix-turn-helix motif; a series of helix-turn-helix motifs is then combined into a super-helix that has a specific central groove. This central groove controls protein binding to specific cis-acting element(s) on the targeted RNA with one PPR motif binding one nucleotide (47,51). *Arabidopsis* species contain approximately 650 C-to-U RNA editing sites in two organelles. These sites are recognized by ~200 members of the PLS subfamily, although it is possible that a single trans-acting factor could recognize more than two sites on average. For example, CRR22 (Chlororespiratory reduction22) and SOL2 recognize at least three cis-acting sites in the plastid and at least six sites in mitochondria, respectively (53,54).

To date, it has been unclear how a single PPR protein recognizes multiple target sequences; however, recently, other accessory proteins such as RNA-editing factor-interacting protein (RIP, also known as multiple sites organellar RNA editing factors, or MORFs) (55-

58) and organelle RNA recognition motif factors (ORRMs) (56,59) in the RNA editing apparatus have been identified. The MORF/RIP family in *Arabidopsis* includes 10 members. Of these, MORF2/RIP2 and MORF9/RIP9 have been reported in plastids, whereas MORF8/RIP1 has been identified in both plastids and mitochondria. RIP10 is encoded by a pseudogene, and the remaining family members have been reported to function in mitochondria. MORF proteins play an important role in C-to-U RNA editing, supporting an ordered spatial connection between PPR and other proteins. Another potential function of MORF proteins may contribute to site-specificity of the editing enzyme to the targeted C and may be associated with their ability to bind metal ions, such as cobalt (55). ORRMs contain an RRM at the C-terminus. The ORRM family has four major members. ORRM1 is a plastid editing factor, whereas ORRM2, ORRM3, and ORRM4 have been identified as mitochondrial RNA editing factors. The functions of ORRM proteins are unclear; however, they may play a similar role to the MORF factors. The interaction between PPR proteins and other trans-acting factors requires further investigation (59,60).

The mechanism of C-to-U substitution editing in plastids and mitochondria is predicted to be very similar to that of apoB mRNA editing, and an APOBEC-1-like cytidine deaminase enzyme may be involved in this process. At least eight cytidine deaminases have been identified in *A. thaliana*. One of these, *A. thaliana* cytidine deaminase 1 (At-CDA-1) has been characterized; however, this protein has no affinity for RNA and cannot perform RNA editing (61). These findings led to the hypothesis that a yet unidentified nuclear encoded protein may be exported to these organelles; to date, the components of the plant RNA editing apparatus are not fully understood.

#### 4. Enzymatic site-directed A-to-I RNA editing

Therapeutic RNA editing or site-directed RNA editing is an approach that corrects mutated mRNA sequences in order to treat genetic diseases caused by point mutations (62). Using mRNA vs. DNA as a gene therapy target is advantageous because targeted mRNA will be replenished after treatment; thus, the applied changes are not maintained or passed on to the next generation as would occur by targeting DNA. Moreover, mRNA-targeted therapy does not alter the physiological level of the endogenous mRNA (63). The site-directed RNA editing machinery requires two main factors: a guide RNA component that specifically recognizes the sequence to be edited and another RNA editing enzyme component that performs the modifying activity (62). RNA editing is naturally prevalent in mammals; when it occurs in coding regions, it results in single amino acid substitutions, and when it occurs in noncoding regions, it leads to changes in RNA

processing. Thus, if RNA editing could be targeted to a user-defined mRNA site, it would have great potential for the treatment of genetic diseases related to point mutations (64). Site-directed RNA editing includes site-directed C-to-U editing and A-to-I editing. Several site-directed RNA editing studies have been conducted recently; and all of which have successfully performed for manipulating site-directed A-to-I transitions (63,64). C-to-U-transition editing has only been hypothetically reviewed. With further refinement of the technology, site-specific C-to-U editing may potentially be accomplished with similar strategies of enzymatic editing. Therefore, in this section, site-directed A-to-I editing will be described and explained in more detail.

A-to-I RNA editing converts adenosine (A) to inosine (I), which is read as guanosine (G); thus, this conversion effectively results in a change from A to G. When A-to-I editing occurs in an mRNA open reading frame, it can recode 12 of the 20 canonical amino acids into a substitute codon, or a start or stop codon (65). Well-known examples of transcripts that undergo A-to-I editing include the calcium-gated glutamate receptor (GluR-B) and the 5-hydroxytryptamine 2C receptor (5HT2c) (66). During RNA editing, the base conversions occur by hydrolytic deamination catalyzed by adenosine deaminase acting on RNA (ADAR) enzymes (65,67). Members of the ADAR family can perform A-to-I RNA editing without additional cofactors *in vitro* (68). ADAR enzyme family includes three members (ADAR1, ADAR2, and ADAR3), which are highly conserved in mammalian cells. The A-to-I editing enzymatic activity of ADAR1 and ADAR2 has been demonstrated, whereas that of ADAR3 has not. ADAR enzymes consist of distinct domains that perform different functions. A catalytic domain containing conserved amino acid residues is situated at the C-terminus. This catalytic domain catalyzes the hydrolytic deamination of A to I. One-to-three repeats of the highly conserved dsRNA-binding domain (dsRBD) (approximately 65 amino acids) that bind(s) both perfect and imperfect RNA duplexes are found at the N-terminus (6).

An early therapeutic RNA editing study involved the design and synthesis of a synthetic complementary RNA oligonucleotide to direct the correction of a premature stop codon mutation in dystrophin RNA. The complementary RNA oligonucleotide was first inserted into the reaction. This complementary RNA oligonucleotide hybridizes perfectly with the targeted sequences that contain a premature stop codon and the hybrid activates the endogenous ADAR enzyme in nuclear extracts or in *Xenopus* embryos. Subsequently, the premature UAG stop codon is corrected to a UGG codon (Trp) both *in vitro* and in *Xenopus* embryos. Importantly, only complementary RNA oligonucleotide was used in the study, and the endogenously expressed enzymes were induced to nonspecifically edit the

region (62).

To obtain specific site-directed RNA editing, the dsRBDs of human ADAR1 (hADAR1) or human ADAR2 (hADAR2) were replaced with an antisense RNA oligonucleotide-guide RNA turning them into guide RNA-dependent enzymes. The antisense RNA oligonucleotide has an important function in guiding the catalytic activity to a specific position on the mRNA and forming the secondary structure required for the highly efficient and selective editing of the single targeted adenosine. An RNA-binding protein that could be genetically encoded is required to link the hADAR deaminase domain and an antisense guide RNA oligonucleotide. The linkage between the hADAR deaminase domain and the RNA-binding protein, and the interaction between the antisense guide RNA and the RNA-binding protein should be small so that they do not interfere with the function of the deaminase domain or the guide RNA. Moreover, high-affinity binding is required to drive the editing process in the complex cellular environment (63). To date, only a few studies have been conducted to examine site-directed enzymatic RNA editing.

In one study, the deaminase domain of hADAR was coupled with the guide RNA by using an *in vitro* reaction. The covalent attachment between human *O*<sup>6</sup>-alkylguanine-DNA-alkyltransferase (AGT) or SNAP-tag and *O*<sup>6</sup>-benzylguanine (BG) was used to couple the deaminase domain of hADAR and the guide RNA. The SNAP-tag is a small protein, which is suitable for direct covalent interactions with BG, resulting in the formation of a stable bond. The guide RNA-dependent deaminase was generated by substituting the N-terminal dsRBD with a SNAP-tag. The gene sequence encoding the hADAR1 deaminase domain was combined with a sequence encoding a SNAP-tag in a single vector, resulting in the expression of a fusion consisting of the hADAR1 deaminase domain fused to a SNAP-tag. Next, synthesis of the BG-guide RNA was conducted by solid-phase peptide synthesis. The vector containing the hADAR1 deaminase domain SNAP-tag fusion and the BG-guide RNA were transfected into cells to generate a guide RNA-deaminase conjugate. The hADAR1 deaminase domain and guide RNA were assembled by a rapid and specific single covalent bond between the SNAP-tag and BG moiety (Figure 1). After the guide RNA-deaminase conjugate was generated, it rapidly carried out site-directed specific RNA editing of the target mRNA, and the results showed the subsequent repair of a premature stop codon (UAG) into a tryptophan codon (UGG) in a fluorescent reporter gene, both *in vitro* and in human cells (293T) (69). Recently, the BG moiety was chemically masked using a light-sensitive 6-nitropiperonyloxymethyl (Npom) protection group, resulting in Npom-protected *O*<sup>6</sup>-benzylguanine (Npom-BG). The Npom group has two regioisomers (N7 and N9); both <sup>N7</sup>Npom-BG

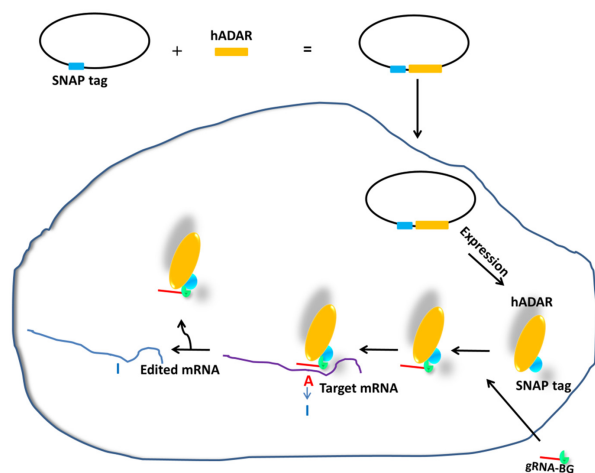


**Figure 1. Schematic of experimental design.** The catalytic domain of the human ADAR1 was fused with the C-terminus of a SNAP-tag. Next, the BG-modified gRNA was reacted with SNAP-deaminase to form guide RNA (gRNA)-deaminase conjugates. Finally, the gRNA-dependent deaminase carried out site-specific A-to-I RNA editing of a target mRNA (64).

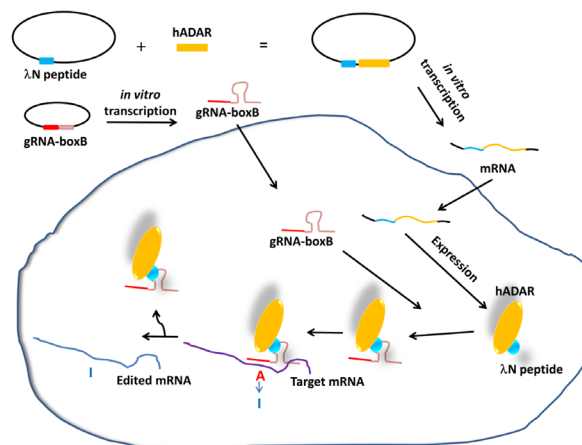


**Figure 2. The overall strategy used for artificial site-directed A-to-I RNA editing.** A site-directed editase was generated by linking the hADAR2 deaminase domain with an antisense guide oligonucleotide through an interaction between the  $\lambda$  phage N protein and the boxB RNA hairpin. Following the generation of the recombinant editase, the guide RNA (gRNA)-dependent deaminase conducted site-specific A-to-I RNA editing of the target mRNA (63).

and  $^{99}\text{mTc}$ -BG efficiently decayed to release BG when irradiated with 365-nm light using a common ultraviolet (UV) light table. Because the repair reaction (enzymatic site-directed A-to-I RNA editing) was dependent on the covalent attachment of guide RNA to the ADAR enzyme, the duration, location, and dosage of the editing reaction could be precisely controlled by triggering the assembly of the covalent RNA-protein conjugate (70).

In another study, the catalytic domain of hADAR2 was linked with antisense guide RNA using a naturally occurring binding reaction;  $\lambda$ -phage N protein-boxB ( $\lambda$ N peptide-boxB) was used to generate a linkage between the hADAR2 deaminase domain and the guide RNA. The  $\lambda$ N peptide consists of 22 amino acids, which were fused to the hADAR2 deaminase domain (DD), and the 17-nucleotide boxB containing a hairpin structure was combined with the guide RNA. The sequences that encode the hADAR2 deaminase domain were combined with the sequences encoding the  $\lambda$ N peptide in a single vector, resulting in expression of the  $\lambda$ N-DD fusion protein. Next, the boxB sequences were linked with the guide RNA sequence in another vector. Both vectors were transcribed using an *in vitro* transcription kits. Then, the synthesized RNAs were directly injected into cells and, following translation, the  $\lambda$ N peptide rapidly bound to boxB with high affinity, thus generating a recombinant enzyme that could be directed efficiently and selectively to edit a single adenosine (Figure 2). *In vitro* assays have shown that this recombinant enzyme can successfully correct a premature termination codon in an mRNA encoding the cystic fibrosis transmembrane conductance regulator anion channel. Moreover, in *Xenopus* oocytes, the recombinant enzyme could also correct cystic fibrosis transmembrane

conductance regulator mRNA, restore the full-length protein, and reestablish functional chloride currents across the plasma membrane; while in human cell lines it could correct a nonfunctional version of enhanced green fluorescent protein containing a premature termination codon (63).

Currently, site-directed enzymatic RNA editing is limited to mutations that can be corrected by recoding A-to-I; however, the same approach should be extended to cytidine deaminases that convert C-to-U. If artificial site-directed enzymatic C-to-U RNA editing could be successfully completed, this enzymatic site-directed RNA editing approach could be applied to a wide variety of codons.

## 5. Non-enzymatic site-directed C-to-U editing

Non-enzymatic site-directed editing has prompted great interest recently because this method does not require the restrictive conditions dictated by enzymatic site-directed RNA editing. Fujimoto *et al.* were the first to report the application of this method for artificial C-to-U DNA and RNA editing. Their method involved the design and synthesis of 5-carboxyvinyl deoxyuridine nucleoside ( $^{CV}U$ )- and 3-cyanovinylcarbazole nucleoside ( $^{CNV}K$ )-modified oligodeoxynucleotides (ODNs) for artificial DNA and RNA editing (71,72) (Figure 3b and Figure 4b). These modified ODNs were synthesized by standard phosphoramidite chemistry on a DNA synthesizer, with a post-modification procedure following ODN synthesis (71). In terms of the chemical structure, if deamination removes the amino group of cytidine (C) at the fourth position in the pyrimidine ring to form a ketone group, cytidine (C) converts to uridine (U).

These modified ODNs are covalently bound to



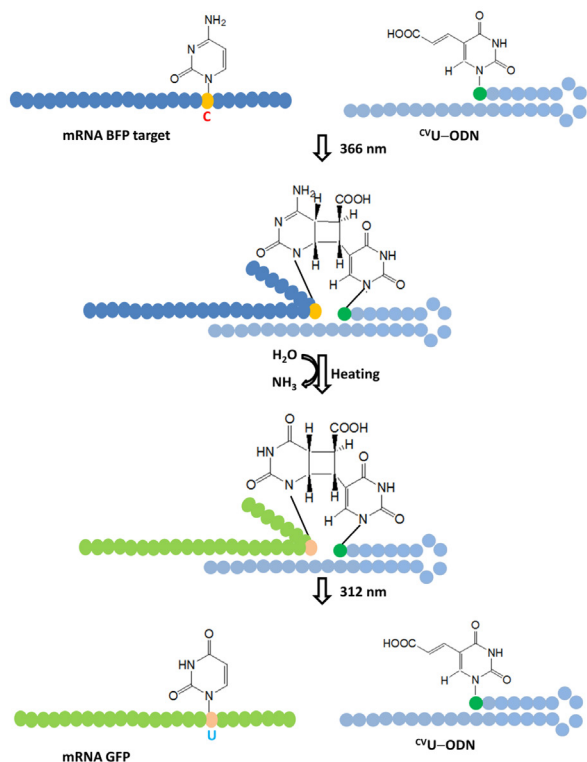


**Figure 5. Schematic representation of the four main reactions of the photo-transition process.** First, hybridization occurs between the modified ODN and the target RNA. Second, photo-crosslinking between the interacting ODNs is achieved by UV irradiation at 366 nm. Third, heat treatment is performed to drive deamination. Fourth, the target RNA and modified ODN are separated by photosplitting (312 nm UV irradiation). Subsequently, artificial editing occurs with a C-to-U photo-transition (71,73).

reaction. Then, the full-length 823-nt RNA and total RNA were used.

Site-directed deamination was performed as described in Figure 5. Base substitution from C to U was confirmed by PCR followed by restriction fragment length polymorphism analysis. *Mva I* could cut the wild-type "CCTGG" sequence, but not the mutant "CCCGG" sequence. Our results demonstrated that successful sequence-specific photochemical base substitution was achieved with various targets, including synthetic single-stranded 72 nucleotide (ss72-nt), ss731-nt, RNA 823-nt, and total RNA from the patient's cells, as targets. Our results showed that approximately 10% of the full-length mRNA was targeted for *in vitro* deamination under physiological temperatures (74).

Cells from the Leigh syndrome patient grew slowly and had difficulties taking up exogenous ODNs; therefore, blue fluorescent protein (BFP), a derivative of green fluorescent protein (GFP), was used as a new and more suitable model. BFP differs from GFP by a single nucleotide; therefore, the nt-199 conversion of cytosine to uridine transforms BFP to GFP. Site-directed deamination was also performed as previously described. Briefly, the responsive <sup>CV</sup>U-modified ODNs

were annealed to the mRNA BFP targets. The mutated cytosine was cross-linked with the responsive ODN by UV radiation (366 nm) and then received heat-treatment. Finally, the cross-linked nucleotide is cleaved by the photosplitting operation (312 nm UV). A C-to-U photo-transition product (mRNA GFP) and <sup>CV</sup>U ODNs were separated after the site-directed deamination process (Figure 5). To confirm the base substitution, PCR-restriction fragment length polymorphism and spectrofluorometry were used. *BtgI*, a restriction enzyme that can digest "CCACGG" in the coding sequence of BFP, but not "CTACGG" in GFP, was suitable for assessing the BFP-to-GFP transition. Our results showed that site-directed photochemical base substitution was successfully achieved using synthetic single-stranded 100 nucleotide (ss100-nt) and *in vitro*-synthesized full-length BFP mRNA targets. Approximately 10% efficiency for the C199U transition was exhibited under a physiological temperature (37°C). Although the efficiency was not high, this result constitutes a first step towards using non-enzymatic site-directed transition to restore mutated mRNAs (73).

The structure and sequence of <sup>CV</sup>U-modified ODNs are key features affecting the biological functions of ODNs. To investigate the relationship between the <sup>CV</sup>U-modified sequences and deamination efficiency, a series of ODNs, including 8 <sup>CV</sup>U-modified ODNs, was subjected to non-enzymatic site-directed C-to-U RNA editing. About structure, the <sup>CV</sup>U-modified ODNs contain three sections: the complementary section, the hairpin loop, and the 5'-terminal photoresponsive nucleobase <sup>CV</sup>U. The complementary section plays an important role in anchoring and site-directing the ODNs to their target; the hairpin loop allows ODNs easy access to cells and increases stability. The 5'-terminal photoresponsive nucleobase-<sup>CV</sup>U constitutes the photoreactive group. Because the 5'-terminal photoresponsive nucleobase <sup>CV</sup>U was the same in all <sup>CV</sup>U-modified ODNs, optimization of the complementary section length and hairpin loop length could be manipulated to control deamination efficiency. First, to investigate the structure-deamination efficiency relationship, the length of the hairpin loop was fixed, and the length of the complementary region was changed. In this case, the deamination efficiency depended on the length of complementary region. The lengths of the hairpin structure were set at 7, 9, and 11 nt, and the lengths of the complementary regions used ranged from 10 to 22 nt in length. Next, to evaluate the effects of the hairpin loop length on the deamination efficiency, the length of complementary region was fixed at 10 nt, and the lengths of hairpin structure used were set at 7, 9, and 11 nt. Photochemical base substitution was performed as described (Figure 5). Using a transition from the cytosine (C) of BFP gene to the uridine (U) of GFP gene at position 199 as a model, we were able to demonstrate that the structural sequence-dependent deamination efficiency was very

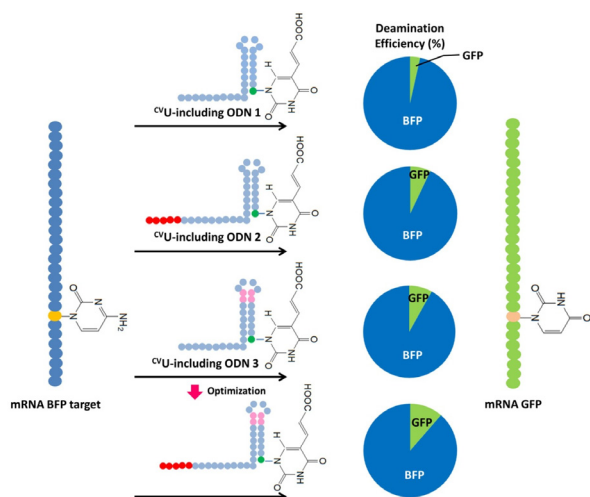


**Figure 6. Schematic representation of the dependence of the deamination efficiency on the lengths of the complementary effector ODN sequence and hairpin loop, which were determined to optimize the <sup>CV</sup>U-modified ODN structure.** In our study, the deamination efficiency reached its maximum values with a complementary sequence length slightly more than 14 nt and a hairpin loop length of 9 nt (75).

tight *in vitro*. The optimum length of the hairpin was 9 nt, and the optimum length of complementary sequence was 15-17 nt (75) (Figure 6).

The advantage of non-enzymatic site-directed RNA editing is that the reaction can occur independently of conditions required for enzymatic activity; however, the disadvantage of this approach is low deamination efficiency. Further studies will be required to create other photoreactive groups to improve the deamination efficiency.

## 6. Conclusion

C-to-U RNA editing is an interesting biological phenomenon; however, to date its underlying enzymatic and complementary components are not fully understood. Further studies are required to elucidate the components and mechanisms of C-to-U RNA editing in both mammals and plants because this process holds great potential for the correction of T>C or A>G genetic mutations. Although enzymatic site-directed C-to-U RNA editing has not yet to be successfully performed, in theory, it involves the same strategy already used successfully for enzymatic A-to-I site-directed RNA editing; thus, in the immediate future, enzymatic site-directed C-to-U editing should be evaluated further in practical applications. In addition, non-enzymatic site-directed C-to-U RNA editing was successfully performed even though it has a lower deamination efficiency. The next steps for non-enzymatic site-directed RNA editing involve the development of other modified ODNs to improve and increase the deamination efficiency at a physiological temperature. In the future, site-directed C-to-U RNA editing

including, enzymatic C-to-U editing and non-enzymatic C-to-U editing, promises to effectively correct a variety of human diseases related to T>C or A>G genetic mutations.

## Acknowledgements

We wish to thank Editage ([www.editage.jp](http://www.editage.jp)) for English language editing. This research was supported in part by a Grant-in-Aid for Scientific Research from the Japan Society for the Promotion of Science in Japan (25290072 and 26670167 to T.T.).

## References

- Gott JM, Emeson RB. Functions and mechanisms of RNA editing. *Annu Rev Genet.* 2000; 34:499-531.
- Chen SH, Habib G, Yang CY, Gu ZW, Lee BR, Weng SA, Silberman SR, Cai SJ, Deslypere JP, Rosseneu M, Gotto AM, Li WH, Chan L. Apolipoprotein B-48 is the product of a messenger RNA with an organ-specific in-frame stop codon. *Science.* 1987; 238:363-366.
- Powell LM, Wallis SC, Pease RJ, Edwards YH, Knott TJ, Scott J. A novel form of tissue-specific RNA processing produces a polipoprotein-B48 in intestine. *Cell.* 1987; 50:831-840.
- Freyer R, Kiefer-Meyer MC, Kössel H. Occurrence of plastid RNA editing in all major lineages of land plants. *Proc Natl Acad Sci USA.* 1997; 94:6285-6290.
- Zanlungo S, Béqu D, Quiñones V, Araya A, Jordana X. RNA editing of a pocytochrome b (cob) transcripts in mitochondria from two genera of plants. *Curr Genet.* 1993; 24:344-348.
- Nishikura K. Functions and regulation of RNA editing by ADAR deaminases. *Annu Rev Biochem.* 2010; 79:321-349.
- Smith HC, Bennett RP, Kizilyer A, McDougall WM, Prohaska KM. Functions and regulation of the APOBEC family of proteins. *Semin Cell Dev Biol.* 2012; 23:258-268.
- Bazak L, Haviv A, Barak M, Jacob-Hirsch J, Deng P, Zhang R, Isaacs FJ, Rechavi G, Li JB, Eisenberg E, Levanon EY. A-to-I RNA editing occurs at over a hundred million genomic sites located in a majority of human genes. *Genome Res.* 2013; 24:365-376.
- Ramaswami G, Lin W, Piskol R, Tan MH, Davis C, Li JB. Accurate identification of human alu and non-alu RNA editing sites. *Nat Methods.* 2012; 9:579-581.
- Li JB, Church GM. Deciphering the functions and regulation of brain-enriched A-to-I RNA editing. *Nat Neurosci.* 2013; 16:1518-1522.
- Rosenber BR, Hamilton CE, Mwangi MM, Dewell S, Papavasiliou FN. Transcriptome-wide sequencing reveals numerous APOBEC1 mRNA-editing targets in transcript 3' UTRs. *Nat Struct Mol Biol.* 2011; 18:230-236.
- Blanc V, Park E, Schaefer S, Miller M, Lin Y, Kennedy S, Billing AM, Hamidane HB, Graumann J, Mortazavi A, Nadeau JH, Davidson NO. Genome-wide identification and functional analysis of Apobec-1-mediated C-to-U RNA editing in mouse small intestine and liver. *Genome Biol.* 2014; 15:R79.
- Harjanto D, Papamarkou T, Oates CJ, Rayon-Estrada V, Papavasiliou FN, Papavasiliou A. RNA editing

- generates cellular subsets with diverse sequence within populations. *Nat Commun.* 2016; 7:12145.
14. Blanc V, Davidson NO. Mouse and other rodent models of C to U RNA editing. *Methods Mol Biol.* 2011; 718:121-135.
  15. Navaratnam N, Patel D, Shah RR, Greeve JC, Powell LM, Knott TJ, Scott J. An additional editing site is present in apolipoprotein B mRNA. *Nucleic Acids Res.* 1991; 19:1741-1744.
  16. Backus JW, Smith HC. Three distinct RNA sequence elements are required for efficient apolipoprotein B (apoB) RNA editing *in vitro*. *Nucleic Acids Res.* 1992; 20:6007-6014.
  17. Backus JW, Smith HC. Apolipoprotein B mRNA sequences 3' of the editing site are necessary and sufficient for editing and editosome assembly. *Nucleic Acids Res.* 1991; 19:6781-6786.
  18. Hersberger M, Innerarity TL. Two efficiency elements flanking the editing site of cytidine 6666 in the apolipoprotein B mRNA support mooring-dependent editing. *J Biol Chem.* 1998; 273:9435-9442.
  19. Nakamuta M, Tsai A, Chan L, Davidson NO, Teng BB. Sequence elements required for apolipoprotein B mRNA editing enhancement activity from chicken enterocytes. *Biochem Biophys Res Commun.* 1999; 254:744-750.
  20. Shah RR, Knott TJ, Legros JE, Navaratnam N, Greeve JC, Scott J. Sequence requirements for the editing of apolipoprotein B mRNA. *J Biol Chem.* 1991; 266:16301-16304.
  21. Mehta A, Kinter MT, Sherman NE, Driscoll DM. Molecular cloning of apobec-1 complementation factor, a novel RNA-binding protein involved in the editing of apolipoprotein B mRNA. *Mol Cell Biol.* 2000; 20:1846-1854.
  22. Navaratnam N, Bhattacharya S, Fujino T, Patel D, Jarmuz AL, Scott J. Evolutionary origins of apoB mRNA editing: Catalysis by a cytidine deaminase that has acquired a novel RNA-binding motif at its active site. *Cell.* 1995; 81:187-195.
  23. MacGinnitie AJ, Anant S, Davidson NO. Mutagenesis of apobec-1, the catalytic subunit of the mammalian apolipoprotein B mRNA editing enzyme, reveals distinct domains that mediate cytosine nucleoside deaminase, RNA binding, and RNA editing activity. *J Biol Chem.* 1995; 270:14768-14775.
  24. Wedekind JE, Dance GS, Sowden MP, Smith HC. Messenger RNA editing in mammals: New members of the APOBEC family seeking roles in the family business. *Trends Genet.* 2003; 19:207-216.
  25. Blanc V, Henderson JO, Newberry EP, Kennedy S, Luo J, Davidson NO. Targeted deletion of the murine apobec-1 complementation factor (acf) gene results in embryonic lethality. *Mol Cell Biol.* 2005; 25:7260-7269.
  26. Fossat N, Tourle K, Radziejew T, Barratt K, Leibhold D, Studdert JB, Power M, Jones V, Loebel DAF, Tam PP. C to U RNA editing mediated by APOBEC1 requires RNA-binding protein RBM47. *EMBO Rep.* 2014; 15:903-910.
  27. Sharma S, Patnaik SK, Taggart RT, Kannisto ED, Enriquez SM, Gollnick P, Baysal BE. APOBEC3A cytidine deaminase induces RNA editing in monocytes and macrophages. *Nat Commun.* 2015; 6:6881.
  28. Sharma S, Patnaik SK, Kemer Z, Baysal BE. Transient overexpression of exogenous APOBEC3A causes C-to-U RNA editing of thousands of genes. *RNA Biol.* 2016; 1-8.
  29. Covello PS, Gray MW. RNA editing in plant mitochondria. *Nature.* 1989; 341:662-666.
  30. Gualberto JM, Lamattina L, Bonnard G, Weil JH, Grienenberger JM. RNA editing in wheat mitochondria results in the conservation of protein sequences. *Nature.* 1989; 341:660-662.
  31. Hiesel R, Wissinger B, Schuster W, Brennicke A. RNA editing in plant mitochondria. *Science.* 1989; 246:1632-1634.
  32. Maier MR, Neckermann K, Igloi GL, Kössel H. Complete sequence of the maize chloroplast genome: Gene content, hotspots of divergence and fine tuning of genetic information by transcript editing. *J Mol Biol.* 1995; 251:614-628.
  33. Bailey-Serres J, Rochaix JD, Wassenegger M, Filipowicz W. Plant, their organelles, viruses and transgenes reveal the mechanisms and relevance of post-transcriptional processes Leysin, VD, Switzerland, February 25-28, 1999. *EMBO J.* 1999; 18:5153-5158.
  34. Kotera E, Tasaka M, Shikanai T. A pentatricopeptide repeat protein is essential for RNA editing in chloroplasts. *Nature.* 2005; 433:326-330.
  35. Sasaki Y, Kozaki A, Ohmori A, Iguchi H, Nagano Y. Chloroplast RNA editing required for functional acetyl-CoA carboxylase in plants. *J Biol Chem.* 2001; 276:3937-3940.
  36. Wintz H, Hanson MR. A termination codon is created by RNA editing in the petunia *atp9* transcript. *Curr Genet.* 1991; 19:61-64.
  37. Unsel M, Marienfeld JR, Brandt P, Brennicke A. The mitochondrial genome of *Arabidopsis thaliana* contains 57 genes in 366,924 nucleotides. *Nat Genet.* 1997; 15:57-61.
  38. Giegé P, Brennicke A. RNA editing in *Arabidopsis* mitochondria effects 441 C to U changes in ORFs. *PNAS.* 1999; 96:15324-15329.
  39. Marchfelder A, Binder S. Plastid and plant mitochondrial RNA processing and RNA stability. In: *Molecular Biology and Biotechnology of Plant Organelles* (Daniell H, Chase CD, eds.). Springer, Dordrecht, 2004; pp. 261-294.
  40. Takenaka M, Verbitskiy D, van der Merwe JA, Zehrmann A, Brennicke A. The process of RNA editing in plant mitochondria. *Mitochondrion.* 2008; 8:35-46.
  41. Chaudhuri S, Carrer H, Maliga P. Site-specific factor involved in the editing of the *psbL* mRNA in tobacco plastids. *EMBO J.* 1995; 14:2951-2957.
  42. Bock R, Hermann M, Kössel H. *In vivo* dissection of cis-acting determinants for plastid RNA editing. *EMBO J.* 1996; 15:5052-5059.
  43. Chaudhuri S, Maliga P. Sequences directing C to U editing of the plastid *psbL* mRNA are located within a 22 nucleotide segment spanning the editing site. *EMBO J.* 1996; 15:5958-5964.
  44. Bock R, Hermann M, Fuchs M. Identification of critical nucleotide positions for plastid RNA editing site recognition. *RNA.* 1997; 3:1194-1200.
  45. Hermann M, Bock R. Transfer of plastid RNA-editing activity to novel sites suggests a critical role for spacing in editing-site recognition. *Proc Natl Acad Sci U S A.* 1999; 96:4856-4861.
  46. Shikanai T. RNA editing in plant organelles: Machinery, physiological function and evolution. *Cell Mol Life Sci.* 2006; 63:698-708.
  47. Small ID, Peeters N. The PPR motif – a TPR-related

- motif prevalent in plant organellar proteins. Trends Biochem Sci. 2000; 25:46-47.
48. Aubourg S, Boudet N, Kreis M, Lecharny A. In *Arabidopsis thaliana*, 1% of the genome codes for a novel protein family unique to plants. Plant Mol Biol. 2000; 42:603-613.
  49. Lurin C, Andrés C, Aubourg S, et al. Genome-wide analysis of *Arabidopsis* pentatricopeptide repeat proteins reveals their essential role in organelle biogenesis. Plant Cell. 2004; 16:2089-2103.
  50. Shikanai T, Endo T, Hashimoto T, Yamada Y, Asada K, Yokota A. Directed disruption of the tobacco *ndhB* gene impairs cyclic electron flow around photosystem I. Proc Natl Acad Sci USA. 1998; 95:9705-9709.
  51. Schmitz-Linneweber C, Small I. Pentatricopeptide repeat proteins: A socket set for organelle gene expression. Trends Plant Sci. 2008; 13:663-670.
  52. Barkan A, Small I. Pentatricopeptide repeat proteins in plants. Annu Rev Plant Biol. 2014; 65:415-442.
  53. Okuda K, Chateigner-Boutin AL, Nakamura T, Delannoy E, Sugita M, Myouga F, Motohashi R, Shinozaki K, Small I, Shikanai T. Pentatricopeptide repeat proteins with the DYW motif have distinct molecular functions in RNA editing and RNA cleavage in *Arabidopsis* chloroplasts. Plant Cell. 2009; 21:147-156.
  54. Zhu Q, Dugardeyn J, Zhang C, Takenaka M, Kühn K, Craddock C, Smalle J, Karampelias M, Denecke J, Peters J, Gerats T, Brennicke A, Eastmond P, Meyer EH, Van Der Straeten D. SLO2, a mitochondrial pentatricopeptide repeat protein affecting several RNA editing sites, is required for energy metabolism. Plant J. 2012; 71:836-849.
  55. Bentolila S, Oh J, Hanson MR, Bukowski R. Comprehensive high-resolution analysis of the role of an *Arabidopsis* gene family in RNA editing. PLoS Genet. 2013; 9:e1003584.
  56. Bentolila S, Heller WP, Sun T, Babina AM, Friso G, vanWijk KJ, Hanson MR. RIP1, a member of an *Arabidopsis* protein family, interacts with the protein RARE1 and broadly affects RNA editing. Proc Natl Acad Sci U S A. 2012; 109:E1453-1461.
  57. Takenaka M, Zehrmann A, Verbitskiy D, Kugelman M, Hartel B, Brennicke A. Multiple organellar RNA editing factor (MORF) family proteins are required for RNA editing in mitochondria and plastids of plants. Proc Natl Acad Sci U S A. 2012; 109:5104-5109.
  58. Boussard C, Avon A, Kindgren P, Bond CS, Challenor M, Lurin C, Small I. The cytidine deaminase signature HxE(x)n CxxC of DYW1 binds zinc and is necessary for RNA editing of *ndhD-1*. New Phytol. 2014; 203:1090-1095.
  59. Sun T, Germain A, Giloteaux L, Hammani K, Barkan A, Hanson MR, Bentolila S. An RNA recognition motif-containing protein is required for plastid RNA editing in *Arabidopsis* and maize. Proc Natl Acad Sci USA. 2013; 110:E1169-1178.
  60. Shi X, Bentolila S, Hanson MR. Organelle RNA recognition motif-containing (ORRM) proteins are plastid and mitochondrial editing factors in *Arabidopsis*. Plant Signal Behav. 2016; 11:e1167299.
  61. Chen M, Herde M, Witte CP. Of the nine cytidine deaminase-like genes in *Arabidopsis*, eight are pseudogenes and only one is required to maintain pyrimidine homeostasis *in vivo*. Plant Physiol. 2016; 171:799-809.
  62. Woolf TM, Chase JM, Stinchcomb DT. Toward the therapeutic editing of mutated RNA sequences. Proc Natl Acad Sci U S A. 1995; 92:8298-8302.
  63. Montiel-Gonzalez MF, Vallecillo-Viejo I, Yudowski GA, Rosenthal JJC. Correction of mutations within the cystic fibrosis transmembrane conductance regulator by site-directed RNA editing. Proc Natl Acad Sci U S A. 2013; 110:18285-18290.
  64. Schneider MF, Wettengel J, Hoffmann PC, Stafforst T. Optimal guideRNAs for re-directing deaminase activity of hADAR1 and ADAR2 in trans. Nucleic Acids Res. 2014; 42:e87.
  65. Bass BL. RNA editing by adenosine deaminases that act on RNA. Annu Rev Biochem. 2002; 71:817-846.
  66. Maas S, Rich A. Changing genetic information through RNA editing. Bioessays. 2000; 22:790-802.
  67. Smith HC, Sowden MP. Base-modification mRNA editing through deamination: The good, the bad and the unregulated. Trends Genet. 1996; 12:418-424.
  68. Chen CX, Cho DS, Wang Q, Lai F, Carter KC, Nishikura K. A third member of the RNA-specific adenosine deaminase gene family, ADAR3, contains both single- and double-stranded RNA binding domains. RNA. 2000; 6:755-767.
  69. Vogel P, Schneider MF, Wettengel J, Stafforst T. Improving site-directed RNA editing *in vitro* and in cell culture by chemical modification of the guideRNA. Angew Chem Int Ed. 2014; 53:6267-6271.
  70. Hanswillemenke A, Kuzdere T, Vogel P, Jekely G, Stafforst T. Site-directed RNA editing *in vivo* can be triggered by the light-driven assembly of an artificial riboprotein. J Am Chem Soc. 2015; 137:15875-15881.
  71. Fujimoto K, Matsuda S, Yoshimura Y, Matsumura T, Hayashi M, Saito I. Site-specific transition of cytosine to uracil *via* reversible DNA photoligation. Chem Commun. 2006; 30:3223-3225.
  72. Fujimoto K, Konishi-Hiratsuka K, Sakamoto T, Yoshimura Y. Site-specific photochemical RNA editing. Chem Commun. 2010; 46:7545-7547.
  73. Vu LT, Nguyen TTK, Alam S, Sakamoto T, Fujimoto K, Suzuki H, Tsukahara T. Change from blue fluorescent protein to green fluorescent protein using chemical RNA editing as a novel strategy in genetic restoration. Chem Biol Drug Des. 2015; 86:242-1252.
  74. Vu LT, Ooka Y, Alam S, Suzuki H, Fujimoto K, Tsukahara T. Chemical RNA editing as a possibility novel therapy for genetic disorders. IJAC. 2012; 2:237-241.
  75. Vu LT, Nguyen TTK, Md Thoufic AA, Suzuki H, Tsukahara T. The relationship between structures and deamination efficiency of carboxyvinyldeoxyuridine ODNs on chemical RNA editing for genetic restoration. Chem Biol Drug Des. 2016; 87:583-593.

(Received March 2, 2017; Revised March 29, 2017; Accepted April 11, 2017)

# The T-Box transcription factor 3 in development and cancer

Tarryn Willmer, Aretha Cooper, Jade Peres, Rehana Omar, Sharon Prince\*

Department of Human Biology, Faculty of Health Sciences, Anzio Road, University of Cape Town, Cape Town, South Africa.

## Summary

T-box factors comprise an archaic family of evolutionary conserved transcription factors that regulate patterns of gene expression essential for embryonic development. The T-box transcription factor 3 (TBX3), a member of this family, is expressed in several tissues and plays critical roles in, among other structures, the heart, mammary gland and limbs and haploinsufficiency of the human *TBX3* gene is the genetic basis for the autosomal dominant disorder, ulnar-mammary syndrome. Overexpression of *TBX3* on the other hand has been linked to several cancers including melanoma, breast, pancreatic, liver, lung, head and neck, ovarian, bladder carcinomas and a number of sarcoma subtypes. Furthermore, there is strong evidence that TBX3 promotes oncogenesis by impacting proliferation, tumour formation, metastasis as well as cell survival and drug resistance. More recently, TBX3 was however shown to also have tumour suppressor activity in fibrosarcomas and thus its functions in oncogenesis appear to be context dependent. Identification of the upstream regulators of TBX3 and the molecular mechanism(s) underpinning its oncogenic roles will make valuable contributions to cancer biology.

**Keywords:** TBX3, transcription factor, embryogenesis, oncogenesis

## 1. Introduction

The T-box family of transcription factors are highly conserved through evolution and based on phylogenetic analysis, the T-box gene family is divided into five subfamilies, namely *Brachyury (T)*, *T-brain (Tbr1)*, *TBX1*, *TBX2*, and *TBX6 (I)*. Members of this family are defined by a unique DNA binding domain known as the T-box which *in vitro*, binds a partially palindromic sequence T(G/C)ACACCT AGGTGTGAAATT, known as the T-element, as well as single T-element half sites in multiple orientations (2). *In vivo* data have, however, revealed that the T-element binding site is highly variable and degenerate and there is evidence that T-box factors can also bind their target genes through co-factor binding sites (3,4). Members of the T-box family have well-established roles in the development of vertebrate and invertebrate species where they are expressed in a wide

array of tissues and their functions range from early cell-fate decisions to organogenesis (5). Their critical roles in development are evident by the number of human congenital developmental syndromes associated with mutations in *T-box* genes (6). In addition, there is overwhelming evidence implicating T-box factors in cancer biology where they behave as oncogenes and/or tumour suppressors (7).

## 2. TBX3

The T-box transcription factor, TBX3, is critical for development and has emerged as an important player in the oncogenic process. It is essential for the formation of, amongst other structures, the heart, limbs, mammary glands, teeth and genitalia and haploinsufficiency of the human *TBX3* gene results in ulnar-mammary syndrome (UMS) which is characterised by malformations of these organs and body structures. On the other hand, the overexpression of *TBX3* is a feature of a wide range of cancers and it has been implicated in several aspects of the oncogenic process ranging from the bypass of senescence to the inhibition of apoptosis, migration and invasion. However, little is known about the molecular basis for the role of TBX3 in development and oncogenesis because there is a paucity of information

Released online in J-STAGE as advance publication June 4, 2017.

\*Address correspondence to:

Dr. Sharon Prince, Department of Human Biology, Faculty of Health Sciences, University of Cape Town, Observatory, 7925, Cape Town, South Africa.  
E-mail: sharon.prince@uct.ac.za

regarding its upstream regulators, its target genes as well as the protein co-factors that it co-operates with to execute its functions.

### 2.1. *TBX3* gene and protein structure

*Tbx3* forms part of the *Tbx2* subfamily of T-box factors, which comprise the closely related *Tbx2*, *Tbx3*, *Tbx4*, and *Tbx5*, all of which originated from a single ancestral gene (8). Based on the branch length of their phylogenetic tree, it is proposed that *Tbx3* was duplicated by unequal crossing over events, giving rise to two gene clusters, namely *Tbx2/Tbx3* and *Tbx4/Tbx5*. An additional duplication of this cluster gave rise to four separate genes, with *Tbx2* and *Tbx4* being situated on chromosome 17q23 and *Tbx3* and *Tbx5* on chromosome 12q24 in humans (8-10). Due to the original duplication event, *TBX3* is more closely related to *TBX2* and in humans they share a 95% identity within their DNA binding domain and approximately 70% homology in their N-termini (11).

In humans, *TBX3* maps to the reverse strand of chromosome 12 at position 12q23-24.1 and alternative splicing results in a number of transcript variants with *TBX3* and *TBX3+2a* being the most extensively studied (9). Fan *et al.* showed that, while *TBX3* and *TBX3+2a* are widely expressed in both mouse and human tissue, their expression ratio is species and tissue dependent (12). The human *TBX3* coding region spans approximately 4.7 kb, contains 7 exons and encodes a 723 amino acid protein (Figure 1). Differential splicing of the second intron, however, results in the addition of the 2a exon, producing the *TBX3+2a* isoform with an additional 20 amino acids in the T-box domain (12,13). It is still unclear whether these variants have overlapping or distinct roles and whether the +2a insertion results in *TBX3+2a* regulating different target genes to *TBX3*. Indeed, Fan *et al.* reported that the isoforms were functionally distinct as, while the overexpression of *TBX3* inhibited senescence in mouse embryonic fibroblasts (MEFs), the overexpression of *TBX3+2a* promoted this process (12). These functional differences were ascribed to the fact that *TBX3*, and not *TBX3+2a*, was able to bind to the consensus T-element *in vitro*. These findings were contradicted by Hoogaars *et al.* who showed that both isoforms bound the consensus T-element in *in vitro* binding assays, repressed the T-elements previously identified in the *Natriuretic peptide A* (*Nppa*) and *p21WAF1* promoters, and interacted with the homeobox co-factor NK2 homeobox 5 (*Nkx2.5*) (14). In addition, using an *in vivo* transgenic mouse model they showed that *TBX3* and *TBX3+2a* were capable of inhibiting heart chamber formation through repression of the cardiac chamber markers *Nppa* and *Gap junction alpha-5* (*Gja5*). Furthermore, a more recent study suggested that, while the overexpression of *Tbx3* and *Tbx3+2a* inhibited *Nanog* promoter activity in pluripotent mouse embryonic

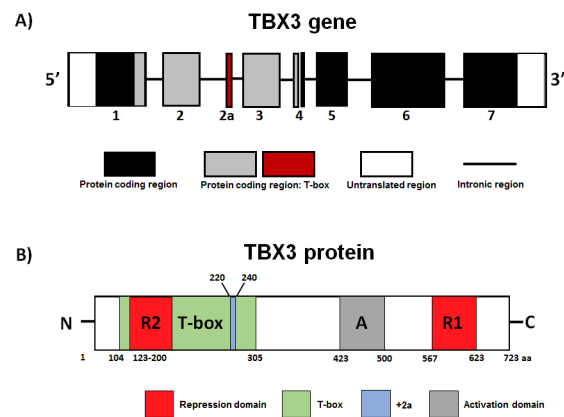


**Figure 1. *TBX3* gene and protein.** Schematic diagram of (A) *TBX3* gene including protein-coding sequences (filled boxes), introns (lines), untranslated sequences (white boxes), highly conserved T-box sequences (grey and red boxes) and exon 2a (red box) which is alternatively transcribed; and (B) *TBX3* protein showing repression domains R1 and R2 (red boxes), T-box (green boxes), activation domain (grey box), additional 20 amino acids in *TBX3+2a* protein splice form (blue box). The number of amino acid residues is shown under each box (adapted from Bamshad *et al.* 1999).

stem cells (mESCs), only *Tbx3+2a* physically interacted with *Nanog* (15). Lastly, Kumar *et al.* highlighted a novel role for *TBX3* in the regulation of RNA splicing and showed that both isoforms regulated this process (16). In summary, while more work is needed to clarify these conflicting findings, it seems likely that the expression pattern and roles of *TBX3* and *TBX3+2a* may vary depending on the cellular context.

The functional domains of the *TBX3* protein (Figure 1B) were mapped using a Gal4 binding domain fused to different regions of *Tbx3* on a luciferase reporter driven by four proximal promoter Gal4 binding sites (17). Constructs expressing either the full length *TBX3* protein or the 123-200 or 567-623 regions of the protein led to a repression of relative luciferase activity. This indicated that *TBX3* was a transcriptional repressor and identified regions 567-623 and 123-200 as repression domains, which the authors called R1 and R2, respectively. Indeed, *TBX3* was subsequently shown to transcriptionally repress *p14ARF/p19ARF*, *p21WAF1*, *Nppa*, *E-cadherin*, and *phosphatase and tensin homolog* (*PTEN*) (7). Furthermore, when R1 or R2 were fused to the VP16 (herpes simplex virus protein 16) activation domain and tested in similar experiments, R1 but not R2, was able to override the VP16 activation domain and to repress transcriptional activity (17). This led to the suggestion that R1 is the dominant repression domain. A putative activation domain at amino acids 423-500 was also mapped and indeed *TBX3* has been shown to activate *Connexin43* (18) and *Gata6* (19) which are both important in heart embryogenesis. Using electrophoretic mobility shift assays (EMSA) the DNA-binding region was found to be located in the N-terminus (position 105-287 (REFSEQ: accession NM 005996.3)) and a

nuclear localization signal (NLS) was found at residues 292 to 297 (17). Bamshad *et al.* characterised mutations in 75 UMS sufferers, from 8 different families and reported that 50% of the mutations resided in the exons encoding the T-box domain and the other 50% occurred in downstream exons which encode the C-terminus (13). Together, these reports highlight the importance of the T-box DNA binding domain and C-terminal regions of TBX3. Further characterisation of the structure of the TBX3 protein and its interaction with DNA were shown by Coll *et al.* when they solved the crystal structure of the TBX3 DNA-binding domain (20). While they demonstrate that TBX3 binds the palindromic consensus T-box binding site as two independent monomers, it is predicted that TBX3 will bind its physiological targets as a single monomer.

As is the case with other T-box factors, it is speculated that post-translational modifications and interaction with co-factors may regulate TBX3 target gene specificity within different cellular contexts but these areas remain poorly understood (21). Indeed, in addition to repressing its known target genes through direct binding to a T-element it can also recruit histone deacetylase (HDAC) 1, 2, 3 and 5 to epigenetically silence promoters and the details will be discussed under relevant sections of this review. Interestingly, mass spectrometry analysis performed in the Moon laboratory revealed that TBX3 interacts with a number of RNA-binding and -splicing proteins which indicated novel roles for TBX3 (16,22). Furthermore, they showed that mutations in the TBX3 NLS, representative of those seen in UMS, disrupt its interaction with its RNA-binding partners. They also reported that TBX3 binds its target RNAs through T-elements present within mRNA transcripts and could directly regulate the alternative splicing of *Disks large homolog 3 (Dlg3)* and *Nuclear factor of kappa light polypeptide gene enhancer in B-cells 1 (Nfkb1)*. TBX3 was also shown to facilitate the recruitment and docking of other RNA-binding proteins and splicing factors, such as the RNA helicase, DEAD box helicase 3 (DDX3), to T-element containing RNAs. Interestingly, the UMS mutations present within the C-terminal region of TBX3 interfered with its RNA splicing functions.

The above findings demonstrate that TBX3 can regulate gene expression at multiple levels.

## 2.2. TBX3 in development and in stem cell biology

During mouse development *Tbx3* is first expressed in the morula, then in the inner cell mass of the blastocyst and at the onset of gastrulation it localises to the proximal pole of the epiblast (23). It is subsequently found in distinct areas of the developing nervous system, musculo-skeleton, eye, heart, kidney, lung, liver, pancreas and mammary gland (24). *TBX3* is also widely expressed in a number of human foetal organs and tissues, including heart, lung, kidney, liver and spleen (13). Consistent

with its extensive expression pattern, TBX3 contributes to the formation of many tissues with its most well characterised roles being in heart, mammary gland and limb development (24). As mentioned earlier, haploinsufficiency of *TBX3* causes the human autosomal dominant UMS which is characterised by a wide range of congenital abnormalities including malformations of the limbs, mammary gland aplasia, loss of areola and defects in the jaw, heart and genitalia (24). These abnormalities can also be observed in mouse models of UMS. For example, homozygous mice die *in utero* around embryonic day E12.5 due to heart abnormalities and embryos exhibit mammary gland aplasia and posterior limb abnormalities (25). Heterozygous mice exhibit minor aberrations of the external genitalia and have a significantly higher incidence of failed nipple and ductal tree development at E18.5 and adult virgins have aplasia of the first three pairs of mammary glands (25,26). It is important to note that there is a large number of tissues and organs where TBX3 is expressed but which are unaffected by UMS, suggesting that specific doses of TBX3 may be required for its functions in different tissues. This is in line with observations that the severity of the UMS phenotype correlates with the level of *TBX3* deficiency (24). It is also possible that other T-box factors, such as TBX2, could compensate for TBX3 in tissues and organs unaffected by UMS.

Consistent with the very early expression of *Tbx3* in the inner cell mass of the blastocyst are numerous studies showing that TBX3/*Tbx3* can promote both self-renewal and differentiation of embryonic stem cells (ESCs) which play important roles in maintaining homeostasis during embryonic development (27). The maintenance of ESC pluripotency involves orchestrated signalling pathways and transcriptional networks including the leukaemia inhibitory factor/signal transducer and activator of transcription (LIF/STAT) pathway, as well as the pluripotency and self-renewal transcription factors, octamer-binding transcription factor 4 (Oct4), Nanog and Sox2. Ivanova *et al.* showed that while *Tbx3* levels were high in undifferentiated mouse ESC (mESC), they were significantly down-regulated in mESCs undergoing retinoic acid (RA) induced differentiation (28). They also demonstrated that high levels of *Tbx3* could block differentiation into mesoderm, ectoderm, trophoblast and neural crest cells. In support of these findings, *Tbx3* was shown to be sufficient to maintain self-renewal of mESCs downstream of LIF/STAT signalling (29). Interestingly, microRNA (miRNA)-137, which plays important roles in neural stem cell differentiation, was recently shown to directly repress *Tbx3* levels by binding its 3' UTR in mESC (30). This repression was also shown to result in disruption of mESC self-renewal and accelerated differentiation *in vitro*. More recently, Cioffi *et al.* also showed that miR-93 represses *Tbx3* and thereby counteracts self-renewal in early adipocyte precursors (31).

Lu *et al.* also showed that Tbx3 overexpression in mESCs promotes differentiation into the extra-embryonic endoderm (ExEn) lineage through direct regulation of the ExEn regulator, *Gata6* (19). Furthermore, they showed that Tbx3 knockdown during embryoid body formation prevented extra-embryonic endoderm differentiation but enhanced ectoderm and trophoderm differentiation. In addition, Zhao *et al.* showed that the overexpression of either Tbx3 or Tbx3+2a in ESCs or induced pluripotent stem cells (iPSCs) could induce differentiation by inhibiting the transcriptional activity of Nanog (15). This was further demonstrated by studies showing that Tbx3 is highly expressed in definitive endoderm progenitor cells and as mentioned earlier, complexes with the histone demethylase, Jmjd3 domain-containing protein 3 (Jmjd3), to transcriptionally activate *Eomes* and promote endoderm differentiation (32,33). Another mechanism by which Tbx3 promotes endoderm differentiation is through the canonical Wntless (Wnt) signalling pathway, where Tbx3 is a downstream effector of Wnt3a and promotes the induction of a primitive endoderm state, giving rise to visceral endoderm (34). Interestingly, Waghray *et al.* recently showed using expression studies and chromatin immunoprecipitation (ChIP) sequencing that Tbx3 directly represses *Developmental pluripotency-associated protein 3* (*Dppa3*) at a region 1.7 kb upstream of its transcriptional start site and consequently induces differentiation of ESCs towards the mesoderm (35). In addition to this, they identified a Wnt/Tbx3/Dppa3 signalling axis that regulates the balance between mESC self-renewal and differentiation, which may provide one possible explanation for how Tbx3 may either promote or inhibit differentiation.

Tbx3 has also been implicated in the generation of mouse iPSCs by, in part, directly activating the *Oct4* promoter (36). In addition, Tbx3 was shown to improve the generation of porcine iPSCs when co-expressed with Oct4, Sox2, Kruppel-like factor 4 (Klf4) and c-Myc (36). Furthermore, iPSC formation increased when *Tbx3* expression was enhanced by Zinc finger protein of the cerebellum 3 (*Zic3*) (37). Ectopic overexpression of Tbx3 in the atria of the adult mouse heart was also shown to reprogramme mature differentiated atrial myocytes into a more naïve pacemaker phenotype by repressing genes required for the working myocardial function and stimulating genes required for pacemaker functions (38). ESCs and iPSC cells can sporadically enter a "two-cell-like embryonic state" (2C-state) which is important for ESC potency (39). Dan *et al.* showed that in 2C mESCs, Tbx3 could activate the promoter activity of a 2-cell gene, *zinc finger and SCAN domain-containing protein 4* (*Zscan4*) and that ectopic overexpression of Tbx3 in these cells resulted in telomere lengthening and genomic stability (40).

The role of TBX3 in promoting differentiation of human ESC (hESC) is somewhat different to that of mESCs, as it promotes neuroepithelial differentiation but

not endoderm differentiation (41). This is possibly due to the different pluripotent states of hESC and mESCs, with mESCs being in a more naïve state (42). TBX3 overexpression cell culture models showed that it could promote hESC proliferation by repressing *p14ARF* and *NFκBIB*, an inhibitor of the NF-kappaB (NF-κB) pathway (41). The knockdown of TBX3 on the other hand resulted in decreased expression of neuroepithelial and neuroectoderm markers paired box 6 (PAX6), LIM homeobox 2 (LHX2), forkhead box G1 (FOXG1), and retina and anterior neural fold homeobox (RAX). Taken together, these studies reveal important, context-dependent roles for TBX3 in the maintenance, self-renewal and differentiation of ESC populations.

### 2.3. TBX3 and cancer

TBX3 is overexpressed in a range of carcinomas (breast, pancreatic, melanoma, liver, gastric, lung, head and neck, ovarian and bladder) and sarcomas (chondrosarcoma, fibrosarcoma, liposarcoma, rhabdomyosarcoma and synovial sarcoma) (7,43,44). Importantly, there is substantial evidence that this overexpression contributes to the oncogenic process at multiple levels including the bypass of senescence and apoptosis as well as the promotion of proliferation, tumour formation and invasion (Figure 2). In addition, recent studies suggest that there are cancer contexts where TBX3 may also function as a tumour suppressor (Figure 2). Given the myriad of cancer processes that TBX3 impacts it is expected to co-operate with other oncogenic factors and to regulate several target genes. There is, however, limited information regarding these areas and nothing is known about what enables TBX3 to switch between tumour promoter and tumour suppressor.

#### 2.3.1. TBX3 in senescence, apoptosis and proliferation

In response to endogenous or exogenous stress signals such as oncogenic stimuli, cells can undergo cell cycle arrests, senescence or apoptosis which protect against inappropriate cell division and/or survival. These processes serve as important barriers to cancer and are regulated at a molecular level by the p14ARF/p53/p21 and p16INK4a/retinoblastoma protein (pRB) tumour suppressor pathways. The inhibition or bypass of these pathways are required for cancer initiation and progression as well as the development of anti-cancer drug resistance.

Senescence is an irreversible/permanent exit from the cell cycle and Tbx3 can bypass this process and consequently immortalise mouse embryonic fibroblasts (MEFs) and ST.HdhQ111 striatal cells through either directly binding or repressing a T- element in the initiator of *p19ARF/p14ARF* or by recruiting HDAC 1, 2, 3 and 5 to epigenetically silence its promoter (7,45). A recent study by Kumar *et al.* demonstrated that TBX3 can also bypass senescence by indirectly repressing

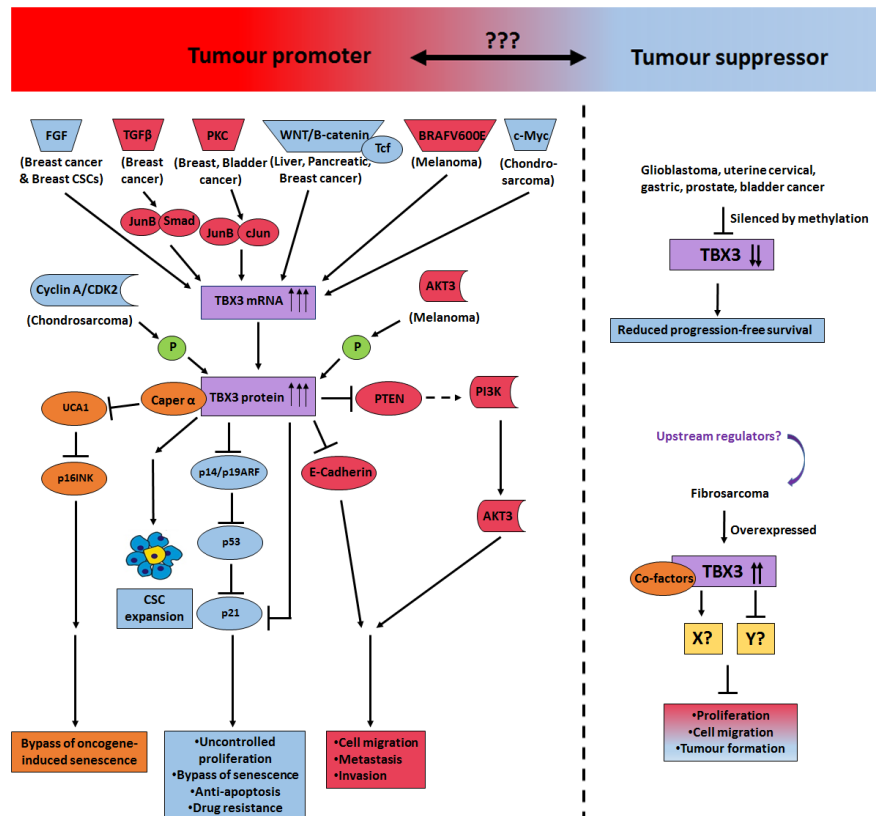


**Figure 2: Mechanisms by which TBX3 contributes to cancer.** Left panel: TBX3 is overexpressed in numerous cancers where it promotes several aspects of the oncogenic process including the bypass of senescence, uncontrolled proliferation, migration, metastasis and drug resistance. In some cancers, the key oncogenic signalling pathways responsible for this overexpression have been identified (see cancer types in brackets and colour coding which match the appropriate oncogenic processes). Right panel: TBX3 also exhibits tumour suppressor activity. It is silenced by methylation in certain cancers and it retards proliferation, cell migration and tumour formation of fibrosarcomas. The factors upstream of TBX3 as well as the co-factors and target genes that mediate the tumour suppressor functions of TBX3 are yet to be elucidated.

*p16INK4a* (22). Indeed, the authors show that Tbx3 in complex with Coactivator of AP1 and Estrogen Receptor (CAPER $\alpha$ ) represses the long non-coding RNA, *Urothelial Cancer Associated 1* (*UCA1*) and this prevents the stabilization of *p16INK4a* mRNA (22). Furthermore, they showed that RAS-induced senescence of human foreskin fibroblasts resulted in dissociation of the CAPER $\alpha$ /TBX3 complex and a concomitant increase in *UCA1* and *p16INK4a* expression. It would be worth investigating whether the CAPER $\alpha$ :TBX3 interaction and *UCA1* repression is required for senescence bypass in TBX3 driven cancers.

Apoptosis, a form of programmed cell death, plays an essential role in the maintenance of tissue homeostasis and negative regulation of this cellular process promotes malignant transformation and chemoresistance (46). There is evidence that TBX3 may contribute to oncogenesis and confer anti-cancer drug resistance by compromising the apoptotic pathway. Indeed, TBX3 co-operated with the Myc oncogene to transform MEFs, where it promoted the bypass of Myc induced apoptosis through the downregulation of p19ARF and p53 levels (47). In addition, TBX3 has been shown to inhibit apoptosis in rat bladder hyperplastic epithelial cells and TBX3 knockdown increased apoptosis in rat

bladder carcinoma cells (7). TBX3 was also linked to protecting cells against anoikis which is a form of apoptosis that occurs when anchorage dependent cells become detached from the surrounding extracellular matrix and its bypass is associated with epithelial mesenchymal transition (EMT). Indeed, head and neck squamous cell carcinoma (HNSCC) cells depleted of TBX3 underwent anoikis (7). The overexpression of TBX3 or TBX3+2a in kidney mesangial cells was also reported to result in the evasion of serum starvation-triggered apoptosis (48). Furthermore, silencing Tbx3 in rat bladder carcinoma cells rendered the cells sensitive to doxorubicin-induced apoptosis and the overexpression of TBX3 was associated with a chemotherapy-resistant phenotype (49). Similar findings showed that knocking down TBX3 sensitized human colorectal carcinoma cells to doxorubicin *via* activating the p14ARF- p53 pathway (50).

A number of studies also support a role for TBX3 in promoting cell cycle progression and proliferation through its ability to disrupt the p19ARF-p53-p21 pathway. Indeed, TBX3 protein and mRNA levels peak in S-phase and chondrosarcoma cells in which TBX3 is depleted accumulate in S-phase with a corresponding increase in p19ARF, p53 and p21 levels (51). The

increased levels of TBX3 in S-phase were shown to occur transcriptionally through activation by c-Myc at E-box motifs located at -1210 and -701 bps and post-translationally by cyclin A-CDK2 phosphorylation (51). Together these results suggest that TBX3 functions as a pro-proliferative factor, in part, by promoting transition into G2/M. TBX3 can also promote cell proliferation of mammary epithelial cells (MECs) by repressing *19ARF*, which was accompanied by the down-regulation of p21 (52). Interestingly, in the same study similar responses were noted in *p53*-null MECs, indicating that the repressive effect of TBX3 on p21 occurred independently of p53. In line with this, depletion of Tbx3 inhibits proliferation of hepatic progenitor cells with a corresponding increase in *p19ARF* mRNA levels and *Tbx3*<sup>-/-</sup> mouse livers exhibit increased p19ARF and p21 levels although p53 levels remained unaffected (53). Importantly, TBX3 can promote cell proliferation by directly binding and repressing the *p21* promoter via a consensus T-element which requires the T-box and R2 repression domains (14,54). It is interesting to note that TBX2 directly represses the *p21* promoter through the same T-element (7). It would therefore be interesting to determine whether TBX2 and TBX3 have redundant pro-proliferative roles in repressing the *p21* promoter in cancers where they are both expressed or whether additional factors, such as post-translational modifications and/or the availability of co-factors, will determine which of the two T-box factors regulates *p21*.

TBX3 may also impinge on other cellular pathways to promote cell cycle progression and proliferation. For example, an inverse correlation between the mRNA and protein levels of TBX3 and the tumour suppressor PTEN was identified in HNSCC cells (55). PTEN is a negative regulator of the phosphoinositide 3-kinase/Protein kinase B (PI3K/AKT) pathway and suppresses oncogenic processes such as proliferation, cell survival and migration (56). Importantly, TBX3 can directly repress *PTEN* by binding a 132 bp DNA region within its promoter (55). Interestingly, the authors found that this region of the *PTEN* promoter does not contain a T-element and thus speculated that TBX3 may repress *PTEN* by either interacting with transcriptional co-repressors or by interfering with positive activators of *PTEN*. It would be interesting to determine the functional significance of *PTEN* repression by TBX3 especially on cell proliferation, survival and migration.

TBX3 has also been shown to negatively regulate proliferation in support of cell migration, a phenomenon known as the proliferation/migration dichotomy (57,58). Knocking down TBX3 by shRNA inhibited migration and enhanced proliferation of breast cancer and melanoma cells which was accompanied by a decrease in the expression of p14ARF, p53 and p21 (57). Furthermore, ectopic overexpression of TBX3 in non-invasive WM1650 radial growth phase (RGP) melanoma cells and the upregulation of TBX3 by RA in

vertical growth phase (VGP) melanoma cells reduced the proliferative capacity of the cells with the former being associated with an increase in migratory ability (58,59). It is important to note that Transforming growth factor-beta (TGF- $\beta$ ) contributes to breast cancer progression by inhibiting cell proliferation and promoting migration and recent studies have shown that TBX3 is required for the anti-proliferative and pro-migratory effects of TGF- $\beta$  in breast epithelial cells (60,61). The mechanism(s) that determines whether TBX3 functions as a pro-proliferative or anti-proliferative factor is not known.

### 2.3.2. TBX3 in tumour formation, invasion and metastasis

TBX3 has also been shown to contribute to tumour formation, migration and invasion (Figure 2, left panel). Indeed, knockdown of TBX3 reduced anchorage-independence of colon and hepatoma carcinoma cell lines and when these cells were engineered to express a Tbx3 mutant, they had significantly reduced ability to form tumours in nude mice (49). A study by Chen *et al.* showed that elevated *TBX3* mRNA levels strongly correlated with metastasis in breast cancer and this was similarly observed by Fillmore *et al.* in (ER)-positive breast cancer tumours (62,63). Importantly, silencing TBX3 by shRNA inhibited *in vitro* tumour forming ability as well as migration of MCF7 breast cancer cells (57). Furthermore, Mowla *et al.* demonstrated that treatment of MCF7 cells with phorbol 12-myristate 13-acetate (PMA) induced TBX3 expression which resulted in increased cell migration (64). Several lines of evidence suggest that TBX3 also plays an important role in the transition of non-malignant RGP melanoma to a malignant VGP melanoma. TBX3 levels increase specifically in VGP and metastatic melanoma cells and whereas ectopic overexpression of TBX3 in RGP melanoma cells was sufficient to promote tumour forming ability and invasion, knockdown of TBX3 in VGP cells inhibited migration and tumour formation (57,58). The overexpression of TBX3 has also been positively linked to migration and invasion of pancreatic ductal adenocarcinoma (PDAC). Compared to normal adjacent and healthy donors, PDAC tissue samples had increased levels of *TBX3* mRNA and stained positive for TBX3 protein (65). Furthermore, *in vitro* assays show that overexpression of TBX3 in Pan1 and BxPC3 pancreatic cell lines significantly enhanced their migratory ability and invasion potential and xenotransplantation experiments revealed that TBX3 overexpressing Pan1 and BxPC3 cells induced significantly larger tumours than their controls. It is interesting to note that the TBX3 overexpressing tumours expressed the angiogenesis associated markers FGF2 and VEGFA which suggests that TBX3 may also be involved in angiogenesis in PDAC. More recently, TBX3 was also linked to tumour formation and migration in several sarcoma subtypes. Ectopic overexpression of

TBX3 in chondrosarcoma cells enhanced their ability to form tumours in mice and knockdown of TBX3 inhibited migration of chondrosarcoma, liposarcoma and rhabdomyosarcoma cells (44).

Decreased expression of E-cadherin in several cancers including melanoma, breast, ovarian and non-small cell lung carcinoma have been shown to be associated with tumour invasiveness, metastasis and poor patient prognosis (66). There is good evidence to suggest that a key mechanism by which TBX3 promotes these oncogenic processes is through its ability to repress *E-cadherin*. A study by Rodriguez *et al.* showed that increased expression of TBX3 correlated with low levels of E-cadherin in metastatic melanoma tissue samples (67). The authors further established using melanoma cells that TBX3 directly binds and represses the *E-cadherin* promoter *in vitro* and *in vivo* through a half consensus T-element close to the transcription initiation site. This repression was shown to be physiologically relevant because when TBX3 was silenced in metastatic melanoma cells, E-cadherin levels increased. Furthermore, TBX3 is transcriptionally indirectly upregulated by the oncoprotein BRAF V600E, which is constitutively activated in 50% of melanomas, and is a substrate and effector of AKT3, which is activated in ~70% of advanced stage melanomas where it plays a critical pro-invasive role (68,69). Importantly, TBX3 was shown to repress *E-cadherin* downstream of both these pathways to promote migration and invasion of melanoma cells. Interestingly, phosphorylation of TBX3 by AKT3 in melanoma enhanced its ability to repress *E-cadherin* and phosphorylation of TBX3 by p38 in normal kidney cells decreased E-cadherin protein levels (70). This suggests that phosphorylation may play an important role in modulating TBX3 target gene regulation. Elevated levels of TBX3 were also shown to correlate with decreased E-cadherin levels in squamous carcinoma cells (71). In addition, work by Du *et al.* revealed that a PKC/TBX3/E-cadherin signalling cascade exists in human bladder cancer cells and that the regulation of *E-cadherin* by TBX3 occurs in a PKC-dependent manner (72). It is noteworthy that in sarcomas, the ability of TBX3 to promote migration was not due to *E-cadherin* repression. This suggests that the molecular mechanism(s) underlying the pro-migratory role of TBX3 in different cancers may be different and future studies identifying TBX3 target genes as well as signalling pathways that upregulate TBX3 would likely shed light on this.

### 2.3.3. *TBX3* and cancer stem cells

Cancer stem cells (CSCs) are a biologically distinct subpopulation of tumour cells which have indefinite potential for self-renewal and they are thought to ultimately drive tumorigenesis. In addition, CSCs are often not targeted by traditional chemotherapeutic agents

and are associated with drug-resistance and clinical relapse after remission (73). A study by Fillmore *et al.* revealed that the addition of oestrogen to a number of ER $\alpha$ -positive breast cancer cell lines resulted in a dramatic increase in the number of CSCs which required TBX3 (63). Importantly, the knockdown of TBX3 significantly reduced CSC numbers in a variety of breast cancer cell lines and abrogated their ability to form tumourspheres, a spherical formation reported to be generated by the proliferation of a single CSC. On the other hand, TBX3 overexpression resulted in a significant increase in CSC numbers, tumoursphere-forming ability and a more than 100-fold increase in tumour-seeding potential *in vivo*. A recent study by Perkhofer *et al.* also demonstrated that TBX3 overexpressing pancreatic cancer cells had increased sphere-forming ability and that TBX3 induced the CSC phenotype of primary pancreatic cancer cells by regulating NODAL/ACTIVIN signalling through an autocrine positive feedback loop (65). In light of this, it would be interesting to determine whether TBX3 impacts similarly on CSCs in other cancers and if this is an additional mechanism through which it contributes to cancer development and anti-cancer drug resistance.

### 2.3.4. *The tumour suppressor role of TBX3*

In contrast to the large body of work implicating TBX3 as an oncoprotein, there are also studies that have implicated it as a tumour suppressor (Figure 2, right panel). Using microarray analyses, Lyng *et al.* demonstrated that *TBX3* gene expression is downregulated in uterine cervical cancer samples, which strongly correlated with lymph node metastasis and reduced progression-free patient survival (74). Subsequent studies have also shown that *TBX3* levels are epigenetically silenced by methylation in glioblastoma, gastric, bladder and prostate cancer (7). Yamashita *et al.* examined methylation-silenced genes in gastric cancer and revealed that the *TBX3* promoter is methylated in at least one primary gastric cancer, but not normal gastric mucosa (75). *TBX3* methylation was subsequently revealed to be associated with a significantly lowered survival rate in a cohort of glioblastoma patients (76). Following this, White-al Habeeb *et al.* demonstrated that *TBX3* is differentially methylated in Gleason score (GS) 8 vs GS6 prostate cancer tumour samples, with increased methylation occurring in the more aggressive GS8 samples (77). Collectively these studies suggest that under certain circumstances TBX3 suppression may promote cancer progression. Furthermore, a study investigating the genome-wide methylation pattern of fresh-frozen bladder cancer tumour tissue revealed that *TBX3* methylation is associated with the progression of non-muscle invasive human bladder tumours (Pta) to muscle-invasive tumours (MI) (78). The authors of this study also showed that *TBX3* methylation was an

independent predictor of bladder cancer progression and that it correlated with reduced progression-free survival. In a follow-up study, the same group performed methylation analyses on formalin-fixed paraffin-embedded tumour tissue from 192 patients with Pta, 40% of whom experienced progression to MI (79). They demonstrated that patients with low *TBX3* methylation experienced significantly increased progression-free survival and that, within 10 years of follow-up time, *TBX3* was an independent prognostic marker of progression risk. Interestingly, both studies revealed that methylation of the *TBX3* homologue, *TBX2*, was also linked to tumour progression of bladder cancer (78,79).

The above studies together suggested that *TBX3* may function as a tumour suppressor and a comprehensive characterisation of the tumour suppressor role of *TBX3* was recently provided by Willmer *et al.* (44). The authors showed that the *TBX3* protein is upregulated in a number of transformed fibroblast and fibrosarcoma cell lines and tissues. Using *TBX3* overexpressing and knock down fibrosarcoma cell culture models they demonstrated that *TBX3* discourages substrate-dependent and -independent cell proliferation, migration and tumour formation. Importantly, whereas the knockdown of *TBX3* was able to significantly increase the *in vivo* tumour forming ability of fibrosarcoma cells in a mouse model, *TBX3* overexpressing cells formed smaller tumours in the same model. These results demonstrate that *TBX3* behaves as a tumour suppressor in transformed fibroblast and fibrosarcoma cells, suggesting it may function as either oncoprotein or tumour suppressor depending on cellular context. It will be important to elucidate the molecular mechanism(s) that enables it to switch between these functions.

#### 2.4. Signalling pathways that regulate *TBX3* expression in cancer

Despite the catastrophic effects observed when *TBX3* expression is deregulated very little is still known about the signalling pathways that regulate *TBX3* levels. In the last few years some developmental pathways, that are important in cancer, have been implicated and these will be discussed below and are indicated in Figure 2.

##### 2.4.1. Wnt/ $\beta$ -catenin signalling pathway

The canonical Wnt/ $\beta$ -catenin pathway plays critical roles during embryogenesis and adult tissue homeostasis, where it regulates a number of key processes including proliferation, differentiation and cell fate determination (80). Aberrant activation of the Wnt/ $\beta$ -catenin pathway, often caused by constitutive activation of  $\beta$ -catenin, has been implicated in a number of cancers and Renard *et al.* have suggested that *TBX3* is a direct target of this pathway in liver tumorigenesis (49). Using microarray analyses, they demonstrated that *TBX3* is upregulated in

mouse hepatocellular carcinoma (HCC) tumour samples carrying an active mutant form of  $\beta$ -catenin. In addition, the authors revealed a correlation of increased *TBX3* expression with a mutant active form of  $\beta$ -catenin in human and mouse HCC and human hepatoblastoma. Furthermore, they demonstrated that  $\beta$ -catenin, in complex with its co-activator Tcf, directly activated the *TBX3* promoter through a Tcf-binding element, resulting in enhanced proliferation, tumour formation, as well as protection from doxorubicin-induced apoptosis. The authors concluded that *TBX3* is a key mediator of the proliferation and survival activities of  $\beta$ -catenin in liver tumorigenesis.

Following this, Lachenmayer *et al.* investigated the effect of the multi-kinase inhibitor Sorafenib, the only Food and Drug Administration (FDA) approved drug for HCC treatment, on the human HepG2 HCC cell line (81). They showed that Sorafenib inhibits  $\beta$ -catenin levels with a corresponding reduction in *TBX3* mRNA levels. In addition, one of the oldest and best known Chinese herbal medicines, rhubarb root, is used to treat liver disease and exhibits anti-cancer properties through the induction of apoptosis in a number of cancers (82). Tsai *et al.* found that it also attenuates Wnt/ $\beta$ -catenin signalling in human HCC cells which was accompanied by decreased *TBX3* protein levels (82).

Interestingly, a study by Cavard *et al.* suggests that the regulation of *TBX3* by the Wnt/ $\beta$ -catenin pathway may not be limited to liver cancer (83). They examined gene expression profiles in solid pseudopapillary pancreatic neoplasms where the Wnt/ $\beta$ -catenin pathway is aberrantly activated and demonstrated that *TBX3* mRNA is overexpressed. The interplay between Wnt signalling and *TBX3* was also reported by Arendt *et al.*, who showed that both Wnt and *TBX3* could regulate proliferation of human breast progenitor cells and that *TBX3* induced autocrine Wnt signalling in these cells, possibly *via* a feedback loop (84).

##### 2.4.2. Fibroblast growth factor (FGF) signalling pathway

FGF signalling has been shown to be important for the regulation of cell proliferation, survival, migration as well as differentiation, and deregulated FGF signalling is important for the pathogenesis of a number of cancers (85). It is well established that *TBX3* regulates this signalling pathway during mammary gland development and it has also been suggested that *TBX3* lies downstream of FGF (86). Fillmore *et al.* demonstrated that oestrogen and FGF signalling upregulated the expression of *TBX3* in breast cancer (63). Treatment of ER $\alpha$ -positive breast cancer cell lines with oestrogen resulted in a substantial increase in secreted FGF9, which in turn resulted in significantly increased *TBX3* mRNA and protein levels. Importantly, when cells were treated with oestrogen and an FGF9 inhibitor this was decreased, while treatment with both oestrogen and FGF9 resulted

in an even greater increase in TBX3 mRNA and protein expression. Similarly, when ER $\alpha$ -negative breast cancer cell lines were treated with FGF9, there was a marked increase in TBX3 protein, suggesting that this regulation is not specific to ER $\alpha$ -positive breast cancer. Taken together, these findings suggest that FGF signalling mediates the upregulation of TBX3 by oestrogen in breast cancer and, as mentioned previously, promotes the expansion of breast CSCs.

#### 2.4.3. Protein kinase C (PKC) signalling pathway

The PKC family consists of phospholipid-dependent serine/threonine-specific protein kinases which mediate various cellular functions including proliferation, apoptosis and differentiation (87). The deregulation of PKC signalling has been implicated in cancer, including breast cancer where it promotes tumourigenesis by modulating cell proliferation, migration, apoptosis and survival (87). Many studies which have investigated the role of the PKC pathway have employed the phorbol ester 12-O-tetradecanoylphorbol-13-acetate (TPA, also called PMA) which activates PKC isoforms by translocating them to specific cellular compartments (87). Mowla *et al.* showed that in prostate epithelial and lung fibroblast cells, PMA, increased TBX3 mRNA and protein in a PKC-dependent manner (64). Furthermore, they demonstrated that the activator protein-1 (AP-1) transcription factors, c-Jun and JunB, bound a degenerate PMA response element in the *TBX3* promoter, mediating its upregulation. Finally, as mentioned previously, they showed that TBX3 mediated the pro-migratory effect of PMA in MCF7 breast cancer cells. The regulation of TBX3 by the PKC pathway has been further supported by Du *et al.* who showed that knocking down Phospholipase C epsilon (PLC $\epsilon$ ) in bladder cancer cell lines resulted in a corresponding inhibition of PKC $\alpha/\beta$ , which in turn reduced TBX3 mRNA and protein levels (72). Importantly, they also demonstrated that in bladder cancer the repression of *E-cadherin* by PKC $\alpha/\beta$  signalling is mediated by TBX3.

#### 2.4.4. Retinoic acid (RA) signalling pathway

All-trans RA, a metabolite of vitamin A (all-trans-retinol), plays an important role in embryo development, where it regulates gene transcription to modulate a number of biological processes, including cell proliferation, differentiation and apoptosis (88). Compromised RA signalling often occurs early in tumourigenesis, including in breast cancer (89). Initial studies provided a preliminary indication that *TBX3* may be regulated by the RA pathway in the development of chick and mouse limbs (90,91). Ballim *et al.* confirmed this regulation during mouse limb development and expanded these findings to show that RA treatment of the ME1402 VGP melanoma cell line resulted in a substantial increase in

TBX3 mRNA and protein, and a correlative decrease in proliferation (59). Furthermore, knockdown of TBX3 expression by a shRNA approach significantly reduced the growth-inhibitory effect of RA. Finally, the authors demonstrated that RA transcriptionally activates *TBX3* through directly binding a degenerate RA response element half site at -87 bp. Together these results suggest that TBX3 partly mediates the RA-regulated inhibition of cell proliferation in the human melanoma cell line tested.

#### 2.4.5. Transforming growth factor-beta 1 (TGF- $\beta$ 1) signalling pathway

The TGF- $\beta$  growth factor cytokine family is composed of a large number of secreted polypeptides that activate cellular responses involved in development, homeostasis and the immune system (92). In addition, TGF- $\beta$ 1 signalling has been widely reported to have a dual role in the progression of cancer. While it acts as a tumour suppressor and inhibits cell proliferation during the early stages of carcinogenesis, it promotes migration and metastasis in the late stages of the disease (92). Similar to TBX3, TGF- $\beta$ 1 signalling is critical for the development of the mammary glands but also contributes to breast cancer progression through the inhibition of cell proliferation and promotion of migration (93). Importantly, Li *et al.* demonstrated that TGF- $\beta$ 1 treatment transcriptionally upregulated *TBX3* in breast epithelial and keratinocyte cells (61). They showed that JunB and Smad4 mediate this effect and directly bind to the *TBX3* promoter at a degenerate Smad Binding Element (SBE). The authors also revealed that TBX3 mediated the anti-proliferative and pro-migratory effects of TGF- $\beta$ 1 in these cells. In a follow-up paper they demonstrated that this anti-proliferative function involves the ability of TBX3 to directly bind and repress the pro-proliferative factor *TBX2* (60). Finally, they showed that the TGF- $\beta$ 1/TBX3/TBX2 axis resulted in the upregulation of *p21WAF1*, leading to cell cycle inhibition. Recent work by Wensing & Campos also showed that TGF- $\beta$ 1 treatment of immortalised human mesangial cells resulted in a substantial increase in *TBX3* and *TBX3+2a* mRNA which resulted in the evasion of serum starvation- triggered apoptosis (48). These findings suggest that TGF- $\beta$ 1 may upregulate TBX3 to simultaneously inhibit proliferation but bypass apoptosis. However, more work is needed to explore this further.

#### 2.4.6. Phosphatidylinositol 3-kinase/Protein kinase B (PI3K/Akt) signalling pathway

PI3Ks constitute a lipid kinase family that activate the serine/threonine kinases, Akt1, Akt2 and Akt3. These highly homologous isoforms phosphorylate a plethora of substrates that are involved in the regulation of key cellular processes including cell proliferation, apoptosis, and migration (94). It is well established that constitutive

activation of Akt, through *PI3K* amplification or *PTEN* mutation, contributes to the oncogenic process and is associated with a poor prognosis and resistance to chemo- and radio-therapy (94). Indeed, Akt activation is one of the most frequent molecular alterations in cancers, including melanoma, gastric, pancreatic, breast, sarcoma and prostate cancer (95-98). While there are instances where the three Akt isoforms are able to compensate for each other, recent research show that their tissue expression patterns and functions are different (99,100). The PI3K/Akt pathway is activated in 70% of all melanoma cases and Peres *et al.* reported that TBX3 is a substrate and effector of this pathway in melanoma (69). Consistent with other reports, the authors demonstrated that Akt3 is the predominant isoform activated in a panel of human melanoma cell lines. Furthermore, Akt3 post-translationally upregulated TBX3 expression through phosphorylation at S720 in ME1402 and MM200 VGP melanoma cells, which promoted protein stabilisation. Lastly, they demonstrated that TBX3 mediated the oncogenic activity of the PI3K/Akt pathway in these cells, as phosphorylation of TBX3 at this site resulted in increased nuclear localisation of TBX3 protein, repression of E-cadherin and promotion of migration and invasion.

### 3. Conclusion

The transcription factor TBX3 provides an important link between embryonic development and cancer. While mutations resulting in decreased levels of TBX3 lead to ulnar-mammary syndrome, increased levels of TBX3 are linked to several epithelial derived cancers and a diverse subset of soft tissue and bone sarcomas. Indeed, TBX3 is a key driver of a number of cancer processes including proliferation, tumour formation, invasion and metastasis and it has therefore been proposed as an important novel molecular target for anti-cancer treatments. There is also evidence that in certain cellular contexts TBX3 may function as a brake to prevent tumour progression. However, there is still very little known about the molecular mechanisms regulating the tumour promoting and tumour suppressor functions of TBX3 and what enables it to switch between these two roles. This information has important implications for targeting TBX3 in anti-cancer drugs especially since directly targeting TBX3 is unlikely to be a viable option. This could involve the following three approaches either alone or in combination: targeting signalling pathways required for TBX3 overexpression; targeting the enzymatic activities of TBX3 co-factors; and targeting the enzymatic activity of genes that encode enzymes that are activated by TBX3.

### Acknowledgements

This project was supported by grants from the SA

Medical Research Council, National Research Foundation (NRF), Cancer Association of South Africa (CANSA), the University of Cape Town and the Harry Crossley foundation.

### References

1. Papaioannou VE. The *T-box* gene family: Emerging roles in development, stem cells and cancer. *Development*. 2014; 141:3819-3833.
2. Wilson V, Conlon FL. The T-box family. *Genome Biol*. 2002; 3:3008.1-3008.7
3. Lingbeek ME, Jacobs JJ, van Lohuizen M. The T-box repressors TBX2 and TBX3 specifically regulate the tumor suppressor gene *p14ARF* via a variant T-site in the initiator. *J Biol Chem*. 2002; 277:26120-26127.
4. van den Boogaard M, Wong LY, Tessadori F, Bakker ML, Dreizehnter LK, Wakker V, Bezzina CR, t Hoen PA, Bakkens J, Barnett P, Christoffels VM. Genetic variation in T-box binding element functionally affects SCN5A/SCN10A enhancer. *J Clin Invest*. 2012; 122:2519-2530.
5. Papaioannou VE. *T-box* genes in development: From hydra to humans. *Int Rev Cytol*. 2001; 207:1-70.
6. Packham EA, Brook JD. *T-box* genes in human disorders. *Hum Mol Genet*. 2003; 12:R37-R44.
7. Wansleben S, Peres J, Hare S, Goding CR, Prince S. T-box transcription factors in cancer biology. *Biochim Biophys Acta*. 2014; 1846:380-391.
8. Agulnik SI, Garvey N, Hancock S, Ruvinsky I, Chapman DL, Agulnik I, Bollag R, Papaioannou V, Silver LM. Evolution of mouse *T-box* genes by tandem duplication and cluster dispersion. *Genetics*. 1996; 144:249-254.
9. Bamshad M, Lin RC, Law DJ, Watkins WC, Krakowiak PA, Moore ME, Franceschini P, Lala R, Holmes LB, Gebuhr TC, Bruneau BG, Schinzel A, Seidman JG, Seidman CE, Jorde LB. Mutations in human TBX3 alter limb, apocrine and genital development in ulnar-mammary syndrome. *Nat Gen*. 1997; 16:311-315.
10. Campbell C, Goodrich K, Casey G, Beatty B. Cloning and Mapping of a Human Gene (*TBX2*) Sharing a Highly Conserved Protein Motif with the *Drosophila omb* Gene. *Genomics*. 1995; 28:255-260.
11. Law DJ, Gebuhr T, Garvey N, Agulnik SI, Silver LM. Identification, characterization and localization to chromosome 17q21-22 of the human TBX2 homolog, member of a conserved developmental gene family. *Mamm Genome*. 1995; 6:793-797.
12. Fan W, Huang X, Chen C, Gray J, Huang T. TBX3 and its isoform TBX3+2a are functionally distinctive in inhibition of senescence and are overexpressed in a subset of breast cancer cell lines. *Cancer Res*. 2004; 64:5132-5139.
13. Bamshad M, Le T, Watkins WS, et al. The spectrum of mutations in TBX3: Genotype/Phenotype relationship in ulnar-mammary syndrome. *Am J Hum Genet*. 1999; 64:1550-1562.
14. Hoogaars WM, Barnett P, Rodriguez M, Clout DE, Moorman AF, Goding CR, Christoffels VM. TBX3 and its splice variant TBX3 + exon 2a are functionally similar. *Pigment Cell Melanoma Res*. 2008; 21:379-387.
15. Zhao D, Wu Y, Chen K. Tbx3 isoforms are involved in pluripotency maintaining through distinct regulation of Nanog transcriptional activity. *Biochem Biophys Res Commun*. 2014; 444:411-414.
16. Kumar PP, Franklin S, Emechebe U, Hu H, Moore B,

- Lehman C, Yandell M, Moon AM. TBX3 regulates splicing *in vivo*: A novel molecular mechanism for Ulnar-mammary syndrome. *PLoS Genet.* 2014; 10:e1004247.
17. Carlson H, Ota S, Campbell CE, Hurlin PJ. A dominant repression domain in Tbx3 mediates transcriptional repression and cell immortalization: Relevance to mutations in Tbx3 that cause ulnar-mammary syndrome. *Hum Mol Genet.* 2001; 10:2403-2413.
  18. Boogerd CJJ, Wong LYE, van den Boogaard M, Bakker ML, Tessadori F, Bakkens J, 't Hoen PAC, Moorman AF, Christoffels VM, Barnett P. Sox4 mediates Tbx3 transcriptional regulation of the gap junction protein Cx43. *Cell Mol Life Sci.* 2011; 68:3949-3961.
  19. Lu R, Yang A, Jin Y. Dual Functions of T-Box 3 (Tbx3) in the Control of Self-renewal and Extraembryonic Endoderm Differentiation in Mouse Embryonic Stem Cells. *J Biol Chem.* 2011; 286:8425-8436.
  20. Coll M, Seidman JG, Muller CW. Structure of the DNA-bound T-box domain of human TBX3, a transcription factor responsible for ulnar-mammary syndrome. *Structure.* 2002; 10:343-356.
  21. Lu J, Li X-P, Dong Q, Kung H-f, He M-L. TBX2 and TBX3: The special value for anticancer drug targets. *Biochim Biophys Acta.* 2010; 1806:268-274.
  22. Kumar PP, Emechebe U, Smith R, Franklin S, Moore B, Yandell M, Lessnick SL, Moon AM. Coordinated control of senescence by lncRNA and a novel T-box3 co-repressor complex. *Elife.* 2014; 3.
  23. Chapman DL, Garvey N, Hancock S, Alexiou M, Agulnik SL, Gibson-Brown JJ, Cebra-Thomas J, Bollag RJ, Silver LM, Papaioannou VE. Expression of the T-box family genes, Tbx1-Tbx5, during early mouse development. *Dev Dyn.* 1996; 206:379-390.
  24. Washkowitz AJ, Gavrillov S, Begum S, Papaioannou VE. Diverse functional networks of Tbx3 in development and disease. *Wiley Interdiscip Rev Syst Biol Med.* 2012; 4:273-283.
  25. Davenport TG, Jerome-Majewska LA, Papaioannou VE. Mammary gland, limb and yolk sac defects in mice lacking *Tbx3*, the gene mutated in human ulnar mammary syndrome. *Development.* 2003; 130:2263-2273.
  26. Jerome-Majewska LA, Jenkins GP, Ernstoff E, Zindy F, Sherr CJ, Papaioannou VE. *Tbx3*, the ulnar-mammary syndrome gene, and Tbx2 interact in mammary gland development through a p19Arf/p53-independent pathway. *Dev Dyn.* 2005; 234:922-933.
  27. Bishop AE, Buttery LD, Polak JM. Embryonic stem cells. *J Pathol.* 2002; 197:424-429.
  28. Ivanova N, Dobrin R, Lu R, Kotenko I, Levorse J, DeCoste C, Schafer X, Lun Y, Lemischka IR. Dissecting self-renewal in stem cells with RNA interference. *Nature.* 2006; 442:533-538.
  29. Niwa H, Ogawa K, Shimosato D, Adachi K. A parallel circuit of LIF signalling pathways maintains pluripotency of mouse ES cells. *Nature.* 2009; 460:118-122.
  30. Jiang K, Ren C, Nair VD. MicroRNA-137 represses Klf4 and Tbx3 during differentiation of mouse embryonic stem cells. *Stem Cell Res.* 2013; 11:1299-1313.
  31. Cioffi M, Vallespinos-Serrano M, Trabulo SM, et al. MiR-93 Controls Adiposity *via* Inhibition of Sirt7 and Tbx3. *Cell Rep.* 2015; 12:1594-1605.
  32. Cheng X, Ying L, Lu L, Galvão AM, Mills JA, Lin HC, Kotton DN, Shen SS, Nostro MC, Choi JK, Weiss MJ, French DL, Gadue P. Self-Renewing Endodermal Progenitor Lines Generated from Human Pluripotent Stem Cells. *Cell Stem Cell.* 2012; 10:371-384.
  33. Kartikasari AE, Zhou JX, Kanji MS, Chan DN, Sinha A, Grapin-Botton A, Magnuson MA, Lowry WE, Bhushan A. The histone demethylase Jmjd3 sequentially associates with the transcription factors Tbx3 and Eomes to drive endoderm differentiation. *Embo J.* 2013; 32:1393-1408.
  34. Price FD, Yin H, Jones A, van Ijcken W, Grosveld F, Rudnicki MA. Canonical Wnt signaling induces a primitive endoderm metastable state in mouse embryonic stem cells. *Stem Cells.* 2013; 31:752-764.
  35. Waghray A, Saiz N, Jayaprakash AD, Freire AG, Papatsenko D, Pereira CF, Lee DF, Brosh R, Chang B, Darr H, Gingold J, Kelley K, Schaniel C, Hadjantonakis AK, Lemischka IR. Tbx3 Controls Dppa3 Levels and Exit from Pluripotency toward Mesoderm. *Stem Cell Reports.* 2015; 5:97-110.
  36. Han J, Yuan P, Yang H, Zhang J, Soh BS, Li P, Lim SL, Cao S, Tay J, Orlov YL, Lufkin T, Ng H-H, Tam W-L, Lim B. Tbx3 improves the germ-line competency of induced pluripotent stem cells. *Nature.* 2010; 463:1096-1100.
  37. Declercq J, Sheshadri P, Verfaillie CM, Kumar A. Zic3 enhances the generation of mouse induced pluripotent stem cells. *Stem Cells Dev.* 2013; 22:2017-2025.
  38. Bakker ML, Boukens BJ, Mommersteeg MT, Brons JF, Wakker V, Moorman AF, Christoffels VM. Transcription factor Tbx3 is required for the specification of the atrioventricular conduction system. *Circ Res.* 2008; 102:1340-1349.
  39. Falco G, Lee SL, Stanghellini I, Bassey UC, Hamatani T, Ko MS. *Zscan4*: A novel gene expressed exclusively in late 2-cell embryos and embryonic stem cells. *Dev Biol.* 2007; 307:539-550.
  40. Dan J, Li M, Yang J, Li J, Okuka M, Ye X, Liu L. Roles for Tbx3 in regulation of two-cell state and telomere elongation in mouse ES cells. *Sci Rep.* 2013; 3:3492.
  41. Esmailpour T, Huang T. TBX3 promotes human embryonic stem cell proliferation and neuroepithelial differentiation in a differentiation stage-dependent manner. *Stem Cells.* 2012; 30:2152-2163.
  42. Weinberger L, Ayyash M, Novershtern N, Hanna JH. Dynamic stem cell states: Naive to primed pluripotency in rodents and humans. *Nat Rev Mol Cell Bio.* 2016; 17:155-169.
  43. Miao ZF, Liu XY, Xu HM, Wang ZN, Zhao TT, Song YX, Xing YN, Huang JY, Zhang JY, Xu H, Xu YY. Tbx3 overexpression in human gastric cancer is correlated with advanced tumor stage and nodal status and promotes cancer cell growth and invasion. *Virchows Archiv.* 2016; 469:505-513.
  44. Willmer T, Cooper A, Sims D, Govender D, Prince S. The T-box transcription factor 3 is a promising biomarker and a key regulator of the oncogenic phenotype of a diverse range of sarcoma subtypes. *Oncogenesis.* 2016; 5:e199.
  45. Yarosh W, Barrientos T, Esmailpour T, Lin L, Carpenter PM, Osann K, Anton-Culver H, Huang T. TBX3 is overexpressed in breast cancer and represses p14 ARF by interacting with histone deacetylases. *Cancer Res.* 2008; 68:693-699.
  46. Elmore S. Apoptosis: A Review of Programmed Cell Death. *Toxicol Pathol.* 2007; 35:495-516.
  47. Carlson H, Ota S, Song Y, Chen Y, Hurlin PJ. Tbx3 impinges on the p53 pathway to suppress apoptosis, facilitate cell transformation and block myogenic differentiation. *Oncogene.* 2002; 21:3827-3835.

48. Wensing LA, Campos AH. TBX3, a downstream target of TGF-beta1, inhibits mesangial cell apoptosis. *Exp Cell Res.* 2014; 328:340-350.
49. Renard CA, Labalette C, Armengol C, Cougot D, Wei Y, Cairo S, Pineau P, Neuveut C, de Reynies A, Dejean A, Perret C, Buendia MA. Tbx3 is a downstream target of the Wnt/beta-catenin pathway and a critical mediator of beta-catenin survival functions in liver cancer. *Cancer Res.* 2007; 67:901-910.
50. Zhang JF, He ML, Qi D, Xie WD, Chen YC, Lin MC, Leung PC, Zhang YO, Kung HF. Aqueous extracts of *Fructus Ligustri Lucidi* enhance the sensitivity of human colorectal carcinoma DLD-1 cells to doxorubicin-induced apoptosis *via* Tbx3 suppression. *Integr Cancer Ther.* 2011; 10:85-91.
51. Willmer T, Peres J, Mowla S, Abrahams A, Prince S. The T-Box factor TBX3 is important in S-phase and is regulated by c-Myc and cyclin A-CDK2. *Cell Cycle.* 2015; 14:3173-3183.
52. Platonova N, Scotti M, Babich P, Bertoli G, Mento E, Meneghini V, Egeo A, Zucchi I, Merlo GR. *TBX3*, the gene mutated in ulnar-mammary syndrome, promotes growth of mammary epithelial cells *via* repression of p19ARF, independently of p53. *Cell Tissue Res.* 2007; 328:301-316.
53. Suzuki A, Sekiya S, Buscher D, Izpisua Belmonte JC, Taniguchi H. Tbx3 controls the fate of hepatic progenitor cells in liver development by suppressing p19ARF expression. *Development.* 2008; 135:1589-1595.
54. Willmer T, Hare S, Peres J, Prince S. The T-box transcription factor TBX3 drives proliferation by direct repression of the p21WAF1 cyclin-dependent kinase inhibitor. *Cell Division.* 2016; 11:6.
55. Burgucu D, Guney K, Sahinturk D, Ozbudak IH, Ozel D, Ozbilim G, Yavuzer U. Tbx3 represses PTEN and is over-expressed in head and neck squamous cell carcinoma. *BMC Cancer.* 2012; 12:481.
56. Chalhoub N, Baker SJ. PTEN and the PI3-kinase pathway in cancer. *Annu Rev Pathol.* 2009; 4:127-150.
57. Peres J, Davis E, Mowla S, Bennett DC, Li JA, Wansleben S, Prince S. The Highly Homologous T-Box Transcription Factors, TBX2 and TBX3, Have Distinct Roles in the Oncogenic Process. *Genes Cancer.* 2010; 1:272-282.
58. Peres J, Prince S. The T-box transcription factor, TBX3, is sufficient to promote melanoma formation and invasion. *Mol Cancer.* 2013; 12:117-117.
59. Ballim RD, Mendelsohn C, Papaioannou VE, Prince S. The ulnar-mammary syndrome gene, *Tbx3*, is a direct target of the retinoic acid signaling pathway, which regulates its expression during mouse limb development. *Mol Bio Cell.* 2012; 23:2362-2372.
60. Li J, Ballim D, Rodriguez M, Cui R, Goding CR, Teng H, Prince S. The Anti-proliferative Function of the TGF-β1 Signaling Pathway Involves the Repression of the Oncogenic TBX2 by Its Homologue TBX3. *J Biol Chem.* 2014; 289:35633-35643.
61. Li J, Weinberg MS, Zerbini L, Prince S. The oncogenic TBX3 is a downstream target and mediator of the TGF-β1 signaling pathway. *Mol Bio Cell.* 2013; 24:3569-3576.
62. Chen ZH, Lu GM, Ji TH. Expression of TBX3 mRNA and its role in the pathogenesis and metastasis of breast cancer. *Nan Fang Yi Ke Da Xue Xue Bao.* 2009; 29:87-89 (in Chinese).
63. Fillmore CM, Gupta PB, Rudnick JA, Caballero S, Keller PJ, Lander ES, Kuperwasser C. Estrogen expands breast cancer stem-like cells through paracrine FGF/Tbx3 signaling. *Proc Natl Acad Sci U S A.* 2010; 107:21737-21742.
64. Mowla S, Pinnock R, Leaner VD, Goding CR, Prince S. PMA-induced up-regulation of TBX3 is mediated by AP-1 and contributes to breast cancer cell migration. *Biochem J.* 2011; 433:145-153.
65. Perkhof L, Walter K, Costa IG, et al. Tbx3 fosters pancreatic cancer growth by increased angiogenesis and activin/nodal-dependent induction of stemness. *Stem Cell Res.* 2016; 17:367-378.
66. Canel M, Serrels A, Frame MC, Brunton VG. E-cadherin-integrin crosstalk in cancer invasion and metastasis. *J Cell Sci.* 2013; 126:393-401.
67. Rodriguez M, Aladowicz E, Lanfrancone L, Goding CR. Tbx3 Represses E-Cadherin Expression and Enhances Melanoma Invasiveness. *Cancer Res.* 2008; 68:7872-7881.
68. Boyd SC, Mijatov B, Pupo GM, Tran SL, Gowrishankar K, Shaw HM, Goding CR, Scolyer RA, Mann GJ, Kefferd RF, Rizos H, Becker TM. Oncogenic B-RAF(V600E) signaling induces the T-Box3 transcriptional repressor to repress E-cadherin and enhance melanoma cell invasion. *J Invest Dermatol.* 2013; 133:1269-1277.
69. Peres J, Mowla S, Prince S. The T-box transcription factor, TBX3, is a key substrate of AKT3 in melanomagenesis. *Oncotarget.* 2015; 6:1821-1833.
70. Yano T, Yamazaki Y, Adachi M, Okawa K, Fort P, Uji M, Tsukita S, Tsukita S. Tara up-regulates E-cadherin transcription by binding to the Trio RhoGEF and inhibiting Rac signaling. *J Cell Biol.* 2011; 193:319-332.
71. Humtsoe JO, Koya E, Pham E, Aramoto T, Zuo J, Ishikawa T, Kramer RH. Transcriptional profiling identifies upregulated genes following induction of epithelial-mesenchymal transition in squamous carcinoma cells. *Exp Cell Res.* 2012; 318:379-390.
72. Du HF, Ou LP, Yang X, Song XD, Fan YR, Tan B, Luo CL, Wu XH. A new PKCalpha/beta/TBX3/E-cadherin pathway is involved in PLCepsilon-regulated invasion and migration in human bladder cancer cells. *Cell Signal.* 2014; 26:580-593.
73. Dean M, Fojo T, Bates S. Tumour stem cells and drug resistance. *Nat Rev Cancer.* 2005; 5:275-284.
74. Lyng H, Brovig RS, Svendsrud DH, Holm R, Kaalhus O, Knutstad K, Oksefjell H, Sundfor K, Kristensen GB, Stokke T. Gene expressions and copy numbers associated with metastatic phenotypes of uterine cervical cancer. *BMC Genomics.* 2006; 7:268.
75. Yamashita S, Tsujino Y, Moriguchi K, Tatematsu M, Ushijima T. Chemical genomic screening for methylation-silenced genes in gastric cancer cell lines using 5-aza-2'-deoxycytidine treatment and oligonucleotide microarray. *Cancer Sci.* 2006; 97:64-71.
76. Etcheverry A, Aubry M, de Tayrac M, Vauleon E, Boniface R, Guenot F, Saikali S, Hamlat A, Riffaud L, Menei P, Quillien V, Mosser J. DNA methylation in glioblastoma: Impact on gene expression and clinical outcome. *BMC Genomics.* 2010; 11:701.
77. White-Al Habeeb NMA, Ho LT, Olkhov-Mitsel E, Kron K, Pethe V, Lehman M, Jovanovic L, Fleshner N, van der Kwast T, Nelson CC, Bapat B. Integrated analysis of epigenomic and genomic changes by DNA methylation dependent mechanisms provides potential novel biomarkers for prostate cancer. *Oncotarget.* 2014; 5:7858-7869.

78. Kandimalla R, van Tilborg AA, Kompier LC, Stumpel DJ, Stam RW, Bangma CH, Zwarthoff EC. Genome-wide analysis of CpG island methylation in bladder cancer identified TBX2, TBX3, GATA2, and ZIC4 as pTa-specific prognostic markers. *Eur Urol.* 2012; 61:1245-1256.
79. Beukers W, Kandimalla R, Masius RG, Vermeij M, Kranse R, van Leenders GJ, Zwarthoff EC. Stratification based on methylation of TBX2 and TBX3 into three molecular grades predicts progression in patients with pTa-bladder cancer. *Mod Pathol.* 2015; 28:515-522.
80. Logan CY, Nusse R. The Wnt signaling pathway in development and disease. *Annu Rev Cell Dev Biol.* 2004; 20:781-810.
81. Lachenmayer A, Alsinet C, Savic R, et al. Wnt-pathway activation in two molecular classes of hepatocellular carcinoma and experimental modulation by sorafenib. *Clin Cancer Res.* 2012; 18:4997-5007.
82. Tsai KH, Hsien HH, Chen LM, Ting WJ, Yang YS, Kuo CH, Tsai CH, Tsai FJ, Tsai HJ, Huang CY. Rhubarb inhibits hepatocellular carcinoma cell metastasis *via* GSK-3-beta activation to enhance protein degradation and attenuate nuclear translocation of beta-catenin. *Food Chem.* 2013; 138:278-285.
83. Cavard C, Audebourg A, Letourneur F, Audard V, Beuvon F, Cagnard N, Radenen B, Varlet P, Vacher-Lavenu MC, Perret C, Terris B. Gene expression profiling provides insights into the pathways involved in solid pseudopapillary neoplasm of the pancreas. *J Pathol.* 2009; 218:201-209.
84. Arendt LM, St. Laurent J, Wronski A, Caballero S, Lyle SR, Naber SP, Kuperwasser C. Human breast progenitor cell numbers are regulated by WNT and TBX3. *PLoS One.* 2014; 9:e111442.
85. Katoh M, Nakagama H. FGF receptors: Cancer biology and therapeutics. *Med Res Rev.* 2014; 34:280-300.
86. Eblaghie MC, Song S-J, Kim J-Y, Akita K, Tickle C, Jung H-S. Interactions between FGF and Wnt signals and Tbx3 gene expression in mammary gland initiation in mouse embryos. *J Anat.* 2004; 205:1-13.
87. Marengo B, De Ciucis C, Ricciarelli R, Pronzato MA, Marinari UM, Domenicotti C. Protein Kinase C: An attractive target for cancer therapy. *Cancers.* 2011; 3:531-567.
88. Das BC, Thapa P, Karki R, Das S, Mahapatra S, Liu TC, Torregroza I, Wallace DP, Kambhampati S, Van Veldhuizen P, Verma A, Ray SK, Evans T. Retinoic acid signaling pathways in development and diseases. *Bioorg Med Chem.* 2014; 22:673-683.
89. Garattini E, Paroni G, Terao M. Retinoids and breast cancer: New clues to increase their activity and selectivity. *Breast Cancer Res.* 2012; 14:111-111.
90. Suzuki T, Takeuchi J, Koshiba-Takeuchi K, Ogura T. Tbx Genes Specify Posterior Digit Identity through Shh and BMP Signaling. *Dev Cell.* 2004; 6:43-53.
91. Tumpel S, Sanz-Ezquerro JJ, Isaac A, Eblaghie MC, Dobson J, Tickle C. Regulation of Tbx3 expression by anteroposterior signalling in vertebrate limb development. *Dev Biol.* 2002; 250:251-262.
92. Imamura T, Hikita A, Inoue Y. The roles of TGF-beta signaling in carcinogenesis and breast cancer metastasis. *Breast Cancer.* 2012; 19:118-124.
93. Tian F, DaCosta Byfield S, Parks WT, Yoo S, Felici A, Tang B, Piek E, Wakefield LM, Roberts AB. Reduction in Smad2/3 signaling enhances tumorigenesis but suppresses metastasis of breast cancer cell lines. *Cancer Res.* 2003; 63:8284-8292.
94. Nitulescu GM, Margina D, Juzenas P, Peng Q, Oлару OT, Saloustros E, Fenga C, Spandidos D, Libra M, Tsatsakis AM. Akt inhibitors in cancer treatment: The long journey from drug discovery to clinical use. *Int J Oncol.* 2016; 48:869-885.
95. Samuels Y, Ericson K. Oncogenic PI3K and its role in cancer. *Current Opinion in Oncology.* 2006; 18:77-82.
96. Yuan TL, Cantley LC. PI3K pathway alterations in cancer: Variations on a theme. *Oncogene.* 2008; 27:5497-5510.
97. Tomita Y, Morooka T, Hoshida Y, Zhang B, Qiu Y, Nakamichi I, Hamada K, Ueda T, Naka N, Kudawara I, Aozasa K. Prognostic significance of activated AKT expression in soft-tissue sarcoma. *Clin Cancer Res.* 2006; 12:3070-3077.
98. Valkov A, Kilvaer TK, Sorbye SW, Donnem T, Smeland E, Bremnes RM, Busund L-T. The prognostic impact of Akt isoforms, PI3K and PTEN related to female steroid hormone receptors in soft tissue sarcomas. *J Transl Med.* 2011; 9:200-200.
99. Gonzalez E, McGraw TE. The Akt kinases: Isoform specificity in metabolism and cancer. *Cell Cycle.* 2009; 8:2502-2508.
100. Fortier AM, Asselin E, Cadrin M. Functional specificity of Akt isoforms in cancer progression. *Biomol Concepts.* 2011; 2:1-11.

(Received February 27, 2017; Revised May 23, 2017; Accepted May 25, 2017)

# Traditional Chinese medicine for human papillomavirus (HPV) infections: A systematic review

Jing Lin<sup>1,2,3,\*</sup>, Lanting Chen<sup>1,2,3,\*</sup>, Xuemin Qiu<sup>1,2,3</sup>, Na Zhang<sup>1,2,3</sup>, Qiting Guo<sup>4</sup>, Yan Wang<sup>1,2,3</sup>, Mingyan Wang<sup>1,2,3</sup>, Hans-Jürgen Guber<sup>5</sup>, Dajin Li<sup>1,2,3</sup>, Ling Wang<sup>1,2,3,\*\*</sup>

<sup>1</sup>Laboratory for Reproductive Immunology, Hospital & Institute of Obstetrics and Gynecology, IBS, Shanghai Medical College, Fudan University, Shanghai, China;

<sup>2</sup>Shanghai Key Laboratory of Female Reproductive Endocrine-related Diseases, Shanghai, China;

<sup>3</sup>The Academy of Integrative Medicine of Fudan University, Shanghai, China;

<sup>4</sup>Public Health of Zhejiang University, Hangzhou, China;

<sup>5</sup>Department of Pharmacy, Kepler University Clinic, Neuromed Campus, Linz, Austria.

## Summary

Human papillomavirus (HPV) infections are common and generally harmless, but persistent infections can bring health problems like cancer and genital warts. For the uninfected group, HPV vaccines provide safe and effective protection, but they're type-restricted and expensive. For those infected, so far there have been a handful of treatments for HPV-associated benign or malignant diseases, traditional Chinese medicine being one of them. This systematic review focuses on the application of traditional Chinese medicine in HPV infection and related diseases on the basis of clinical findings. Moreover it covers compositions and mechanisms based on *in vitro* laboratory methods and animal models. Traditional Chinese medicine improves clinical index in the treatment of cervical cancer and genital warts; the mechanisms behind the effectiveness might be the regulation of cell apoptosis, viral gene transcription and translation, cell signal transduction pathways, and immune function.

**Keywords:** Traditional Chinese medicine, human papillomavirus (HPV), HPV infection, cervical cancer, genital warts

## 1. Introduction

Human papillomavirus (HPV) infection, one of the most common sexually transmitted diseases, is detectable at least once in the lifetime of most sexually active people (1). According to a study on a large sample in China, HPV positive rate was 21.7% by hybrid capture II test (HCII) and 15.7% by multiplex polymerase chain reaction fluorescence testing (MPFT) method (2). The virus can be divided into two categories: low-risk types and high-risk types. In most cases, low-risk HPV

infections resolve spontaneously due to human immune defense, taking HPV type 1, 2, 3, and 4 as examples. In very few cases, the infection persists and causes warts, benign papilloma, precancerous lesions, and even cancer. High-risk types, HPV 16 and 18 included, are known as a definite biological carcinogen for cancers of the cervix, vulva, vagina, penis, anus, and oropharynx. HPV infection was associated with 4.8% of cancers in 2008 globally, 86.9% of cases being cervical cancer (3). A recent study pointed out that HPV infection explained around 660,000 cases of cancer and 350 million genital warts (4). Genes E6 and E7 are the oncogenes of HPV, which modulate p53 and PDZ-domain proteins and target the retinoblastoma protein family (5). E6 and E7 proteins facilitate viral genome amplification in ways driving cell cycle entry, promoting basal cell proliferation, and causing neoplasia.

There are three HPV vaccines available on the global market, all being safe and effective. Bivalent and quadrivalent vaccines provide protection against

Released online in J-STAGE as advance publication May 6, 2017.

\*These authors contributed equally to this work.

\*\*Address correspondence to:

Dr. Ling Wang, Laboratory for Reproductive Immunology, Hospital & Institute of Obstetrics and Gynecology, IBS, Fudan University Shanghai Medical College, 413 Zhaozhou Road, Shanghai 200011, China.

E-mail: Dr.wangling@fudan.edu.cn

nearly 70% of HPV-associated cervical precancerous and cancerous problems, while the nine-valent vaccine protects against 90% (6). But controversy remains when it comes to the high cost, incomplete protection, nontherapeutic activity and unknown co-factors that influence the efficacy of vaccines. Listed below are the current therapies for cervical intraepithelial neoplasia with HPV infections: *i*) antiviral drugs like cidofovir, *ii*) immunoenhancers like interferon and imiquimod, *iii*) cytotoxic agents like 5-fluorouracil (5-FU), *iv*) photodynamic therapy (PDT), *v*) therapeutic vaccines, and *vi*) ablative or excisional treatment (7). However, these approaches are expensive and of limited efficacy with side effects and safety concerns, which greatly restricts their application. Thus, traditional Chinese medicine gains increasing popularity to cover their limitations.

## 2. Mechanisms

The potential role of traditional Chinese medicine for HPV related diseases has been demonstrated by *in vitro* and *in vivo* experiments, which take a step further in the exploration of the underlying mechanism of its active components. Presented below (Table 1) is a brief outline of some recent research on the pharmacology of common Chinese medicine, whose findings can be

summarized as follows.

### 2.1. Induce apoptosis

In 1999, Zheng *et al.* carried out an *in vitro* study to examine the effect of arsenic trioxide ( $As_2O_3$ ), a widely used ingredient in the practice of traditional Chinese medicine, on HPV 16 DNA-immortalized human cervical epithelial cells (HCE16/3 cell line).  $As_2O_3$  was discovered to increase apoptosis of HCE16/3 cells at a low concentration, which might have a connection with viral oncogene suppression (8). Another study revealed that butein, isolated from the stem extract of *Rhus verniciflua*, exhibited an inhibitory effect on MCF-7 human breast cancer cell line and human cervical carcinoma cell line HeLa. Butein treatment was found to reduce cell viability, induce apoptosis, and cause DNA damage compared with untreated cells (9).

### 2.2. Modulate gene transcription and protein synthesis

Pinellia extract fraction treatment notably decreased the mRNA expression and protein level of HPV E6 while increasing the mRNA and protein level of p53 in CaSki and HeLa cervical cancer cells. The down-regulation of HPV E6 gene expression and up-regulation of the

**Table 1. The methodologies and findings of recent researches on Traditional Chinese Medicine for HPV infections**

Component, Year	Material	Methods	Mechanism of action
Arsenic trioxide (8), 1999	HCE16/3 cells	MTT assay, DNA-fragmentation assay, RT-PCR, flow cytometry, western blot	Decrease intestinal alkaline phosphatase level, repress oncogenes, reactivate p53 and p21, increase apoptosis
Yigan Kang (12), 2006	HeLa cells, NOD-SCID mice	MTT assay, intestinal alkaline phosphatase activity assay, reversion frequency assay, semi-quantitative RT-PCR, flow cytometry, western blot, tumorigenicity testing	Decrease intestinal alkaline phosphatase level, repress oncogenes, reactivate p53 and p21, increase apoptosis
Baofukang (13), 2007	CaSki and H8 cells	MTT assay, flow cytometry, RT-PCR	Inhibit cell proliferation, arrest cell cycle, down-regulate oncogene expression, increase apoptosis
Pinellia extract fraction (10), 2012	CaSki and HeLa cells	RT-PCR, western blot	Down-regulate E6, up-regulate p53
Youdujing (15), 2012	Cervical tissue of HPV infected patients	RT-PCR	Inhibit hTERT expression
Tanshinone IIA (11), 2015	CaSki, SiHa, HeLa, and C33a cells, athymic nude mice	MTT assay, DNA-binding dyes, flow cytometry, western blot, tumor xenograft, real-time PCR	Inhibit oncogene expression, arrest cell cycle, induce p53 and cause apoptosis
Dehydrocostus lactone (16), 2015	HeLa and C33a cells	MTT assay, flow cytometry, transwell analysis, western blot	Inhibit cell proliferation, inhibit invasion, induce apoptosis, down-regulate phospho-Akt
Butein (9), 2016	MCF-7, HeLa, and ME180 cells	MTT assay, DNA ladder assay, flow cytometry, alkaline comet assay	Reduce cell viability, increase apoptosis, cause DNA damage
Erhuang Powder (17), 2016	Vaginal lavage and cervical tissue of HPV infected CIN I patients	ELISA and immunohistochemistry assay	Regulate Th1/Th2 balance, increase IFN- $\gamma$ and T-bet

**Abbreviations:** HPV, human papillomavirus; MTT, 3-(4,5-dimethyl-2-thiazolyl)-2,5-diphenyl-2-H-tetrazolium bromide; RT-PCR, reverse transcription polymerase chain reaction; hTERT, human telomerase reverse transcriptase; Akt, protein kinase B; CIN, cervical intraepithelial neoplasia; ELISA, enzyme-linked immunosorbent assay; IFN, interferon.

p53 gene was thought to be critical to the anti-tumor effect of Pinellia extract fraction (10). In examination of HPV positive CaSki cells, the Tanshinone IIA, active component of Danshen (*Salvia miltiorrhiza*), was proven to repress the expression of viral oncogenes like E6 and E7 genes, reactivate p53 gene, and modulate proteins like E6AP ubiquitin-protein ligase (E6AP), E2F1, and retinoblastoma protein (pRb). This research revealed that the apoptotic effect of Tanshinone IIA was p53-mediated with Bax, Bcl2, and caspase-3 involved (11). In another experiment with Yigan Kang, it was discovered that Yigan Kang down-regulated E6 and E7 oncogenes while up-regulating p53 and p21 expression in the HeLa cervical cancer line (12). Studies of the Baofukang suppository reported reduction of HPV E6 and E7 mRNA along with inhibition of cell proliferation in the H8 immortalized cervical epithelial cell line, and the CaSki and SiHa cervical cancer cell lines (13,14). Highly expressed in most malignant tumors, human telomerase reverse transcriptase (hTERT) was detected to be down-regulated and deactivated after Youdujing treatment (15).

### 2.3. Regulate cell signal transduction pathways

As one of the traditional Chinese medicines for a broad range of diseases, dehydrocostus lactone could inhibit proliferation and invasion of HeLa (HPV 18 positive) and C33a (HPV negative) human cervical cancer cell lines associated with a reduced level of phospho-protein kinase B (Akt) phosphorylation in a time- or dose-dependent manner. These inhibitions were particularly enhanced combined with specific phosphatidylinositol 3-kinase (PI3K)/Akt inhibitors, which suggested that dehydrocostus lactone might give play to the anti-tumor role *via* the PI3K/Akt pathway (16).

### 2.4. Boost immunity

Tumor genesis is closely linked with immune function of the human body. Immunocompromised hosts are at a higher risk for developing HPV related diseases or malignancies. The anti-tumor activity relies mainly on cell immunity, where Th1 cells play an important role. In the study of the clinical effect of Erhuang Powder in HPV-infected cervical intraepithelial neoplasia (CIN) I patients, it was found that the level of interferon- $\gamma$  (IFN- $\gamma$ ) in vaginal lavage was significantly higher after treatment accompanied by increased expression of T-bet in the cervical tissue, which indicated the regulation of Th1/Th2 balance and improvement of the cervical immune microenvironment (17).

## 3. Traditional Chinese Medicine

Since there have not been any clinically recommended pharmacological therapies for HPV related health problems, traditional Chinese medicine continues to be

an alternative for reasons of efficacy, safety, low cost, and so on. Basic laboratory research has demonstrated the multi-target effectiveness of traditional Chinese medicine for HPV related diseases. Presented below (Table 2) is a brief outline of application of traditional Chinese medicine in HPV related diseases on the basis of clinical findings.

### 3.1. Internal treatment

Traditional Chinese doctors have treated cervical diseases based on the symptoms and signs since a long time ago. According to the theory formed in practice, Rhizoma Atractylodis, Cortex Phellodendri, Semen Coicis, and Poria have a beneficial effect on spleen function and fluid metabolism; Radix Astragali and Radix Angelicae Sinensis are prescribed to enhance immunity; Faeces Trogopterpi, Flos Lonicerae, Herba Hedyotidis Diffusae, Herba Scutellariae Barbatae, and Herba Lobeliae Chinensis are heat-clearing and detoxifying herbs which are capable of relieving genital itching and pain.

Modified Simiao Decoction, main components containing Radix Astragali 20 g, Rhizoma Atractylodis 15 g, Cortex Phellodendri 15 g, Semen Coicis 30 g, Radix Angelicae Sinensis 15 g, Poria 15 g, Faeces Trogopterpi 10 g, Flos Lonicerae 15 g, Herba Hedyotidis Diffusae 30 g, Herba Scutellariae Barbatae 10 g, Herba Lobeliae Chinensis 10 g, Radix Glycyrrhizae 10 g, exhibited better improvement of clinical symptoms compared with the classic Chinese medicine formulation Baofukang in patients with cervical HPV infection (18). In addition, Modified Simiao Decoction had greater performance of virus clearance and a higher level of IFN- $\alpha$  and tumor necrosis factor- $\alpha$  (TNF- $\alpha$ ) which confirmed its antiviral and immune-regulatory effect (19).

Yiqi Huashi Jiedu Decoction, composed of Radix Astragali 15 g, Poria 20 g, Rhizoma Atractylodis Macrocephalae 15 g, Cortex Phellodendri 10g, Rhizoma Cyrtomii 10 g, Fructus Amomi 10 g, Radix Angelicae Sinensis 10 g, Rhizoma Chuanxiong 10 g, Radix Gentianae 6g, Radix Glycyrrhizae 6 g, was another classic formulation that had the power of activating blood circulation, dissipating blood stasis, eliminating necrotic tissues, promoting granulation, dissipate heat, and enhancing diuresis. Adding Fructus Toosendan and Rhizoma Corydalis for patients with abdominal pain, Cortex Magnoliae Officinalis for poor appetite, Semen Euryales for leukorrhagia, and Yiqi Huashi Jiedu Decoction showed higher clinical healing rate, better virus clearance, and less recurrence than routine western medical treatment in patients with HPV infection and cervicitis (20).

### 3.2. External treatment

Evidence has been accumulating on topical Chinese medicine effecting HPV related cervical infection.

**Table 2. The application of Traditional Chinese Medicine in HPV related diseases on the basis of clinical findings**

Experimental group, Year	Sample size	Control group	Sample size	Patients	Clinical index
Modified Simiao Decoction (18), 2013	44	Baofukang	42	Cervical HPV infection	Symptoms, HPV negative rate
Modified Simiao Decoction (19), 2015	43	Baofukang	43	Cervical HPV infection	Symptoms, histopathology, HPV negative rate, IFN- $\alpha$ , TNF- $\alpha$
Yiqi Huashi Jiedu Decoction (20), 2015	49	Routine western medical treatment	49	Cervicitis with HPV infection	Symptoms, colposcopic observation, HPV negative rate
Baofukang (21), 2010	137	No	131	Cervicitis with HPV infection	LCT, HCII, colposcopic observation
Baofukang (22), 2013	113	IFN- $\alpha$ 2b	143	CIN I, high risk type HPV infection	LCT, colposcopic observation and biopsy, HCII, HPV negative rate
Radix Sophorae Flavescens Ointment (23), 2013	120	No	103	Cervical HPV infection	HPV negative rate
ZMLS (24), 2007	94	IFN- $\alpha$ 2a	92	Cervicitis, CIN I, HPV infection	Symptoms, HPV negative rate
Realgar (25), 2012	26	No	25	CIN I, HPV infection	TCT, HPV negative rate, colposcopic observation and biopsy
Paiteling (26), 2011	80	No	40	CIN I/II, high risk type HPV infection	TCT, HPV detection, colposcopic observation and biopsy
Zibai gel (27), 2012	32	No	30	High risk type HPV infection	Symptoms, HCII, LCT, colposcopic observation and biopsy
Youdujing (28), 2012	35	Physiological saline	35	High risk type HPV infection	HPV detection, colposcopic observation and biopsy, hTERT mRNA expression
Chinese medicine (33), 2016	34	IFN- $\alpha$ 2b, Levamisole	34	HPV infection	Flow cytometry, HPV detection
Fuzheng Jiedu Decoction (34), 2014	40	Pure Chinese medicine/IFN- $\alpha$	40/40	High risk type HPV infection	Symptoms, HPV detection, IL-6 level
Chinese medicine and Baofukang (35), 2016	40	Baofukang	40	High risk type HPV infection	Gynecological examinations, HPV detection, HCII
Qingre Fuzheng (36), 2010	64	Water	64	High risk type HPV infection	HPV detection, LCT, biopsy, measure of IgA, IgG, IgM, C3, and C4
Ezhuyou-N-CWS (37), 2009	30	No	30	High risk type HPV infection	HPV detection, LCT, biopsy, levels of IgA, IgG, IgM, C3, and C4
CO <sub>2</sub> laser and Baofukang (38), 2016	80	CO <sub>2</sub> laser and polycresol sulfonic aldehyde	60	Intraepithelial neoplasia and high risk type HPV infection	HPV detection, TCT, colposcopic biopsy
Microwave therapy and Baofukang (39), 2013	121	Microwave	60	Chronic cervicitis with high risk type HPV infection	TCT, colposcopic observation, HPV detection
Microwave therapy and Baofukang (40), 2009	278	Microwave	279	Chronic cervicitis with HPV infection	Symptoms, colposcopic observation, HPV detection
Electrocauterization and Baofukang (41), 2016	47	Electrocauterization /Baofukang	56/43	High risk type HPV infection	Colposcopic observation, HCII, HPV detection
Baofukang and interferon (42), 2014	110	Baofukang/interferon	110/100	Cervical erosion and HPV infection	HPV detection, colposcopic observation and biopsy, cytology
Recombinant human IFN- $\alpha$ 2b and Baofukang (43), 2016	53	Baofukang	53	High risk type HPV infection	HPV detection, colposcopic observation and biopsy, levels of TNF- $\alpha$ and IL-6
Jiawei Jiapi Decoction and XinFuNing (44), 2016	30	XinFuNing, recombinant human IFN- $\alpha$ 2b	30	HPV infection	Symptoms, HPV detection
Xunxi No. 1 and radiotherapy (45), 2016	40	Radiotherapy	40	Cervical cancer with high risk type HPV infection	ISH for HPV16/18, 5-year disease-free survival, pelvic lymphnode metastasis

*Abbreviations:* HPV, human papillomavirus; IFN, interferon; TNF, tumor necrosis factor; LCT, liquid based cytology; HCII, hybrid capture II test; CIN, cervical intraepithelial neoplasia; ZMLS, Zhimiling suppository; TCT, thinprep cytologic test; hTERT, human telomerase reverse transcriptase; IL, interleukin; ISH, *in situ* hybridization.

As one of the representative drugs for external use, Baofukang suppository was reported to have a higher cure rate and effectivity in a test group evaluated by gynecological examination, hybrid capture II test (HCII) and liquid based cytology (LCT). Rhizoma Curcumae and Borneolum are the main contents of Baofukang suppository. After a 3-month medication, it showed a 38% HPV negative rate and a 37% relative light units/cutoff (RLU/CO) ratio improvement rate (21). Comparison of Baofukang and IFN- $\alpha$ 2b indicated that Baofukang reached a higher HPV negative rate and CIN I reversal rate (22). Radix Sophorae Flavescentis ointment is known as a heat-clearing and damp-drying drug whose antitumor and antiviral function has been gradually recognized in the application of hepatic and gastric carcinoma. Clinical study proved that it had a 36% viral conversion rate which was remarkably higher than the spontaneous regression rate of the blank control group (23). Zhimiling suppository (ZMLS) intravaginal suppository, ingredients including Cortex Phellodendri, Radix Sophorae Flavescentis, Catechu, and Borneolum, had a 93.6% efficacy rate versus 93.5% for the IFN- $\alpha$ 2a treatment (24). It emphasized a similar clinical remission result for ZMLS which is more cost-effective. Verified by clinical trials, external application of realgar, 1 g each time every 3 days in the cervical surface of patients tested with HPV infection and CIN I pathological changes, yielded a 53% HPV negative rate and 50% CIN I reversal rate. (25). Paiteling, composed of Herba Hedyotidis Diffusae, Folium Isatidis, Fructus Cnidii, and Fructus Bruceae, had a cytotoxic effect for repressing proliferation of cancer cells and damaging the HPV pathogen which took effect in CIN I/II patients (26). Zibai gel, the active ingredient being Radix Arnebiae, Rhizoma Curcumae, Cortex Phellodendri, Flos Lonicerae, and Radix Sophorae Flavescentis, was found to reduce viral load, effectively relieve symptoms, and improve cytological and pathological results for cervical infected patients (27). Apart from the clinical effectiveness of Youdujing cream in cervical infected patients from etiological, cytological, and pathological levels (28), it was a popular choice for condyloma acuminatum as well. The active components of Youdujing include Fructus Bruceae, Rhizoma Curcumae, Radix Arnebiae, and so on. To investigate the therapeutic effect of Youdujing in genital lesions, *in vitro* experiments were conducted showing the inhibition of HPV-DNA amplification (29,30).

As another form of traditional Chinese medicine, acupuncture is useful in treating a variety of dermatologic disorders, human papillomavirus warts included. As the research work goes further and becomes more detailed, increased importance has been attached to the neuro-immuno-modulation role of acupuncture in pathogenesis of dermatological HPV infections (31). There was a case report about the long-term therapy of traditional Chinese acupuncture clearing away a giant HPV wart that an HIV

infected patient developed when cryotherapy failed (32).

### 3.3. Internal and external treatment

Various combinations of internal and external medicine, focusing on both the local lesion and whole body, have been used to treat HPV infection. Modern pharmacology of traditional Chinese medicine has demonstrated the power of those herbs. For instance, Folium Isatidis, Radix Isatidis, and Herba Portulacae are able to clear heat-toxin and eliminate dampness; Semen Persicae, Flos Carthami, and Rhizoma Cyperi can promote blood circulation and dissipate stasis; Concha Margaritifera, Concha Ostreae, and Spica Prunellae are capable of removing lumps and warts; Radix Astragali, Rhizoma Atractylodis Macrocephalae, and Poria strengthen the spleen and stomach; and Fructus Lycii, Radix Polygoni Multiflori, and Radix Rehmanniae are beneficial to the liver and kidney. Oral administration and fumigation of Chinese medicine has proven to have clinical value (33). Compared with pure external use of Chinese medicine or IFN- $\alpha$ , the combined use of oral decoction and topical powder received better clinical effects assessed by symptoms and signs in line with the decline of viral load (34). A decoction containing Poria 30 g, Rhizoma Dioscoreae Hypoglaucae 15 g, Radix Achyranthis Bidentatae 12 g, Semen Coicis 30 g, Radix Stephaniae Tetrandrae 10 g, Fructus Forsythiae 12 g, Radix Angelicae Dahuricae 10 g, Rhizoma Atractylodis Macrocephalae 10 g, Herba Violae 15 g, Cortex Phellodendri 12 g, Radix Glycyrrhizae 6 g, with Herba Hedyotidis Diffusae, Herba Patriniae, and Herba Portulacae for patients with excessive heat and toxin, Flos Carthami and Semen Persicae for genital drying, Fructus Kochiae and Cortex Dictamnii for genital itching, exhibited significant improvement of cervicitis combined with intravaginal Baofukang suppository (35). According to the study, the associative action of internal treatment and external intervention yielded a notably higher level of IgG, IgA, and IgM (36).

### 3.4. Integrated medicine

Although western medicine is scientifically sound for treating HPV related health conditions and widely acknowledged for its fast onset, Chinese medicine has been well accepted due to its rich philosophical content. Integrated medicine complements each other. Ezhuyou-N-CWS, a combination of Nocardia rubra cell wall skeleton (N-CWS) and Chinese medicine Ezhuyou, which brought the potent adjuvant and antitumor activities of N-CWS to the broad spectrum of the anti-microorganism effect of Ezhuyou, inhibited the proliferation of HeLa cells *in vitro* and exhibited effective results in patients with cervical HPV infection (37). In patients with vaginal intraepithelial neoplasia and HPV infections after a cervical cancer operation, CO<sub>2</sub> laser

combined with Baofukang suppository showed a superior curative effect compared to pure laser treatment (38). Both, retrospective and prospective studies confirmed the better clinical effect of microwave therapy combined with Baofukang in chronic HPV infected patients (39,40). The application of electrocauterization and Baofukang was also reported to have a better therapeutic effect (41). A clinical trial showed that the HPV negative rate was 92.8% in cervical infected patients after the combined use of Baofukang and IFN, higher than 61% in the IFN group and 59.1% in the Baofukang group (42). Moreover, further research pointed out this combination could regulate immune function measured by TNF- $\alpha$  and interleukin-6 (IL-6) level (43). For cervical HPV infected patients, Jiawei Jianpi Decoction plus recombinant IFN- $\alpha$ 2b exhibited a higher effective rate and HPV negative rate and a lower symptoms score than the pure IFN group (44). Chinese medical intervention (Xunxi No.1) plus radiotherapy benefited cervical cancer patients, whose 5-year disease-free survival rate was higher and metastasis rate was much lower compared with a radiotherapy group (45).

#### 4. Conclusion

Persistent infections of human papillomavirus (HPV) bring various health problems. HPV vaccines provide type-restricted and expensive protection for uninfected groups. Perfect treatments for HPV-associated benign or malignant diseases are not available at the moment. Chinese medicine emphasizes integrity and has fewer side effects. This systematic review summarized the clinical findings and laboratory research with the theme of the application of traditional Chinese medicine in HPV infection and related diseases. It explored the composition and mechanisms of some most frequently used prescriptions. To conclude, traditional Chinese medicine improves clinical index in the treatment of cervical cancer and genital warts as a result of its regulation in cell apoptosis, viral gene expression, cell signal transduction pathways and body immune function.

#### Acknowledgements

This work was supported by the National Natural Science Foundation of China (grant no. 31571196 to Ling Wang), the Science and Technology Commission of Shanghai Municipality 2015 YIXUEYINGDAO project (grant no.15401932200 to Ling Wang), the FY2008 JSPS Postdoctoral Fellowship for Foreign Researchers (P08471 to Ling Wang), the National Natural Science Foundation of China (grant no. 30801502 to Ling Wang), the Shanghai Pujiang Program (grant no. 11PJ1401900 to Ling Wang), the National Natural Science Foundation of China (grant no. 81401171 to Xue-Min Qiu), the Development Project of Shanghai Peak Disciplines-Integrated Chinese and

Western Medicine (grant no. 20150407).

#### References

1. Park IU, Introcaso C, Dunne EF. Human papillomavirus and genital warts: A review of the evidence for the 2015 centers for disease control and prevention sexually transmitted diseases treatment guidelines. *Clin Infect Dis*. 2015; 61:S849-855.
2. Zeng Z, Austin RM, He X, Chen X, Guo X, Zheng B, Wu S, Yang H, Zhao C. Prevalence of high-risk human papillomavirus infection in China: Analysis of 671,163 human papillomavirus test results from China's largest college of American pathologists-certified laboratory. *Am J Clin Pathol*. 2016; 145:622-625.
3. Forman D, Martel CD, Lacey CJ, Soerjomataram I, Tieulent JL, Bruni L, Vignat J, Ferlay J, Bray F, Plummer M, Franceschi S. Global burden of human papillomavirus and related diseases. *Vaccine*. 2012; 30:12-23.
4. Denny L. Epidemiology and burden of disease associated with HPV infection. *Curr Obstet Gynecol Rep*. 2016; 5:189-195.
5. Doorbar J, Quint W, Banks L, Bravo IG, Stoler M, Broker TR, Stanley MA. The biology and life-cycle of human papillomaviruses. *Vaccine*. 2012; 30:55-70.
6. Angioli R, Lopez S, Aloisi A, Terranova C, Cicco CD, Scaletta G, Capriglione S, Miranda A, Luvero D, Ricciardi R, Montera R, Plotti F. Ten years of HPV vaccines: State of art and controversies. *Crit Rev Oncol Hematol*. 2016; 102:65-72.
7. Hampson L, Martin-Hirsch P, Hampson IN. An overview of early investigational drugs for the treatment of human papilloma virus infection and associated dysplasia. *Expert Opin Investig Drugs*. 2015; 24:1529-1537.
8. Zheng J, Deng YP, Lin C, Fu M, Xiao PG, Wu M. Arsenic trioxide induces apoptosis of HPV16 DNA-immortalized human cervical epithelial cells and selectively inhibits viral gene expression. *Int J Cancer*. 1999; 82:286-292.
9. Tong XQ, Lv W, Luo WQ, Lu WX, Li N. Treatment of human cervical cancer cells with butein leads to apoptosis and DNA damage. *Int J Clin Exp Med*. 2016; 9:11084-11089.
10. Li GL, Xia Q, Chen SH, Gui SQ, Xu CJ. Effects of Pinellia extract fraction on expressions of HPV16 and P53 genes in cervical cancer cell lines. *China J Tradit Chin Med Pharm*. 2012; 27:113-116. (in Chinese)
11. Munagala R, Aqil F, Jeyabalan J, Gupta RC. Tanshinone IIA inhibits viral oncogene expression leading to apoptosis and inhibition of cervical cancer. *Cancer Lett*. 2015; 356:536-546.
12. Deng WP, Chao MW, Lai WF, Sun C, Chung CY, Wu CC, Lin IH, Hwang JJ, Wu CH, Chiu WT, Chen CY, Redpath JL. Correction of malignant behavior of tumor cells by traditional Chinese herb medicine through a restoration of p53. *Cancer Lett*. 2006; 233:315-327.
13. Zhang XY, Bian ML, Fang Q, Chen QY, Chen ZH, Xu M. Study on the mechanism of the proliferative inhibition of Baofukang suppository on human papillomavirus *in vitro*. *J China-Japan Friendship Hosp*. 2007; 21:216-219+259. (in Chinese)
14. Shang YH, Bai LX, Wei LH. The molecular mechanism of Baofukang suppository as a potential inhibitor for cervical carcinoma cell. *Chin J Clin Obstet Gynecol*. 2003; 4:336-338+381. (in Chinese)

15. Xiao J, Wu J, Yu B, Xie HH. Therapeutic efficacy of Youdujing preparation in treating cervical high-risk human papilloma virus infection patients. *Chin J Integr Tradit West Med* 2012; 32:1212-1215. (in Chinese)
16. Jiang EP, Sun XW, Kang HX, Sun LP, An WF, Yao YH, Hu XR. Dehydrocostus Lactone inhibits proliferation, antiapoptosis, and invasion of cervical cancer cells through PI3K/Akt signaling pathway. *Int J Gynecol Cancer*. 2015; 25:1179-1186.
17. Xu YX, Yuan L. Improvement of cervical microenvironment and effect of Erhuang Powder on CIN I accompanied by human papillomavirus infection according to Th1/Th2 immune balance. *Liaoning J Tradit Chin Med*. 2016; 43:962-965+1118. (in Chinese)
18. Dou BF, Zhang JG, Liu B. Analysis on effect of Modified Simiao Decoction in treatment of cervical HPV infection. *Liaoning J Tradit Chin Med*. 2013; 40:1141-1142. (in Chinese)
19. Cheng JM, Tong Y, Chen SC, Zhang L. Clinical effect of modified Simiao Decoction in treating cervical HPV infection. *Pharm Clin Chin Mater Med*. 2015; 31:149-150. (in Chinese)
20. He JM, Huo DZ, Chen YM. Influence of Yiqi Huashi Jiedu Decoction on TCM symptom score and HPV turn rate of cervicitis with HPV infection. *Chin Arch Tradit Chin Med*. 2015; 33:2390-2392. (in Chinese)
21. Bian ML, Chen QY, Zhu J, Ma L, Hao M, Liu J, Chen Y. The efficacy of baofukang suppository for treatment of cervicitis combined with persistent HPV infection. *Chin J Pract Gynecol Obstet*. 2010; 26:383-385. (in Chinese)
22. Shen JJ, Liu ZH, Li J, Zhou YQ, Wang C, Wu RF. The clinical observation for Baofukang and interferon in promoting the regression of low-grade cervical intraepithelial neoplasia. *Chin J Clin Obstet Gynecol*. 2013; 14:509-512. (in Chinese)
23. Wang YH, Wang F, Li YQ. Clinical study on treatment of cervical HPV infection by Radix Sophorae Flavescens ointment. *Med J Natl Defending Forces Southwest China*. 2013; 23:189-191. (in Chinese)
24. Zhang Y, Wang XY, Ding ZY. Treatment of female patients with vaginal and cervical HPV infection. *Chin J Infect Chemother*. 2007; 7:293-294. (in Chinese)
25. Zhang MY. Clinical study on the interventive effect of realgar on the clearance of HPV and CIN. *J Clin Exp Med*. 2012; 11:580-581. (in Chinese)
26. Chen R, Zhao J, Liao QP. The clinical observation report of paiteling on treatment of CIN1/2. *Chin J Pract Gynecol Obstet*. 2011; 27:703-705. (in Chinese)
27. Ma XL, Xue XO, Li S, Wang Y, Xie W. Clinical study of Zibai gel on treatment of cervical high-risk human papillomavirus infection. *Chin J Inform TCM*. 2012; 19:9-12. (in Chinese)
28. Xiao J, Huang JL, Cai LE. Study of Youdujing in treating HR-HPV infected cervical lesions. *Guangdong Med J*. 2011; 32:2036-2039. (in Chinese)
29. Hou MJ, Fan RQ, Sun J, Xuan GW, Chi FH. Effect of Chinese medicine Youdujing for human papilloma virus DNA. *J Guangzhou Univ Tradit Chin Med*. 1998; 15:57-60. (in Chinese)
30. Feng Y, Deng YH, Xuan GW, Zhou D, Sun J, Yuan XH, Zhao RZ. Preparation and *in vitro* pharmacodynamics effect of the Youdujing cream. *Chin Hosp Pharm J*. 2004; 24:7-8. (in Chinese)
31. Ma C, Sivamani RK. Acupuncture as a treatment modality in dermatology: A systematic review. *J Altern Complement Med*. 2015; 21:520-529.
32. Ursini T, Polilli E, Congedo G, Tontodonati M, Masi FD, Mazzotta E, Parruti G, Pippa L. Complete healing of a giant wart in a severely immune-compromised patient with HIV infection treated with acupuncture. *Case Rep Dermatol*. 2011; 3:175-180.
33. Mai LX, Yang GZ, Yuan SH, Wang DN, Zhang T, Deng WC, Huang PJ. Effect of treatment by Chinese herbs for subclinical papillomavirus infection (SPI) and change of T cell subpopulation. *Liaoning J Tradit Chin Med*. 2016; 43:750-752. (in Chinese)
34. Ye LQ, Lou KL, Chen Y, Jiang Y. Clinical study of Chinese medicine intervention in treating cervical HR-HPV infection. *Acta Chin Med Pharm*. 2014; 42:79-82. (in Chinese)
35. Qin JL, Fu MX, Cheng JJ. Clinical effect of Chinese medicine and Baofukang in treating high-risk human papilloma virus. *Modern J Integr Tradit Chin West Med*. 2016; 25:1538-1540. (in Chinese)
36. Zhang PY, Wang XB, Xu X, Yang J, Yang HY. Study of intervention by traditional Chinese medicine for cervical precancerous lesion infected by high-risk HPV. *Liaoning J Tradit Chin Med*. 2010; 37:1191-1194. (in Chinese)
37. Chi Y, Li J. Ezhuyou-N-CWS carrier suppository for antagonizing HPV infection and preventing cervical cancer. *J Beijing Univ Tradit Chin Med*. 2009; 32:419-421. (in Chinese)
38. Wang Y, Su L, Kong WM, Wu YM, Duan W. Clinical study of CO2 laser combined with Baofukang suppository in the treatment of vaginal intraepithelial neoplasia with high risk HPV infection. *Oncol Prog*. 2016; 14:441-443+448. (in Chinese)
39. Zhao MJ, Wang SJ, Wei WH. Analysis of microwave therapy plus Baofukang in treating chronic cervicitis with high risk HPV infection. *Matern Child Health Care China*. 2013; 28:5730-5731. (in Chinese)
40. Yan LS, Yan JF. Clinical value of microwave therapy plus Baofukang in treating chronic cervicitis with HPV infection. *Matern Child Health Care China*. 2009; 24:4182-4183. (in Chinese)
41. Yu J, Yang HY, Zhang LJ, Zhang HP, Liu Y. Clinical study on the treatment of high risk HPV infection. *Chin J Nosocomiol*. 2016; 26:3069-3071. (in Chinese)
42. Xu JQ, Xu JG, Song XZ. Clinical observation of Baofukang combined with interferon in the treatment of cervical erosion complicated with HPV infection. *Chin Arch Tradit Chin Med*. 2014; 32:2028-2030. (in Chinese)
43. Li MX, Xue HY, Chen JP, Zhang XQ, Zhang YL. Effects of treatment efficacy and immune function of recombinant human interferon  $\alpha$ -2b with Baofukang vaginal for patients combined with human papillomavirus infection. *Chin J Nosocomiol*. 2016; 26:3296-3298. (in Chinese)
44. Tang QJ, Guo SS, Wang ZZ. Clinical study of cervical HPV infection treated by Jiawei Jianpi Decoction combined with XinFuNing. *Shanghai J Tradit Chin Med*. 2016; 50:55-57. (in Chinese)
45. Xu X, Zhang B, Hao L, Gu J, Liu L, Wang X, Wu M, Zhang P, Cheng H. Combined use of Xunxi No. 1 and radiotherapy have clinical benefits in stage Ia-IIb cervical cancer patients with high-risk human papilloma virus infection. *Minerva Biotechnol*. 2014; 26:309-313. (in Chinese)

(Received March 8, 2017; Revised April 17, 2017; Accepted April 20, 2017)

# Liver fibrosis after antiretroviral therapy in a longitudinal cohort of sexually infected HIV patients in eastern China

Qian Wei<sup>1,2,§</sup>, Haijiang Lin<sup>3,§</sup>, Yingying Ding<sup>1</sup>, Xing Liu<sup>1</sup>, Qionghai Wu<sup>3</sup>, Weiwei Shen<sup>3</sup>, Meiyang Gao<sup>1</sup>, Na He<sup>1,2,\*</sup>

<sup>1</sup> Department of Epidemiology, School of Public Health, Fudan University, and The Key Laboratory of Public Health Safety of Ministry of Education, Shanghai, China;

<sup>2</sup> Key Laboratory of Health Technology Assessment of Ministry of Health, Fudan University, Shanghai, China;

<sup>3</sup> Taizhou City Center for Disease Control and Prevention, Taizhou city of Zhejiang Province, China.

## Summary

We assessed the factors that influenced improvement or progression in human immunodeficiency virus (HIV)-infected patients who were receiving combination antiretroviral therapy (cART). This was a retrospective cohort study of HIV-infected patients receiving cART in Taizhou, Zhejiang, China, 2009-2015. Liver fibrosis was assessed by Fibrosis-4 (FIB-4) score. Improvement of liver fibrosis was defined as having > 30% decrease in FIB-4 from baseline, whereas progression of liver fibrosis was defined as having > 30% increase in FIB-4 score from baseline. A total of 955 HIV-infected patients were included. Of these, 808 (84.6%) were HIV-monoinfection, 125 (13.1%) were HIV/hepatitis B virus (HBV) coinfection and 29 (3.0%) were HIV/hepatitis C virus (HCV) coinfection. The median duration of treatment was 15 months. After treatment, 37.1% participants had > 30% decreases in FIB-4 index, 14.8% had > 30% increases in FIB-4 index, while the remaining 48.2% had stabilized FIB-4 index. In multivariate analysis, improvement of liver fibrosis was negatively associated with an older age, but was positively associated with baseline FIB-4 index and > 30% increases in CD4 cell count after ART. Progression of liver fibrosis was positively associated with an older age, but was negatively associated with gender and HIV transmission mode (male homosexual vs. male heterosexual, female heterosexual vs. male heterosexual), and baseline FIB-4 index. Our findings indicate that improvement of liver fibrosis could be achieved by early initiation of ART through better CD4 cell recovery. Liver fibrosis and hepatotoxicity associated with ART should be monitored as early as possible and throughout till the end of treatment, with special attention to the elderly and heterosexual men.

**Keywords:** Antiretroviral therapy, HIV, HBV, liver fibrosis, sexual transmission

## 1. Introduction

The liver is a major target of human immunodeficiency virus (HIV) infection and a wide spectrum of liver disease can be seen in patients with HIV infection, ranging from steatosis, steatohepatitis, cirrhosis,

non-cirrhotic portal hypertension and hepatocellular carcinoma (1). HIV infection adversely impacts on the progression of liver diseases. For example, HIV/hepatitis B virus (HBV) co-infected patients had significantly decreased rate of hepatitis B surface antigen (HBsAg) clearance and increased HBV replication than HBV monoinfected individuals (2-3), and HIV/hepatitis C virus (HCV) coinfecting patients had lower rate of HCV viral suppression than HCV monoinfected controls (4). Consequently, progression to cirrhosis is more rapid in HIV-infected patients with chronic liver diseases (5-6). End stage liver disease (ESLD) has become a major cause of mortality in HIV-infected individuals receiving antiretroviral therapy (ART), accounting for a greater proportion of deaths than cardiovascular disease or non-

Released online in J-STAGE as advance publication May 6, 2017.

<sup>§</sup>These authors contributed equally to this works.

\*Address correspondence to:

Dr. Na He, Department of Epidemiology, School of Public Health, and the Key Laboratory of Public Health Safety of Ministry of Education, Fudan University, P.O.Box 289,138 Yi Xue Yuan Road, Shanghai 200032, China.

E-mail: nhe@fudan.edu.cn

acquired immune deficiency syndrome (AIDS)-related cancers (7-8).

In China, common risk factors for liver disease such as alcohol use, HBV and HCV infections are more prevalent in HIV-infected patients than those without HIV infection (9-12). All-cause mortality was also higher in HIV-infected patients with HBV and/or HCV co-infection(s) than in those with HIV only, although ART has generally increased life expectancy of HIV-infected patients (13). Nevertheless, little is known about the impact of ART on the development and progression of liver diseases among people living with HIV and AIDS (PLWHA) in China. In a recently published study, Li *et al.* examined progression of liver fibrosis among ART receiving HIV-infected patients, and found that ART was associated with reduction in liver fibrosis scores in the majority of HIV-hepatitis co-infected and HIV-mono-infected Chinese participants (14). Unfortunately, this study had only a 48 weeks observation period and did not allow for long-term evaluation of progression of liver fibrosis among HIV patients with ART. Given that Chinese PLWHA are now living much longer owing to life-long ART and are at high risk of non-AIDS deaths particularly liver diseases (15-17), research to solicit long-term effects of ART on the development and the outcome of liver diseases especially liver fibrosis is urgently needed.

Liver biopsy is the gold standard technique for diagnosis of liver fibrosis, but it is an invasive procedure and does carry a small risk for complications (18). Thus, there is a need for a noninvasive method to assess liver fibrosis for monitoring liver disease progression and for pursuing epidemiological analysis. Fibrosis-4 (FIB-4) index has been developed and validated as an inexpensive and accurate noninvasive marker for liver fibrosis in HIV-infected patients (19-21), and is increasingly used for studying hepatic fibrosis in HIV-infected patients (14, 22-23).

In this retrospective cohort study, we proposed to assess the long-term impact of ART on liver fibrosis measured by FIB-4 index among HIV-infected patients in a rural prefecture of Eastern China.

## 2. Materials and Methods

### 2.1. Study design and subject selection

This was a retrospective cohort study of HIV-infected patients receiving ART in Taizhou prefecture of Zhejiang province, Eastern China. To be eligible for the study, participants must fulfill the following selection criteria: *i*) were sexually infected with HIV, *ii*) started ART during January 2009 through December 2015, *iii*) aged  $\geq 18$  years at ART initiation, *iv*) had CD4 cell count prior to ART initiation, and *v*) had available information of age, platelet (PLT) count, alanine transaminase (ALT) and aspartate transaminase (AST) levels for calculation

of FIB-4 index at both ART initiation and at least one follow-up visit.

For all participants, the observation period was from the date of ART initiation (*i.e.* baseline) to December 31, 2016. According to China National Guidelines for Free Antiretroviral Treatment for HIV/AIDS, the first line treatment regimen comprises 2 nucleotide reverse transcriptase inhibitors (NRTIs) plus 1 non-nucleotide reverse transcriptase inhibitors (NNRTI). Most commonly, the 2 NRTIs are either zidovudine (AZT) or stavudine (d4T, replaced by tenofovir disoproxil fumarate (TDF) since 2010) and either lamivudine (3TC) or didanosine (DDI) (stopped in 2008), and the 1 NNRTI is either nevirapine (NVP) or efavirenz (EFV).

This study was approved by the Institutional Review Board (IRB) of the Chinese National Center for AIDS/STD Control and Prevention and the IRB of Fudan University, Shanghai, China.

### 2.2. Data collection

Demographical, epidemiological and clinical data were extracted from the China AIDS Comprehensive Response Information Management System (CRIMS) which is a unified web-based national information system. All eligible participants were tested for HBsAg and anti-HCV antibody (HCVAb) using enzyme linked immunoabsorbent assay (ELISA) (Kehua Biotechnology Co. Ltd., Shanghai, China). Patients with CD4 cell count decreased from baseline more than 30% were defined as being decreased in CD4 cell count and with increased from baseline higher than 30% were defined as increased in CD4+ (24).

### 2.3. Study outcomes

Liver fibrosis was determined by FIB-4 score, using Sterling's formula calculated as  $(\text{age} [\text{years}] \times \text{AST} [\text{IU/L}]) / (\text{PLT count} [10^9/\text{L}] \times (\text{ALT}^{1/2} [\text{IU/L}]))$  (19). FIB-4 was ranked into 3 classes according to standard cut-off values:  $< 1.45$  for class 1 (no significant fibrosis);  $1.45-3.25$  for class 2 (moderate fibrosis) and  $> 3.25$  for class 3 (severe fibrosis) (25). Improvement of liver fibrosis was defined as having  $> 30\%$  decrease in FIB-4 from baseline, whereas progression of liver fibrosis was defined as having  $> 30\%$  increase in FIB-4 score from baseline (26-27).

### 2.4. Statistical analysis

All statistical analyses were performed using SPSS version 22.0. Bivariate statistical analyses were performed with the Chi-square test or Fisher's exact test for categorical variables, and Mann-Whitney *U* test or Kruskal-Wallis test for continuous variables. Two separate logistic regression analyses were performed to determine risk factors for improvement ( $> 30\%$  decrease

in FIB-4 index) or progression (> 30% increase in FIB-4 index) of liver fibrosis after ART, respectively. For each of the two logistic regression models, independent variables were selected based on existing knowledge of potential causal relationships between risk factors and liver fibrosis. In this regard, variables of appropriate baseline and follow-up characteristics such as demographic variables, HIV transmission mode, HBV and HCV coinfection status, ART regimen and duration as well as CD4 cell count were subject to univariate logistic regression analysis and were included in the final multiple logistic regression models using the "forced entry" criteria for variable selection. A *p*-value < 0.05 was chosen as the significance level.

### 3. Results

#### 3.1. Baseline characteristics

##### 3.1.1. Sociodemographic characteristics and CD4 cell count

A total of 955 HIV-infected patients participated in the study. Of them, 75.2% were male, 75.1% were married, 69.2% were HIV-infected through heterosexual transmission and 30.8% through homosexual transmission. The median age of the study participants was 37.0 years, and the median CD4 cell count was 211 cells/ $\mu$ L (Table 1).

##### 3.1.2. HBV and HCV coinfection

As shown in Table 1, 125 participants (13.1%) were seropositive for HBsAg and 29 (3.0%) were seropositive for HCVAb. Seven patients (0.7%) were seropositive for both HBsAg and HCVAb. The proportion of HIV monoinfection, HIV/HBV coinfection, HIV/HCV

**Table 1. Baseline and follow-up characteristics of study participants by FIB-4 changes after ART**

Characteristics	Total, N (%) <sup>*</sup>	FIB-4 Unchanged (within $\pm$ 30%), N (%) <sup>**</sup>	FIB-4 Decreased > 30%, N (%) <sup>**</sup>	FIB-4 Increased > 30%, N (%) <sup>**</sup>	<i>P</i> <sup>a</sup>
<i>n</i>	955	460	354	141	
<i>Baseline characteristics</i>					
<i>Age (years)</i>					
Median (IQR)	37.0 (28.0-47.0)	36.0 (28.0-48.0)	39.0 (29.0-47.0)	37.0 (28.0-48.0)	0.935
18-24	131 (13.7)	67 (51.2)	48 (36.6)	16 (12.2)	0.565
25-34	263 (27.5)	137 (52.1)	87 (33.1)	39 (14.8)	
35-44	268 (28.1)	119 (44.4)	109 (40.7)	40 (14.9)	
$\geq$ 45	293 (30.7)	137 (46.8)	110 (37.5)	46 (15.7)	
<i>Gender</i>					
Male	718 (75.2)	341 (47.5)	261 (36.4)	116 (16.2)	0.107
Female	237 (24.8)	119 (50.2)	93 (39.2)	25 (10.6)	
<i>Marital status</i>					
Unmarried	238 (24.9)	117 (49.2)	81 (34.0)	40 (16.8)	0.417
Married	717 (75.1)	343 (47.8)	273 (38.1)	101 (14.1)	
<i>HIV transmission mode</i>					
Homosexual	294 (30.8)	152 (51.7)	105 (35.7)	37 (12.6)	0.262
Heterosexual	661 (69.2)	308 (46.6)	249 (37.7)	104 (15.7)	
<i>CD4 count (cells/<math>\mu</math>L)</i>					
Median (IQR)	211 (133-287)	230 (150-303)	194 (125-271)	212 (112-286)	0.634
<i>HBV coinfection</i>					
Yes	125 (13.1)	52 (41.6)	53 (42.4)	20 (16.0)	0.281
No	830 (86.9)	408 (49.2)	301 (36.3)	121 (14.6)	
<i>HCV coinfection</i>					
Yes	29 (3.0)	10 (34.5)	14 (48.3)	5 (17.2)	0.303
No	926 (97.0)	450 (48.6)	340 (36.7)	136 (14.7)	
<i>FIB-4 Index</i>					
Median (IQR)	1.1 (0.7-1.7)	0.99 (0.7-1.5)	1.4 (0.99-2.3)	0.8 (0.5-1.3)	< 0.001
< 1.45	640 (67.0)	343 (53.6)	181 (28.3)	116 (18.1)	< 0.001
1.45-3.25	255 (26.7)	106 (41.6)	125 (49.0)	24 (9.4)	
> 3.25	60 (6.3)	11 (18.3)	48 (80.0)	1 (1.7)	
<i>Follow-up characteristics</i>					
<i>ART regimen</i>					
AZT+3TC+EFV/NVP	883 (92.5)	422 (47.8)	331 (37.5)	130 (14.7)	0.635
TDF+3TC+EFV/NVP	72 (7.5)	38 (52.8)	23 (31.9)	11 (15.3)	
<i>Duration of ART (months)</i>					
< 3	220 (23.0)	115 (52.3)	74 (33.6)	31 (14.1)	0.192
3-12	232 (24.3)	118 (50.9)	76 (32.8)	38 (16.4)	
13-36	279 (29.2)	134 (48.0)	105 (37.6)	40 (14.3)	
> 36	224 (23.5)	93 (41.5)	99 (44.2)	32 (14.3)	
<i>CD4 change (last follow-up vs. baseline)</i>					
Unchanged (within $\pm$ 30%)	303 (31.7)	171 (56.4)	93 (30.7)	39 (12.9)	0.002
Increased > 30%	609 (63.8)	267 (43.8)	250 (41.1)	92 (15.1)	
Decreased > 30%	43 (4.5)	22 (51.2)	11 (25.3)	10 (23.3)	

<sup>\*</sup>The proportion was calculated in row; <sup>\*\*</sup>The proportion was calculated in column; <sup>a</sup>Chi-square test for categorical variables or Kruskal-Wallis test for continuous variables, as appropriate; IQR, interquartile range; 3TC, lamivudine; TDF, tenofovir.

coinfection and HIV/HBV/HCV coinfection was 84.6% (808/955), 12.4% (118/955), 2.3% (22/955) and 0.7% (7/955), respectively.

### 3.1.3. FIB-4 index or liver fibrosis

The prevalence of liver fibrosis, *i.e.*, FIB-4  $\geq 1.45$ , was 33.0% (315/955) overall, 31.6% (255/808) for HIV mono-infections, 39% (46/118) for HIV/HBV coinfections, 45.5% (10/22) for HIV/HCV coinfections, and 57.1% (4/7) for HIV/HBV/HCV coinfections (Table 1). The prevalence of liver fibrosis was significantly different by HBV and/or HCV coinfection status, with participants co-infected with HBV and/or HCV being more likely to be living with liver fibrosis (Fisher's exact test,  $p = 0.043$ ). Furthermore, the proportion of participants with severe liver fibrosis, *i.e.*, FIB-4  $> 3.25$ , was 6.3% (60/955) overall, 5.3% (43/808) for HIV mono-infections, 11.9% (14/118) for HIV/HBV coinfections, 9.1% (2/22) for HIV/HCV coinfections, and 14.3% (1/7) for HIV/HBV/HCV coinfections.

### 3.2. Antiretroviral therapy

As shown in Table 1, 92.5% of the participants were prescribed with AZT+3TC+EFV/NVP while the other 7.5% were prescribed with TDF+3TC+EFV/NVP. The combination use of TDF+3TC, both of which are efficacious for HBV suppression, was more prevalent among HIV/HBV co-infected participants (15.2%, or 19/125) than among HIV mono-infected participants (6.4%, or 53/830) ( $\chi^2 = 12.11$ ,  $p < 0.001$ ). About 23% of the participants had received ART for less than three months, whereas 52.7% had received ART for more than one year (Table 1).

### 3.3. Follow-up characteristics

#### 3.3.1. CD4 cell count

After antiretroviral therapy, 63.8% of the participants had  $> 30\%$  increases in CD4 cell count or CD4 cell recovery, whereas 4.5% had  $> 30\%$  decreases in CD4 cell count. CD4 cell count remained constant from the baseline to the last follow-up after ART among 31.7% of the participants (Table 1).

#### 3.3.2. FIB-4 index or liver fibrosis

After antiretroviral therapy, 354 participants (37.1%) had  $> 30\%$  decreases in FIB-4 index (*i.e.*, improvement of liver fibrosis), 141 (14.8%) had  $> 30\%$  increases in FIB-4 index (*i.e.*, progression of liver fibrosis), while the remaining 460 participants (48.2%) had stabilized FIB-4 index. As shown in Table 1, The FIB-4 changing status after ART was significantly associated with the participant's baseline FIB-4 score but not significantly

associated with other baseline characteristics. Participants with different CD4 cell count changing status also showed different FIB-4 changing status after ART, with a higher proportion of FIB-4 increase observed among those with decreased CD4 cell count (Table 1).

### 3.4. Predictors for improvement of liver fibrosis after ART

According to univariate logistic regression analysis, improvement of liver fibrosis after ART was significantly associated with baseline FIB-4 index, duration of ART and CD4 cell count changing status (Table 2). After adjusted for potential confounding effects of the other variables using multiple logistic regression model, improvement of liver fibrosis after ART was negatively associated with an older age (aOR <sub>$\geq 45$  vs. 18-24</sub> = 0.42, 95% CI: 0.23-0.76), but was positively associated with baseline FIB-4 index (aOR<sub>1.45-3.25 vs. <1.45</sub> = 3.53, 95% CI: 2.44-5.10; aOR <sub>$> 3.25$  vs. <1.45</sub> = 16.25, 95% CI: 7.93-33.29) and  $> 30\%$  increases in CD4 cell count after ART (aOR<sub>increased $> 30\%$  vs. unchanged</sub> = 1.46, 95% CI: 1.05-2.04) (Table 2).

### 3.5. Predictors for progression of liver fibrosis after ART

According to univariate logistic regression analysis, progression of liver fibrosis after ART was significantly associated with gender and HIV transmission mode, and baseline FIB-4 index (Table 3). After adjusted for potential confounding effects of the other variables using multiple logistic regression model, progression of liver fibrosis after ART was positively associated with an older age (aOR <sub>$\geq 45$  vs. 18-24</sub> = 2.62, 95% CI: 1.21-5.65), but was negatively associated with gender and HIV transmission mode (aOR<sub>male homosexual vs. male heterosexual</sub> = 0.50, 95% CI: 0.32-0.80; aOR<sub>female heterosexual vs. male heterosexual</sub> = 0.54, 95% CI: 0.32-0.90), and baseline FIB-4 index (aOR<sub>1.45-3.25 vs. <1.45</sub> = 0.31, 95% CI: 0.19-0.53; aOR <sub>$> 3.25$  vs. <1.45</sub> = 0.04, 95% CI: 0.01-0.34) (Table 3).

## 4. Discussion

This study, to the best of our knowledge, is the first community-based longitudinal cohort study to assess impact of ART on liver fibrosis among HIV-infected patients in Eastern China. We observed that one-third of the HIV-infected patients were living with liver fibrosis before ART and the majority of them had attenuated or stabilized liver fibrosis after ART. In a multicenter cross-sectional study of HIV-positive ART-naïve patients across twelve provinces in China, the proportion of participants with liver fibrosis or FIB-4  $\geq 1.45$  was 26.2% (12). Recently, Ding *et al* reported that the prevalence of liver fibrosis was as high as 42.5% among 3900 HIV-infected ART-naïve patients in

**Table 2. Logistic regression analyses of predictors for > 30% FIB-4 decrease or improvement of liver fibrosis after ART**

Characteristics	Crude OR (95% CI)	p	Adjusted OR (95% CI)	p
<i>Baseline characteristics</i>				
Age (years)				
18-24	1.00		1.00	
25-34	0.86 (0.55-1.32)	0.483	0.83 (0.52-1.33)	0.431
35-44	1.18 (0.77-1.82)	0.439	0.74 (0.44-1.25)	0.258
≥ 45	1.04 (0.68-1.59)	0.859	0.42 (0.23-0.76)	0.004
Marital status				
Unmarried	1.00		1.00	
Married	1.19 (0.87-1.62)	0.263	1.09 (0.72-1.65)	0.681
Gender and HIV transmission mode				
Male, heterosexual	1.00		1.00	
Male, homosexual	0.95 (0.70-1.30)	0.767	1.26 (0.88-1.80)	0.214
Female, heterosexual	1.10 (0.80-1.53)	0.533	1.16 (0.80-1.68)	0.441
FIB-4 Index				
< 1.45	1.00		1.00	
1.45-3.25	2.43 (1.80-3.29)	< 0.001	3.53 (2.44-5.10)	< 0.001
> 3.25	10.1 (5.26-19.5)	< 0.001	16.25 (7.93-33.29)	< 0.001
HBV coinfection				
No	1.00		1.00	
Yes	1.29 (0.88-1.89)	0.186	1.12 (0.74-1.71)	0.595
HCV coinfection				
No	1.00		1.00	
Yes	1.61 (0.77-3.37)	0.208	1.37 (0.61-3.10)	0.444
<i>Follow-up characteristics</i>				
ART regimen				
AZT+3TC+EFV/NVP	1.00		1.00	
TDF+3TC+EFV/NVP	0.78 (0.46-1.30)	0.350	0.74 (0.42-1.32)	0.314
Duration of ART (months)				
< 3	1.00		1.00	
3-12	0.96 (0.64-1.42)	0.842	0.95 (0.62-1.44)	0.799
13-36	1.19 (0.82-1.72)	0.355	1.11 (0.74-1.68)	0.608
> 36	1.56 (1.06-2.29)	0.022	1.29 (0.83-2.00)	0.257
CD4 change (last follow-up vs baseline)				
Unchanged (within ± 30%)	1.00		1.00	
Increased > 30%	1.57 (1.17-2.11)	0.002	1.46 (1.05-2.04)	0.024
Decreased > 30%	0.78 (0.38-1.61)	0.495	0.75 (0.34-1.65)	0.480

OR, odds ratio; CI, confidence interval.

**Table 3. Logistic regression analyses of predictors for a > 30% FIB-4 increase or progression of liver fibrosis after ART**

Characteristics	Crude OR (95% CI)	p	Adjusted OR (95% CI)	p
<i>Baseline characteristics</i>				
Age (years)				
18-24	1.00		1.00	
25-34	1.25 (0.67-2.33)	0.481	1.30 (0.67-2.50)	0.437
35-44	1.26 (0.67-2.34)	0.465	1.63 (0.79-3.35)	0.184
≥ 45	1.33 (0.72-2.46)	0.349	2.62 (1.21-5.65)	0.014
Marital status				
Unmarried	1.00		1.00	
Married	0.81 (0.54-1.21)	0.305	0.65 (0.39-1.10)	0.109
Gender and HIV transmission mode				
Male, heterosexual	1.00		1.00	
Male, homosexual	0.62 (0.41-0.95)	0.031	0.50 (0.32-0.80)	0.004
Female, heterosexual	0.51 (0.31-0.83)	0.006	0.54 (0.32-0.90)	0.018
FIB-4 Index				
< 1.45	1.00		1.00	
1.45-3.25	0.46 (0.29-0.74)	0.001	0.31 (0.19-0.53)	< 0.001
> 3.25	0.07 (0.01-0.55)	0.011	0.04 (0.01-0.34)	0.002
HBV coinfection				
No	1.00		1.00	
Yes	1.11 (0.66-1.86)	0.676	1.17 (0.68-2.03)	0.565
HCV coinfection				
No	1.00		1.00	
Yes	1.21 (0.45-3.22)	0.702	1.32 (0.47-3.71)	0.605
<i>Follow-up characteristics</i>				
ART regimen				
AZT+3TC+EFV/NVP	1.00		1.00	
TDF+3TC+EFV/NVP	1.04 (0.53-2.03)	0.898	0.96 (0.47-1.97)	0.910
Duration of ART (months)				
< 3	1.00		1.00	
3-12	1.19 (0.71-1.99)	0.499	1.11 (0.65-1.91)	0.698
13-36	1.02 (0.61-1.69)	0.937	0.94 (0.54-1.61)	0.813
> 36	1.01 (0.59-1.73)	0.953	0.97 (0.54-1.74)	0.926
CD4 change (last follow-up vs baseline)				
Unchanged (within ± 30%)	1.00		1.00	
Increased > 30%	1.20 (0.80-1.80)	0.365	1.30 (0.84-2.01)	0.241
Decreased > 30%	2.05 (0.93-4.48)	0.072	1.79 (0.78-4.10)	0.170

OR, odds ratio; CI, confidence interval.

a rural prefecture of Yunnan province in Southwestern China (28). Obviously, these studies observed varied prevalence of liver fibrosis among HIV patients, which are mostly attributable to different sources and characteristics of the study participants. Nevertheless, all the aforementioned studies including the present study reported that liver fibrosis was more prevalent among patients with HBV and/or HCV coinfection than those with HIV monoinfection, which is also consistent with findings from other countries (22,29-31).

The existing literature extensively evaluates liver disease progression among HIV/HCV or HIV/ HBV coinfecting patients receiving ART (27,32-33), with only a few studies examining liver disease progression and potential risk factors among HIV-monoinfected patients. In the present study, we found that a substantial proportion of HIV-infected patients, regardless of HBV and/or HCV coinfection status, had remarkable reduction or improvement of liver fibrosis after ART, further corroborating long-term benefits of ART on liver diseases in Chinese HIV patients (28). Such improvement of liver fibrosis was significantly associated with age, baseline FIB-4 score and post-ART CD4 cell recovery. It is by definition that patients with higher baseline FIB-4 score had more chances to present a reduced FIB-4 score after ART while having less chances to present an increased FIB-4 score during the follow-up, as long as ART had beneficiary effects on liver fibrosis. In this study, HIV patients aged over 45 years were less likely to gain improvement of liver fibrosis than younger patients. This is not surprise given that the development of liver cirrhosis is generally a slow disease progression and takes over 20-30 years. In fact, a study of HBV infected patients in China revealed that the protective effect of female gender against hepatic cirrhosis gradually lost with increasing age (34). Therefore, the less improvement of liver fibrosis among the elders underscores the importance of more closely monitoring and intervening liver disease progression in HIV-infected elderly people. Furthermore, the significant association between increased CD4 cell count and improved liver fibrosis after ART observed by the present study as well as studies in China and other countries further indicates the importance of promotion of CD4 cell recovery and maintenance of normal immune status through combination antiretroviral therapy (cART) for HIV patients (23,35). Since early initiation of cART remarkably improves CD4 cell recovery and generally slows down the disease progression (14,36-38), it is highly recommended that HIV-infected patients should get treated soonest possible after HIV diagnosis.

On the other hand, about 14.8% of the HIV patients had development or progression of liver fibrosis during ART. In fact, rapid fibrosis development from ART as well as from the chronic HIV infection itself is of serious concern to HIV patients (28,39-41). The

pathophysiology of liver fibrosis in patients with HIV is a multifactorial process whereby chronic immune activation and inflammation that are unable to be fully suppressed by ART promote production of liver fibrosis. In addition, mitochondrial toxicity, triggered by both ART and HIV, contributes to intrahepatic damage, which is even more severe in patients coinfecting with viral hepatitis (42).

More progression of liver fibrosis was observed among the elders. As mentioned above, HIV patients suffered more and rapid progression in various chronic diseases including liver fibrosis as they are getting old. In the meantime, we also found that female gender was a protective predictor of liver fibrosis progression among treated HIV patients, especially compared with heterosexual men. This is consistent with observations among both HIV-infected and HIV-uninfected populations (34,43). Although this is most likely due to pathophysiological differences and differential responses to ART between males and females (44-46), the less exposure of female patients to behaviors that favorite liver disease progression such as smoking and drinking cannot be ruled out (10,47-48). Interestingly, we found that homosexual men or men who have sex with men (MSM) were less likely to encounter liver fibrosis progression than heterosexual men. The mechanisms are unknown and remain to be defined.

This study has a couple of limitations. First, misclassification of liver fibrosis is unavoidable when a noninvasive marker instead of liver biopsy was used to define liver fibrosis. However, the misclassification should be non-differential and in turn made the association estimates biased to be more conservative. Moreover, liver biopsy was not feasible in this large epidemiologic study. Second, life style data including alcohol use and physical exercise that have potential impacts on liver diseases were not collected in this study, further limiting our capacity to draw a powerful causal inference.

Despite the limitations, this large longitudinal study has several important clinical and public health implication. First, improvement of liver fibrosis is achievable among HIV patients with better CD4 cell recovery which can be expectable through early initiation of ART. Second, liver fibrosis and hepatotoxicity associated with ART should be monitored as early as possible and throughout till the end of treatment, with special attention to the elderly and heterosexual men.

#### Acknowledgements

This study was supported by Natural Science Foundation of China (Grant No. 81373062; 81361120385; 81402725), and Shanghai Municipal Health and Family Planning Commission (Grant No. GWTD2015S05; 15GWZK0101; 15GWZK0801).

## References

- Crane M, Iser D, Lewin SR. Human immunodeficiency virus infection and the liver. *World J Hepatol.* 2012; 4:91-98.
- Chun H M, Mesner O, Thio CL, *et al.* HIV outcomes in Hepatitis B virus coinfecting individuals on HAART. *J Acquir Immune Defic Syndr.* 2014; 66:197.
- Gilson RJ, Hawkins AE, Beecham MR, Ross E, Waite J, Briggs M, McNally T, Kelly GE, Tedder RS, Weller IV. Interactions between HIV and hepatitis B virus in homosexual men: Effects on the natural history of infection. *AIDS.* 1997; 11:597-606.
- Liu X, He N, Fu Z, Duan S, Gao M, Zhang ZF. Plasma HCV viral load among HCV mono-infected and HCV/HIV co-infected individuals in Yunnan Province, China. *Hepat Mon.* 2012; 12:453-459.
- de Lédighen V, Barreiro P, Foucher J, Labarga P, Castéra L, Vispo ME, Bernard PH, Martin-Carbonero L, Neau D, García-Gascó P, Merrouche W, Soriano V. Liver fibrosis on account of chronic hepatitis C is more severe in HIV-positive than HIV-negative patients despite antiretroviral therapy. *J Viral Hepat.* 2008; 15:427-433.
- Macías J, Berenguer J, Japón MA, Girón JA, Rivero A, López-Cortés LF, Moreno A, González-Serrano M, Iribarren JA, Ortega E, Miralles P, Mira JA, Pineda JA. Fast fibrosis progression between repeated liver biopsies in patients coinfecting with human immunodeficiency virus/hepatitis C virus. *Hepatology.* 2009; 50:1056-1063.
- Weber R, Sabin CA, Friis-Moller N, *et al.* Liver-related deaths in persons infected with the human immunodeficiency virus: The D:A:D study. *Arch Intern Med.* 2006; 166:1632-1641.
- Data Collection on Adverse Events of Anti-HIV drugs (D:A:D) Study Group, Smith C, Sabin CA, Lundgren JD, Thiebaut R, Weber R, Law M, Monforte Ad, Kirk O, Friis-Moller N, Phillips A, Reiss P, El Sadr W, Pradier C, Worm SW. Factors associated with specific causes of death amongst HIV-positive individuals in the D: A: D Study. *AIDS.* 2010; 24:1537-1548.
- He N, Chen L, Lin HJ, Zhang M, Wei J, Yang JH, Gabrio J, Rui BL, Zhang ZF, Fu ZH, Ding YY, Zhao GM, Jiang QW, Detels R. Multiple Viral Coinfections among HIV/AIDS Patients in China. *Biosci Trends.* 2011; 5:1-9.
- Luo X, Duan S, Duan Q, Pu Y, Yang Y, Ding Y, Gao M, He N. Alcohol use and subsequent sex among HIV-infected patients in an ethnic minority area of Yunnan Province, China. *PLoS One.* 2013; 8:e61660.
- Shen YZ, Wang ZY, Qi TK, Jiang XY, Song W, Tang Y, Wang JR, Liu L, Zhang RF, Zheng YF, Dai ZS, Lu HZ. Serological survey of viral hepatitis markers among newly diagnosed patients with HIV/AIDS in China. *HIV Med.* 2013; 14:167-175.
- Xie J, Han Y, Qiu Z, Li Y, Li Y, Song X, Wang H, Thio CL, Li T. Prevalence of hepatitis B and C viruses in HIV-positive patients in China: A cross-sectional study. *J Int AIDS Soc.* 2016; 19:20659.
- Zhang F, Zhu H, Wu Y, Dou Z, Zhang Y, Kleinman N, Bulterys M, Wu Z, Ma Y, Zhao D, Liu X, Fang H, Liu J, Cai WP, Shang H. HIV, hepatitis B virus, and hepatitis C virus co-infection in patients in the China National Free Antiretroviral Treatment Program, 2010-12: A retrospective observational cohort study. *Lancet Infect Dis.* 2014; 14:1065-1072.
- Li Y, Xie J, Han Y, Wang H, Lv W, Guo F, Qiu Z, Li Y, Du S, Song X, Zhu T, Thio CL, Li T. Combination Antiretroviral Therapy Is Associated With Reduction in Liver Fibrosis Scores in HIV-1-Infected Subjects. *Medicine (Baltimore).* 2016; 95:e2660.
- Zhang F, Dou Z, Ma Y, Zhao Y, Liu Z, Bulterys M, Chen RY. Five-year outcomes of the China National Free Antiretroviral Treatment Program. *Ann Intern Med.* 2009; 151:241-251.
- Dou Z, Zhang F, Zhao Y, Jin C, Zhao D, Gan X, Ma Y. Progress on China's national free antiretroviral therapy strategy in 2002-2014. *Zhonghua Liu Xing Bing Xue Za Zhi.* 2015; 36:1345-1350. (in Chinese)
- Yang J, Su S, Zhao H, Wang D, Wang J, Zhang F, Zhao Y. Prevalence and mortality of cancer among HIV-infected inpatients in Beijing, China. *BMC Infect Dis.* 2016; 16:82.
- Cadranel JF, Rufat P, Degos F. Practices of liver biopsy in France: Results of a prospective nationwide survey. *Hepatology.* 2000; 32:477-481.
- Sterling RK, Lissen E, Clumeck N, Sola R, Correa MC, Montaner J, Sulkowski M, Torriani FJ, Dieterich DT, Thomas DL, Messinger D, Nelson M. Development of a simple noninvasive index to predict significant fibrosis in patients with HIV/HCV coinfection. *Hepatology.* 2006; 43:1317-1325.
- Bruno R, Sacchi P, Cima S, Maiocchi L, Patruno SF, Klersy C, Barbarini G, Zuccaro V, Camma C, Filice G. Correlation between FIB4, liver stiffness and metabolic parameters in patients with HIV and hepatitis C virus co-infection. *Dig Liver Dis.* 2011; 43:575-578.
- Ucar F, Sezer S, Ginis Z, Ozturk G, Albayrak A, Basar O, Ekiz F, Coban S, Yuksel O, Armutcu F, Akbal E. APRI, the FIB-4 score, and Forn's index have noninvasive diagnostic value for liver fibrosis in patients with chronic hepatitis B. *Eur J Gastroenterol Hepatol.* 2013; 25:1076-1081.
- Park LS, Tate JP, Justice AC, Lo Re V 3rd, Lim JK, Bräu N, Brown ST, Butt AA, Gibert C, Goetz MB, Rimland D, Rodriguez-Barradas MC, Dubrow R. FIB-4 index is associated with hepatocellular carcinoma risk in HIV-infected patients. *Cancer Epidemiol Biomarkers Prev.* 2011; 20:2512-2517.
- Kooij KW, Wit FW, van Zoest RA, Schouten J, Kootstra NA, van Vugt M, Prins M, Reiss P, van der Valk M. Liver fibrosis in HIV-infected individuals on long-term antiretroviral therapy: Associated with immune activation, immunodeficiency and prior use of didanosine. *AIDS.* 2016; 30:1771-1780.
- Tincati C, Merlini E, Braidotti P, Ancona G, Savi F, Tosi D, Borghi E, Callegari ML, Mangiavillano B, Barassi A, Bulfamante G, d'Arminio Monforte A, Romagnoli S, Chomont N, Marchetti G. Impaired gut junctional complexes feature late-treated individuals with suboptimal CD4+ T-cell recovery upon virologically suppressive combination antiretroviral therapy. *AIDS.* 2016; 30:991-1003.
- Mendeni M, Focà E, Gotti D, Ladisa N, Angarano G, Albini L, Castelnuovo F, Carosi G, Quiros-Roldan E, Torti C. Evaluation of liver fibrosis: Concordance analysis between noninvasive scores (APRI and FIB-4) evolution and predictors in a cohort of HIV-infected patients without hepatitis C and B infection. *Clin Infect Dis.* 2011; 52:1164-1173.
- Boursier J, Konaté A, Gorea G, Reaud S, Quemener E, Oberti F, Hubert-Fouchard I, Dib N, Calès P. Reproducibility of liver stiffness measurement by

- ultrasonographic elastometry. *Clin Gastroenterol Hepatol.* 2008; 6:1263-1269.
27. ANRS CO13 HEPAVIH Cohort. Regression of liver stiffness after sustained hepatitis C virus (HCV) virological responses among HIV/HCV-coinfected patients. *AIDS.* 2015; 29:1821.
  28. Ding Y, Duan S, Ye R, Yang Y, Yao S, Wang J, Cao D, Liu X, Lu L, Jia M, Wu Z, He N. More Improvement than Progression of Liver Fibrosis Following Antiretroviral Therapy in A Longitudinal Cohort of HIV-infected Patients With or Without HBV and HCV Co-infections. *J Viral Hepat.* 2016; doi: 10.1111/jvh.12658.
  29. Martinez SS, Campa A, Li Y, Fleetwood C, Stewart T, Ramamoorthy V, Baum MK. Low Plasma Zinc Is Associated with Higher Mitochondrial Oxidative Stress and Faster Liver Fibrosis Development in the Miami Adult Studies in HIV Cohort. *J Nutr.* 2017; 147:556-562.
  30. Wandeler G, Mulenga L, Vinikoor MJ, Kovari H, Battagay M, Calmy A, Cavassini M, Bernasconi E, Schmid P, Bolton-Moore C, Sinkala E, Chi BH, Egger M, Rauch A. Liver fibrosis in treatment-naïve HIV-infected and HIV/HBV co-infected patients: Zambia and Switzerland compared. *Int J Infect Dis.* 2016; 51:97-102.
  31. Bailey H, Nizova N, Martsynovska V, Volokha A, Malyuta R, Cortina-Borja M, Thorne C. HCV co-infection and markers of liver injury and fibrosis among HIV-positive childbearing women in Ukraine: Results from a cohort study. *BMC Infect Dis.* 2016; 16:755.
  32. Schmid P, Bregenzer A, Huber M, Rauch A, Jochum W, Müllhaupt B, Vernazza P, Opravil M, Weber R. Progression of liver fibrosis in HIV/HCV co-infection: A comparison between non-invasive assessment methods and liver biopsy. *PLoS One.* 2015; 10:e0138838.
  33. Audsley J, Robson C, Aitchison S, Matthews GV, Iser D, Sasadeusz J, Lewin SR. Liver fibrosis regression measured by transient elastography in human immunodeficiency virus (HIV)-Hepatitis B virus (HBV)-coinfected individuals on long-term HBV-active combination antiretroviral therapy. *Open Forum Infect Dis.* 2016; 3:ofw035.
  34. You H, Kong Y, Hou J, *et al.* Female gender lost protective effect against disease progression in elderly patients with chronic hepatitis B. *Sci Rep.* 2016; 6:37498.
  35. Focà E, Fabbiani M, Prosperi M, *et al.* Liver fibrosis progression and clinical outcomes are intertwined: Role of CD4+ T-cell count and NRTI exposure from a large cohort of HIV/HCV-coinfected patients with detectable HCV-RNA: A MASTER cohort study. *Medicine(Baltimore).* 2016; 95:e4091.
  36. Ding Y, Duan S, Wu Z, Ye R, Yang Y, Yao S, Wang J, Xiang L, Jiang Y, Lu L, Jia M, Detels R, He N. Timing of antiretroviral therapy initiation after diagnosis of recent HIV infection and CD4+ T-cell recovery. *Clin Microbiol Infect.* 2016; 22:290. e5-8.
  37. Martin NK, Devine A, Eaton JW, Miners A, Hallett TB, Foster GR, Dore GJ, Easterbrook PJ, Legood R, Vickerman P. Modeling the impact of early antiretroviral therapy for adults coinfecting with HIV and hepatitis B or C in South Africa. *AIDS.* 2014; 28:S35-S46.
  38. Bräu N, Salvatore M, Ríos-Bedoya CF, Fernández-Carbia A, Paronetto F, Rodríguez-Orengo JF, Rodríguez-Torres M. Slower fibrosis progression in HIV/HCV-coinfected patients with successful HIV suppression using antiretroviral therapy. *J Hepatol.* 2006; 44:47-55.
  39. Limketkai BN, Mehta SH, Sutcliffe CG, Higgins YM, Torbenson MS, Brinkley SC, Moore RD, Thomas DL, Sulkowski MS. Relationship of liver disease stage and antiviral therapy with liver-related events and death in adults coinfecting with HIV/HCV. *JAMA.* 2012; 308:370-378.
  40. Pacheco YM, Jarrin I, Rosado I, Campins AA, Berenguer J, Iribarren JA, Rivero M, Muñoz-Medina L, Bernal-Morell E, Gutiérrez F, Leal M. Increased risk of non-AIDS-related events in HIV subjects with persistent low CD4 counts despite cART in the CoRIS cohort. *Antiviral Res.* 2015; 117:69-74.
  41. Konerman MA, Mehta SH, Sutcliffe CG, Vu T, Higgins Y, Torbenson MS, Moore RD, Thomas DL, Sulkowski MS. Fibrosis progression in human immunodeficiency virus/hepatitis C virus coinfecting adults: Prospective analysis of 435 liver biopsy pairs. *Hepatology.* 2014; 59:767-775.
  42. Debes JD, Bohjanen PR, Boonstra A. Mechanisms of Accelerated Liver Fibrosis Progression during HIV Infection. *J Clin Transl Hepatol.* 2016; 4:328-335.
  43. Boyd A, Bottero J, Mialhes P, Lascoux-Combe C, Rougier H, Girard PM, Serfaty L, Lacombe K. Liver fibrosis regression and progression during controlled hepatitis B virus infection among HIV-HBV patients treated with tenofovir disoproxil fumarate in France: A prospective cohort study. *J Int AIDS Soc.* 2017; 20:1-12.
  44. Maskew M, Brennan AT, Westreich D, McNamara L, MacPhail AP, Fox MP. Gender differences in mortality and CD4 count response among virally suppressed HIV-positive patients. *J Womens Health (Larchmt).* 2013; 22:113-120.
  45. Means AR, Risher KA, Ujeneza EL, Maposa I, Nondi J, Bellan SE. Impact of Age and Sex on CD4+ Cell Count Trajectories following Treatment Initiation: An Analysis of the Tanzanian HIV Treatment Database. *PloS One.* 2016; 11:e0164148.
  46. Cornell M, Myer L, Kaplan R, Bekker LG, Wood R. The impact of gender and income on survival and retention in a South African antiretroviral therapy programme. *Trop Med Int Health.* 2009; 14:722-731.
  47. Luo X, Duan S, Duan Q, Pu Y, Yang Y, Ding Y, Gao M, He N. Tobacco Use among HIV-infected Individuals in a Rural Community in Yunnan Province, China. *Drug Alcohol Depend.* 2014; 134:144-150.
  48. Lim JK, Tate JP, Fultz SL, Goulet JL, Conigliaro J, Bryant KJ, Gordon AJ, Gibert C, Rimland D, Goetz MB, Klein MB, Fiellin DA, Justice AC, Lo Re V 3rd. Relationship between alcohol use categories and noninvasive markers of advanced hepatic fibrosis in HIV-infected, chronic hepatitis C virus-infected, and uninfected patients. *Clin Infect Dis.* 2014; 58:1449-1458.

(Received March 17, 2017; Revised April 11, 2017; Accepted April 20, 2017)

# Re-entry and related predictors among HIV-infected clients receiving methadone maintenance treatment in Guangdong province, China

Xiaofeng Luo<sup>1,2</sup>, Xiao Gong<sup>1,2</sup>, Peizhen Zhao<sup>3</sup>, Xia Zou<sup>1,2</sup>, Wen Chen<sup>1,2</sup>, Li Ling<sup>1,2,\*</sup>

<sup>1</sup> Faculty of Medical Statistics and Epidemiology, School of Public Health, Sun Yat-sen University, Guangzhou, China;

<sup>2</sup> Sun Yat-sen Center for Migrant Health Policy, Sun Yat-sen University, Guangzhou, China;

<sup>3</sup> Guangdong Provincial Center for Skin Disease and STI Control, Guangzhou, China.

## Summary

This study examined the re-entry characteristics and related predictors among HIV-infected methadone maintenance treatment (MMT) clients in Guangdong, China. Data on HIV-infected MMT clients was obtained from the clinic MMT registration system in Guangdong. Of the 653 participants, only 9.0% remained in the MMT program until the end of the study. For the drop-outs, 70.0% returned to MMT at least once by the end of the study. Re-entry was independently associated with marital status ( $OR_{\text{never married}} = 2.24$ , 95% CI: 1.02-4.93;  $OR_{\text{married currently}} = 2.34$ , 95% CI: 1.05-5.22), being unemployed ( $OR = 1.92$ , 95% CI: 1.12-3.27), lower positive percentages of urine tests ( $OR_{<40\%} = 4.08$ , 95% CI: 2.21-7.54;  $OR_{40\%-80\%} = 2.52$ , 95% CI: 1.39-4.56), higher maintenance doses ( $OR = 3.78$ , 95% CI: 2.21-7.54) and poorer MMT attendance percentages ( $OR_{<20\%} = 282.02$ , 95% CI: 62.75-1268.11;  $OR_{20-49\%} = 20.75$ , 95% CI: 10.52-40.93;  $OR_{50-79\%} = 6.07$ , 95% CI: 3.44-10.73). A higher re-entry frequency was independently associated with lower education level ( $OR_{\text{junior high school}} = 0.49$ , 95% CI: 0.26-0.93), average drug use times less than twice ( $OR = 0.64$ , 95% CI: 0.41-1.00), lower positive percentages of urine tests ( $OR = 0.39$ , 95% CI: 0.22-0.70) and poorer percentages of MMT attendance ( $OR_{<20\%} = 7.24$ , 95% CI: 2.99-17.55;  $OR_{20-49\%} = 14.30$ , 95% CI: 5.94-34.42;  $OR_{50-79\%} = 6.15$ , 95% CI: 2.55-14.85). Re-entry and repeated re-entry were prevalent among HIV-infected MMT clients in Guangdong, underscoring the urgent needs of tailored interventions and health education programs for this population.

**Keywords:** Re-entry, methadone maintenance treatment (MMT), HIV, China

## 1. Introduction

Opioid dependence is a worldwide health problem that leads to enormous economic, personal and public health consequences (1). The World Health Organization (WHO) statistics show that an estimated 69,000 people die from opioid overdose each year; an estimated 15 million people suffer from opioid dependence, yet only 10% of them are receiving effective treatments (2).

Methadone is a safe, low-cost, convenient and effective substitute treatment drug for opioid dependence (3). Decades of experience have demonstrated that methadone maintenance treatment (MMT) is currently the most effective intervention measure for controlling opioid use and its related HIV transmission among opioid users (4-6). Meanwhile, MMT could improve stability for society (7) and help drug users recover their physical and social functions (8-10).

China has the largest number of intravenous drug users (IDUs) in the world (11), and it is well recognized that the national epidemic of HIV originated and spread rapidly in this group by sharing needles (11). In response, the Chinese government introduced MMT in 2004 to control the rapid spread of both heroin use and HIV transmission (12,13). From 2006, MMT was quickly expanded from its original 8 clinics in 2004 to

Released online in J-STAGE as advance publication April 18, 2017.

\*Address correspondence to:

Dr. Li Ling, School of Public Health, Sun Yat-sen University, 74 Zhongshan Road II, Guangzhou 510080, China.

E-mail: lingli@mail.sysu.edu.cn

767 clinics covering 28 Chinese provinces as of April 2015 (14,15). In the past decade, MMT has effectively reduced heroin use (14,16,17) and curbed the spread of HIV/AIDS among heroin addicts (17-19). According to official statistics, HIV incidence among clients has decreased from 0.95% in 2006 to 0.12% in 2014 since the implementation of the MMT program (15). As estimated, 15,000 new HIV infections among opioid addicts were prevented; consumption of heroin was reduced by 100 tons; and 65 billion Yuan (RMB) in heroin trade were avoided (15).

Nonetheless, MMT in China faces many challenges, such as low coverage (14) and high drop-out rates (20). So far, retention has proven to be a valuable indicator of MMT effectiveness (21). High drop-out means many clients terminated the treatment before obtaining therapeutic benefits. However, repeated drop-out and re-entry remains prevalent among clients in MMT programs, often for multiple episodes (22,23). With the expansion of the MMT program and the increase of treatment accessibility, this phenomenon appears to have increased (23). HIV-infected drug users have been regarded as a "dual risk" subgroup (24). They transmit HIV via either sharing needles or having unprotected sex with partners. A study has demonstrated that MMT not only decreased the frequency of drug use but also improved the health-related quality of life among HIV-infected opioid addicts (25). Therefore, it becomes particularly important to strengthen MMT retention in this subgroup. Given that there are limited resources for drug treatment programs in China, it is imperative to know the re-entry characteristics of HIV-infected attendees to maximize the impact of MMT and tailor it to effectively target the population. Therefore, we used the data from 14 clinics in Guangdong to evaluate the re-entry and correlates among HIV-infected MMT clients.

## 2. Materials and Methods

### 2.1. Ethics approval

This study was approved by the Institutional Review Board (IRB) of the School of Public Health of Sun Yat-sen University, Guangzhou, China (No: 2013-26).

### 2.2. Study site and participants

Fourteen MMT clinics located in 9 cities of Guangdong Province were chosen as the study site for this study. From July 2006 to December 2013, all registered HIV-infected MMT clients in the unified MMT management system who met the Chinese Classification of Mental Disorders version 3 criteria for opioid dependence (26), were 18 years old or above, tested to be HIV-infected and able to provide written informed consent were included in this study.

### 2.3. Study procedure

At admission, a structured interview was developed to assess demographic characteristics, drug use history and sexual activity history. An interview was conducted by local clinic staff that had been trained in administration of the interview schedule. In China, to help insure security, clients were asked to attend the clinic daily once they have been enrolled in the program to take their methadone doses under the supervision of clinic staff, and the data on doses and date were routinely collected and stored in the national unified MMT management system. Urine morphine tests were performed on a random day each month. Participants were provided with no incentives.

In China, each client has a unique MMT ID based on personal ID regardless of the re-entry times. The study period was defined as the duration between the first and the last methadone uptake date.

### 2.4. Measures

#### 2.4.1. Methadone maintenance doses and attendance

The average daily maintenance dose during the study period was calculated according to the following formula:

The average daily maintenance dose = total intake doses/total number of days taking methadone.

The percentage of MMT attendance during the study period was calculated according to the following formula:

The percentage of MMT attendance = (total actual number of days taking methadone/total expected number of days taking methadone) × 100%.

#### 2.4.2. Positive percentages of urine morphine tests

The percentage of urine morphine tests during the study period was calculated according to the following formula:

The percentage of urine morphine tests = (total number of positive urine morphine test results/total number of testing times) × 100%.

According to the positive percentage distribution, it was classified as < 40%, 40-80% and > 80%.

#### 2.4.3. Re-entry during the study period

In this study, "drop-out" was defined as a participant failing to continue MMT for 14 consecutive days (21,22), and the drop-outs included "loss-to-follow-up" and "re-entry". Those drop-outs who did not return by the end of the study were classified into the "loss-to-follow-up" group, while those who returned at least once by the end of the study were classified into the "re-entry" group.

For the "re-entry" group, the re-entry frequency was calculated based on the returned times over the study period, and it was classified as low (< once/year), moderate (1-2 times/year) and frequent (> twice/year) based on the distribution.

#### 2.4.4. HIV and urine morphine tests

Anti-HIV antibody was screened using an enzyme-linked immunosorbent assay (ELISA) technique (Beijing BGI-GBI BiotechCo., Ltd, Beijing, China). Any samples that screened HIV positive were confirmed using a Western blot assay (Abbott, MP Biomedicals, LLC, Singapore) by the local CDC (Centers for Disease Control).

Urine morphine was screened using a Morphine Diagnostic Kit (Colloidal Gold) technique (ABON Biopharm Co., Ltd, Hangzhou, China).

#### 2.5. Statistical analysis

All analyses were performed in SPSS version 17.0 for Windows (SPSS Inc., Chicago). Categorical variables were presented with percentages. Binary logistic regression analyses (including univariate and multivariate analyses) were performed to explore correlates of re-entry; and multivariate ordinal logistic regression analysis was conducted to explore correlates of higher frequency of re-entry. The criterion for statistical significance was  $p < 0.05$ .

### 3. Results

#### 3.1. Study participants and demographic characteristics

Totally, there were 805 registered HIV-infected MMT clients between Jul. 2006 and Dec. 2013 in the unified MMT management system. Among them, 81.1% (653 of 805) were eligible for this study.

Among the 653 participants, 22.1% were older than 40; 93.4% were males; 99.1% were ethnic Han, 53.1% were never married; 63.4% had received junior high school education; 64.2% were unemployed; only 23.7% had a harmonious family relationship; and 61.7% relied on their family or friends (Table 1).

#### 3.2. Multiple sex partners at baseline

Among all participants, 17.3% had had sexual activity with multiple sex partners (Table 1).

#### 3.3. Heroin use

Table 1 presents detailed information about opioid use at baseline among the study participants. Among the participants, only 21.4% had used drugs less than 10 years; 64.8% participants used drugs on average at

least 3 times per day; 97.7% abused heroin, and 98.6% abused drugs by injection. Among the IDUs, 58.7% shared intravenous needles to inject drugs. Only 12.4% reported never meeting drug users.

As Table 1 summarizes, the positive percentage of urine morphine results that < 0%, 40-80% and > 80% were 29.0%, 32.6% and 38.4% respectively during the study period.

#### 3.4. Average maintenance dose and attendance

Of the participants, only 39.4% received doses of more than 60 mg/day. Also, 20.1% participants' attendance rates were less than 20%, and only 35.8% over 80% (Table 1).

#### 3.5. Re-entry during the study period

Only 9.0% (59 of 653) participants remained in the MMT during the study period. For the 594 drop-outs, 70.0% (416 of 594) returned to MMT at least once by the end of the study (Table 1). Of the 416 participants who experienced re-entries, the re-entry frequencies of < 1, 1- and 2- times/year were 51.9%, 22.6% and 9.4% respectively; and 5.3% returned to MMT  $\geq 5$  times/year (Table 2). The distribution of re-entry frequency at different entry years and institutions are listed in Table 3.

After controlling for potential confounding variables, multivariate binary logistic regression analysis indicated that re-entry was independently associated with marital status, being unemployed, lower positive proportion of urine tests, higher maintenance doses and poorer percentages of MMT attendance (Table 4).

Multivariate ordinal logistic regression analysis indicated that after controlling for potential confounding variables among the re-entries, a higher re-entry frequency was independently associated with lower education level, average drug use times less than twice, lower positive proportion of urine tests and poorer MMT attendance percentages (Table 5).

### 4. Discussion

Although MMT re-entry of general clients has previously been reported in China (22), to our knowledge, this is the first study to reveal the re-entry and re-entry frequency characteristics among HIV-infected MMT clients. In the present analyses, we observed a high re-entry rate (70.0%) among HIV-infected drug users, which was similar to that (two-thirds) reported by Bell and colleagues (23). However, this was lower than the rate of 81.2% in whole MMT clients in our previous study (22). This may be due to the fact that the HIV-infected clients (1) have much higher mortality than general clients (27); and (2) have higher continued heroin use rate than general clients (according to our previous studies, the rates were 75% for all clients

**Table 1. Characteristics of the participants**

Characteristics	Retain (n = 59) No. (%)	Re-entry (n = 416) No. (%)	Non-re-entry (n = 178 ) No. (%)	Total (n = 653) No. (%)
Age (years)				
≤ 30	8 (13.6)	83 (20.0)	24 (13.5)	115 (17.6)
31-35	13 (22.0)	127 (30.5)	53 (29.8)	193 (29.6)
36-40	15 (25.4)	133 (32.0)	53 (29.8)	201 (30.8)
≥ 41	23 (39.0)	73 (17.5)	48 (27.0)	144 (22.1)
Gender				
Male	54 (91.5)	388 (93.3)	168 (94.4)	610 (93.4)
Female	5 (8.5)	28 (6.7)	10 (5.6)	43 (6.6)
Ethnic				
Han	59 (100.0)	412 (99.0)	176 (98.9)	647 (99.1)
Others	0 (0)	4 (1.0)	2 (1.1)	6 (0.9)
Marital Status				
Single	32 (54.2)	230 (55.3)	85 (47.8)	347 (53.1)
Married Currently	18 (30.5)	146 (35.1)	67 (37.6)	231 (35.4)
Others	9 (15.3)	40 (9.6)	26 (14.6)	75 (11.5)
Education Level				
Elementary or lower	11 (18.6)	110 (26.4)	49 (27.5)	170 (26.0)
Junior high school	39 (66.1)	261 (62.7)	114 (64.0)	414 (63.4)
Senior high school or higher	9 (15.3)	45 (10.8)	15 (8.4)	69 (10.6)
Employed Status at Baseline				
Unemployed	39 (66.1)	273 (65.6)	107 (60.1)	419 (64.2)
Employed	20 (33.9)	143 (34.4)	71 (39.9)	234 (35.8)
Family Relationship at Baseline				
Harmonious	12 (20.3)	94 (22.6)	49 (27.5)	155 (23.7)
Inharmonious	47 (79.7)	322 (77.4)	129 (72.5)	498 (76.3)
Mainly Financial Sources at Baseline				
Family and Friends	35 (59.3)	263 (63.2)	105 (59.0)	403 (61.7)
Others	24 (40.7)	153 (36.8)	73 (41.0)	250 (38.3)
Duration of Drug Abuse (years)				
≤ 10	9 (15.3)	88 (21.2)	43 (24.2)	140 (21.4)
11-15	21 (35.6)	179 (43.0)	68 (38.2)	268 (41.0)
≥ 16	29 (49.2)	149 (35.8)	67 (37.6)	245 (37.5)
Type of Drug Use at Baseline				
Heroin	57 (96.6)	408 (98.1)	173 (97.2)	638 (97.7)
Others	2 (3.4)	8 (1.9)	5 (2.8)	15 (2.3)
Drug administration method at Baseline				
Inhaled only	2 (3.4)	18 (4.3)	15 (8.4)	35 (5.4)
Injected only	54 (91.5)	387 (93.0)	159 (89.3)	600 (91.9)
Mixed (injected and inhaled)	3 (5.1)	11 (2.6)	4 (2.2)	18 (2.8)
Injected Drugs at Baseline				
Yes	58 (98.3)	413 (99.3)	173 (97.2)	644 (98.6)
No	1 (1.7)	3 (0.7)	5 (2.8)	9 (1.4)
Shared Needles to Inject Drugs at Baseline				
Yes	29 (50.0)	248 (60.0)	101 (58.4)	378 (58.7)
No	29 (50.0)	165 (40.0)	72 (41.6)	266 (41.3)
Average Times of Drug Use per Day at Baseline				
≤ 2	15 (25.4)	154 (37.0)	61 (34.3)	230 (35.2)
≥ 3	44 (74.6)	262 (63.0)	117 (65.7)	423 (64.8)
Frequency of Meeting with Peer Users at Baseline				
none	14 (23.7)	46 (11.1)	21 (11.8)	81 (12.4)
1-4/month	11 (18.6)	100 (24.0)	51 (28.7)	162 (24.8)
1-6/week	20 (33.9)	100 (24.0)	47 (26.4)	167 (25.6)
> 1/day	14 (23.7)	170 (40.9)	59 (33.1)	243 (37.2)
Multiple Sex Partners at Baseline				
Yes	5 (8.5)	79 (19.0)	29 (16.3)	113 (17.3)
No	54 (91.5)	337 (81.0)	149 (83.7)	540 (82.7)
Positive Proportion of Urine Tests* (%)				
< 40	32 (58.2)	111 (27.1)	40 (23.8)	183 (29.0)
40-80	13 (23.6)	146 (35.7)	47 (28.0)	206 (32.6)
> 80	10 (18.2)	152 (37.2)	81 (48.2)	243 (38.4)
Average Maintenance Dose (ml/day)				
≥ 60	37 (62.7)	176 (42.3)	44 (24.7)	257 (39.4)
< 60	22 (37.3)	240 (57.7)	134 (75.3)	396 (60.6)
Percentages of MMT Attendance (%)				
< 20	0 (0)	129 (31.0)	2 (1.1)	131 (20.1)
20-	0 (0)	121 (29.1)	20 (11.2)	141 (21.6)
50-	5 (8.5)	101 (24.3)	41 (23.0)	147 (22.5)
≥ 80%	54 (91.5)	65 (15.6)	115 (64.6)	234 (35.8)

\*: 21 participants had no urine test results.

**Table 2. Re-entry frequency among the re-entries during study period (n = 416)**

Frequency (times/year)	Number (n)	Percentage (%)
< 1	216	51.9
1-	94	22.6
2-	39	9.4
3-	28	6.7
4-	17	4.1
≥ 5	22	5.3

**Table 3. Re-entry frequency at the different entrant year and institution (n = 416)**

Variables	< 1 (n = 216) No. (%) <sup>a</sup>	1- (n = 94) No. (%) <sup>a</sup>	2- (n = 39) No. (%) <sup>a</sup>	3- (n = 28) No. (%) <sup>a</sup>	4- (n = 17) No. (%) <sup>a</sup>	≥ 5 (n = 22) No. (%) <sup>a</sup>	Total (n = 416) No. (%) <sup>b</sup>
<b>Year</b>							
2006	31 (64.6)	14 (29.2)	2 (4.2)	0 (0)	1 (2.1)	0 (0)	48 (11.5)
2007	64 (65.3)	16 (16.3)	10 (10.2)	3 (3.1)	1 (1.0)	4 (4.1)	98 (23.6)
2008	44 (53.7)	19 (23.2)	6 (7.3)	7 (8.)	2 (2.4)	4 (4.9)	82 (19.7)
2009	29 (54.7)	11 (20.8)	4 (7.5)	4 (7.5)	2 (3.8)	3 (5.7)	53 (12.7)
2010	11 (34.4)	11 (34.4)	2 (6.3)	2 (6.3)	2 (6.3)	4 (12.5)	32 (7.7)
2011	25 (44.6)	16 (28.9)	7 (12.5)	4 (7.1)	2 (3.6)	2 (3.6)	56 (13.5)
2012	11 (35.5)	6 (19.4)	4 (12.9)	2 (6.5)	6 (19.4)	2 (6.5)	31 (7.5)
2013	1 (6.3)	1 (6.3)	4 (25.0)	6 (37.5)	1 (6.3)	3 (18.8)	16 (3.8)
<b>Institution</b>							
No. 1	17 (60.7)	5 (17.9)	3 (10.7)	0 (0)	0 (0)	3 (10.7)	28 (6.7)
No. 2	2 (40.0)	2 (40.0)	0 (0)	0 (0)	0 (0)	1 (20.0)	5 (1.2)
No. 3	2 (20.0)	5 (50.0)	0 (0)	2 (20.0)	1 (10.0)	0 (0)	10 (2.4)
No. 4	4 (40.0)	1 (10.0)	2 (20.0)	1 (10.0)	1 (10.0)	1 (10.0)	10 (2.4)
No. 5	18 (62.1)	3 (10.3)	1 (3.4)	2 (6.9)	3 (10.3)	2 (6.9)	29 (7.0)
No. 6	12 (40.0)	12 (40.0)	1 (3.3)	2 (6.7)	0 (0)	3 (10.0)	30 (7.2)
No. 7	35 (48.6)	19 (26.4)	8 (11.1)	3 (4.2)	4 (5.6)	3 (4.2)	72 (17.3)
No. 8	30 (63.8)	6 (12.8)	4 (8.5)	2 (4.3)	1 (2.1)	4 (8.5)	47 (11.3)
No. 9	16 (57.1)	8 (28.6)	1 (3.6)	2 (7.1)	1 (3.6)	0 (0)	28 (6.7)
No. 10	6 (54.5)	3 (27.3)	0 (0)	1 (9.1)	1 (9.1)	0 (0)	11 (2.6)
No. 11	29 (46.8)	14 (22.6)	8 (12.9)	7 (11.3)	2 (3.2)	2 (3.2)	62 (14.9)
No. 12	12 (52.2)	6 (26.1)	4 (17.4)	0 (0)	1 (4.3)	0 (0)	23 (5.5)
No. 13	10 (45.5)	4 (18.2)	3 (13.6)	3 (13.6)	0 (0)	2 (9.1)	22 (5.3)
No. 14	23 (59.0)	6 (15.4)	4 (10.3)	3 (7.7)	2 (5.1)	1 (2.6)	39 (9.4)

<sup>a</sup>calculated by row, <sup>b</sup>calculated by column.

(28) and 98.4% for HIV-infected clients (unpublished) during the first 12 months after treatment initiation), and subsequent more likelihood of being incarcerated. Of course, the reasons for not re-entry become the next step, which needs to be solved urgently. In addition, we also found the re-entry frequency exceeded once per year among 48.1% clients. Given that repeated drop-out and re-entry could not reach the expected treatment targets, tailored intervention measures are urgently needed for the study population.

China has made impressive progress in the MMT program since 2004. The agencies that were tasked with the program's expansion have been confronted with many challenges (14). The major concern is retention. We found that marital status was associated with re-entry in our study. For many clients, marriage provides the primary form of social support. In China, those who were never married always lived with their parents and other members. The study suggested that being married and having a close relationship with a spouse were associated with better treatment outcomes over time (29). Therefore,

family members and/or spouse potentially played a crucial role in encouraging re-entry (30). It is widely recognized that drug-abuse will cause a huge loss of both life and wealth. For the HIV-infected MMT clients, most of them had lost work capacity and had prolonged unemployment. Economic pressures might force them into re-entry MMT. Literature has demonstrated that a poor knowledge level often contributes to the misconceptions about MMT, which could be potential factors causing drop-out (31). Our study found that clients with lower education levels were associated with lower re-entry frequency. This probably is because those misconceptions lead to immature drop-outs and re-entries (31). Hence, interventions strengthening accurate MMT information propagation should be greatly warranted.

Positive morphine urine results generally indicate heroin use by the clients within the last 2-3 days (32). Heroin use would decrease the retention rate among HIV-infected MMT clients (33). Concurrent heroin use was extremely prevalent among HIV-infected MMT clients, and our 12 month follow-up study has

**Table 4. Correlates of re-entry among the drop-outs (n = 577)**

Variables	Univariate		Multivariate	
	OR (95% CI) <sup>a</sup>	p	OR (95% CI)	p
Age (years)				
≤ 30	2.27 (1.27-4.07)	0.006	1.20 (0.49-2.94)	0.693
31-35	1.58 (0.97-2.56)	0.066	0.82 (0.40-1.68)	0.587
36-40	1.65 (1.020-2.68)	0.042	0.96 (0.49-1.88)	0.900
≥ 41	1.00		1.00	
Gender				
Male	0.83 (0.39-1.74)	0.825	1.03 (0.40-2.68)	0.955
Female	1.00		1.00	
Marital Status				
Single	1.76 (1.01-3.06)	0.045	2.24 (1.02-4.93)	0.045
Married Currently	1.42 (0.80-2.51)	0.233	2.34 (1.05-5.22)	0.038
Others	1.00		1.00	
Education Level				
Elementary or lower	0.75 (0.38-1.47)	0.399	0.89 (0.34-2.33)	0.814
Junior high school	0.76 (0.41-1.43)	0.396	0.82 (0.34-2.00)	0.667
Senior high school or higher	1.00		1.00	
Employed Status at Baseline				
Unemployed	1.27 (0.88-1.82)	0.200	1.92 (1.12-3.27)	0.017
Employed	1.00		1.00	
Family Relationship at Baseline				
Harmonious	0.77 (0.52-1.15)	0.198	0.93 (0.53-1.63)	0.794
Inharmonious	1.00		1.00	
Mainly Financial Sources at Baseline				
Family and Friends	1.20 (0.84-1.71)	0.331	0.97 (0.58-1.63)	0.914
Others	1.00		1.00	
Duration of Drug Abuse (years)				
≤ 10	0.92 (0.58-1.47)	0.920	0.74 (0.36-1.50)	0.401
11-15	1.18 (0.79-1.77)	0.410	1.14 (0.64-2.01)	0.658
≥ 16	1.00		1.00	
Shared Needles at Baseline				
Yes	1.13(0.79-1.61)	0.515	1.09 (0.65-1.84)	0.723
No	1.00		1.00	
Average Times of Drug Use per Day at Baseline				
≤ 2	1.13(0.78-1.63)	0.523	1.09 (0.65-1.84)	0.732
≥ 3	1.00		1.00	
Frequency of Meeting with Peer Users at Baseline				
none	0.76 (0.42-1.38)	0.367	0.96 (0.43-2.12)	0.915
1-4/month	0.68 (0.43-1.07)	0.093	0.83 (0.46-1.53)	0.557
1-6/week	0.74 (0.47-1.17)	0.192	0.74 (0.39-1.36)	0.344
> 1/day	1.00		1.00	
Multiple Sex Partners at Baseline				
Yes	1.20(0.76-1.92)	0.435	1.30 (0.68-2.48)	0.430
No	1.00		1.00	
Positive Percentages of Urine Tests (%)				
< 40	1.48 (0.94-2.32)	0.089	4.08 (2.21-7.54)	< 0.001
40-80	1.66 (1.08-2.53)	0.020	2.52 (1.39-4.56)	0.002
> 80	1.00		1.00	
Average Maintenance Dose (ml/day)				
≥ 60	2.23 (1.51-3.31)	< 0.001	3.78 (2.21-7.54)	< 0.001
< 60	1.00		1.00	
Percentages of MMT Attendance (%)				
< 20	114.12 (27.33-476.54)	< 0.001	282.08 (62.75-1268.11)	< 0.001
20-49	10.70 (6.10-18.78)	< 0.001	20.75 (10.52-40.93)	< 0.001
50-79	4.36 (2.71-7.00)	< 0.001	6.07 (3.44-10.73)	< 0.001
≥ 80%	1.00		1.00	

Note. <sup>a</sup>OR: Odds Ratio, CI: Confidence Interval, obtained from binary logistic regression analysis.

shown the concurrent heroin use rate reached 98.4% (unpublished data). We found that clients with lower positive percentages of urine morphine tests have more likelihood to return to the MMT, yet have a lower frequency of re-entry. These components should be

considered: *i*) after a period of treatment, addictive syndrome was clearly alleviated, so many clients might consider themselves recuperated enough to leave the program (34). However, not long after leaving MMT, they would experience the abstinence symptoms again

**Table 5. Correlates of higher frequency of re-entry among the re-entries (n = 416)**

Variables	low No. (%) <sup>*</sup>	moderate No. (%) <sup>*</sup>	frequent No. (%) <sup>*</sup>	OR (95% CI) <sup>a,b</sup>	p <sup>b</sup>
Age (years)					
≤ 30	51 (61.4)	17 (20.5)	15 (18.1)	0.63 (0.29-1.37)	0.246
31-35	63 (49.6)	30 (23.6)	34 (26.8)	0.82 (0.43-1.56)	0.547
36-40	68 (51.1)	30 (22.6)	35 (26.3)	0.83 (0.45-1.52)	0.540
≥ 41	34 (46.6)	17 (23.3)	22 (30.1)	1.00	
Gender					
Male	202 (52.1)	89 (22.9)	97 (25.0)	0.80 (0.35-1.84)	0.598
Female	14 (50.0)	5 (17.9)	9 (32.1)	1.00	
Marital Status					
Single	126 (54.8)	48 (20.9)	56 (24.3)	0.90 (0.43-1.88)	0.781
Married Currently	74 (50.7)	32 (21.9)	40 (27.4)	0.81 (0.39-1.69)	0.569
Others	16 (40.0)	14 (35.0)	10 (25.0)	1.00	
Education Level					
Elementary or lower	53 (48.2)	28 (25.5)	29 (26.4)	0.55 (0.27-1.13)	0.104
Junior high school	144 (55.2)	55 (21.1)	62 (23.8)	0.49 (0.26-0.93)	0.030
Senior high school or higher	19 (42.2)	11 (24.4)	15 (33.3)	1.00	
Employed Status at Baseline					
Unemployed	147 (53.8)	60 (22.0)	66 (24.2)	0.71 (0.45-1.11)	0.134
Employed	69 (48.3)	34 (23.8)	40 (28.0)	1.00	
Family Relationship at Baseline					
Harmonious	51 (54.3)	21 (22.3)	22 (23.4)	0.86 (0.52-1.42)	0.558
Inharmonious	165 (51.2)	73 (22.7)	84 (26.1)	1.00	
Mainly Financial Sources at Baseline					
Family and Friends	138 (52.5)	61 (23.2)	64 (24.3)	0.84 (0.55-1.29)	0.433
Others	78 (51.0)	33 (21.6)	42 (27.5)	1.00	
Duration of Drug Abuse (years)					
≤ 10	50 (56.8)	17 (19.3)	21 (23.9)	0.72 (0.39-1.32)	0.288
11-15	98 (54.7)	39 (21.8)	42 (23.5)	0.73 (0.46-1.17)	0.196
≥ 16	68 (45.6)	38 (25.5)	43 (28.9)	1.00	
Shared Needles Drugs at Baseline					
Yes	120 (48.4)	65 (26.2)	63 (25.4)	1.37 (0.89-2.09)	0.149
No	96 (57.1)	29 (17.3)	43 (25.6)	1.00	
Average Times of Drug Use per Day at Baseline					
≤ 2	89 (57.8)	34 (22.1)	31 (20.1)	0.64 (0.41-1.00)	0.050
≥ 3	127 (48.5)	60 (22.9)	75 (28.6)	1.00	
Frequency of Meeting with Peer Users at Baseline					
none	23 (50.0)	8 (17.4)	15 (32.6)	1.40 (0.70-2.79)	0.344
1-4/month	55 (55.0)	20 (20.0)	25 (25.0)	0.90 (0.53-1.51)	0.685
1-6/week	48 (48.0)	30 (30.0)	22 (22.0)	1.28 (0.76-2.16)	0.358
> 1/day	90 (52.9)	36 (21.2)	44 (25.9)	1.00	
Multiple Sex Partners at Baseline					
Yes	46 (58.2)	15 (19.0)	18 (22.8)	0.70 (0.41-1.20)	0.194
No	170 (50.4)	79 (23.4)	88 (26.1)	1.00	
Positive Percentages of Urine Tests (%)					
< 40	73 (65.8)	24 (21.6)	14 (12.6)	0.39 (0.22-0.70)	0.001
40-80	80 (54.8)	32 (21.9)	34 (23.3)	0.65 (0.40-1.05)	0.078
> 80	61 (40.1)	38 (25.0)	53 (34.9)	1.00	
Average Maintenance Dose (ml/day)					
≥ 60	96 (54.5)	41 (23.3)	39 (22.2)	0.92 (0.60-1.40)	0.684
< 60	120 (50.0)	53 (22.1)	67 (27.9)	1.00	
Percentages of MMT Attendance (%)					
< 20	59 (45.7)	27 (20.9)	43 (33.3)	7.24 (2.99-17.55)	<0.001
20-49	47 (38.8)	29 (24.0)	45 (37.2)	14.30 (5.94-34.42)	<0.001
50-79	53 (52.5)	30 (29.7)	18 (17.8)	6.15 (2.55-14.85)	<0.001
≥ 80%	57 (87.7)	8 (12.3)	0 (0)	1.00	

Note. <sup>a</sup> OR: Odds Ratio, CI: Confidence Interval; <sup>b</sup> Obtained from multivariate ordinal logistic regression analysis adjusting for potential confounding variables listed in the table; \* Proportions were calculated in the row.

and had to return to MMT; *ii*) the clients with lower positive percentages of urine morphine tests had a stronger desire to abstain from drug use, and if they had drug desire, they would prefer to receive MMT; *iii*) the clients with higher positive percentages of urine morphine tests might have a poorer desire to

abstain from drug use, which subjected them to drug expenditure concerns, and therefore they exhibited repeated drop-out and re-entry.

Doses have already been well documented to be a crucial component of MMT retention in varied settings (20,35-37). Higher doses of MMT are associated with

longer retention (37-39). The prescribed dose should be able to prevent withdrawal, block craving and discourage patients from reverting to heroin use (20). Our study revealed that clients (1) with higher maintenance doses or (2) with higher frequency of drug use at baseline had more likelihood to return to the MMT program. We speculated that those two group clients depended more seriously on heroin use, but given their low affordability for the drug fees, the clients had to return to the MMT program to alleviate the cravings. The US National Institutes of Health has recommended methadone doses should be not less than 60 mg/day (40). However, both staff and clients have a preference for lower doses in China (41). Concurrent heroin use was a common phenomenon among MMT clients (28,42), especially among HIV-infected clients (our unpublished data has shown the concurrent opioid use rate for 12 months was 98.4%), which could directly lead to drop-out (33). A study demonstrated that clients needed higher doses when they continued to use drugs during MMT (43). Also some scholars hold that HIV-infected clients probably require a higher methadone dose (27). However, further research is needed to provide solid evidence.

A daily MMT dose could relieve the drug craving for only 24-36 hours (44). If clients do not sufficiently adhere to the MMT, the effectiveness of the MMT program would be greatly compromised. We found that poorer attendance was associated with both re-entry and higher frequency of re-entry. The literature suggested that MMT-related misconceptions were very prevalent among newly recruited MMT clients in China, which eventually led to poor compliance and drop-outs (31,45). The primary reasons could be *i*) the clients regard MMT as a transient program for drug detoxification, and most of them did not want to remain on treatment once their addictive reactions are alleviated. However, once they leave MMT, they experience the abstinence symptoms again and cannot afford heroin, and they had to return to MMT (22); *ii*) many clients did not intend to terminate the service completely, since they want to switch back and forth freely between heroin use and MMT depending on the affordability for drug fees.

The present study has limitations. First, like most other studies involving high-risk behavior measures, recall bias and deliberate concealment are inevitable. Second, we could not obtain the reasons for not re-entry among those who have been lost to follow-up. Third, the enrolment period of this study lasted for seven years, demographic characteristics, risk behaviors and treatment performance may vary temporally. Fourth, the data of this study was extracted from the Chinese National MMT Program data system. Characteristics related to the participant's HIV infection and antiretroviral treatment status (*e.g.*, CD4 counts, HIV viral load, comorbidities, biochemical testing results particularly liver functions given a substantial proportion of drug users could be co-infected with HCV) might play an important role in re-

entry to MMT. Yet, that information was registered and managed by other special institutions, and we failed to obtain them in this study.

Despite these limitations, this study identified some important implications for future harm reduction programs targeting re-entry among HIV-infected MMT clients in Guangdong. Study results underscore the importance of *i*) providing continuous and efficient MMT consulting and health education interventions to HIV-infected clients as a strategy to address re-entry; also, the study showed that even health professionals had misconceptions about MMT (46). Clinic staff plays a critical role in retaining the participants in treatment, so it is necessary to provide on-going staff training to improve the quality of their services, increase their understanding of drug addiction and enhance their professionalism; and *ii*) strengthening and/or improving supervision measures to potentially improve MMT attendance. In addition, the effectiveness of higher-dose MMT vs. the standard dose deserves further research investigation.

#### Acknowledgements

This study was supported by the National Natural Science Foundation of China (grant no. 71173245 and 81473065 to L.L.) and China Medical Board (12-111 to L.L.). The funding agencies played no role in the study design, data collection, and data analysis, interpretation of study results and writing of the manuscript. We are grateful to the staff of MMT clinics in the study site for their valuable assistance in subject recruitment and data collection. We appreciate the HIV-infected MMT participants spending time and sharing with us their information.

#### References

1. World Health Organization. Guidelines for the psychosocially assisted pharmacological treatment of opioid dependence. Geneva, 2009.
2. World Health Organization. Information sheet on opioid overdose. Geneva 2014.
3. Gambashidze N, Sikharulidze Z, Piralishvili G, Gvakharia N. Evaluation of pilot methadone maintenance therapy in Georgia (Caucasus). *Georgian Med News*. 2008;25-30.
4. Gowing LR, Farrell M, Bornemann R, Sullivan LE, Ali RL. Brief report: Methadone treatment of injecting opioid users for prevention of HIV infection. *J Gen Intern Med*. 2006; 21:193-5.
5. Michels II, Stover H, Gerlach R. Substitution treatment for opioid addicts in Germany. *Harm Reduct J*. 2007; 4:5.
6. MacArthur GJ, Minozzi S, Martin N, Vickerman P, Deren S, Bruneau J, Degenhardt L, Hickman M. Opiate substitution treatment and HIV transmission in people who inject drugs: Systematic review and meta-analysis. *BMJ*. 2012; 345:e5945-e5945.
7. Nguyen TTM, Nguyen LT, Pham MD, Vu HH, Mulvey KP. Methadone maintenance therapy in Vietnam: An overview and scaling-up plan. *Adv Prev Med*. 2012;

- 2012:1-5.
8. Xiao L, Wu Z, Luo W, Wei X. Quality of Life of Outpatients in Methadone Maintenance Treatment Clinics. *J Acquir Immune Defic Syndr.* 2010; 53:S116-S120.
  9. Chou YC, Shih SF, Tsai WD, Li CS, Xu K, Lee TS. Improvement of quality of life in methadone treatment patients in northern Taiwan: A follow-up study. *BMC Psychiatry.* 2013; 13:190.
  10. Sun HM, Li XY, Chow EPF, Li T, Xian Y, Lu YH, Tian T, Zhuang X, Zhang L. Methadone maintenance treatment programme reduces criminal activity and improves social well-being of drug users in China: A systematic review and meta-analysis. *BMJ Open.* 2015; 5:e005997-e005997.
  11. Mathers BM, Degenhardt L, Phillips B, Wiessing L, Hickman M, Strathdee SA, Wodak A, Panda S, Tyndall M, Toufik A, Mattick RP. Global epidemiology of injecting drug use and HIV among people who inject drugs: A systematic review. *Lancet.* 2008; 372:1733-45.
  12. Sullivan SG, Wu Z. Rapid scale up of harm reduction in China. *Int J Drug Policy.* 2007; 18:118-128.
  13. Wu Z, Rou K, Cui H. The HIV/AIDS epidemic in China: History, current strategies and future challenges. *AIDS Educ Prev.* 2004; 16:7-17.
  14. Yin W, Hao Y, Sun X, Gong X, Li F, Li J, Rou K, Sullivan SG, Wang C, Cao X, Luo W, Wu Z. Scaling up the national methadone maintenance treatment program in China: Achievements and challenges. *Int J Epidemiol.* 2010; 39:ii29-ii37.
  15. The National Health and Family Planning Commission of the People's Republic of China. The national health and family planning commission published online. <http://www.nhfpc.gov.cn/zhuz/zxfb1/201506/f2bd445f5ec04085adb9b84d995cb22b.shtml> (accessed June 26, 2015). (in Chinese)
  16. Zhang L, Chow EP, Zhuang X, Liang Y, Wang Y, Tang C, Ling L, Tucker JD, Wilson DP. Methadone maintenance treatment participant retention and behavioural effectiveness in China: A systematic review and meta-analysis. *PLoS One.* 2013; 8:e68906.
  17. Pang L, Hao Y, Mi G, Wang C, Luo W, Rou K, Li J, Wu Z. Effectiveness of first eight methadone maintenance treatment clinics in China. *AIDS.* 2007; 21 Suppl 8:S103-7.
  18. Zou X, Ling L, Zhang L. Trends and risk factors for HIV, HCV and syphilis seroconversion among drug users in a methadone maintenance treatment programme in China: A 7-year retrospective cohort study. *BMJ Open.* 2015; 5:e008162.
  19. Dai J, Zhao L, Liang Y. Policy implementation of methadone maintenance treatment and HIV infection: Evidence from Hubei province, China. *Subst Abuse Treat Prev Policy.* 2013; 8:38.
  20. Zhou K, Zhuang G. Retention in methadone maintenance treatment in mainland China, 2004-2012: A literature review. *Addict Behav.* 2014; 39:22-29.
  21. Lin C, Hung C, Peng C, Chao E, Lee TS. Factors associated with methadone treatment duration: A Cox regression analysis. *PLoS One.* 2015; 10:e0123687.
  22. Zhang L, Zou X, Zhang D, Li X, Zhao P, Ling L. Investigation of repeat client drop-out and re-enrolment cycles in fourteen methadone maintenance treatment clinics in Guangdong, China. *PLoS One.* 2015; 10:e0139942.
  23. Bell J, Burrell T, Indig D, Gilmour S. Cycling in and out of treatment; participation in methadone treatment in NSW, 1990–2002. *Drug Alcohol Depen.* 2006; 81:55-61.
  24. Liu H, Grusky O, Li X, Ma E. Drug users: A potentially important bridge population in the transmission of sexually transmitted diseases, including AIDS, in China. *Sex Transm Dis.* 2006; 33:111-117.
  25. Tran BX, Ohinmaa A, Duong AT, Do NT, Nguyen LT, Nguyen QC, Mills S, Jacobs P, Houston S. Changes in drug use are associated with health-related quality of life improvements among methadone maintenance patients with HIV/AIDS. *Qual Life Res.* 2012; 21:613-623.
  26. National Working Group on Community-based Methadone Maintenance Treatment for Opium Dependents, National Training Center for Methadone Maintenance Treatment. Clinical guidelines of methadone maintenance treatment. 2005.
  27. Liu E, Rou K, McGoogan JM, Pang L, Cao X, Wang C, Luo W, Sullivan SG, Montaner JSG, Bulterys M, Detels R, Wu Z. Factors associated with mortality of HIV-positive clients receiving methadone maintenance treatment in China. *J Infect Dis.* 2013; 208:442-453.
  28. Luo X, Zhao P, Gong X, Zhang L, Tang W, Zou X, Chen W, Ling L. Concurrent heroin use and correlates among methadone maintenance treatment clients: A 12-month follow-up study in Guangdong Province, China. *Int J Environ Res Public Health.* 2016; 13:305.
  29. Heinz AJ, Wu J, Witkiewitz K, Epstein DH, Preston KL. Marriage and relationship closeness as predictors of cocaine and heroin use. *Addict Behav.* 2009; 34:258-263.
  30. Liu H, Li J, Lu Z, Liu W, Zhang Z. Does Chinese culture influence psychosocial factors for heroin use among young adolescents in China? A cross-sectional study. *BMC Public Health.* 2010; 10:563.
  31. Xu H, Gu J, Lau JTF, Zhong Y, Fan L, Zhao Y, Hao C, He W, Ling W. Misconceptions toward methadone maintenance treatment (MMT) and associated factors among new MMT users in Guangzhou, China. *Addict Behav.* 2012; 37:657-662.
  32. Couper FJ, Logan BK. Drug and human performance fact sheets. <https://one.nhtsa.gov/people/injury/research/job185drugs/index.htm> (accessed April, 2014).
  33. Jiang H, Cao X, Wang C, Luo W, Li J, Rou K, Zhang B, Fang Y, Li C. Study on the adherence and related determinants among HIV-positive clients under methadone maintenance treatment in Dali, Yunnan province from 2005 to 2013. *Chin J Epidemiol (in Chinese).* 2014; 35:255-258.
  34. Gu J, Xu H, Lau JTF, Hao Y, Zhong Y, Fan L, Zhao Y, Hao C, Ling W. Misconceptions predict dropout and poor adherence prospectively among newly admitted first-time methadone maintenance treatment clients in Guangzhou, China. *Addiction.* 2012; 107:1641-1649.
  35. Wickersham JA, Zahari MM, Azar MM, Kamarulzaman A, Altice FL. Methadone dose at the time of release from prison significantly influences retention in treatment: Implications from a pilot study of HIV-infected prisoners transitioning to the community in Malaysia. *Drug Alcohol Depen.* 2013; 132:378-382.
  36. Yang F, Lin P, Li Y, He Q, Long Q, Fu X, Luo Y. Predictors of retention in community-based methadone maintenance treatment program in Pearl River Delta, China. *Harm Reduct J.* 2013; 10:3.
  37. Bao YP, Liu ZM, Epstein DH, Du C, Shi J, Lu L. A meta-analysis of retention in methadone maintenance by dose and dosing strategy. *Am J Drug Alcohol Abuse.* 2009;

- 35:28-33.
38. Amato L, Davoli M, Perucci CA, Ferri M, Faggiano F, Mattick RP. An overview of systematic reviews of the effectiveness of opiate maintenance therapies: Available evidence to inform clinical practice and research. *J Subst Abuse Treat.* 2005; 28:321-9.
  39. Strain EC, Bigelow GE, Liebson IA, Stitzer ML. Moderate- vs high-dose methadone in the treatment of opioid dependence: A randomized trial. *JAMA.* 1999; 281:1000-5.
  40. NIH Consensus Conference. Effective medical treatment of opiate addiction. National Consensus Development Panel on Effective Medical Treatment of Opiate Addiction. *JAMA.* 1998; 280:1936-43.
  41. Lin C, Wu Z, Detels R. Family support, quality of life and concurrent substance use among methadone maintenance therapy clients in China. *Public Health.* 2011; 125:269-274.
  42. Wang R, Ding Y, Bai H, Duan S, Ye R, Yang Y, Wang J, Tang R, Gao M, He N. Illicit heroin and methamphetamine use among methadone maintenance treatment patients in Dehong Prefecture of Yunnan Province, China. *PLoS One.* 2015; 10:e0133431.
  43. Fareed A, Casarella J, Amar R, Vayalapalli S, Drexler K. Methadone maintenance dosing guideline for opioid dependence, a literature review. *J Addict Dis.* 2010; 29:1-14.
  44. Joseph H, Stancliff S, Langrod J. Methadone maintenance treatment (MMT): A review of historical and clinical issues. *Mt Sinai J Med.* 2000; 67:347-364.
  45. Gossop M, Stewart D, Marsden J. Treatment process components and heroin use outcome among methadone patients. *Drug Alcohol Depen.* 2003; 71:93-102.
  46. Leavitt SB. Methadone dosing & safety in the treatment of opioid addiction. *Funct Ecol.* 2001; 15:696-699.

(Received December 16, 2016; Revised March 9, 2016; Accepted March 27, 2017)

# Time series analysis of weekly influenza-like illness rate using a one-year period of factors in random forest regression

Hongyan Wu<sup>1</sup>, Yunpeng Cai<sup>1</sup>, Yongsheng Wu<sup>2</sup>, Ren Zhong<sup>1</sup>, Qi Li<sup>1</sup>, Jing Zheng<sup>3</sup>, Denan Lin<sup>3,\*</sup>, Ye Li<sup>1,\*</sup>

<sup>1</sup> Shenzhen Institutes of Advanced Technology, Chinese Academy of Sciences, China;

<sup>2</sup> Shenzhen Center for Disease Control and Prevention, Shenzhen, China;

<sup>3</sup> Shenzhen Health Information Center, Shenzhen, China.

## Summary

Influenza, a disease caused by a respiratory virus, sickened over 5,043,127 citizens in Shenzhen, China, from January 2014 to April 2016. An accurate forecasting of outbreaks of influenza-like illness (ILI, here we refer to ILI as the upper respiratory infection) could facilitate public health officials to suggest public health actions earlier. In this study, a random forest regression constructed with a one-year period of factors was adopted to forecast the weekly ILI rate using the clinical data from Shenzhen Health Information Center. The following conclusions were drawn based on this method: *i*) Compared to the predication with 52 (one-year) history observations, the accuracy of the predication was improved by adding another 52 first-order difference variables: mean absolute percentage error (MAPE) decreased from 5.04% to 4.35% and mean squared error (MSE) decreased from 2.85E-04 to 1.97E-04. *ii*) The variables with the first-order difference seemed more significant than the original history observations during the predication. In addition, both the recent observations and the later observations seemed important in the predicating procedure. *iii*) Analysis using the Pearson correlation concluded that weather conditions, the influence of which could have been implied by history observations and seemed insignificant for the predication, showed correlation to the weekly average temperature and maximum temperature. The correlation coefficients were -0.3656 and -0.3583, respectively.

**Keywords:** Time series analysis, random forest regression, influenza-like illness (ILI), mean absolute percentage error (MAPE), mean squared error (MSE), correlation

## 1. Introduction

Influenza is a disease caused by a respiratory virus, and can infect any age group. The illness ranges from mild to severe, and results in the death of thousands annually. An outbreak puts tremendous pressure on both clinicians

and patients. The accurate forecasting of influenza outbreaks could facilitate public health officials in taking more timely public health actions, such as suggesting school closures and allocating or temporarily readjusting medical resources for hospitals and medical centers. Studies suggest that by accurately forecasting the outbreak of influenza and by taking preventative and control measures, such as school closures, the impact of influenza could be minimized (1-3).

Time-series forecasting methods, which play an important role in disease prediction, analyze the patterns of past outbreaks and formulate a forecasting model from underlying temporal relationships (4). The autoregressive integrated moving average (ARIMA) method was first popularized by Box-Jenkins for analyzing time-series data (5). The study used this approach to investigate the influence of winter holiday break on

Released online in J-STAGE as advance publication May 8, 2017.

\*Address correspondence to:

Dr. Denan Lin, Shenzhen Health Information Center, 2210 North of Renmin Road, Luohu, Shenzhen, 518000, China.  
E-mail: ldn308@163.com

Dr. Ye Li, Shenzhen Institutes of Advanced Technology, Chinese Academy of Sciences, 1068 Xueyuan Avenue, Shenzhen University Town, Nanshan, Shenzhen 518055, China.  
E-mail: ye.li@siat.ac.cn

weekly influenza-like illness rates (6). Unfortunately, the ARIMA model suffers from two drawbacks. First, it assumes linear relationships between independent and dependent variables, and second, a constant standard deviation in errors develops in the model over time. Reference compared the performance of ARIMA and random forest time series to predict avian influenza H5N1 outbreaks (7,8), which revealed that random forest time series modeling provided enhanced results over existing time series models for the prediction of infectious disease outbreaks. Instead of utilizing clinical data, Google Flu Trends attempted to make accurate predictions by aggregating search queries. Although it achieved an impressive accuracy of 97% in its early stage, Google Flu Trends team no longer published current estimates because of its drop in accuracy in the interval of 2011-2013 (9,10). A study by the Institute of Cognitive Science Osnabrück also attempted to predicate flu trends by combining social media data (e.g. Twitter) with CDC data (11).

A key intuition in this study is that a flu season could be influenced by the conditions of the past year. Therefore the forecasting of weekly influenza-like illness (ILI) rate should consider not only recent observations as used in the traditional approaches (7,8) but also much later observations and their difference. Therefore, this paper adopted the weekly rate of the previous one-year observations and their first-order difference to the recent observation as the predictor space, and applied this novel predictor space to the random forest regression method to forecast the weekly ILI rate.

## 2. Materials and Methods

### 2.1. Data sources

Weather data were obtained from the Weather Channel (<https://weather.com/>), and clinical data were obtained from Shenzhen Health Information Center, which collected clinic visit information from January 1, 2014 to April 10, 2016, from 60 state hospitals, 6 mother and child care centers, and 619 community rehabilitation centers. Figure 1 illustrates the data, in which the Y axis represents the weekly ILI rate and the X axis represents outbreak time.

### 2.2. Methodology

*Random forest regression* is a tree-based method that involves stratifying or segmenting the predictor space into a number of simple regions. To make a prediction for a given observation, the mean of the response values of the training observations in the same region is typically applied. There are two steps to build a regression tree as follows:

i) Divide the predictor space  $X_1, X_2, \dots, X_p$  into  $j$

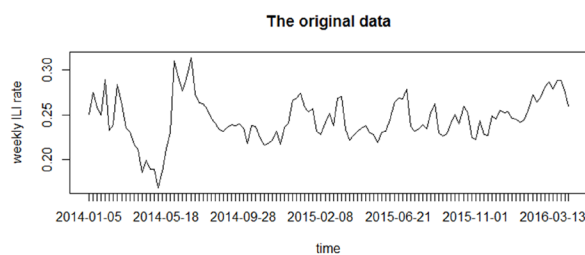


**Figure 1. Data from Shenzhen Health Information Center.** Y axis represents the weekly ILI rate; X axis represents outbreak time.

distinct and non-overlapping regions,  $R_1, R_2, \dots, R_j$ ;

ii) For every observation that falls into region  $R_j$ , the same prediction is made, which is simply the mean of the response values for the training observations in  $R_j$ .

By bootstrapping the entire training data set multiple times, bagging reduces the high variance to overcome the coherent overfitting problem in decision trees. For  $K$  bootstrapped training sets, the final prediction for the point  $x$  is as follows:

$$f(X) = \frac{1}{K} \sum_{k=1}^K T_k(x)$$

All bagged trees look similar to each other if a very strong predictor is always selected in the top split. Random forest de-correlates decision trees by allowing a randomly sampled subset ( $m$  features) from the full predictor space ( $p$  features). Random forest utilizes a group of "weak learners" to form a "strong learner" thereby improving the classification or regression performance. Two parameters are important in the random forest algorithm – the number of trees in the forest ( $n_{tree}$ ), and the number of predictors in each tree ( $m_{try}$ ). In this study, package "randomForest" in R was used. The default value for  $n_{tree}$  was adopted, and the function *tuneRF* was used to choose the optimal value of  $m_{try}$ .

*Predictor space* In this study, three kinds of components were chosen as the predictor space: history observations, first-order difference values and weather conditions. Assuming the current predicted point was  $X_0$ ; the first component was the sequence  $X_1, X_2, X_3, \dots, X_{t-1}, X_t$ , where  $t$  was 52, and was filled with the values of the previous 52 observations before  $X_0$ . The second component was the sequence  $D_1, D_2, D_3, \dots, D_t$ , where  $t$  was 52, and  $D_t$  meant the first order difference between  $X_1$  and the previous  $t$ th observation. The third component was composed of weather conditions *Temperature*, *Humidity*, *Wind\_speed*, and *Maximum\_temperature*, which denoted the weekly average of temperature, humidity, wind speed, and maximum temperature, respectively.

*Metrics* Mean absolute percentage error (MAPE) and mean squared error (MSE) were used to measure the prediction accuracy (12). MAPE and MSE are

defined as the following formula, respectively:

$$MAPE = \frac{100}{n} \sum_{t=1}^n \left| \frac{A_t - F_t}{A_t} \right|$$

$$MSE = \frac{1}{n} \sum_{t=1}^n (F_t - A_t)^2$$

where  $A_t$  is the actual value and  $F_t$  is the forecasted value.

*Variable importance* is a predictor ranking based on the contribution that predictors make to construct a tree. In this study, variable importance was computed using the percent increase in MSE, based upon the mean decrease of accuracy in predications on the out of bag samples when a given variable was excluded from the model.

### 3. Results

#### 3.1. Improved predication accuracy

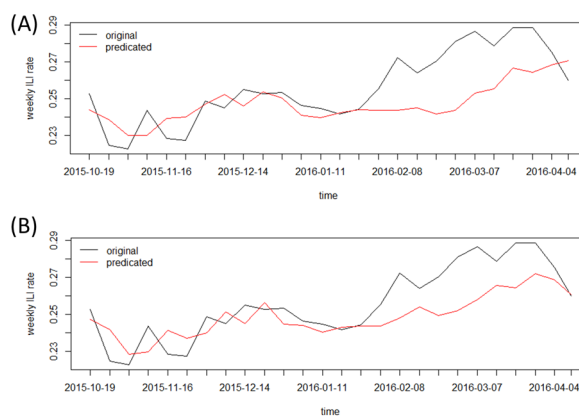
The data from Jan. 1, 2014, to Oct. 12, 2015 (93 week) were used as training data, and the half-year data from Oct. 19, 2015, to Apr. 10, 2016 (26 weeks) were used as the test data. The experiments were performed by iteratively adding a new week of data, training a new model based on the updated data, and predicating the value for the following week. To investigate the influence of different predictors on the predication accuracy, the experiments were carried out four times by gradually combining more predictors into the predictor space. In the first process, 52 recent observation variables X1,X2,X3,...,X51,X52 were chosen. In the second, 52 difference variables D1,...,D52 were combined into the predictor space. In the third, the weather conditions were added into the predictor space. Finally, the weather conditions were changed into the first-order difference values of each weather condition.

Figure 2A illustrates the first experiment of the weekly ILI rate with the predictor space of 52 recent

observations. Figure 2B shows the results of 104 predictors (52 difference predictors were added), which shows that the predication accuracy was improved. Compared to the forecast without using difference predictors, Table 1 shows that by adding the difference predictors MAPE decreased from 5.04% to 4.35% and MSE decreased from 2.85E-04 to 1.97E-04. Here, the detailed results of the last two experiments were not provided anymore because the weather conditions had almost made no influence on the predication accuracy.

#### 3.2. Comparison of variable importance

The top six variables in each model were checked according to their weights. Then, each variable was summed up in all the models, and the average weight was obtained and shown in Table 2. The following observations were made: *i*) Without using difference predictors, besides the recent variables (such as



**Figure 2. Prediction of Weekly ILI rate with different predictor spaces. (A).** The predictor space was composed of 52 recent observations. The black line illustrates the original data, and the red line shows the corresponding predicted values. **(B).** Here, 52 difference predictors were combined into the predictor space. The black line illustrates the original data, and the red line shows the corresponding predicted values

**Table 1. Comparison of forecasting with and without difference predictors**

Predictor space	MAPE (%)	MSE
Without difference predictors	5.04	2.85E-04
With difference predictors	4.35	1.97E-04

**Table 2. Comparisons of variable importance**

Variables	V1	V2	V3	V4	V5	V6
Without difference predictors						
Name	X1	X5	X24	X25	X52	X23
Weight (%)	9.11	6.85	4.21	3.64	2.44	1.86
With difference predictors						
Name	D3	D4	D8	X5	D34	D43
Weight (%)	5.58	4.35	4.15	3.65	2.12	1.64

**Table 3. Analysis of correlation between weather conditions and weekly ILI rate**

Variables	T	H	WS	MaxT	T <sub>d</sub>	H <sub>d</sub>	WS <sub>d</sub>	MaxT <sub>d</sub>
Coefficient	-0.3656	-0.08224	0.03954	-0.3583	0.1229	-0.1015	-0.1575	0.334
P-Value	0.00235	0.5082	0.7507	0.002907	0.3219	0.4135	0.2029	0.1199

X1, X5, etc.), the variables of the middle-distance observations (such as X24, X25) and the one-year-away observation (such as X52) seemed to be important; *ii*) The variables with the first-order difference seemed more important than the original history observations since D3, D4 and D8 have heavier weights than X5.

### 3.3. Analysis of weather conditions

The third and fourth experiments revealed that the addition of weather conditions into the predicator space did not significantly change the predication accuracy. The analysis of variable importance also showed that the weather-condition-related variables have no significant influence on the predication. However, it is already known that weather conditions are somewhat related to ILI, the influence of which could be implied by the history observations during the predication. In this section we did Pearson correlation analysis between ILI and weather conditions. We investigated the Pearson correlation between weekly ILI rate and the weekly average of temperature (*T*), humidity (*H*), wind speed (*WS*), the maximum temperature (*MaxT*), and their first-order difference (the corresponding variables are notated with a subscript *d*), respectively. Table 3 shows the weekly ILI rate in Shenzhen correlated to the weekly average temperature and the maximum temperature. The correlation coefficients were calculated as -0.3656 and -0.3583, respectively.

## 4. Discussion

Although every flu season is different because of environmental conditions and changes in the flu virus itself, influenza outbreaks could be influenced and predicated by the conditions of past years. The random forest methods used in the current studies (7,13,14) utilize the window size for lags is no bigger than three, which means the influence of later observations are not considered. In this study, by evaluating the variable importance, we found that both the recent observations and the later observations were interesting and had significant influence on the predication. The top six variables of the Shenzhen data were X1, X5, X24, X25, X52, and X23 without the difference predicators, and D3, D4, D8, X5, D34, and D43 with the difference predicators. However, because of changes in the virus and environmental factors, it is difficult to explain how and why the later observations influence the current predictions of influenza outbreaks.

Shenzhen has a humid subtropical maritime

climate. In the analysis of variable importance, we also checked weather conditions, which could influence influenza virus transmission (15-17). The weather conditions, including the weekly average temperature, humidity, wind speed, and maximum temperature, seemed insignificant for predication because their influence could be implied by the history observations. By analyzing the Pearson correlation, we found that the weekly average temperature and maximum temperature showed correlation to the predicated values with correlation coefficients of -0.3656 and -0.3583, respectively. Other factors, such as humidity, showed no apparent relationship. It was also noticed that by averaging the weekly value, the influence of weather conditions could be weakened. In the future, this conclusion should be verified with the investigation of more detailed daily data.

## 5. Conclusion

In this study, the random forest regression approach was adopted to forecast the weekly ILI rate. Compared to the predication with 52 one-year-previous observations, by adding an additional 52 first-order difference variables the accuracy was improved: the error decreased from 4.35% to 5.04% in MAPE and from 2.85E-04 to 1.97E-04 in MSE for the predication of the weekly ILI rate using the clinic data from the Shenzhen Health Information Center in China. The variables with the first-order difference seemed more important than the original history observations. However, both the recent observations and the later observations seemed to be important in the predicating procedure. By analyzing the Pearson correlation, the weather conditions, the influence of which could have been implied by the history observations and seemed insignificant for the predication, showed correlation coefficients of -0.3656 and -0.3583, respectively, to the weekly average temperature and the maximum temperature.

## Acknowledgements

This work has been supported by National High-tech R&D Program (863 Program) of China (SS2015AA020109) and by National Natural Science Foundation of China (81601575).

## References

1. Earn DJ, He D, Loeb MB, Fonseca K, Lee BE, Dushoff J. Effects of school closure on incidence of pandemic

- influenza in Alberta, Canada. *Ann Intern Med.* 2012; 156:173-181.
2. Cauchemez S, Valleron AJ, Boëlle PY, Flahault A, Ferguson NM. Estimating the impact of school closure on influenza transmission from Sentinel data. *Nature.* 2008; 452:750-754.
  3. Heymann AD, Hoch I, Valinsky L, Kokia E, Steinberg DM. School closure may be effective in reducing transmission of respiratory viruses in the community. *Epidemiol Infect.* 2009; 137:1369-1376.
  4. Chatfield C. *The analysis of time series: An introduction.* CRC press, New York, USA, 2016; pp. 1-15.
  5. Box GE, Jenkins GM, Reinsel GC. *Time series analysis: Forecasting and control.* John Wiley & Sons, Hoboken, New Jersey, USA, 2015; pp. 92-100.
  6. Gao H, Wong KK, Zheteyeva Y, Shi J, Uzicanin A, Rainey JJ. Comparing observed with predicted weekly influenza-like illness rates during the winter holiday break, United States, 2004-2013. *PLoS One.* 2015; 10:e0143791.
  7. Kane MJ, Price N, Scotch M, Rabinowitz P. Comparison of ARIMA and random forest time series models for prediction of avian influenza H5N1 outbreaks. *BMC Bioinformatics.* 2014; 15:276.
  8. Breiman L. Random forests. *Machine learning.* 2001; 45:5-32.
  9. Lazer D, Kennedy R, King G, Vespignani A. The parable of Google flu: Traps in big data analysis. *Science.* 2014; 343:1203-1205.
  10. Butler D. When Google got flu wrong. *Nature.* 2013; 494:155.
  11. IBM, University of Osnabrück cooperate to study innovative use of Twitter to predict flu outbreaks. <http://www.research-in-germany.org/en/research-landscape/news/2016/09/2016-09-14-ibm--university-of-osnabr-ck-cooperate-to-study-innovative-use-of-twitter-to-predict-flu-outbreaks.html> (accessed December 16, 2016).
  12. Lehmann EL, Casella G. *Theory of point estimation.* Springer Science & Business Media, New York, USA, 2006.
  13. Akhoondzadeh M. Decision Tree, Bagging and Random Forest methods detect TEC seismo-ionospheric anomalies around the time of the Chile, ( $M_w = 8.8$ ) earthquake of 27 February 2010. *Adv Space Res.* 2016; 57:2464-2469.
  14. Gopakumar S, Tran T, Luo W, Phung D, Venkatesh S. Forecasting patient outflow from wards having no real-time clinical data. *Healthcare Informatics (ICHI), 2016 IEEE International Conference on.* 2016. IEEE. <http://ieeexplore.ieee.org/document/7776342/?reload=true> (accessed December 16, 2016).
  15. Lowen AC, Steel J. Roles of humidity and temperature in shaping influenza seasonality. *Virology.* 2014; 88:7692-7695.
  16. Lowen AC, Mubareka S, Steel J, Palese P. Influenza virus transmission is dependent on relative humidity and temperature. *PLoS Pathog.* 2007; 3:1470-6.
  17. Oong XY, Ng KT, Lam TT, Pang YK, Chan KG, Hanafi NS, Kamarulzaman A, Tee KK. Epidemiological and evolutionary dynamics of influenza B viruses in Malaysia, 2012-2014. *PLoS One.* 2015; 10:e0136254.

(Received February 22, 2017; Revised April 7, 2017; Accepted April 18, 2017)

## Posttraumatic stress disorder eliminates association of *TrkB rs1187327* with HDL-C in Chinese Han adolescents

Ting Cao, Qiwei Guo, Mi Su, Yue Feng, Mei Fan, Yanjun Si, Nazakat H Memon, Jia Lin, Dingzhi Fang\*

Department of Biochemistry and Molecular Biology, West China School of Preclinical and Forensic Medicine, Sichuan University, Chengdu, China.

### Summary

Tropomyosin-related kinase receptor B (TrkB) has been observed to be a common player in posttraumatic stress disorder (PTSD) and the regulation of serum lipids levels. However, interplays of PTSD with TrkB on serum lipids levels have not been explored yet. This study was to investigate the interplays of PTSD and *TrkB rs1187327* on serum lipid profiles. Variants of *TrkB rs1187327* of 709 high school students were identified by polymerase chain reaction-restriction fragment length polymorphism (PCR-RFLP) analyses and verified by DNA sequencing. The PTSD Checklist Civilian Version (PCL-C) was used to assess PTSD. Colorimetric methods were used to determine the serum levels of triglyceride (TG), total cholesterol (TC), high-density lipoprotein cholesterol (HDL-C), low-density lipoprotein cholesterol (LDL-C) and glucose. The results show that the GG homozygotes had a significantly higher level of HDL-C than the A allele carriers of *TrkB rs1187327* after the adjustment for gender, age and body mass index (BMI) ( $1.44 \pm 0.299$  mmol/L vs.  $1.39 \pm 0.266$  mmol/L,  $p = 0.036$ ). When PTSD was taken into account, the higher than the A allele carriers level of HDL-C of the GG homozygotes was observed significant after the adjustment for gender, age and BMI only in the subjects without PTSD ( $1.44 \pm 0.293$  mmol/L vs.  $1.39 \pm 0.267$  mmol/L,  $p = 0.030$ ), but not in the subjects with PTSD. These results suggest that the A allele of *TrkB rs1187327* may be associated with decreased levels of serum HDL-C in general healthy adolescents, but not in adolescents with PTSD.

**Keywords:** BDNF-TrkB, SNP, lipids, PCR-RFLP

### 1. Introduction

Post-traumatic stress disorder (PTSD) is a prevalent, chronic and disabling anxiety disorder (1). It usually develops following exposures to traumatic events such as natural disasters, threatened deaths, serious injuries and sexual violence, and is characterized by an inability to extinguish fear memories (2-4). Evidences have been reported for a strong link between PTSD and

higher prevalence of cardiovascular diseases (CVD) (5,6). Meanwhile, abnormalities of serum lipid profiles are the major traditional risk factors of CVD, which include increased levels of serum triglycerides (TG), total cholesterol (TC) and more widely recognized low-density lipoprotein cholesterol (LDL-C), and decreased levels of high-density lipoprotein cholesterol (HDL-C) (7,8). Moreover, it was found that the levels of TC, TG and LDL-C were elevated but the level of HDL-C was reduced in war veterans with chronic PTSD when compared with healthy control subjects (9-11). However, in other studies, no significant differences were found in the levels of serum TC, LDL-C and HDL-C between veterans with and without PTSD (12). The mechanisms of these discrepancies have not been elucidated yet.

Brain-derived neurotrophic factor (BDNF) is one of the neurotrophins, which can exert its functions by

Released online in J-STAGE as advance publication June 18, 2017.

\*Address correspondence to:

Dr. Dingzhi Fang, MD, PhD, Department of Biochemistry and Molecular Biology, West China School of Preclinical and Forensic Medicine, Sichuan University, Chengdu 610041 P. R. China.

E-mail: dzfang@scu.edu.cn

activating the tropomyosin-related kinase receptor B (TrkB) (13), the high affinity receptor of BDNF. It was observed that BDNF was associated with memory and learning (14). Decreased levels of BDNF in various brain regions have been reported to be involved in psychiatric disorders and neurodegenerative pathogenesis (15). Single-nucleotide polymorphisms (SNPs) at the gene of BDNF were demonstrated to be indispensable to establish genetic risk factors for the onset and development of mental disorders including PTSD (16). For example, the SNP of Val66Met polymorphism has been confirmed to be related with PTSD (17). This polymorphism was tested to be associated with impaired fear extinction that was an indispensable character of PTSD (18). Moreover, previous studies have demonstrated that BDNF plays an important role in the regulation of glucose and lipids metabolisms. It was revealed that the serum level of BDNF was positively correlated with the serum levels of TG, TC and LDL-C (19-21). On the other hand, the transgenic mice overexpressing *TrkB* gene were reported to have enhanced ability to extinct fear memories (22), although this effect was not confirmed by the knockout of the gene because it resulted in that mice rarely survived beyond three weeks and the rest survived mice had serious health problems (23,24). Furthermore, the association of TrkB with serum lipid profiles has also been revealed. It was reported that there was a decreasing trend of HDL-C level in the transgenic mice overexpressing *TrkB* when compared with the control mice (25). All these evidences suggest that TrkB is involved in not only the development of PTSD but also the regulation of serum lipid profiles. Exploring the interactions between PTSD and TrkB on serum lipid profiles may provide novel insights into the regulation of lipoprotein metabolisms and the pathophysiological mechanism of dyslipidemia. Therefore, we hypothesized that PTSD may affect the association of TrkB with the levels of serum lipids. To test our hypothesis in the present study, the effect of PTSD on the levels of serum lipids was analyzed in high school students with different genotypes of the *rs1187327* polymorphism at the gene of *TrkB* (*TrkB rs1187327*) 6 months after Wenchuan earthquake, a catastrophic disaster occurred on May 12, 2008. The earthquake, measuring 8.0 on the Richter scale, extended about 10 thousand km<sup>2</sup>, destroyed about 6.5 million houses and left about 15 million people evacuated from their homes. According to the official statistics, 69 thousand people were confirmed dead and 37 thousand people injured. *TrkB rs1187327* polymorphism was selected in this study because it had been frequently studied and may have an effect on splicing or expression (26). In addition, studies have shown that *TrkB rs1187327* may contribute to the risk of mental diseases (27,28). To our knowledge, interactions between PTSD and *TrkB rs1187327* on the levels of serum lipids have not been explored before.

## 2. Materials and Methods

### 2.1. Study population

This study was conducted at the 6<sup>th</sup> month after the 2008 Wenchuan Earthquake in a boarding high school situated 10 kilometers away from the epicenter of the earthquake. The earthquake destroyed almost all the buildings at the school. The students lived and studied in temporary houses after the earthquake before their school was rebuilt.

The students were selected from grade 11 for this study. A total of 746 students participated in the questionnaire survey, 737 (98.8%) of the students completed the questionnaire. A total of 709 students were finally included in the study. The other students were excluded because (i) they did not complete all the questionnaires in the survey; (ii) they provided more than one answers for single-answer question, and/or no answers were chosen for any questions; (iii) their blood were not sampled because of personal reasons; and (iv) they had diseases, medications or other interferences that influenced serum lipid profiles or PTSD. The included 709 students were all Chinese Han people. All the students and their guardians provided written consents. This study was approved by the Human Ethics Committee of Sichuan University. All procedures performed in studies involving human participants were in accordance with the ethical standards of the institutional and/or national research committee and with the 1964 Helsinki declaration and its later amendments or comparable ethical standards.

### 2.2. Measurements

The measurement instrument consisted of two parts. The first part was used to assess demographic characteristics including gender, age, height and weight. Body mass index (BMI) was calculated. In the second part, the PTSD Checklist Civilian Version (PCL-C) was used to assess the symptoms of PTSD. It consists of 17 items based on Diagnostic and Statistical Manual of Mental Disorders, 4th edition (ASM-IV) criteria (27), with a total score from 17 to 85 (28). Cronbach's  $\alpha$  coefficient of the PCL-C ranged from 0.891 to 0.894 in the present study. The score of 50 was selected as cut-off point for PTSD (29-31).

### 2.3. DNA extraction and genotyping

Peripheral venous blood was sampled into sterile anticoagulant tubes. Genomic DNA was extracted using Wizard Genomic DNA Purification Kit (Tiandz, China) according to the procedure provided by the manufacture. *TrkB rs1187327* was genotyped by polymerase chain reaction restriction-fragment length polymorphism (PCR-RFLP) method and verified by

**Table 1. Distribution of the genotypes of *TrkB rs1187327***

Genotype	Total n (%)	Hardy-Weinberg <i>p</i>	Males n (%)	Females n (%)	<i>p</i> <sup>†</sup>
AA	125 (17.6)	0.987	60 (19.2)	65 (16.4)	0.401
AG	342 (48.2)		153 (49.0)	189 (47.6)	
GG	242 (34.1)		99 (31.7)	143 (36.0)	

<sup>†</sup> Males vs. females by Chi-Square tests.

**Table 2. Prevalence of PTSD in the subjects with different genotypes of *TrkB rs1187327***

PTSD	AX			GG		
	All (%)	Males (%)	Females (%)	All (%)	Males (%)	Females (%)
With	48 (10.3)	14 (6.6)	34 (13.4) <sup>#</sup>	27 (11.2)	4 (4.0)	23 (16.1) <sup>#</sup>
Without	419 (89.7)	199 (93.4)	22 (86.6)	215 (88.8)	95 (96.0)	120 (89.3)

Data are expressed as n (%). <sup>#</sup>*p* < 0.05 when compared with that of the male students.

DNA sequencing. The DNA fragments containing *TrkB rs1187327* were amplified using primers of 5'-GATGTTGAGCAGGCGTGATA-3' (forward) and 5'-GCAACACACAACCTTGCTGAAA-3' (reverse). DNA templates were denatured at 95°C for 5 min followed by 30 cycles consisting of denaturing at 95°C for 30 s, annealing at 56°C for 30 s and extension at 72°C for 30 s, with a final extension at 72°C for 5 min. The 341 bp PCR products were incubated with 4 units of *Eco471* (Shanghai) at 37°C for 12 hours. The digested fragments were then separated by electrophoresis on 2% agarose gel. The separated DNA fragments were 341 bp for the AA genotype, and 245 and 96 bp for the GG genotype.

#### 2.4. Blood collection and serum lipids analyses

Venous blood samples were collected between 7:00 a.m. and 8:00 a.m. after twelve-hour fasting. Enzymatic methods were used to determine the serum concentrations of TC, TG and glucose. HDL-C concentration was measured enzymatically after phosphotungstic-Mg<sup>2+</sup> precipitation of apolipoprotein B-containing lipoproteins. LDL-C concentration was quantified in the semi-automated biochemistry analyzer by the polyvinyl sulfate precipitation method. All biochemical parameters were measured three times, and the average values were used for statistical analyses.

#### 2.5. Statistical analyses

All the data are presented as mean ± standard deviation (SD) unless otherwise stated. The  $\chi^2$  goodness-of-fit test was performed to assess whether the genotypes of *TrkB rs1187327* were in the Hardy-Weinberg equilibrium. Chi-square tests were used to analyze the distribution of genotypes and PTSD prevalence between the male and female subjects, or PTSD prevalence between the subjects with different genotypes of

*TrkB rs1187327*. One-way ANOVAs were used to evaluate the differences of serum lipid levels and the related metabolic indices in the subjects with different genotypes of *TrkB rs1187327* before the adjustment for age, gender and BMI as covariates. Analyses of covariance (ANCOVA) with age, gender and BMI as covariates were used to analyze the differences of TC, TG, HDL-C, LDL-C and glucose in subjects with and without PTSD or/and with different genotypes of *TrkB rs1187327*. Age, gender and BMI were used as covariates because impacts of these variables were observed on serum lipids concentrations (12,32). All statistical analyses were 2-tailed with *p* ≤ 0.05 as the level of significance.

### 3. Results

#### 3.1. Distribution of the genotypes of *TrkB rs1187327*

As shown in Table 1, there was no significant deviation from Hardy-Weinberg equilibrium in the distribution of the genotypes of *TrkB rs1187327* (*p* = 0.987). Moreover, no significant differences were found of the genotypes between the male and female subjects (*p* = 0.401).

#### 3.2. Prevalence of PTSD in the subjects with different genotypes of *TrkB rs1187327*

For the further analyses, the AA homozygotes were combined with the heterozygotes and designated as the A allele carriers (AA/AG) because of the limited number. The prevalence of PTSD is shown in Table 2 for the subjects with different genotypes of *TrkB rs1187327*. There was no significant difference between the GG homozygotes and the A allele carriers in the all subjects, the male subjects or the female ones. However, the female subjects had higher prevalence of PTSD than the male subjects in both the GG homozygotes (*p*

**Table 3. Anthropometric and biochemical characteristics of the subjects with different genotypes of *TrkB rs1187327***

Variables	AX, n = 467	GG, n = 242	p-Value	ANCOVA, p-Value <sup>a</sup>
Gender: female, n (%)	254 (54.4%)	143 (59.1%)	0.012	–
Age, year	16.9 ± 0.574	16.9 ± 0.613	0.370	–
BMI, kg/m <sup>2</sup>	20.2 ± 2.21	20.4 ± 2.48	0.368	–
TC, mmol/L	3.56 ± 0.559	3.64 ± 0.600	0.178	0.178
TG, mmol/L	1.10 ± 0.419	1.14 ± 0.479	0.074	0.613
HDL-C, mmol/L	1.39 ± 0.266	1.44 ± 0.299	0.119	0.036
LDL-C, mmol/L	1.66 ± 0.476	1.68 ± 0.511	0.702	0.858
Glucose, mmol/L	5.08 ± 0.422	5.06 ± 0.460	0.374	0.619

BMI: body mass index; TG: triglycerides; TC: total cholesterol; HDL-C: High-density lipoprotein cholesterol; LDL-C: Low-density lipoprotein cholesterol; ANCOVA: analysis of covariance. <sup>a</sup>Analyses of covariance with the adjustment for age, gender and BMI.

**Table 4. Effects of PTSD on the association of *TrkB rs1187327* with anthropometric and biochemical characteristics**

Variables	Group	AX	GG	p-Value <sup>a</sup>	ANCOVA, p-Value <sup>a,b</sup>
Gender: female, n (%)	Control	220 (52.5%)	120 (70.8%)	0.450	–
	PTSD	34 (55.8%)	23 (85.2%)	0.260	–
Age, year	Control	16.9 ± 0.571	16.9 ± 0.608	0.459	–
	PTSD	16.9 ± 0.598	17.0 ± 0.649	0.525	–
BMI, kg/m <sup>2</sup>	Control	20.1 ± 2.18	20.2 ± 2.31	0.870	–
	PTSD	21.0 ± 2.32	22.1 ± 3.17	0.130	–
TC, mmol/L	Control	3.54 ± 0.547	3.62 ± 0.592	0.122	0.128
	PTSD	3.72 ± 0.631	3.77 ± 0.661	0.740	0.798
TG, mmol/L	Control	1.08 ± 0.376	1.12 ± 0.447	0.030	0.351
	PTSD	1.29 ± 0.665	1.29 ± 0.671	0.890	0.277
HDL-C, mmol/L	Control	1.39 ± 0.267	1.44 ± 0.293	0.229	0.030
	PTSD	1.41 ± 0.263	1.41 ± 0.340	0.247	0.866
LDL-C, mmol/L	Control	1.65 ± 0.463	1.67 ± 0.474	0.629	0.853
	PTSD	1.72 ± 0.577	1.78 ± 0.621	0.878	0.880
Glucose, mmol/L	Control	5.09 ± 0.427	5.06 ± 0.439	0.566	0.623
	PTSD	5.00 ± 0.371	4.99 ± 0.466	0.358	0.895

<sup>a</sup>Comparisons of those between the GG homozygotes and the A allele carriers in the control or PTSD subjects. <sup>b</sup>Analyses of covariance with the adjustment for gender, age and BMI.

= 0.003) and the A allele carriers ( $p = 0.016$ ).

### 3.3. Anthropometric and biochemical characteristics of the subjects with different genotypes of *TrkB rs1187327*

As presented in Table 3, there were no significant differences of the serum lipids levels between the GG homozygotes and the A allele carriers before the adjustment for age, gender and BMI. However, the GG homozygotes had a significantly higher level of HDL-C than the A allele carriers after the adjustment for gender, age and BMI although no other differences were observed after the adjustment.

### 3.4. Effects of PTSD on the association of *TrkB rs1187327* with anthropometric and biochemical characteristics

Table 4 presented the anthropometric and biochemical characteristics of the subjects with different genotypes of *TrkB rs1187327* and with or without PTSD. Before the adjustment for age, gender and BMI, the GG homozygotes without PTSD had significantly higher level of TG than the A allele carriers without PTSD. No other significant differences were observed between the

GG homozygotes and the A allele carriers in control or PTSD subjects. After the adjustment of age, gender and BMI, the GG homozygotes had significantly higher level of HDL-C than the A allele carriers only in the control subjects, but not in the subjects with PTSD. No other significant differences were tested between the GG homozygotes and the A allele carriers in control or PTSD subjects.

## 4. Discussion

BDNF-TrkB signaling pathway has been found to play an important role in lipid metabolism (19). However, the association of TrkB with serum lipid profiles has not been explored yet in human being, although it has been reported that there is a decreasing trend of HDL-C level in the transgenic mice overexpressing *TrkB* when compared with the control mice (25). Moreover, BDNF-TrkB signaling pathway has also been found to be an important player in the development of PTSD after stressed (15-17). Therefore, exploring the interplays of TrkB with PTSD on serum lipid profiles may provide novel insights into the mechanism of the regulation of serum lipids levels and pathophysiology of CVD,

especially in the subjects with PTSD. However, these interplays have not reported yet. In the present study, the association of *TrkB rs1187327* with the levels of serum lipids was investigated in high school students with or without PTSD. The results demonstrated that the GG homozygotes of *TrkB rs1187327* had significantly higher levels of HDL-C than the A allele carriers after the adjustment for gender, age and BMI (Table 3). When PTSD was taken into account, the higher than the A allele carriers levels of HDL-C of the GG homozygotes were observed significant after the adjustment for gender, age and BMI only in the subject without PTSD, but not in the subjects with PTSD (Table 4). These results suggest that *TrkB rs1187327* may be associated with the serum level of HDL-C and PTSD can modify and eliminate the association.

Plasma BDNF was found to be correlated with TG levels (33). In contrast, the expression of *TrkB* in endothelium was reduced in atherosclerotic lesions in the patients with high levels of TC, TG, LDL-C and glucose, when compared with that in the subjects with normal lipid profiles (34). Low levels of BDNF were reported to be in concurrence with reduced glucose metabolism and decreased HDL-C levels in Chinese people (35,36). However, a decreasing trend of HDL-C level was observed in the transgenic mice overexpressing *TrkB* when compared with the control mice (25). All these evidences suggest associations of *TrkB* with serum lipid profiles although they are indirect and inconstant. In the present study, the levels of HDL-C of the GG homozygotes were observed significant higher than the A allele carriers after the adjustment for gender, age and BMI only in the subject without PTSD, but not in the subjects with PTSD (Table 4). This result may be one of the explanations of the inconsistent relationship reported before between *TrkB* and the levels of serum lipids, and suggest that psychological factors such as PTSD need to be taken into account when the relationship is investigated. *TrkB rs1187327* is located in introns (26). The structure and the related functions of the encoded protein should not be changed. However, it has been observed that *TrkB rs1187327* is associated with psychiatric disorders such as bipolar disorder (26) and Alzheimer's disease (37). Therefore, the mutants of *TrkB rs1187327* may play a role in splicing or expression levels (26). Other mechanism such as linkage disequilibrium is also needed to be taken into account. There were some limitations in the present study. Firstly, serum levels of *TrkB* were not measured. Secondly, the levels of *TrkB* mRNA were not tested.

In conclusion, there may be some interplays of *TrkB rs1187327* with PTSD on serum lipid profiles, together with age, gender and BMI. After the adjustment of age, gender and BMI, the GG homozygotes had a significantly higher level of HDL-C than the A allele carriers. When PTSD was taken into account, the GG homozygotes had significantly higher levels of HDL-C

than the A allele carriers only in the control subjects, but not in the subjects with PTSD. These results suggest that the A allele of *TrkB rs1187327* may be associated with decreased level of serum HDL-C in general healthy adolescents, but not in adolescents with PTSD. This finding of the present study may provide new insights into the regulations of serum lipids levels and their mechanisms, and pave the way to precision medical intervention to reduce risks of cardiovascular diseases in young subjects, especially those with different genotypes of *TrkB rs1187327* and with or without PTSD.

### Acknowledgements

This study was supported by the Program of Sichuan Province for International Cooperation and Exchanges of Sciences and Technologies (Grant no. 2017HH0074). Professor Ding Zhi Fang is the recipient of the grant.

### References

1. Wentworth BA, Stein MB, Redwine LS, Xue Y, Taub PR, Clopton P, Nayak KR, Maisel AS. Post-traumatic stress disorder: A fast track to premature cardiovascular disease? *Cardiol Rev.* 2013; 21:16-22.
2. Lancaster CL, Teeters JB, Gros DF, Back SE. Posttraumatic Stress Disorder: Overview of Evidence-Based Assessment and Treatment. *J Clin Med.* 2016; 5:105.
3. Goenjian AK, Walling D, Steinberg AM, Karayan I, Najarian LM, Pynoos R. A prospective study of posttraumatic stress and depressive reactions among treated and untreated adolescents 5 years after a catastrophic disaster. *Am J Psychiatry.* 2005; 162:2302-2308.
4. Roussos A, Goenjian AK, Steinberg AM, Sotiropoulou C, Kakaki M, Kabakos C, Karagianni S, Manouras V. Posttraumatic stress and depressive reactions among children and adolescents after the 1999 earthquake in Ano Liosia, Greece. *Am J Psychiatry.* 2005; 162:530-537.
5. Lewis TT. Trauma and Posttraumatic Stress Disorder: Emerging Risk Factors for Cardiovascular Disease in Women? *Circulation.* 2015; 132:227-229.
6. Brudey C, Park J, Wiaderkiewicz J, Kobayashi I, Mellman TA, Marvar PJ. Autonomic and inflammatory consequences of posttraumatic stress disorder and the link to cardiovascular disease. *Am J Physiol Regul Integr Comp Physiol.* 2015; 309:R315-321.
7. Baigent C, Keech A, Kearney PM, Blackwell L, Buck G, Pollicino C, Kirby A, Sourjina T, Peto R, Collins R, Simes R. Efficacy and safety of cholesterol-lowering treatment: Prospective meta-analysis of data from 90,056 participants in 14 randomised trials of statins. *Lancet.* 2005; 366:1267-1278.
8. Mihaylova B, Emberson J, Blackwell L, Keech A, Simes J, Barnes EH, Voysey M, Gray A, Collins R, Baigent C. The effects of lowering LDL cholesterol with statin therapy in people at low risk of vascular disease: Meta-analysis of individual data from 27 randomised trials. *Lancet.* 2012; 380:581-590.
9. Vilibic M, Jukic V, Pandzic-Sakoman M, Bilic P, Milosevic M. Association between total serum cholesterol

- and depression, aggression, and suicidal ideations in war veterans with posttraumatic stress disorder: A cross-sectional study. *Croat Med J.* 2014; 55:520-529.
10. Karlovic D, Buljan D, Martinac M, Marcinko D. Serum lipid concentrations in Croatian veterans with post-traumatic stress disorder, post-traumatic stress disorder comorbid with major depressive disorder, or major depressive disorder. *J Korean Med Sci.* 2004; 19:431-436.
  11. Kagan BL, Leskin G, Haas B, Wilkins J, Foy D. Elevated lipid levels in Vietnam veterans with chronic posttraumatic stress disorder. *Biol Psychiatry.* 1999; 45:374-377.
  12. Jendricko T, Vidovic A, Grubisic-Ilic M, Romic Z, Kovacic Z, Kozaric-Kovacic D. Homocysteine and serum lipids concentration in male war veterans with posttraumatic stress disorder. *Prog Neuropsychopharmacol Biol Psychiatry.* 2009; 33:134-140.
  13. Huang EJ, Reichardt LF. Neurotrophins: Roles in neuronal development and function. *Annu Rev Neurosci.* 2001; 24:677-736.
  14. Barde YA. Neurotrophins: A family of proteins supporting the survival of neurons. *Prog Clin Biol Res.* 1994; 390:45-56.
  15. Mattson MP, Maudsley S, Martin B. A neural signaling triumvirate that influences ageing and age-related disease: Insulin/IGF-1, BDNF and serotonin. *Ageing Res Rev.* 2004; 3:445-464.
  16. Mahan AL, Ressler KJ. Fear conditioning, synaptic plasticity and the amygdala: Implications for posttraumatic stress disorder. *Trends Neurosci.* 2012; 35:24-35.
  17. Frielingsdorf H, Bath KG, Soliman F, Difede J, Casey BJ, Lee FS. Variant brain-derived neurotrophic factor Val66Met endophenotypes: Implications for posttraumatic stress disorder. *Ann N Y Acad Sci.* 2010; 1208:150-157.
  18. Soliman F, Glatt CE, Bath KG, *et al.* A genetic variant BDNF polymorphism alters extinction learning in both mouse and human. *Science.* 2010; 327:863-866.
  19. Suwa M, Kishimoto H, Nofuji Y, Nakano H, Sasaki H, Radak Z, Kumagai S. Serum brain-derived neurotrophic factor level is increased and associated with obesity in newly diagnosed female patients with type 2 diabetes mellitus. *Metabolism.* 2006; 55:852-857.
  20. Nurjono M, Tay YH, Lee J. The relationship between serum brain-derived neurotrophic factor (BDNF) and cardiometabolic indices in schizophrenia. *Schizophr Res.* 2014; 157:244-248.
  21. Golden E, Emiliano A, Maudsley S, Windham BG, Carlson OD, Egan JM, Driscoll I, Ferrucci L, Martin B, Mattson MP. Circulating brain-derived neurotrophic factor and indices of metabolic and cardiovascular health: Data from the Baltimore Longitudinal Study of Aging. *PLoS One.* 2010; 5:e10099.
  22. Koponen E, Voikar V, Riekkari R, Saarelainen T, Rauramaa T, Rauvala H, Taira T, Castren E. Transgenic mice overexpressing the full-length neurotrophin receptor *trkB* exhibit increased activation of the *trkB*-PLC $\gamma$  pathway, reduced anxiety, and facilitated learning. *Mol Cell Neurosci.* 2004; 26:166-181.
  23. Ernfors P, Lee KF, Jaenisch R. Mice lacking brain-derived neurotrophic factor develop with sensory deficits. *Nature.* 1994; 368:147-150.
  24. Klein R, Smeyne RJ, Wurst W, Long LK, Auerbach BA, Joyner AL, Barbacid M. Targeted disruption of the *trkB* neurotrophin receptor gene results in nervous system lesions and neonatal death. *Cell.* 1993; 75:113-122.
  25. Jiang H, Huang S, Li X, Li X, Huang S, Zhang Y, Chen ZY. Endothelial tyrosine kinase receptor B prevents VE-cadherin cleavage and protects against atherosclerotic lesion development in ApoE<sup>-/-</sup> mice. *Oncotarget.* 2015; 6:30640-30649.
  26. Dmítrzak-Węglarz M, Rybakowski JK, Suwalska A, Skibinska M, Leszczynska-Rodziewicz A, Szczepankiewicz A, Hauser J. Association studies of the BDNF and the NTRK2 gene polymorphisms with prophylactic lithium response in bipolar patients. *Pharmacogenomics.* 2008; 9:1595-1603.
  27. Trull TJ, Verges A, Wood PK, Jahng S, Sher KJ. The structure of Diagnostic and Statistical Manual of Mental Disorders (4th edition, text revision) personality disorder symptoms in a large national sample. *Personal Disord.* 2012; 3:355-369.
  28. Blanchard EB, Jones-Alexander J, Buckley TC, Forneris CA. Psychometric properties of the PTSD Checklist (PCL). *Behav Res Ther.* 1996; 34:669-673.
  29. Dobie DJ, Kivlahan DR, Maynard C, Bush KR, McFall M, Epler AJ, Bradley KA. Screening for post-traumatic stress disorder in female Veteran's Affairs patients: Validation of the PTSD checklist. *Gen Hosp Psychiatry.* 2002; 24:367-374.
  30. Jia Z, Tian W, Liu W, Cao Y, Yan J, Shun Z. Are the elderly more vulnerable to psychological impact of natural disaster? A population-based survey of adult survivors of the 2008 Sichuan earthquake. *BMC Public Health.* 2010; 10:172.
  31. Liu ZY, Yang YF, Ye YL, Zeng ZQ, Xiang YJ, Yuan P. One-year follow-up study of post-traumatic stress disorder among adolescents following the Wen-Chuan earthquake in China. *Biosci Trends.* 2010; 4:96-102.
  32. Craig WY, Palomaki GE, Haddow JE. Cigarette smoking and serum lipid and lipoprotein concentrations: An analysis of published data. *BMJ.* 1989; 298:784-788.
  33. Soavi C, Marusic U, Sanz JM, Morieri ML, Dalla Nora E, Simunic B, Pisot R, Zuliani G, Passaro A. Age-related differences in plasma BDNF levels after prolonged bed rest. *J Appl Physiol.* 2016; 120:1118-1123.
  34. Jiang H, Huang S, Li X, Li X, Zhang Y, Chen ZY. Tyrosine kinase receptor B protects against coronary artery disease and promotes adult vasculature integrity by regulating Ets1-mediated VE-cadherin expression. *Arterioscler Thromb Vasc Biol.* 2015; 35:580-588.
  35. Li B, Lang N, Cheng ZF. Serum Levels of Brain-Derived Neurotrophic Factor Are Associated with Diabetes Risk, Complications, and Obesity: A Cohort Study from Chinese Patients with Type 2 Diabetes. *Mol Neurobiol.* 2016; 53:5492-5499.
  36. Liu W, Han X, Zhou X, Zhang S, Cai X, Zhang L, Li Y, Li M, Gong S, Ji L. Brain derived neurotrophic factor in newly diagnosed diabetes and prediabetes. *Mol Cell Endocrinol.* 2016; 429:106-113.
  37. Vepsäläinen S, Castren E, Helisalmi S, Iivonen S, Mannermaa A, Lehtovirta M, Hanninen T, Soininen H, Hiltunen M. Genetic analysis of BDNF and *TrkB* gene polymorphisms in Alzheimer's disease. *J Neurol.* 2005; 252:423-428.

(Received February 24, 2017; Revised June 7, 2017; Accepted June 9, 2017)

# Unique *Trichomonas vaginalis* gene sequences identified in multinational regions of Northwest China

Jun Liu<sup>1,2</sup>, Meng Feng<sup>1</sup>, Xiaolan Wang<sup>3</sup>, Yongfeng Fu<sup>1</sup>, Cailing Ma<sup>4,\*</sup>, Xunjia Cheng<sup>1,\*</sup>

<sup>1</sup>Department of Medical Microbiology and Parasitology, School of Basic Medical Sciences, Fudan University, Shanghai, China;

<sup>2</sup>Department of Medical Parasitology, Xinjiang Medical University, Urumqi, China;

<sup>3</sup>Department of Prenatal Diagnosis Laboratory, the First Affiliated Hospital of Xinjiang Medical University, Urumqi, China;

<sup>4</sup>Department of Gynecology, the First Affiliated Hospital of Xinjiang Medical University, Urumqi, China.

## Summary

*Trichomonas vaginalis* (*T. vaginalis*) is a flagellated protozoan parasite that infects humans worldwide. This study determined the sequence of the 18S ribosomal RNA gene of *T. vaginalis* infecting both females and males in Xinjiang, China. Samples from 73 females and 28 males were collected and confirmed for infection with *T. vaginalis*, a total of 110 sequences were identified when the *T. vaginalis* 18S ribosomal RNA gene was sequenced. These sequences were used to prepare a phylogenetic network. The rooted network comprised three large clades and several independent branches. Most of the Xinjiang sequences were in one group. Preliminary results suggest that Xinjiang *T. vaginalis* isolates might be genetically unique, as indicated by the sequence of their 18S ribosomal RNA gene. Low migration rate of local people in this province may contribute to a genetic conservativeness of *T. vaginalis*. The unique genetic feature of our isolates may suggest a different clinical presentation of trichomoniasis, including metronidazole susceptibility, *T. vaginalis* virus or *Mycoplasma* co-infection characteristics. The transmission and evolution of Xinjiang *T. vaginalis* is of interest and should be studied further. More attention should be given to *T. vaginalis* infection in both females and males in Xinjiang.

**Keywords:** *Trichomonas vaginalis*, genetic diversity, 18S ribosomal RNA gene, multinational regions, Northwest China

## 1. Introduction

*Trichomonas vaginalis* (*T. vaginalis*) is a flagellated protozoan parasite that inhabits the vagina of females and the urethra, prostate gland, and epididymis of males (1). The WHO estimates that trichomoniasis affects more than 276 million people each year, with a worldwide prevalence of 22% for women and 2.2% for men (2). Trichomoniasis is more symptomatic in females than

males. Symptoms in females can be debilitating and severe, such that 89% of the diagnosed cases are in women. *T. vaginalis* has emerged as a major pathogen of non-gonococcal urethritis and may contribute to male infertility (3-5).

The traditional method for detecting trichomoniasis involves examination of samples using direct light microscopy. More recent studies have used culturing, serological diagnosis, and other molecular methods to detect trichomoniasis. For example, the 18S ribosomal RNA gene is conserved in primary structure, making it a good target for detecting *T. vaginalis* by PCR. In addition, PCR-based gene sequencing has been used to examine *T. vaginalis* genotypes (6-9). Conrad *et al.* used 27 polymorphic markers, including 21 microsatellite and 6 single-copy genes, to study genetic diversity in *T. vaginalis* and identified two population types (6). Previous studies had also been done on the relationship between its genotype and the clinical presentation of trichomoniasis, including drug susceptibility and

Released online in J-STAGE as advance publication June 11, 2017.

\*Address correspondence to:

Dr. Xunjia Cheng, Department of Medical Microbiology and Parasitology, School of Basic Medical Sciences, Fudan University, Shanghai 200032, China.

E-mail: xjcheng@shmu.edu.cn

Dr. Cailing Ma, Department of Gynecology, the First Affiliated Hospital of Xinjiang Medical University, Urumqi 830054, China.

E-mail: hymcl@sina.com

microbial symbiosis (6-9).

Most studies of *T. vaginalis* focus on women, with samples collected from vaginal swabs. Genetic information from *Trichomonas* in male patients remains largely unknown. In this study, we extracted DNA from vaginal swabs of women and semen samples of men, respectively, infected with *T. vaginalis* in Xinjiang Province, China. The 18S ribosomal gene of *T. vaginalis* was amplified and analyzed to evaluate the molecular epidemiology of *T. vaginalis* in this multi-ethnic region. Preliminary results suggest that a unique 18S ribosomal RNA gene of *T. vaginalis* was detected in these samples.

## 2. Materials and Methods

### 2.1. Sample collection

Seventy-three women and 28 men of childbearing age (range, 20-39 years) who attended the First Affiliated Hospital of Xinjiang Medical University and produced leukorrhea or semen infected with *T. vaginalis* were selected for the present study. The participants included several ethnic groups, including 63 Han, 20 Uyghur, 6 Mongolian, 6 Kazakh, 3 Hui, 1 Khalkhas, and 2 foreigners (from Russia, 22 and 38 years old). Detailed

participant information is presented in Table 1. The institutional ethics committees of the First Teaching Hospital of Xinjiang Medical University approved the protocol (Ethics approval number: 20150402-06).

### 2.2. Sample evaluation by microscopy and genomic DNA extraction

Leukorrhea from women or semen from men was collected after 3-5 days of sexual abstinence. Leukorrhea was examined from a direct smear, and semen analysis was conducted strictly according to the WHO guidelines (10). All samples were examined using a microscope to verify the presence of a *T. vaginalis* infection. Samples were then sent immediately to the protozoan laboratory. Total genomic DNA from all fresh samples was extracted using the DNeasy Blood and Tissue Kit (Tiangen, Beijing, China) according to the manufacturer's protocol. Extracts were stored at -20°C before being tested.

### 2.3. PCR amplification and sequencing

A set of primers was designed to target the conserved regions of the 18S ribosomal genes of *T. vaginalis*. The sequences were selected from regions of the 18S

**Table 1. Ethnicity and age of patients included in this study**

Sample	Ethnicity	Age	Sample	Ethnicity	Age	Sample	Ethnicity	Age
XJ-F3	Uyghur	28	XJ-F62	Han	27	XJ-F130	Han	39
XJ-F4	Han	36	XJ-F64	Han	39	XJ-F132	Uyghur	29
XJ-F8	Han	23	XJ-F65	Han	28	XJ-F133	Uyghur	23
XJ-F9	Han	27	XJ-F68	Han	37	XJ-F134	Han	33
XJ-F11	Han	27	XJ-F73	Han	38	XJ-F135	Uyghur	38
XJ-F13	Han	24	XJ-F74	Han	34	XJ-M1	Han	28
XJ-F15	Uyghur	29	XJ-F77	Uyghur	36	XJ-M2	Han	29
XJ-F16	Mongolian	38	XJ-F78	Kazakh	24	XJ-M3	Han	27
XJ-F17	Kazakh	27	XJ-F79	Han	25	XJ-M4	Han	39
XJ-F18	Han	39	XJ-F81	Kazakh	27	XJ-M5	Han	39
XJ-F19	Han	24	XJ-F83	Uyghur	25	XJ-M6	Han	25
XJ-F21	Han	32	XJ-F85	Han	24	XJ-M7	Uyghur	39
XJ-F22	Han	32	XJ-F86	Han	37	XJ-M8	Han	39
XJ-F23	Uyghur	26	XJ-F88	Han	26	XJ-M9	Uyghur	28
XJ-F25	Han	32	XJ-F90	Hui	30	XJ-M11	Uyghur	35
XJ-F27	Uyghur	26	XJ-F93	Kazakh	31	XJ-M12	Han	24
XJ-F28	Han	21	XJ-F94	Han	26	XJ-M13	Other ethnic	22
XJ-F32	Mongolian	36	XJ-F98	Khalkhas	26	XJ-M14	Hui	26
XJ-F33	Han	29	XJ-F101	Mongolian	25	XJ-M15	Han	38
XJ-F34	Han	34	XJ-F102	Uyghur	38	XJ-M16	Han	38
XJ-F36	Han	25	XJ-F104	Uyghur	37	XJ-M17	Hui	22
XJ-F37	Uyghur	32	XJ-F106	Han	39	XJ-M18	Han	31
XJ-F38	Kazakh	24	XJ-F107	Uyghur	39	XJ-M19	Other ethnic	38
XJ-F42	Mongolian	31	XJ-F109	Han	38	XJ-M21	Han	39
XJ-F45	Han	20	XJ-F110	Uyghur	31	XJ-M22	Han	30
XJ-F47	Han	25	XJ-F111	Uyghur	23	XJ-M23	Han	31
XJ-F50	Han	25	XJ-F113	Uyghur	39	XJ-M24	Han	26
XJ-F51	Han	20	XJ-F117	Mongolian	27	XJ-M25	Han	28
XJ-F52	Han	39	XJ-F119	Han	38	XJ-M26	Han	34
XJ-F57	Han	32	XJ-F120	Mongolian	27	XJ-M27	Han	38
XJ-F58	Kazakh	30	XJ-F123	Han	32	XJ-M28	Han	36
XJ-F59	Han	24	XJ-F127	Han	25	XJ-M29	Han	31
XJ-F60	Uyghur	26	XJ-F128	Han	35	XJ-M30	Han	39
XJ-F61	Han	23	XJ-F129	Han	27			

ribosomal gene that differed from those of *T. tenex*, *Tritrichomonas foetus*, *Candida albicans*, and other common pathogens found in the human urogenital system. The primer sequences were as follows: *T. vaginalis* S, 5'-ATC AGA GGC ACG CCA TTC-3'; *T. vaginalis* AS, 5'-CGC CCT TGA TCG ACA GAA-3'. PCR was performed using the thermal cycler Gene Amp PCR system (BIO-RAD).

Standard PCR was conducted using a total volume of 50  $\mu$ L. The master mix contained 5  $\mu$ L 10 $\times$  *ExTaq* buffer (Mg<sup>2+</sup> plus), 4  $\mu$ L of the four deoxynucleoside triphosphates (2.5  $\mu$ M each), 2.5  $\mu$ L of each primer (20  $\mu$ M each), 0.25  $\mu$ L *ExTaq* DNA polymerase (5 U/ $\mu$ L, Takara), 2  $\mu$ L DNA, and 33.75  $\mu$ L double distilled sterile water. The amplification procedure included 3 min of denaturation at 94°C followed by 35 cycles of 15 s denaturation at 94°C, 30 s annealing at 60°C, and 30 s extension at 72°C. A final extension step at 72°C for 7 min was also included in each cycle.

PCR products were separated by horizontal gel electrophoresis at 100 volts on a 2% agarose gel in Tris-acetate-EDTA buffer and visualized using an ultraviolet transilluminator after ethidium bromide staining. The size of the amplified product (582 bp) was determined by comparison to a commercial 100-bp DNA ladder (Takara). The AxyPrep DNA Gel Extraction kit (Corning, Inc., Corning, NY, USA) was used to extract the desired band, and the product was sequenced. For the double peak signal products, the pMD 19T vector (Takara), *E. coli* JM109 (Takara), and the AxyPrep Plasmid Miniprep kit (Corning) were used to clone the products. At least five clones of each sample were sent for sequencing.

#### 2.4. Gene analysis

Gene sequences were analyzed to ensure that the sequences were from *T. vaginalis*. Multiple sequence comparisons were made using Clustal W in software BioEdit 7.0.5.3 (11). Genetic distances were calculated using the Maximum Composite Likelihood settings in the software MEGA 5 (12) and were then sent to SplitsTree 4.13.1 (13) to create a phylogenetic network that accounts for reticulation events such as hybridization, horizontal gene transfer, and recombination.

A factorial correspondence analysis (FCA) representing the proximity between each individual genotype in a 2D plot was performed based on the 18S ribosomal gene frequencies using GenAlEx 6.5. The haplotype diversity and nucleotide diversity of these gene sequences between different groups were calculated using DnaSPv5 software.

### 3. Results

After extracting DNA from fresh samples, partial *T. vaginalis* 18S ribosomal gene sequences were amplified

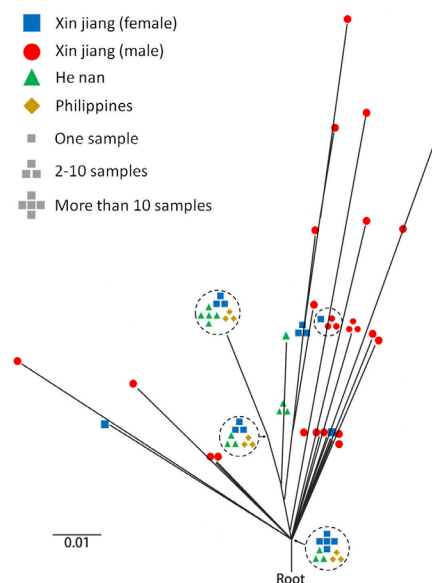


**Figure 1. Network based on the 18S ribosomal RNA gene sequence of *T. vaginalis*.** Network presenting the genetic relationships between Chinese and Philippine isolates as determined using SplitsTree 4. Colors indicate Xinjiang females (blue), Xinjiang males (red), Chinese Henan (green), and Philippine (yellow) sequences. Single symbol, one sample included; 3-symbol stack, 2-10 samples included; 5 symbol stack, > 10 samples included.

and sequenced. PCR analysis of 73 samples from females identified 75 *T. vaginalis* 18S ribosomal RNA sequences (labeled XJ-F1 through XJ-F75). In the samples from 28 males, 35 *T. vaginalis* 18S ribosomal RNA sequences were identified (labeled XJ-M1 through XJ-M35). To construct a rooted phylogenetic network, the 110 sequences identified in this study and another 46 reference sequences reported in Genbank were included.

In the distance-based network generated from the 18S ribosomal RNA gene, *T. vaginalis* separated into three main clusters (Figure 1). The majority of Philippine sequences were located close to the root, while the majority of the Xinjiang sequences were located far from the root. The network revealed high diversity in 18S ribosomal RNA gene sequences in isolates from Xinjiang males' isolates.

Sequences of *T. vaginalis* clearly separated into three groups using visual assessment of the FCA plot (Figure 2). The majority of Xinjiang sequences differed from the majority of Henan and Philippine sequences. Group sequence compositions are as follows: Group 1, 59 from Xinjiang females, 32 from Xinjiang males of this study, with 16 previously reported sequences (4 Philippine, 12 Henan); Group 2, 12 Xinjiang females, 3 Xinjiang males, 8 Henan, and 3 Philippine; Group 3, 4 Xinjiang females, 12 Henan, and 7 Philippine. No significant differences between groups were observed with respect to Xinjiang sample ethnicity or age in this study (Figure 3).

Quantifiable data revealed both high haplotype diversity (0.957) and nucleotide diversity (0.00738) of 18S ribosomal RNA gene sequences from Xinjiang

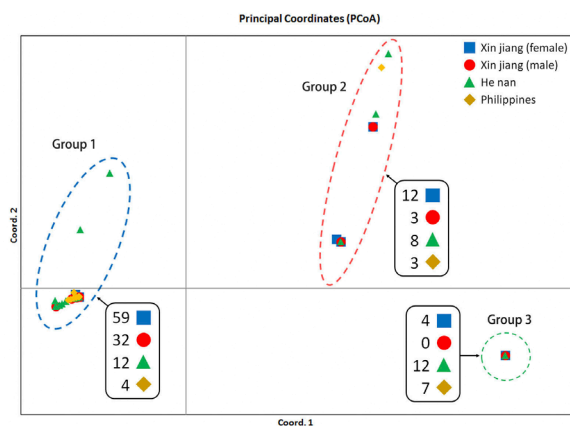


**Figure 2. Principal coordinate analysis of *T. vaginalis* populations.** The first and second coord extracted 38.75% and 11.76% of the total genetic variance, respectively. Colors indicate Xinjiang females (blue), Xinjiang males (red), Chinese Henan (green), and Philippine (yellow) sequences. The number of different populations included in each group is presented in the black textbox.

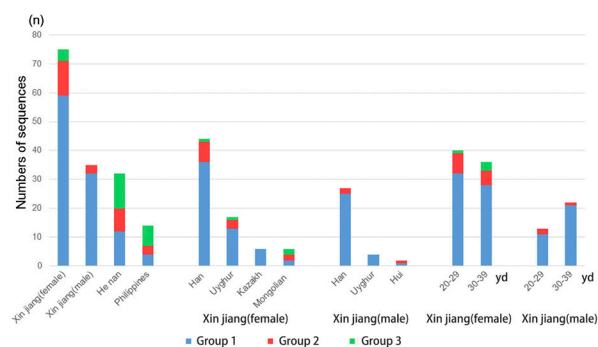


**Figure 3. Group distribution of Xinjiang samples with respect to ethnicity and age.** Y-axis, number of sequences; X-axis, sequence diversity of Xinjiang samples with respect to ethnicity and age. Sequences were divided into 3 groups according to principal coordinates analysis (as in Figure 2); Xinjiang females (blue), Xinjiang males (red), Chinese Henan (green), and Philippine (yellow) sequences

males. Mongolian samples of Xinjiang females also indicated high haplotype diversity (0.867) and nucleotide diversity (0.00289). No significant diversity was observed between Xinjiang samples with respect to ages (Table 2).

#### 4. Discussion

Approximately 1% of male patients in the First Affiliated Hospital of Xinjiang Medical University were positive for *T. vaginalis* upon examination of urine samples by microscopy. However, the detection rate of *T. vaginalis* in semen samples was about 4%. PCR has been used to study the related molecular epidemiology of *T. vaginalis* infection (14-16). In this study, all the samples were confirmed for the existence of trophozoites of *T. vaginalis* in semen by microscopy and unique sequences of the 18S ribosomal RNA gene of *T. vaginalis* existed in Xinjiang male patients.

**Table 2. Diversity of 18S ribosomal RNA gene sequence in *T. vaginalis***

Items	Haplotype diversity $\pm$ SD	Nucleotide diversity $\pm$ SD
China Xinjiang (females)	0.737 $\pm$ 0.036	0.00374 $\pm$ 0.00034
China Xinjiang (males)	0.957 $\pm$ 0.026	0.00738 $\pm$ 0.00083
China Henan	0.81 $\pm$ 0.031	0.00325 $\pm$ 0.00026
Philippines	0.703 $\pm$ 0.095	0.0023 $\pm$ 0.00042
China Xinjiang (females)		
Han	0.397 $\pm$ 0.09	0.0015 $\pm$ 0.00039
Uyghur	0.404 $\pm$ 0.13	0.00103 $\pm$ 0.00038
Kazakh	0	0
Mongolian	0.867 $\pm$ 0.129	0.00289 $\pm$ 0.00053
China Xinjiang (male)		
Han	0.961 $\pm$ 0.028	0.00711 $\pm$ 0.00095
Uyghur	1 $\pm$ 0.177	0.01055 $\pm$ 0.00261
Hui	1 $\pm$ 0.5	0.00842 $\pm$ 0.00421
China Xinjiang (females)		
20 - 29 years old	0.39 $\pm$ 0.092	0.00122 $\pm$ 0.00034
30 $\pm$ 39 years old	0.442 $\pm$ 0.1	0.00168 $\pm$ 0.00042
China Xinjiang (males)		
20 $\pm$ 29 years old	0.987 $\pm$ 0.035	0.00864 $\pm$ 0.00104
30 $\pm$ 39 years old	0.931 $\pm$ 0.046	0.00632 $\pm$ 0.00106

Several *T. vaginalis* sequences have been reported to date, and most of the 18S gene sequences have been reported in Chinese and Philippine studies (17-19). Previous studies indicate a relationship between *T. vaginalis* genotype and the clinical presentation of trichomoniasis (7,20,21). In this study, a distance-based network was constructed with three large clusters and many branches. The data suggest that Xinjiang *T. vaginalis* isolates might be genetically unique, although the results are preliminary. Thus the transmission and evolution of Xinjiang *T. vaginalis* is of interest and should be studied further.

A previous study showed that ethnicity is associated with *T. vaginalis* infection (22). In our study, Mongolian Xinjiang females were highly diverse with respect to haplotype and nucleotide sequences, comprising 3 groups. Samples from individuals other than Han were too few to make a reliable conclusion. The relationship between patient age and *T. vaginalis* 18S ribosomal RNA gene sequence was also investigated, but no significant clustering of samples was indicated based on age. The clusters indicated in this study must be confirmed using a larger patient cohort. Awareness of the molecular epidemiology of *T. vaginalis* in both females and males may be beneficial for disease diagnosis and treatment.

Previous study determined high genetic diversity within the *T. vaginalis* parasite isolated from worldwide regions in North America, Africa, Europe, Asia and Australia, and it was also found that the genotype characteristics remained stable in parasites. These studies had been done on the genotype of *T. vaginalis* and the relationship between its genotype and the clinical presentation of trichomoniasis, including metronidazole susceptibility, the presence of *T. vaginalis* virus (TVV) and *Mycoplasma hominis* (6-9). In this study, all the samples were collected from Xinjiang and the low

migration rate of local people in this province may contribute to genetic conservativation of *T. vaginalis*. Our results demonstrated that the genetic diversity of Chinese *T. vaginalis* isolates was associated with geographic distance based on the 18S ribosomal RNA gene. The unique genetic feature of our isolates may suggest a different metronidazole susceptibility, TVV or *Mycoplasma* co-infection characteristics. The results provided insight into the genetic features of *T. vaginalis* isolates and differences in genetic distance among China and other countries in different continents.

PCR analysis of the 18S ribosomal RNA gene sequence of *T. vaginalis* in 73 females and 28 males identified 110 sequences. The majority of these sequences formed a group that differed from most sequences reported in Genbank. These data suggest that *T. vaginalis* isolates from patients living in Xinjiang Province differ genetically from those of patients in other locations. Greater awareness of the molecular epidemiology of *T. vaginalis* in Xinjiang may be beneficial for disease diagnosis and treatment.

#### Acknowledgements

This work was supported by the National Nature Science Foundation of China (81171594) and the Major Project of the Twelfth Five-Year Plan (2012ZX10004220).

#### References

1. Hezarjaribi HZ, Fakhar M, Shokri A, Teshnizi SH, Sadough A, Taghavi M. *Trichomonas vaginalis* infection among Iranian general population of women: A systematic review and meta-analysis. *Parasitol Res.* 2015; 114:1291-1300.
2. World Health Organization. Global incidence and prevalence of selected curable sexually transmitted infections. 2008.
3. Pellati D, Mylonakis I, Bertoloni G, Fiore C, Andrisani A, Ambrosini G, Armanini D. Genital tract infections and infertility. *Eur J Obstet Gynecol Reprod Biol.* 2008; 140:3-11.
4. Shiadeh MN, Niyiyati M, Fallahi S, Rostami A. Human parasitic protozoan infection to infertility: A systematic review. *Parasitol Res.* 2016; 115:469-477.
5. Soper D. Trichomoniasis: Under control or under-controlled? *Am J Obstet Gynecol.* 2004; 190:281-290.
6. Conrad M, Zubacova Z, Dunn LA, Upcroft J, Sullivan SA, Tachezy J, Carlton JM. Microsatellite polymorphism in the sexually transmitted human pathogen *Trichomonas vaginalis* indicates a genetically diverse parasite. *Mol Biochem Parasit.* 2011; 175:30-38.
7. Conrad MD, Gorman AW, Schillinger JA, Fiori PL, Arroyo R, Malla N, Dubey ML, Gonzalez J, Blank S, Secor WE, Carlton JM. Extensive genetic diversity, unique population structure and evidence of genetic exchange in the sexually transmitted parasite *Trichomonas vaginalis*. *Plos Neglect Trop D.* 2012; 6:e1573.
8. Hampl V, Vanáčová S, Kulda J, Flegr J. Concordance between genetic relatedness and phenotypic similarities of *Trichomonas vaginalis* strains. *BMC Evol Biol.* 2001; 1:11.
9. Vanáčová S, Tachezy J, Kulda J, Flegr J. Characterization of trichomonad species and strains by PCR fingerprinting. *J Eukaryot Microbiol.* 1997; 44:545-552.
10. World Health Organization. WHO laboratory manual for the examination of human semen and semen-cervical mucus interaction. 4th ed. New York: Cambridge University Press; 1999.
11. Hall TA. BioEdit: A user-friendly biological sequence alignment editor and analysis program for Windows 95/98/NT. *Nucleic Acids Symp Ser.* 1999; 41:95-98.
12. Tamura K, Peterson D, Peterson N, Stecher G, Nei M, Kumar S. MEGA5: Molecular evolutionary genetics analysis using maximum likelihood, evolutionary distance, and maximum parsimony methods. *Mol Biol Evol.* 2011; 28:2731-2739.
13. Huson DH, Bryant D. Application of phylogenetic networks in evolutionary studies. *Mol Biol Evol.* 2006; 23:254-267.
14. Crucitti T, van Dyck E, Tehe A, Abdellati S, Vuylsteke B, Buve A, Laga M. Comparison of culture and different PCR assays for detection of *Trichomonas vaginalis* in self collected vaginal swab specimens. *Sex Transm Infect.* 2003; 79:393-398.
15. Radonjic IV, Dzamic AM, Mitrovic SM, Arsic Arsenijevic VS, Popadic DM, Kranjic Zec IF. Diagnosis of *Trichomonas vaginalis* infection: The sensitivities and specificities of microscopy, culture and PCR assay. *Eur J Obstet Gynecol Reprod Biol.* 2006; 126:116-120.
16. van der Schee C, van Belkum A, Zwiijgers L, van der Brugge E, O'Neill EL, Luijendijk A, van Rijsoort-Vos T, van Der Meijden WI, Verbrugh H, Sluiter HJ. Improved diagnosis of *Trichomonas vaginalis* infection by PCR using vaginal swabs and urine specimens compared to diagnosis by wet mount microscopy, culture, and fluorescent staining. *J Clin Microbiol.* 1999; 37:4127-4130.
17. Dimasuy KG, Rivera WL. First report of *Trichomonas tenax* infection in the Philippines. *Parasitol Int.* 2014; 63:400-402.
18. Gunderson, J, Hinkle, G, Leipe, D, Morrison, HG, Stickel, SK, Odelson, DA, Breznak JA, Nerad TA, Müller M, Sogin ML. Phylogeny of trichomonads inferred from small-subunit rRNA sequences. *J Eukaryot Microbiol.* 1995; 42:411-415.
19. Mao M, Liu HL. Genetic diversity of *trichomonas vaginalis* clinical isolates from Henan province in central China. *Pathog Glob Health.* 2015; 109:241-246.
20. Cornelius DC, Robinson DA, Muzny CA, Mena LA, Aanensen DM, Lushbaugh WB, Meade JC. Genetic characterization of *Trichomonas vaginalis* isolates by use of multilocus sequence typing. *J Clin Microbiol.* 2012; 50:3293-3300.
21. Hawksworth J, Levy M, Smale C, Cheung D, Whittle A, Longhurst D, Muir P, Gibson W. Population structure and genetic diversity of the parasite *Trichomonas vaginalis* in Bristol, UK. *Infect Genet Evol.* 2015; 34:36-43.
22. Mitchell HD, Lewis DA, Marsh K, Hughes G. Distribution and risk factors of *Trichomonas vaginalis* infection in England: An epidemiological study using electronic health records from sexually transmitted infection clinics, 2009-2011. *Epidemiol Infect.* 2014; 142:1678-1687.

(Received May 16, 2017; Revised June 4, 2017; Accepted June 5, 2017)

## Paeoniflorin prevents TLR2/4-mediated inflammation in type 2 diabetic nephropathy

Tingmin Zhang<sup>§</sup>, Qijin Zhu<sup>§</sup>, Yunxia Shao, Kun Wang, Yonggui Wu\*

Department of Nephrology, the First Affiliated Hospital, Anhui Medical University Hefei, Anhui, China.

### Summary

Paeoniflorin is an effective Chinese traditional medicine with anti-inflammatory and immunoregulatory effects. The aim of this study was to investigate the underlying renoprotective mechanism of Paeoniflorin. *In vivo*, db/db mice were intraperitoneally injected with Paeoniflorin at a dose of 15, 30, or 60 mg/kg respectively. The immunostaining of TLR2, TLR4, CD68, NF- $\kappa$ B p65 and the mRNA level of inflammatory factors, together with the protein expression of TLR2/4 signaling were evaluated. Our data demonstrated that Paeoniflorin could decrease the urinary albumin excretion rate and inhibit macrophage infiltration and activation through blockage of the TLR2/4 signaling pathway compared with the db/db group *in vivo*. *In vitro*, RAW264.7 cells were categorized into control, bovin serum albumin (BSA)-stimulated, advanced glycation end products (AGEs)-stimulated, Paeoniflorin intervention and oxidized phospholipid (OxPAPC)-inhibited groups. The cell viability, the optimal stimulated time and concentration were measured as well as the TLR2/4 signaling activation determined by RT-PCR, Western blot and ELISA. Our data demonstrated that Paeoniflorin reduced the AGEs-induced TLR2/4 activation and inflammatory responses, which was consistent with the TLR2/4 inhibitor group. These findings indicate that Paeoniflorin prevents macrophage activation *via* inhibition of TLR2/4 signaling expression in type 2 diabetic nephropathy.

**Keywords:** Paeoniflorin, TLR 2/4, diabetic nephropathy, inflammation, macrophage

### 1. Introduction

Diabetic nephropathy (DN), as the most common diabetic microvascular complication, accounts for a third of all patients with diabetes mellitus (1-2). Data from developed countries show that diabetic nephropathy is the first cause of renal replacement therapy (3). However, existing clinical interventions which contain strict control of hyperglycemia and hypertension, and block the renin-angiotensin-aldosterone axis have been demonstrated only to delay the progression of DN, not to cease or reverse the pathological state (4-5).

Recent studies have appreciated that the central pathogenesis of DN resulting from diabetes is oxidative injury, as well as inflammatory and immune responses (6). Numerous studies have proposed that macrophage infiltration and activation in diabetic kidney initiate inflammation *via* the release of some related factors, which subsequently lead to the development and progression of DN. Toll-like receptors (TLRs) are germline-encoded receptors which have been found on either antigen-presenting cells (including macrophages, and monocytes) or kidney intrinsic cells, especially renal tubular epithelial cells and endothelial cells (7). The recognition of TLRs ligands triggers the innate immune response for the activation of TLRs signaling promotes the transcription of NF- $\kappa$ B, which causes an inflammatory cascade with a high release of pro-inflammatory cytokines and chemokines (8). Nevertheless, *in vivo* and *in vitro* studies, showed increased expression in TLR2 was observed respectively in a streptozocin (STZ) induced diabetic model and high glucose circumstances (9), while it was also noted

Released online in J-STAGE as advance publication June 18, 2017.

<sup>§</sup>These authors contributed equally to this work.

\*Address correspondence to:

Dr. Yonggui Wu, Department of Nephrology, the First Affiliated Hospital, Anhui Medical University, No.218 Jixi Road, Hefei, Anhui, China.

E-mail: wuyonggui@medmail.com.cn

that an attenuation in NF- $\kappa$ B and pro-inflammatory cytokines activation with silenced or inhibited TLR4 expression (10), indicates the significance of TLRs in mediating the whole process. Furthermore, TLR2 and TLR4 can be found in macrophages, which are strongly related to its activation. Thus, we assume that the terminal kidney injury called DN resulted from the TLR2/4-mediated inflammatory state triggered by a certain diabetic microenvironment.

Paeoniflorin, a typical Chinese herbal medicine ingredient, is a primary component of total glucosides of paeony, isolated from the dried root of *Paeonia lactiflora* Pall (Family: Ranunculaceae) which was used in traditional Chinese prescriptions for anti-inflammatory, analgesic and diuretic effects (11). The drug has been admitted by US Food and Drug Administration for marketing since 1998 and Paeoniflorin itself has been shown to have not only anti-inflammatory, immune-regulatory, anti-allergic (12), and antinociceptive effects (13), but also antioxidative (14) and antiproliferative (15) activities as well by a growing number of scientific research studies. An experiment conducted by Fu *et al.* discovered a lower level of urinary albumin and ameliorated glomerular hypertrophy, together with decreased macrophage infiltration and inflammatory factor production in Paeoniflorin-treated rats (16). Also, Huang *et al.* revealed TLR as one of the paeonol target genes relevant to the anti-inflammatory effect (17). Therefore, the former evidence implicated that Paeoniflorin might mediate the inflammatory response *via* the TLRs signaling pathway in DN. Our study was designed to investigate the mechanism of how Paeoniflorin prevents TLR2/4-mediated inflammation in type 2 diabetic nephropathy.

## 2. Materials and Methods

### 2.1. Drugs and reagents

Paeoniflorin [C<sub>23</sub>H<sub>28</sub>O<sub>11</sub>, MW: 480.45, purity: 98.78% (HPLC)], LD<sub>50</sub>: 9,530 mg/kg] was bought from Nanjing GOREN BIO Technology Co., Ltd (Nanjing, China) as the commercial product. Its molecular structure is shown in Figure 1. OxPAPC was prepared by invivoGen Biotechnology (invivoGen, USA). CCK-8 Cell Counting Kit was obtained from Vazyme Biotech Co. (Nanjing, China). The rabbit anti-TLR4, MyD88, Trif, iNOS antibodies were purchased from Abcam Biotechnology (Abcam, Cambridge, UK) and p-IRF3, NF- $\kappa$ B p65, NF- $\kappa$ B p-p65 were from Cell Signaling Technology (CST Beverly, MA, USA), together with TLR2 from EMD Millipore Corporation (EMD Millipore, USA). The rabbit anti- p-IRAK1 were from Santa Cruz Biotechnology (Santa Cruz, California, USA). TNF- $\alpha$  and IL-1 $\beta$  ELISA kit were from R&D Systems (R&D Systems, USA), while MCP-1 ELISA

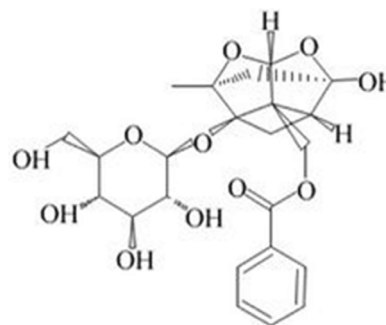


**Figure 1.** The chemical structures of Paeoniflorin.

kit was obtained from RIBIO TECH ( RIBIO TECH , Beijing, China).

### 2.2. Animals

The wild db/m littermates and db/db mice were purchased from the Model Animal Research Center of Nanjing University and housed individually in cages under standard conditions with 12-hour light-dark cycle, free access to food and water, room temperature of 24°C and humidity of 60%. The experimental protocols were approved by Ethical Committee of Animal Research of Anhui Medical University and executed according to the recommendations of Laboratory Animal Care and Use.

### 2.3. Experimental design

The db/m mice were recognized as the non-diabetic control group ( $n = 12$ ). The db/db mice whose blood glucose levels were over 16.7 mmol/L, were regarded as diabetic and were randomly divided into four groups (diabetic control group and Paeoniflorin intervention groups) among which there existed no differences, number of rats in each group was 12. Paeoniflorin intervention groups were intraperitoneally injected with Paeoniflorin daily at the dose of 15, 30, or 60 mg/kg respectively at 10-weeks of age, while the non-diabetic control group and diabetic control group were injected with an equivalent amount of saline. All the mice were sacrificed at 12-weeks-of-age and the kidneys were harvested for further analyses. The weight of the body and kidney, as well as blood glucose of each mouse were recorded using an electronic scale and glucose analyzer, while the blood samples were obtained by jugular artery catheterization.

### 2.4. Metabolic data analysis

Prior to sacrifice, samples for 24 h urine were gathered from the mice for the calculation of urinary albumin excretion. Creatinine clearance rates were calculated by urinary creatinine concentration/serum creatinine  $\times$  urine flow per minute.

### 2.5. Cell culture

RAW264.7 cells were purchased from Shanghai cell bank of Chinese Academy of Science, China and seeded in high glucose DMEM medium with an osmotic pressure of 250 mmol/L, which was supplemented with 10% fetal bovine serum (FBS) and 1% penicillin G, streptomycin. The serum free medium was used to culture the cells for 24 h in order to synchronize the cells. Prior to the experiment, the cells were inoculated in 96-well plates, at a density of 5,000-10,000 cells per plate. Different concentrations of Paeoniflorin were added in cell culture for a day and a CCK-8 assay kit was used to determine cell viability. Under 200 µg/mL AGEs stimulation, the cells were collected at different time points, and the total protein was extracted to observe the expression of TLR2, TLR4 and iNOS protein in order to determine the optimal time of stimulation. In addition, different concentrations of Paeoniflorin were also added half an hour ahead of AGEs stimulation and TLR2, TLR4 and iNOS expression was assessed to determine the best concentration for Paeoniflorin treatment. Then the synchronized RAW264.7 cells were divided into the control group, BSA-stimulated group, AGEs-stimulated group, Paeoniflorin intervention group and oxidized phospholipid (OxPAPC)-inhibited group. The BSA-stimulated group was cultured with 200 µg/mL BSA and the AGEs-stimulated group, Paeoniflorin intervention group as well as the OxPAPC-inhibited group were all cultured with 200 µg/mL AGEs respectively for 24 hours. The Paeoniflorin intervention group was treated with various concentrations of Paeoniflorin half an hour before AGEs. Furthermore, an hour before the AGEs stimulation, the OxPAPC-inhibited group was added in OxPAPC to block the TLR2/4 signaling pathway.

### 2.6. Immunohistochemistry

Fresh renal tissues were fixed with 4% paraformaldehyde and embedded with paraffin, which were later cut into 2 µm sections. After deparaffinization, the tissue slices were treated with 3% hydrogen peroxide and then heated in a microwave in order to enclose the endogenous peroxidase and retrieve the antigen. Primary antibody (CD68, TLR2, TLR4, NF-κB p65) was incubated at 37°C with polyperoxidase-anti-mouse/rabbit IgG, followed by 3,3-diaminobenzidine (DAB, Sigma) and hematoxylin staining. Quantitation for CD68 positive cells, representing the recruitment of macrophages in tissue sections were counted randomly in 20 high-power (×400) interstitial fields. However, the staining of TLR2, TLR4 and NF-κB p65 was analyzed by a computer system.

### 2.7. Western blot

Animal protein of homogeneous kidney samples and

cell protein were lysed and combined with loading buffer, boiled, then separated using 10-12% SDS-PAGE. Proteins were electro blotted onto a nitrocellulose membrane, incubated with primary antibody TLR2, TLR4, MyD88, p-IRAK1, Trif, p-IRF3, NF-κB p-p65, or NF-κB p65 overnight at 4°C after blocking with skimmed milk for 1 hour. The combination of secondary antibody (the goat anti-rabbit IgG) was applied once the membrane was washed. Finally the observation of the image using enhanced chemiluminescence and the protein content was quantitated using the documentation system.

### 2.8. RT-PCR

The RNA extracted from the kidney and the cells *via* Trizol reagent (Invitrogen, California, USA) was used to reverse transcribe to cDNA with the help of a Reverse transcription Kit (Promega, USA), which was in turn augmented by RT-PCR using Power SYBR Green PCR Master Mix (Bio-Rad, USA) and GAPDH primers (Sangon Biotech, Shanghai, China). The forward and reverse primer for the detected RNA sequence were as follows: TNF-α: 5'-CCCTCCTGGCCAACGGCATG-3' and 5'-TCGGGGCAGCCTTGTCCTT-3'; the TLR2 (MQP030650), TLR4 (MQP032465), MCP-1 (MQP027672), IL-1β (MQP027422), iNOS (MQP029793). Primers were bought from GeneCopoeia, USA. Finally, the relative expression of genes was analyzed by using 2<sup>-ΔΔCt</sup>.

### 2.9. ELISA

At the end of the experiment, the culture medium of the RWA 264.7 cells was collected and the content of TNF-α, IL-1β, and MCP-1 in it was determined by ELISA kits.

### 2.10. Statistical analyses

Data were analyzed with the help of SPSS 16.0 and continuous variables were expressed as mean ± SD. All the data were compared by ANOVA analysis. The difference between groups was tested using the LSD and Levene method for a homogeneity test of variance, in which a *p* value under 0.05 was considered significant.

## 3. Results

### 3.1. Clinical parameters

The mice in the control group were responsive with active behavior, bright body hair, normal diet, water and a good mental state. Diabetes mellitus model group mice gradually showed obvious symptoms of diabetes: eating and drinking more, increased urine output,

**Table 1. Changes of clinical and metabolic parameters in five groups of mice**

Group	Dose (mg/kg)	Blood glucose (mmol/L)	Body weight (g)	Kidney weight (g)	Albumin excretion rate ( $\mu\text{g}/24\text{ h}$ )	Creatinine clearance rate (mL/min)
db/m	–	7.06 $\pm$ 1.22	24.64 $\pm$ 1.14	0.18 $\pm$ 0.02	16.91 $\pm$ 4.89	0.97 $\pm$ 0.29
db/db	–	33.46 $\pm$ 3.28**	45.35 $\pm$ 2.38**	0.25 $\pm$ 0.03**	1144.5 $\pm$ 81.3**	2.47 $\pm$ 0.64**
db/db+ paeoniflorin	15	34.08 $\pm$ 2.40	43.46 $\pm$ 2.69	0.25 $\pm$ 0.05	589.17 $\pm$ 69.42###	1.89 $\pm$ 0.57###
	30	32.67 $\pm$ 3.59	45.61 $\pm$ 2.97	0.23 $\pm$ 0.02#	497.32 $\pm$ 51.22###	1.71 $\pm$ 0.49###
	60	31.08 $\pm$ 2.56	43.39 $\pm$ 2.36	0.22 $\pm$ 0.03###	456.98 $\pm$ 55.46###	1.59 $\pm$ 0.53###

\*\* $p < 0.01$ , compared with the db/m group; # $p < 0.05$ ; ### $p < 0.01$ , compared with the db/db group. Data are presented as Mean  $\pm$  SD. Number of rats in each group was 12.

weight loss, bleak coat, messy, dirty, delayed behavior and were apathetic. Diabetic mice given paeoniflorin intervention and TLR2/4 knockout showed a mild performance compared to diabetes mellitus model group mice.

The metabolic data and the monitored clinical parameters of the five groups of mice are demonstrated in Table 1. On average, the enhanced blood glucose level and body weight were observed in the db/db group compared to db/m mice, but differences with Paeoniflorin treatment were not noticed. Despite the similar blood glucose level and body weight, mice given Paeoniflorin treatment exhibited a considerable dose-dependent decrease in albuminuria compared to the db/db group, which was still higher than that of db/m group.

### 3.2. Immunohistochemical analysis for distribution of TLR2, TLR4, CD-68 and NF- $\kappa$ B p65 in mice kidneys

Immunohistochemistry showed that staining of TLR2 was mainly observed in the tubulointerstitium, while the expression of TLR4 was found on glomeruli in addition to tubulointerstitium. In db/m mice kidneys, the positive result of IHC staining for TLR2 and TLR4 was barely noted, however the db/db mice illustrated typical manifestation of TLR2 and TLR4, which was recognized as overexpression. Compared with the db/db, the intensity of TLR2 and TLR4 immunostaining was significantly decreased parallel to the concentration of the Paeoniflorin given to the db/db mice, proving that the treatment with Paeoniflorin can decrease the expression of TLR2 and TLR4 in diabetic models. In order to gain better insight into the inflammatory level, we introduced macrophage recruitment into our investigation. CD68, as a parameter representing renal macrophage accumulation, was occasionally noticed in db/m mice kidneys, yet, the CD68 positive macrophage infiltration was found markedly increased in db/db mice. Immunohistochemical staining indicated a statistical reduction in CD68 positive expression in kidneys from Paeoniflorin treated mice with diabetes as compared to db/db mice, which verifies the effects of Paeoniflorin on macrophage accumulation and infiltration. NF- $\kappa$ B p65 was highly expressed in the nucleus and cytoplasm of glomerular mesangial cells and renal tubular epithelial cells from db/db mice

compared to the rare expression in db/m mice, however, NF- $\kappa$ B p65-positive expression was decreased with the Paeoniflorin treatment in a dose-dependent manner (Figures 2 and 3, Table 2).

### 3.3. The mRNA results of iNOS, TNF- $\alpha$ , IL-1 $\beta$ and MCP-1 in mice kidneys

As shown in Figure 4, low level expression of iNOS, TNF- $\alpha$ , IL-1 $\beta$  and MCP-1 was discovered in conformity with transcriptional regulation of mRNA levels in db/m mice. In contrast, the mRNA levels of iNOS, TNF- $\alpha$ , IL-1 $\beta$  and MCP-1 was significantly elevated in db/db mice and fell remarkably with Paeoniflorin treatment, which was highly consistent with the Western blot results.

### 3.4. Western blot analysis of TLR2, TLR4, MyD88, p-IRAK1, Trif, p-IRF3, NF- $\kappa$ B p-p65, NF- $\kappa$ B p65, and IL-1 $\beta$ expression in mice kidneys

TLR2 and TLR4 together with the downstream signaling molecule protein expression in the experimental subjects was further confirmed by Western blot analysis, which showed a significant upregulation of TLR2, TLR4, MyD88, p-IRAK1, Trif, p-IRF3, NF- $\kappa$ B p-p65, and NF- $\kappa$ B p65 in db/db mice compared to db/m mice. The same goes with the inflammatory cytokines-IL-1 $\beta$ . By comparison, the expression of the above protein was significantly attenuated by 15, 30 and 60 mg/kg Paeoniflorin treatment (Figure 5).

### 3.5. Effect of Paeoniflorin on AGEs-stimulated production of TLR2, TLR4 and iNOS

To determine the stimulated time of AGEs and concentration of Paeoniflorin intervention, we evaluated the viability of RAW 264.7 cells under different concentrations of Paeoniflorin and TLR2, TLR4, iNOS expressions when stimulated with AGEs for various lengths of time. In Figure 6, the Cytotoxicity assay showed that the viability of RAW 264.7 cells declined at  $10^{-4}$  mol/L Paeoniflorin intervention while there was no influence at concentrations between  $10^{-4}$  and  $10^{-8}$ . Figure 7 also demonstrated the overexpression of TLR2 and iNOS 4 hours after AGEs stimulation in RAW 264.7 cells, while TLR4 was remarkably elevated from

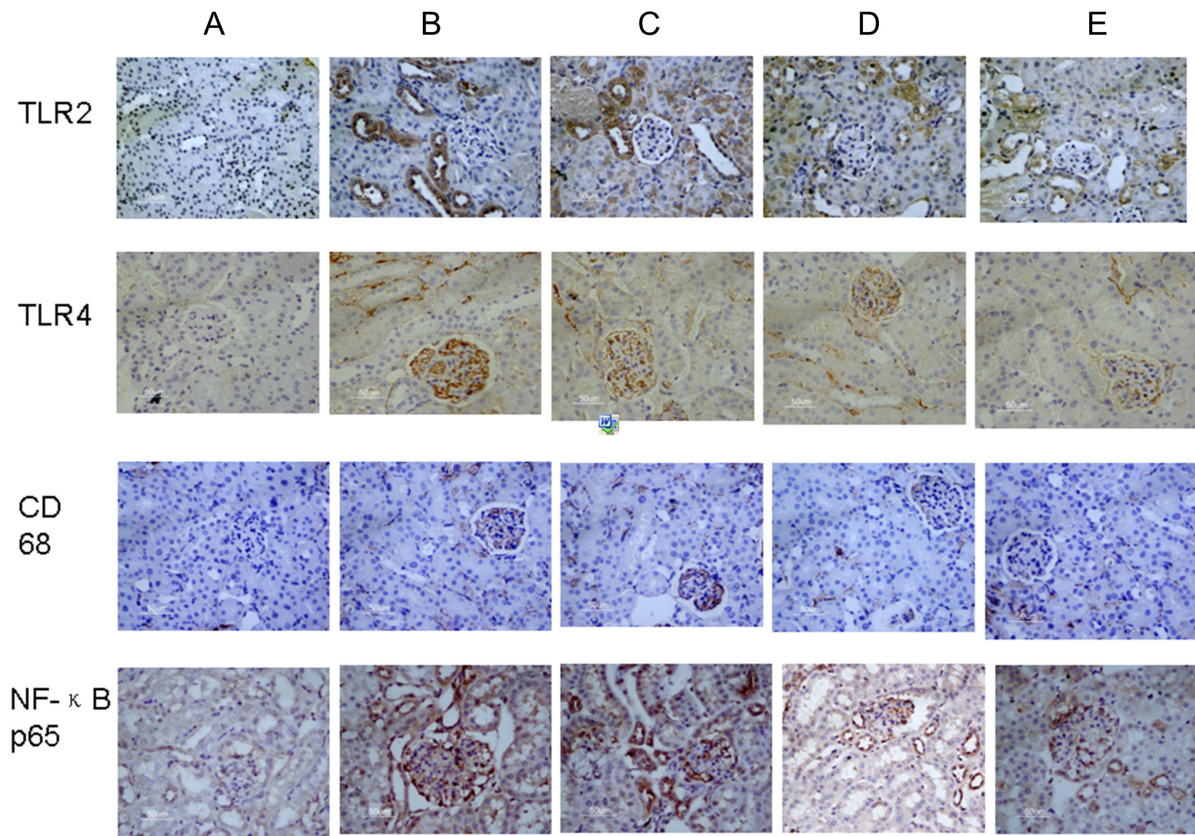


Figure 2. Effects of Paeoniflonin on TLR2, TLR4, CD 68 and NF-κB p65 immunostaining in mice kidney. (A), db/m group; (B), db/db group; (C), db/db+PF 15 mg/kg group; (D), db/db+PF 30 mg/kg group; (E), db/db+PF 60 mg/kg group. Original magnification 400×.

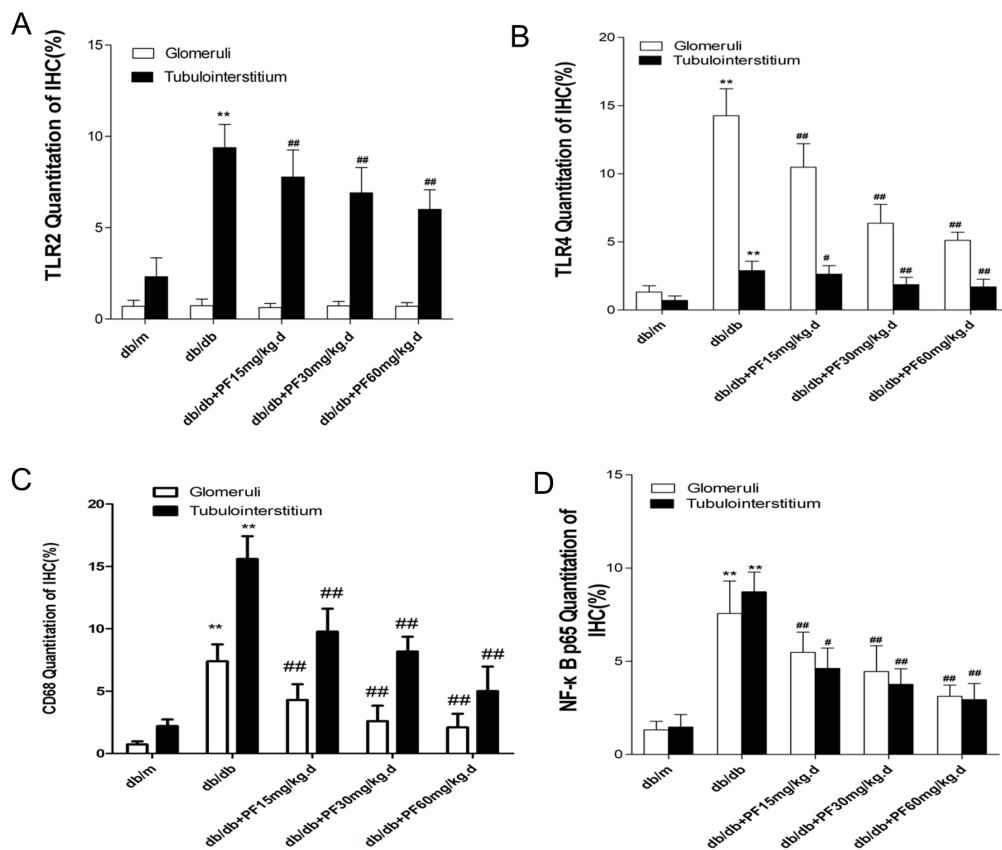


Figure 3. (A-D), Quantitative analyses of the TLR2, TLR4, CD 68 and NF-κB p65 immunohistochemical staining results. The results are presented as Mean ± SD. \*\**p* < 0.01 vs. db/m group, #*p* < 0.05 vs. db/db group, ##*p* < 0.01 vs. db/db group.

Table 2. Quantition of IHC in glomeruli and tubelointerstitium(cells/mm<sup>2</sup>)

Group	Dose (mg/kg)	TLR2		TLR4		CD68		NF-κB P65	
		glomeruli	tubelointerstitium	glomeruli	tubelointerstitium	glomeruli	tubelointerstitium	glomeruli	tubelointerstitium
db/m	-	0.700 ± 0.330	2.320 ± 1.040	1.320 ± 0.460	0.700 ± 0.330	0.730 ± 0.250	2.200 ± 0.540	1.320 ± 0.460	1.470 ± 0.670
db/db	-	0.730 ± 0.360	9.390 ± 1.260**	14.260 ± 1.980**	2.890 ± 0.680**	7.400 ± 1.360**	15.600 ± 1.830**	7.560 ± 1.750**	8.730 ± 1.050**
db/db+ paeoniflorin	15	0.630 ± 0.220	7.780 ± 1.480##	10.480 ± 1.730##	2.630 ± 0.620#	4.300 ± 1.260##	9.780 ± 1.840##	5.480 ± 1.080##	4.620 ± 1.090#
	30	0.720 ± 0.240	6.910 ± 1.390##	6.370 ± 1.380##	1.860 ± 0.540##	2.600 ± 1.240##	8.180 ± 1.190##	4.450 ± 1.380##	3.760 ± 0.840##
	60	0.700 ± 0.200	6.000 ± 1.080##	5.120 ± 0.590##	1.700 ± 0.560##	2.1000 ± 1.100##	5.000 ± 1.980##	3.120 ± 0.600##	2.950 ± 0.860##

\*\**p* < 0.01, compared with the db/m group; #*p* < 0.05; ##*p* < 0.01, compared with the db/db group. Data are presented as Mean ± SD. Number of rats in each group was 12.

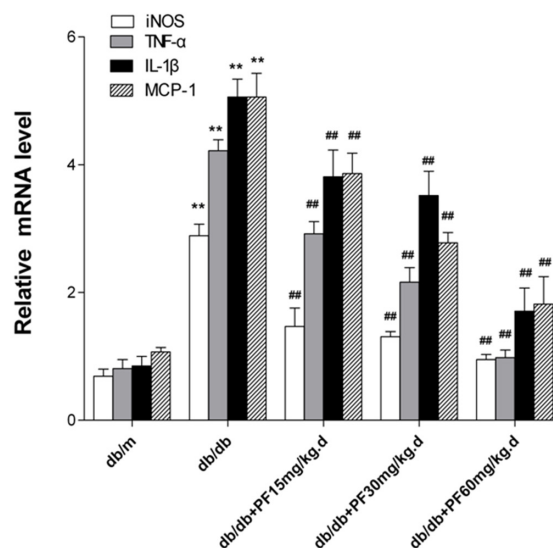


Figure 4. The mRNA results of iNOS, TNF-α, IL-1β and MCP-1 in mice kidneys. The results are presented as Mean ± SD of at least three repeated experiments. \*\**p* < 0.01 vs. db/m group, #*p* < 0.01 vs. db/db group.

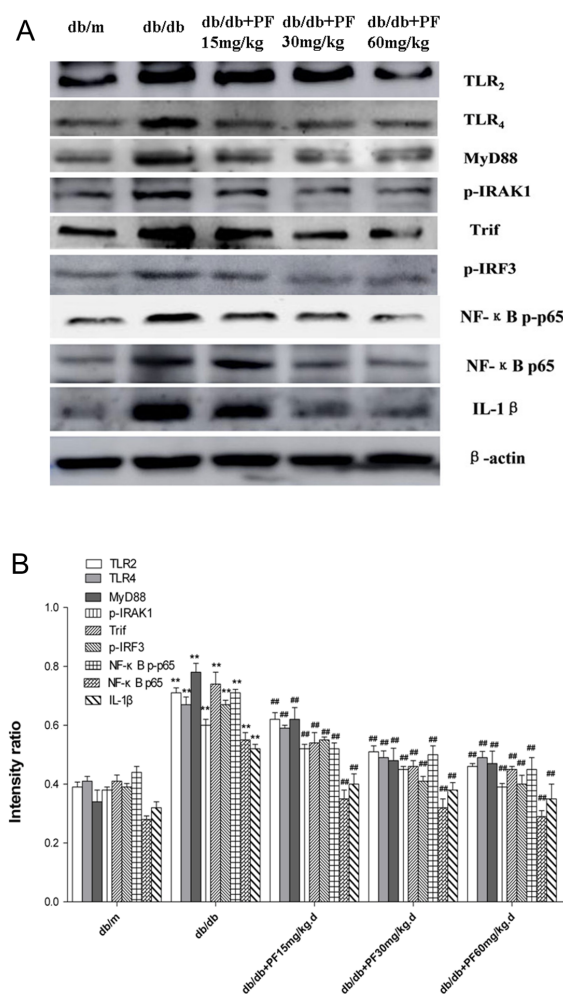
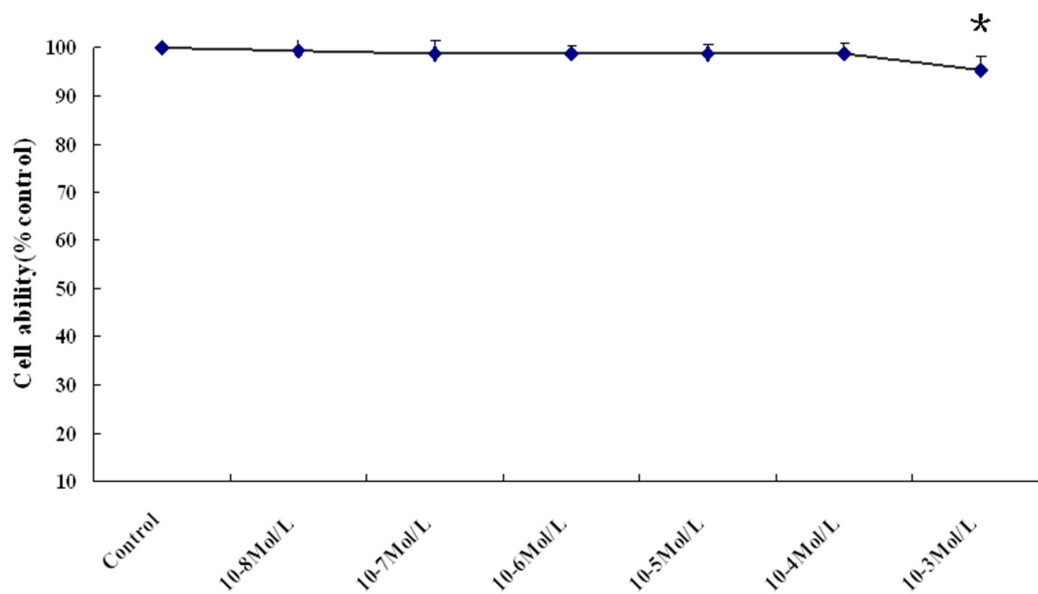
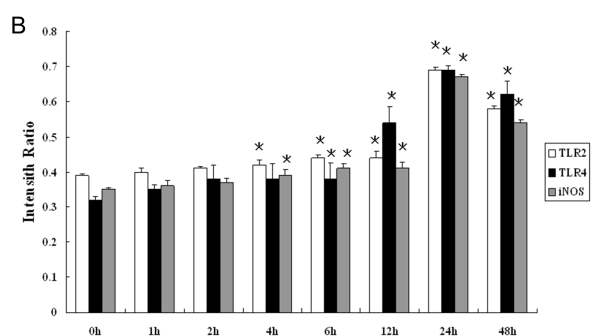
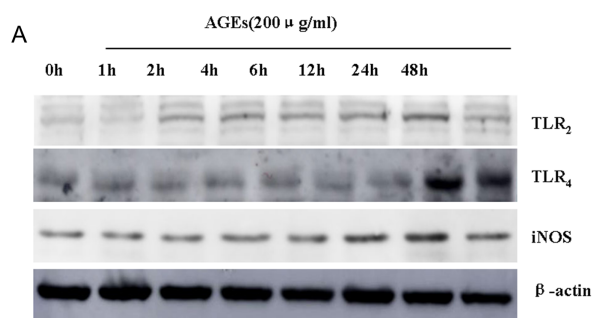


Figure 5. Effects of Paeoniflorin on TLRs signaling activation and IL-1β expression in db/db mice. (A), The db/db mice were treated with different Paeoniflorin concentrations. (B), The protein levels of TLR2, TLR4, MyD88, p-IRAK1, Trif, p-IRF3, IRF3, NF-κB p-p65, NF-κB p65 and IL-1β were assessed by Western blot analyses. The values are presented as Mean ± SD of at least three repeated experiments. \*\**p* < 0.01 vs. db/m group, #*p* < 0.01 vs. db/db group.



**Figure 6.** Cell viability analysis of Paoniflorin treatment on RAW 264.7 cells.  $10^{-8}$ - $10^{-3}$  mol/L Paoniflorin was respectively treated on RAW 264.7 cells and cell viability was detected by using a CCK-8 assay. The results are expressed as Mean  $\pm$  SD of at least three repeated experiments. \* $p < 0.05$  vs. control group.



**Figure 7.** Effects of AGEs on TLRs and macrophage activation at different time points. (A), RAW 264.7 cells were cultured with 200 ug/mL AGEs for time of 0, 1, 2, 4, 6, 12, 24 and 48 h. (B), The protein levels of TLR2, TLR4 and iNOS were determined by Western blot. Values are presented as Mean  $\pm$  SD of at least three repeated experiments. \*\* $p < 0.01$  vs. 0 h group.

6 h, which all peaked at 24 h. Thus, we cultured cells with AGEs for 24 h in the subsequent experiments. In the selected four doses ( $10^{-5}$  to  $10^{-8}$  mol/L), TLR2, TLR4, and iNOS expression could be inhibited in a concentration dependent manner by Paoniflorin when stimulated by AGEs, compared to the AGEs stimulated

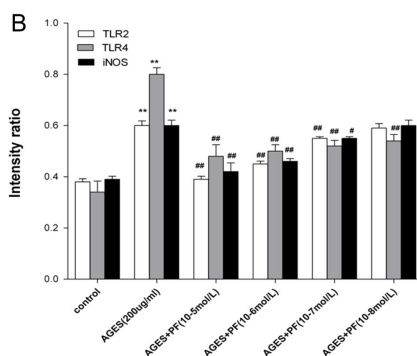
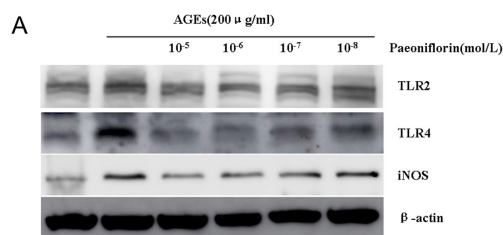


**Figure 8.** Involvement of TLRs and macrophage activation under different Paoniflorin concentrations on AGEs-stimulated cells. (A), AGEs-stimulated RAW 264.7 cells were treated respectively with  $10^{-8}$ - $10^{-3}$  mol/L Paoniflorin. (B), The protein levels of TLR2, TLR4 and iNOS were determined by Western blot. Values are presented as Mean  $\pm$  SD of at least three repeated experiments. \*\* $p < 0.01$  vs. 0 h group.

group. Therefore, we chose  $10^{-5}$  mol/L as the intervention dose (Figure 8).

3.6. Advanced glycation end products (AGEs) activated the expression of TLRs signaling and macrophage activation on RAW 264.7

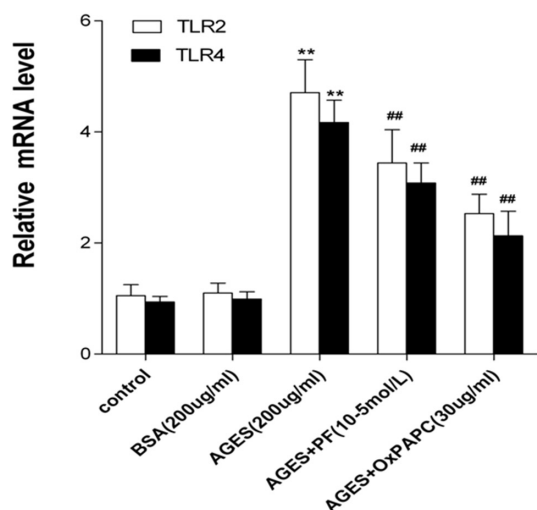


**Figure 9.** Effects of Paeniflorin and OxPAPC on TLR2 and TLR4 mRNA level in AGEs-stimulated RAW 264.7 cells. Values are presented as Mean ± SD of at least three repeated experiments. \*\**p* < 0.01 vs. control group, ##*p* < 0.01 vs. AGEs group.

To identify whether the activated inflammatory effect of hyperglycemia on macrophages is mediated by TLRs, we cultured RAW 264.7 with AGEs *in vitro*. As we can see in Figure 9, the mRNA level of TLR2 and TLR4 was elevated in the AGEs group, but decreased in both the Paeniflorin and OxPAPC group. Western blot analysis in Figures 10A and 10B showed that proteins of TLRs signaling pathway including TLR2, TLR4, MyD88, p-IRAK1, Trif, p-IRF3, NF-κB p-p65, NF-κB p65 and iNOS were prominently increased on RAW 264.7 under AGEs condition, while the Paeniflorin treatment and OxPAPC intervention both exhibited a significant reduction in the expression of TLR2, TLR4, MyD88, p-IRAK1, Trif, p-IRF3, NF-κB p65, NF-κB p-p65 and iNOS.

### 3.7. TLRs mediated pro-inflammatory responses in RAW 264.7 exposed to AGEs

To visualize the effects of hyperglycemia on inflammation initiated by macrophages, the following events were carried out *in vitro* with RAW 264.7 cells. The secretion of TNF-α, IL-1β and MCP-1 were determined *via* ELISA, finding that RAW 264.7 exposed to AGEs demonstrated a higher concentration of TNF-α, IL-1β and MCP-1, whereas TNF-α, IL-1β and MCP-1 in Paeniflorin treated cells were profoundly diminished. In order to further clarify the pivotal role of TLRs in inflammatory responses and Paeniflorin treatment, the inhibitor of the TLRs was introduced. The results of RAW 264.7 cultured in OxPAPC were similar to those seeded in Paeniflorin after exposure to AGEs, which corresponded to what was obtained from Western blots (Figure 11).

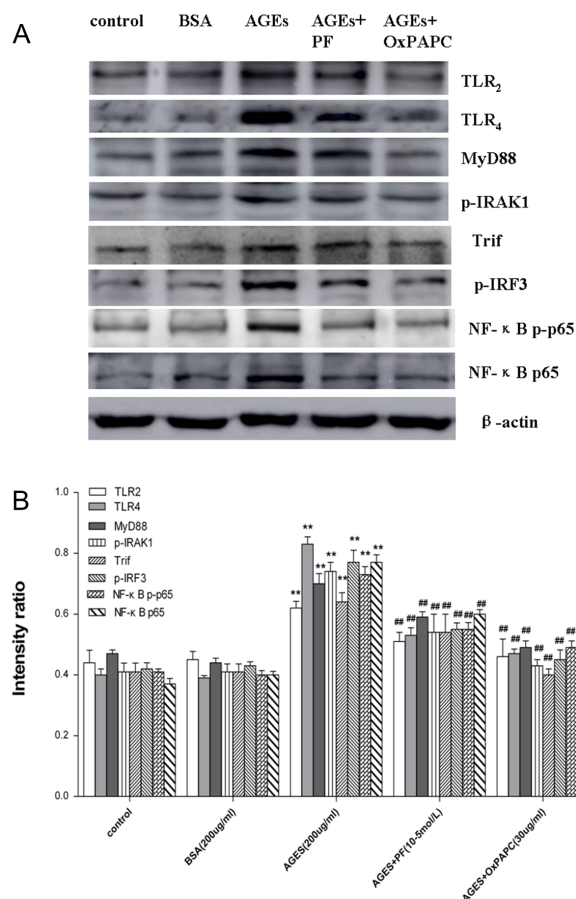


**Figure 10.** Effects of Paeniflorin and OxPAPC on the cell signaling activation in AGEs-stimulated RAW 264.7 cells. (A), Cells were pretreated with Paeniflorin for 0.5 h or OxPAPC for 1 h and then stimulated with AGEs. (B), The protein levels of TLR2, TLR4, MyD88, p-IRAK1, Trif, p-IRF3, IRF3, NF-κB p-p65, NF-κB p65 were assessed by Western blot analyses. Values are presented as Mean ± SD of at least three repeated experiments. \*\**p* < 0.01 vs. control group, ##*p* < 0.01 vs. AGEs group.

## 4. Discussion

DN is a long-term complication, and the prevention of its progression remains to be a challenge. Increasing evidence reviewed lately, indicates that TLR2/4-mediated inflammation might be a promising factor leading to an effective approach to DN blockage and treatment. In renal biopsy of DN patients, macrophages accumulated and turned out to play a pathogenic role in DN progression (18). In addition, research on type 1 diabetic patients showed the increasing expression of TLR2, pro-inflammatory cytokines in blood leukocytes (19) and upregulation of TLR4 in human renal tubules (10). Studies performed by Alaa S. *et al.* demonstrated that the absence of macrophage TNF-α stimulated by TLRs could prevent diabetic mice from having complications like DN and chronic renal injuries, which could be mainly expressed in albuminuria decrease and hypertrophy reduction (4). Also, the introduction of Chinese traditional medicine – Paeniflorin, which

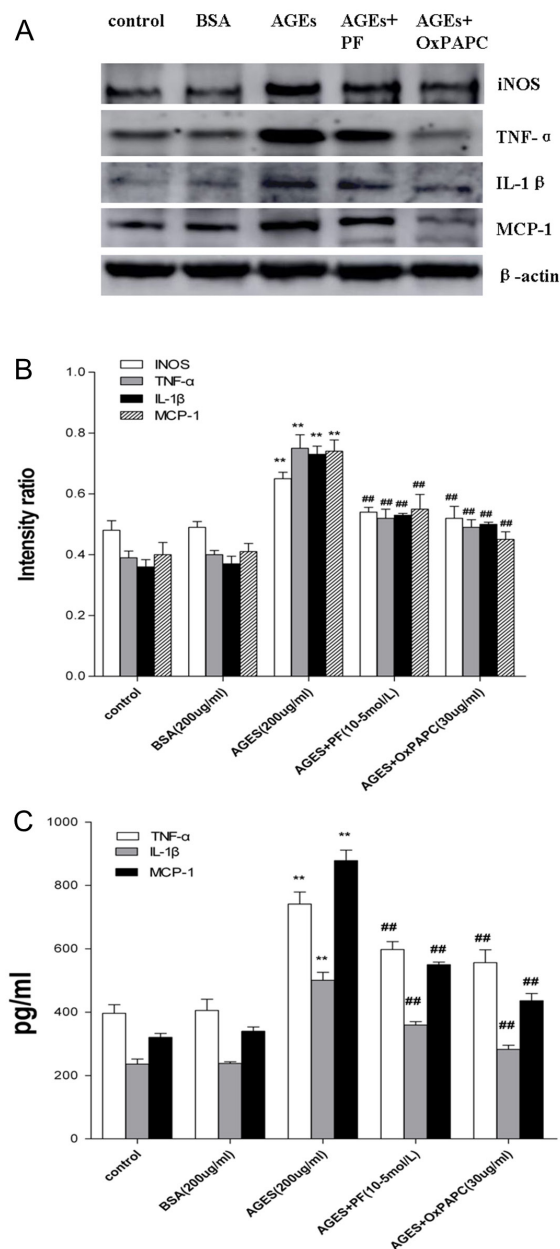


**Figure 11. Effects of Paeoniflorin and OxPAPC on macrophage activation and inflammatory cytokines expression in AGEs-stimulated RAW 264.7 cells.** (A), Cells were pretreated with Paeoniflorin for 0.5 h or OxPAPC for 1 h and then stimulated with AGEs. (B), The protein levels of TNF- $\alpha$ , IL-1 $\beta$ , MCP-1 and iNOS were assessed by Western blot analyses. (C), Expression of secreted TNF- $\alpha$ , IL-1 $\beta$ , MCP-1 were determined by ELISA kit. Values are presented as Mean  $\pm$  SD of at least three repeated experiments. \*\* $p < 0.01$  vs. control group, ## $p < 0.01$  vs. AGEs group.

was reported to have anti-inflammatory and immunoregulatory effects, was found to be helpful for DN treatment and prevention (14,16), though the underlying protective mechanism of its action was largely unclear. In the present study, we demonstrated that the mechanism of Paeoniflorin treatment in DN might be through the TLR-involved anti-inflammatory process.

Paeoniflorin as a typical main principal bioactive component of *Paeoniae Radix* (20), is one of the major

constituents that form total glucosides of paeony (TGP) (21) and has been put into clinical treatment for rheumatoid arthritis (22), hepatitis (21), systemic lupus erythematosus, and mesenteric hyperplastic nephritis (23-25). Xu *et al.* has done research on rats, which suggested that the protective affect of TGP on DN was associated with the blockage of TLR2 and TLR4 activation (26). In our study, we illustrated that Paeoniflorin therapy decreased proteinuria and ameliorated creatinine clearance rate in db/db mice. We also presented the blocking of NF- $\kappa$ B activation and macrophage recruitment, together with the suppression of the inflammatory cytokines and chemokines (TNF- $\alpha$ , IL-1 $\beta$ , MCP-1, and iNOS) in the Paeoniflorin group, which was highly consistent with that reported by Fu *et al.* (16). The reduction of selective TLRs signaling molecule expression was also observed and the above results are compatible with those *in vitro* experiments on AGEs-induced RAW 264.7 cells when treated with Paeoniflorin suggesting the renoprotective role Paeoniflorin played in TLRs-mediated DN progression.

Previous essays have reported that macrophage infiltration and activation play an essential role in the pathogenesis of DN. In recent studies, increasing evidence demonstrated that the phenotype of the infiltrated macrophage was the major character that ultimately decided the sequelae of DN (27). M1 macrophages promote the inflammatory response and tissue injury, while the M2 macrophages provide the anti-inflammatory and tissue protective effects (28). The transformation of M1 phenotype could be initiated by pro-inflammatory cytokines such as IFN- $\gamma$ , and TNF- $\alpha$ , which in turn enhanced the secretion of these pro-inflammatory cytokines (27). In our experiment, iNOS, as the key M1 macrophage marker, was shown to estimate the population of activated macrophages and the severity of inflammation in DN models. Our data revealed the similar results to Devaraj *et al.*, finding the increased expression of iNOS in db/db mice and the M1 phenotype in RAW264.7 cells when exposed to AGEs (8). Furthermore, we exhibited that Paeoniflorin treatment not only reduced macrophage recruitment but also the M1 phenotype in a dose-dependent manner, resulting in a decrease of proinflammatory cytokine production, which corresponded to our *in vitro* experiments. Thus, we have reason to speculate that the renoprotective effect of Paeoniflorin on DN is likely related to the blockage of M1 macrophage phenotype activation.

Insight into the full mechanism of TLR2/4 signaling pathway has caused increasing attention. A great quantity of research executed in DN models exhibited that once ligand binding occurred, the downstream signaling pathway could be categorized as the MyD88-dependent and the MyD88-independent pathway. The former, was characterized by both TLR2 and TLR4, signals through IRAKs, while the latter pathway only

implemented in TLR4 not TLR2, signals through TRIF and then IRF3. Despite the different pathways, they both reach to activation of NF- $\kappa$ B which can ultimately up-regulate the transcription of factors related to inflammatory responses and thereby initiate inflammation. NF- $\kappa$ B p65 as a family member of NF- $\kappa$ B transcription factors, was monitored as a parameter in our experiment (29). Data presented in our study further verified the previous TLRs signal pathway, showing the synergistically enhanced downstream signaling proteins in db/db and AGEs-induced RAW 264.7 models. Therefore, termination of inflammation in diabetes taking TLRs as a target seems to be a suitable treatment project to ameliorate inflammation and progressive DN. In addition, *in vivo* and *in vitro* experiments, these proteins were found synergistically decreased in Paeoniflorin treatment groups, which indicated that Paeoniflorin might inhibit macrophages from activation through the blockage of TLRs expression in DN.

Our strategies designed to further state that the TLRs-inhibited renoprotection of Paeoniflorin theory using TLR2 and TLR 4 inhibitor was carried out in RAW264.7 macrophages. We and others have already displayed that the hyperglycemic environment can activate TLRs and M1 macrophages which strikingly increased in mice kidneys with diabetes. In our subsequent experiment, we incubated the AGEs- induced RAW264.7 macrophages with OxPAPC- an inhibitor of TLR signaling restricted to TLR2/4 (30). The results of the statistic reduction of TLR2, TLR4, MyD88, p-IRAK1, p-IRF3, and NF- $\kappa$ B p65, together with TNF- $\alpha$ , IL-1 $\beta$ , MCP-1 and iNOS, which is similar to the Paeoniflorin treatment, making our TLR-mediated macrophage activation and TLR-inhibited Paeoniflorin treatment sensible.

In summary, our findings suggest that the activation of TLR2/4 initiate M1 macrophage polarization and infiltration, resulting in the release of inflammatory cytokines and chemokines, which in turn exacerbate inflammation and ultimately aggravate DN. The research we did on Paeoniflorin treatment for the first time demonstrate that Paeoniflorin prevents macrophage activation *via* inhibition of TLR2/4 expression in type 2 diabetic nephropathy and provides supportive evidence for paeoniflorin therapeutic strategies in DN patients.

### Acknowledgements

The project was financially granted by Natural Science Foundation of China (No. 81374034, 81470965).

### References

1. Middleton RJ, Foley RN, Hegarty J, Cheung CM, McElduff P, Gibson JM, Kalra PA, O'Donoghue DJ, New JP. The unrecognized prevalence of chronic kidney disease in diabetics. *Nephrol Dial Transplant*. 2006; 21:88-92

2. Grace BS, Clayton P, McDonald SP. Increases in renal replacement therapy in Australia and New Zealand: understanding trends in diabetic nephropathy. *Nephrology (Carlton)*. 2012; 17:76-84.
3. Ansell D, Feehally J, Fogarty D, *et al*. UK renal registry 2009: 12th annual report of the renal association. *Nephron Clin Pract*. 2010;115 suppl 1:c1-c370.
4. Awad AS, You H, Gao T, Cooper TK, Nedospasov SA, Vacher J, Wilkinson PF, Farrell FX, Brian Reeves W. Macrophage-derived tumor necrosis factor-alpha mediates diabetic renal injury. *Kidney Int*. 2015; 88:722-733.
5. Leoncini G, Viazzi F, Pontremoli R. RAAS inhibition and renal protection. *Curr Pharm Des*. 2012; 18:971-980.
6. Awad AS, You H, Gao T, Gvritshvili A, Cooper TK, Tombran-Tink J. Delayed treatment with a small pigment epithelium derived factor (PEDF) peptide prevents the progression of diabetic renal injury. *PLoS One*. 2015; 10:e0133777.
7. Ma J, Wu H, Zhao C.Y, Panchapakesan U, Pollock C, Chadban SJ. Requirement for TLR2 in the development of albuminuria, inflammation and fibrosis in experimental diabetic nephropathy. *Int J Clin Exp Pathol*. 2014; 7:481-495.
8. Devaraj S, Tobias P, Kasinath B.S, Ramsamooj R, Afify A, Jialal I. Knockout of toll-like receptor-2 attenuates both the proinflammatory state of diabetes and incipient diabetic nephropathy. *Arterioscler Thromb Vasc Biol*. 2011; 31:1796-1804.
9. Mudaliar H, Pollock C, Komala M.G, Chadban S, Wu H, Panchapakesan U. The role of Toll-like receptor proteins (TLR) 2 and 4 in mediating inflammation in proximal tubules. *Am J Physiol Renal Physiol*. 2013; 305:F143-154.
10. Lin M, Yiu WH, Wu HJ, Chan LY, Leung JC, Au WS, Chan KW, Lai KN, Tang SC. Toll-like receptor 4 promotes tubular inflammation in diabetic nephropathy. *J Am Soc Nephrol*. 2012; 23:86-102.
11. Liu HQ, Zhang WY, Luo XT, Ye Y, Zhu XZ. Paeoniflorin attenuates neuroinflammation and dopaminergic neurodegeneration in the MPTP model of Parkinson's disease by activation of adenosine A<sub>1</sub> receptor. *Br J Pharmacol*. 2006; 148:314-325.
12. Wang C, Yuan J, Wu HX, Chang Y, Wang QT, Wu YJ, Liu LH, Wei W. Paeoniflorin inhibits inflammatory responses in mice with allergic contact dermatitis by regulating the balance between inflammatory and anti-inflammatory cytokines. *Inflamm Res*. 2013; 62:1035-1044.
13. Yu HY, Liu MG, Liu DN, Shang GW, Wang Y, Qi C, Zhang KP, Song ZJ, Chen J. Antinociceptive effects of systemic various paeoniflorin on bee venom-induced various phenotypes of nociception and hypersensitivity. *Pharmacol Biochem Behav*. 2007; 88:131-140.
14. Zhang MH, Feng L, Zhu MM, Gu JF, Wu C, Jia XB. Antioxidative and anti-inflammatory activities of paeoniflorin and oxypaeoniflora on AGEs-induced mesangial cell damage. *Planta Med*. 2013; 79:1319-1323.
15. Hung JY, Yang CJ, Tsai YM, Huang HW, Huang MS. Antiproliferative activity of paeoniflorin is through cell cycle arrest and the Fas/Fas ligand-mediated apoptotic pathway in human non-small cell lung cancer A549 cells. *Clin Exp Pharmacol Physiol*. 2008; 35:141-147.
16. Fu J, Li Y, Wang L, Gao B, Zhang N, Ji Q. Paeoniflorin prevents diabetic nephropathy in rats. *Comp Med*. 2009; 59:557-566.
17. Huang H, Chang EJ, Lee Y, Kim JS, Kang SS, Kim

- HH. A genome-wide microarray analysis reveals anti-inflammatory target genes of paeonol in macrophages. *Inflamm Res*. 2008; 57:189-198.
18. Nguyen D, Ping F, Mu W, Hill P, Atkins RC, Chadban SJ. Macrophage accumulation in human progressive diabetic nephropathy. *Nephrology (Carlton)*. 2006; 11:226-231.
  19. Ururahy MA, Loureiro MB, Freire-Neto FP, de Souza KS, Zuhl I, Brandao-Neto J, Hirata RD, Doi SQ, Arrais RF, Hirata MH, Almeida Md, de Rezende AA. Increased TLR2 expression in patients with type 1 diabetes: Evidenced risk of microalbuminuria. *Pediatr Diabetes*. 2012; 13:147-154.
  20. Liu DZ, Xie KQ, Ji XQ, Ye Y, Jiang CL, Zhu XZ. Neuroprotective effect of paeoniflorin on cerebral ischemic rat by activating adenosine A1 receptor in a manner different from its classical agonists. *Br J Pharmacol*. 2005; 146:604-611.
  21. He DY, Dai SM. Anti-inflammatory and immunomodulatory effects of paeonia lactiflora pall, a traditional chinese herbal medicine. *Front Pharmacol*. 2011; 2:10.
  22. Zhang W, Dai SM. Mechanisms involved in the therapeutic effects of Paeonia lactiflora Pallas in rheumatoid arthritis. *Int Immunopharmacol*. 2012; 14:27-31.
  23. Ding ZX, Yang SF, Wu QF, Lu Y, Chen YY, Nie XL. Therapeutic effect of total glucosides of paeony on lupus nephritis in MRL/lpr mice. *Nan Fang Yi Ke Da Xue Xue Bao*. 2011; 31:656-660. ( in Chinese)
  24. Wu H, Wei W, Song L, Zhang L, Chen Y, Hu X. Paeoniflorin induced immune tolerance of mesenteric lymph node lymphocytes *via* enhancing beta 2-adrenergic receptor desensitization in rats with adjuvant arthritis. *Int Immunopharmacol*. 2007; 7:662-673.
  25. Zhang HF, Xiao WG, Hou P. 2011. Clinical study of total glucosides of paeony in patients with systemic lupus erythematosus. *Zhongguo Xi Yi Jie He Za Zhi*. 2011; 31:476-479. (in Chinese)
  26. Xu XX, Qi XM, Zhang W, Zhang CQ, Wu XX, Wu YG, Wang K, Shen JJ. Effects of total glucosides of paeony on immune regulatory toll-like receptors TLR2 and 4 in the kidney from diabetic rats. *Phytomedicine*. 2014; 21:815-823
  27. Zhang XL, Guo YF, Song ZX, Zhou M. Vitamin D prevents podocyte injury *via* regulation of macrophage M1/M2 phenotype in diabetic nephropathy rats. *Endocrinology*. 2014; 155:4939-4350.
  28. Ricardo SD, van Goor H, Eddy AA. Macrophage diversity in renal injury and repair. *J Clin Invest*. 2008; 118: 3522-3530.
  29. Mudaliar H, Pollock C, Panchapakesan U. Role of Toll-like receptors in diabetic nephropathy. *Clin Sci (Lond)*. 2014; 126:685-694.
  30. Erridge C, Kennedy S, Spickett CM, Webb DJ. Oxidized phospholipid inhibition of Toll-like receptor (TLR) signaling is restricted to TLR2 and TLR4 - Roles for CD14, LPS-binding protein, and MD2 as targets for specificity of inhibition. *J Biol Chem*. 2008; 283:24748-24759.

(Received April 30, 2017; Revised May 30, 2017; Accepted June 1, 2017)

# Preoperative biliary drainage versus direct surgery for perihilar cholangiocarcinoma: A retrospective study at a single center

Yulong Cai<sup>1</sup>, Qi Tang<sup>2</sup>, Xianze Xiong<sup>1</sup>, Fuyu Li<sup>1</sup>, Hui Ye<sup>1</sup>, Peipei Song<sup>3</sup>, Nansheng Cheng<sup>1,\*</sup>

<sup>1</sup> Department of Bile Duct Surgery, West China Hospital, Sichuan University, Chengdu, Sichuan, China;

<sup>2</sup> Department of Social Medicine and Medical Service Management, School of Public Health, Shandong University, Ji'nan, Shandong, China;

<sup>3</sup> Graduate School of Frontier Sciences, The University of Tokyo, Kashiwa-shi, Chiba, Japan.

## Summary

Perihilar cholangiocarcinoma (pCC, also known as a Klatskin tumor) is the most common type of cholangiocarcinoma (CC). Preoperative biliary drainage (PBD) is indicated for pCC patients with acute cholangitis or patients who need portal vein embolization (PVE). However, the routine performance of PBD in other patients with pCC is still controversial. The current study retrospectively examined patients with pCC who did not undergo PVE and who did not have cholangitis who were seen at this Hospital to assess the advantages and disadvantages of PBD. This study also sought to find an optimal value of total bilirubin (TB) to indicate performing PBD. Between 2009 and 2014, after excluding patients with acute cholangitis and PVE, patients who had undergone hepatectomy for pCC were enrolled in this study. First, the surgical outcomes and postoperative outcomes were compared between PBD group and direct surgery group. Second, ROC curve analysis of a subgroup of patients was performed to find the best cut off value of TB for indicating the PBD. Third, the costs for patients, including the total charges and the charges per day were compared between the two groups. Subjects were 218 patients in total. Fifty-five patients underwent PBD. This group had a longer operative time [390 (210-700) vs. 360 (105-730) min,  $p = 0.013$ ], and a longer hospital stay [20 (9-48) vs. 17 (6-93) days,  $p = 0.007$ ], but underwent vascular resection and reconstruction less often [8 (14.5%) vs. 50 (30.7%),  $p = 0.019$ ]. Mortality and morbidity were comparable between the two groups. ROC curve analysis of a subgroup of patients indicated that the cut-off value for total bilirubin was 218.75  $\mu\text{mol/L}$  (12.4 mg/dL). The total hospital charges and the charges per day did not differ significantly for the two groups. Disadvantages of PBD were a longer operating time and a longer duration of hospitalization, but the short-term surgical outcomes and hospital charges of PBD group were comparable to the direct surgery group. PBD should be considered for patients when the diagnosis is still suspicious of pCC. Based on the current data, the optimal cut-off value for preoperative TB was 218.75  $\mu\text{mol/L}$  (12.4 mg/dL) to indicate PBD for patients with pCC.

**Keywords:** Cholangiocarcinoma, Klatskin tumor, preoperative biliary drainage, bilirubin, hospital cost

## 1. Introduction

Perihilar cholangiocarcinoma (also known as a Klatskin

Released online in J-STAGE as advance publication May 22, 2017.

\*Address correspondence to:

Dr. Nansheng Cheng, Department of Bile Duct Surgery, West China Hospital, Sichuan University, Chengdu, Sichuan Province, China.

E-mail: nanshengcheng2012@163.com

tumor) is the most common type of cholangiocarcinoma (CC). Perihilar cholangiocarcinoma (pCC) is defined as CC located in the extrahepatic bile duct and involving the confluence of the left and right main hepatic ducts (1). At present, the only potential curative treatment for pCC is surgical resection. In order to achieve an R0 resection (negative margins), a major hepatectomy, in a form such as a right or left trisegmentectomy, must be performed (2). Moreover, patients with pCC are known to have obstructive jaundice. Given this fact, patients

have higher postoperative morbidity and mortality rates due to hepatic insufficiency and infections (3).

Preoperative biliary drainage (PBD) and portal vein embolization (PVE) are used for preoperative optimization of the liver. PBD is performed to prevent cholestasis-associated toxicities and PVE is performed to improve regeneration of a small future remnant liver (FLR) (4). According to current evidence and guidelines regarding pCC, biliary drainage is definitely indicated for a patient with pCC and acute cholangitis, but the routine performance of biliary drainage is controversial (5). In addition, PBD is recommended for patients who are eligible for PVE (6).

A meta-analysis has indicated that PBD provided no advantage when treating a tumor causing obstructive jaundice (7). Therefore, whether PBD should be undergone by patients without acute cholangitis and who do not need PVE is still controversial. Moreover, surgeons usually choose to perform PBD depending on the level of total bilirubin (TB), but few studies have examined an appropriate value for TB to indicate the need for PBD.

The current study retrospectively examined patients with pCC who did not undergo PVE and who did not have cholangitis who were seen at this Hospital to assess the advantages and disadvantages of PBD. This study also sought to determine an optimal value for TB to indicate the need for PBD.

## 2. Materials and Methods

### 2.1. Patients

Potential subjects were patients had undergone hepatectomy for pCC between 2009 and 2014 at a tertiary care facility (Department of Bile Duct/Pancreat/Liver Surgery, West China Hospital, Sichuan University, China). Patients with acute cholangitis and patients who underwent PVE were excluded, resulting in 218 patients in total. The clinical records of these patients were retrospectively reviewed using the Hospital's database. pCC was confirmed based on pathological findings in all patients. Fifty-five patients underwent PBD and the remaining 163 patients directly underwent surgery. Patients who died or who had serious complications (Dindo-Clavien III-IV) causing hospitalization for over 30 days were excluded to identify a subgroup of patients with a good prognosis postoperatively ( $n = 184$ ). A receiver operating characteristic (ROC) curve analysis of this subgroup of patients was performed. In general, patients were routinely followed for 90 days to analyze the 90-day mortality and morbidity.

### 2.2. Study design

This study was divided into three parts. First, the outcomes of patients who underwent PBD and those

who did not were compared to assess the advantages and disadvantages of PBD. Second, ROC curve analysis of a subgroup of patients was performed to find the optimal value for TB to indicate PBD. Third, the cost for patients, including the total charges and the charges per day, were compared for patients who underwent PBD and patients who did not.

### 2.3. Definitions

PBD was defined as insertion of a biliary drain for percutaneous transhepatic drainage (PTBD) or endoscopic biliary drainage (EBD). Patients underwent surgery one week after PBD, and patients who directly underwent surgery usually did so two weeks after they were diagnosed with pCC. The Bismuth-Corlette classification was used to gauge the extent of pCC (8). The American Society of Anesthesiologists (ASA) Physical Status classification system was used to evaluate a patient's physical state before undergoing surgery. Bilirubin levels were measured in units of  $\mu\text{mol/L}$  ( $1\text{mg/dL} = 17.1\mu\text{mol/L}$ ). Postoperative mortality was defined as any death occurring within 90 days of surgery. R0 resection was considered curative treatment when the resection margin was free of the tumor according to microscopy. Postoperative morbidity included grade I to IV complications according to the Dindo-Clavien classification (9). Tumors were identified a mass-forming, periductal-infiltrating, and intraductal-growing types based on the classification proposed by the Liver Cancer Study Group of Japan (10).

The surgical procedure depended on the location of the tumor. Generally, a right/left hepatectomy with caudate resection, lymph node dissection, common bile duct resection, and Roux-en-Y biliary-enteric anastomosis was performed. Simple extrahepatic bile duct resection was performed only for patients with Bismuth-Corlette type I pCC. The initial rationale for surgery was to achieve an R0 resection. The total cost for patients included the hospital basic fee and the cost of medications, surgery, and anesthesia. In China, National Health Insurance covers most of the costs, but costs for some surgical instruments are borne by patients themselves.

### 2.4. Statistical analysis

Statistical analyses were performed using SPSS (version 19.0, SPSS Inc. Chicago, IL, USA). Continuous variables with a normal distribution were expressed as the mean  $\pm$  standard deviation (SD) and compared using an independent Student's *t* test. Other continuous variables were expressed as the median (range) and compared using the Mann-Whitney *U* test. Categorical data were expressed as the number (percentage) and compared using a chi-square or Fisher's exact test as appropriate. ROC curve analysis was used in the subgroup with a

good prognosis to determine the best cut-off value for TB to indicate the need for PBD. Sensitivity, specificity, positive predictive values (PPV), and negative predictive values (NPV) were calculated for the cut-off point. A *p* value < 0.05 was deemed to be significant.

### 3. Results

#### 3.1. PBD versus direct surgery

The flowchart in Figure 1 shows how patients were selected. Patients with acute cholangitis and who underwent PVE were excluded, resulting in a total of 218 patients. Fifty-five patients underwent PBD before surgery and 163 patients directly underwent surgery. The demographic and clinical characteristics of the two groups are shown in Table 1. There were no significant differences between PBD group and direct surgery group in terms of age, gender, BMI, smoking, infection with the hepatitis B virus, Bismuth-Corlette classification, or ASA physical status score. In regard to preoperative laboratory data, Aspartate transaminase (AST) levels in

the two groups were similar. The PBD group had higher levels of total bilirubin before PBD [281.1 (8.2-565.4) vs. 161.0 (8.4-455.6), *p* = 0.000] and lower levels of Alanine aminotransferase (ALT) [81 (13-383) vs. 113 (13-765), *p* = 0.032]. And the direct surgery group had lower levels of albumin (ALB) [35.7 (28.1-50.1) vs. 37.7 (22.2-71.0), *p* = 0.029]. Importantly, after patients underwent PBD, the total bilirubin (TB) level one day before surgery did not differ significantly between the two groups [140.9 (7.2-497.4) vs. 161.0 (8.4-455.6), *p* = 0.467].

The surgical and postoperative outcomes are shown in Table 2. The PBD group associated with longer operative time [390 (210-700) vs. 360 (105-730) min, *p* = 0.013] and hospital stay [20 (9-48) vs. 17 (6-93) days, *p* = 0.007]. Although there were no deaths in the PBD group, mortality did not differ significantly between the two groups [0 (0%) vs. 7 (4.3%), *p* = 0.263]. Morbidity was higher in the PBD group but did not differ significantly from that in the other group. Interestingly, fewer patients in the PBD group underwent vascular resection and reconstruction in comparison to the direct surgery group [8 patients (14.5%) vs. 50 (30.7%), *p* = 0.019]. Total

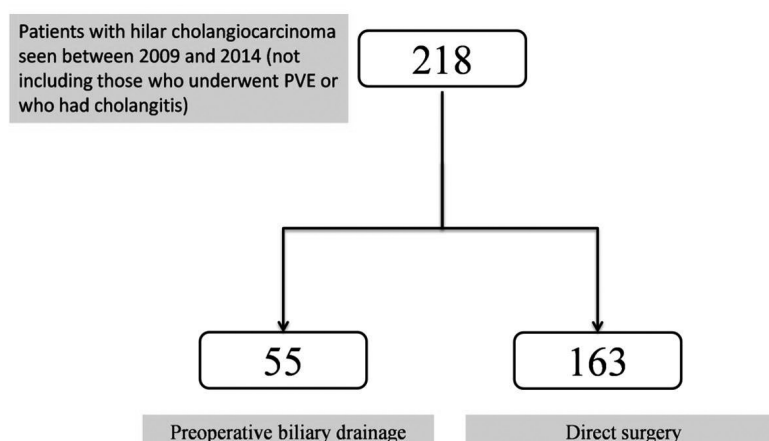


Figure 1. Flowchart of the included participants. PVE, portal vein embolization.

Table 1. Demographic and clinical characteristics

Variables	PBD (n = 55)	Direct surgery (n = 163)	<i>p</i> value
Age (years)	59 ± 11	60 ± 9	0.349
Gender (male/female)	30/25	74/89	0.240
BMI	21.8 ± 5.9	22.5 ± 6.8	0.519
Smoking	20 (36.4%)	65 (39.9%)	0.644
HBV infection	5 (9.1%)	9 (5.5%)	0.538
Bismuth-Corlette classification			
I/ II/ IIIA/ IIIB/ IV	9/13/10/8/5	24/28/24/42/45	0.469
ASA physical status score			
I/II/III/IV/V	2/26/26/0/1	1/83/78/0/1	0.189
ALB (g/L)	35.7 (28.1-50.1)	37.7 (22.2-71.0)	0.029
ALT (U/L)	81 (13-383)	113 (13-765)	0.032
AST (U/L)	74 (24-255)	89 (14-836)	0.114
T-Bil before PBD (µmol/L)	281.1 (8.2-565.4)	161.0 (8.4-455.6)	0.000
T-Bil after PBD (µmol/L)	140.9 (7.2-497.4)	161.0 (8.4-455.6)	0.467

Age and BMI are expressed as the mean ± standard deviation; other variables are expressed as the number (%) or median (range). PBD, preoperative biliary drainage; ALB, albumin; ALT, alanine aminotransferase; AST, aspartate transaminase; T-Bil, total bilirubin.

**Table 2. Surgical and postoperative outcomes**

Variables	PBD (n = 55)	Direct surgery (n =163)	p value
Surgical procedure, n (%)			
Right or extended right hepatectomy	29 (52.7%)	71 (43.6%)	0.238
Left or extended left hepatectomy	17 (30.9%)	68 (41.7%)	0.155
Simple bile duct resection	9 (16.4%)	24 (14.7%)	0.769
Operative time, min	390 (210-700)	360 (105-730)	0.013
Operative bloody loss, ml	500 (100-2000)	500 (50-3000)	0.324
Transfusion	26 (47.3%)	57 (35.0%)	0.104
Vascular reconstruction	8 (14.5%)	50 (30.7%)	0.019
Morbidity Dindo-Clavien			
Total	26 (47.2%)	56 (34.4%)	0.087
Grade I and II, n (%)	13 (23.6%)	35 (21.5%)	0.738
Grade III and IV, n (%)	13 (23.6%)	21 (12.9%)	0.057
Mortality	0 (0.0%)	7 (4.3%)	0.263
Second laparotomy	1 (1.8%)	10 (6.1%)	0.364
Tumor size, cm	2.9 (1.0-6.0)	3.0 (0.8-8.0)	0.987
Surgical margin			
R0/R1/R2	42 (76.4%)	125 (76.6%)	0.961
Tumor type			
Periductal-infiltrating/ mass-forming/intraductal-growing	39/11/5	101/44/18	0.482
T-Bil (μmol/L)	180.6 (17.0-540.8)	120.2 (6.2-461.0)	0.000
POD 3	106.5 (7.0-601.1)	75.4 (8.6-299.6)	0.004
POD 7			
ALT (U/L)	160 (17-5524)	187 (21-1753)	0.235
POD 3	70 (12-336)	67 (8-1576)	0.843
POD 7			
AST (U/L)	102 (24-24804)	118 (23-4528)	0.646
POD 3	55 (29-394)	47 (14-1591)	0.382
POD 7			
ALB (g/L)	29.1 (21.3-38.3)	29.8 (20.0-163.0)	0.355
POD 3	31.0 (21.2-86.0)	32.8 (20.1-67.0)	0.031
POD 7	20 (9-48)	17 (6-93)	0.007
Total hospital stay			

T-Bil, ALT, AST, and ALB levels for 7 patients who died were excluded. POD, postoperative day.

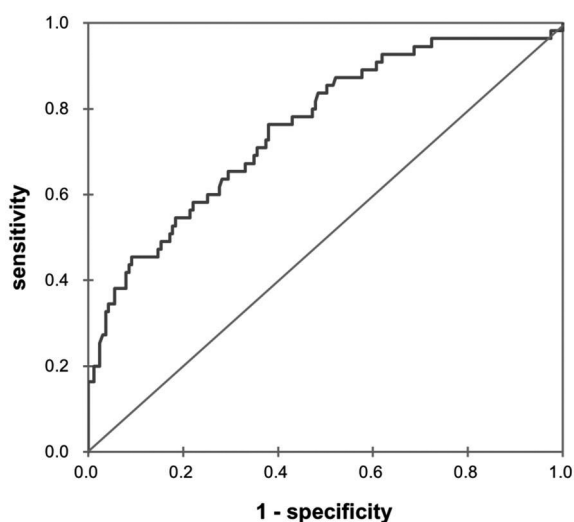


**Figure 2. Results of ROC curve analysis of preoperative total bilirubin to predict the need for preoperative biliary drainage in a subgroup of patients.** Cut-off value: 218.75 μmol/L; ROC area: 0.780; 95%CI: 0.699-0.862; Sensitivity (%): 70.5; Specificity (%): 72.1; PPV (%):44.3; NPV (%): 88.6.

bilirubin was higher on POD 1 and POD 3 in the PBD group, and ALB was lower on POD 7. The surgical

procedure, operative blood loss, number of transfusions needed, whether a second laparotomy was performed, tumor size, R0 resection, tumor type, and AST and ALT levels on POD 1 and 7 were similar for the two groups.

The current findings revealed that the PBD group and the direct surgery group had nearly the same postoperative outcomes. Patients in the PBD group had a longer operating time and longer duration of hospitalization but underwent vascular resection and reconstruction less often. There were no deaths in the group that underwent PBD, but mortality did not differ significantly from the other group according to the current findings.

### 3.2. ROC curve analysis

ROC curve analysis of a subgroup of patients was performed. In order to find the optimal reference value of TB to indicate the need for PBD, patients who died and patients who had major complications that caused hospitalization for over 30 days were excluded. This subgroup of patients had a good prognosis and they can be regarded as right and standard choice of performing PBD on pCC patients. This subgroup consisted of 184

**Table 3. Financial outcomes in the PBD and direct surgery groups**

Variables	PBD (n = 55)	Direct surgery (n =163)	p value
Total charge for the treatment			
RMB	93,946 ± 40,198	84,223 ± 56,759	0.588
(US\$)	(14,270 ± 6,106)	(12793 ± 8,621)	
Charge per day			
RMB	4,096 ± 1,526	4,738 ± 2,082	0.331
(US\$)	(622 ± 231)	(719 ± 316)	

Cost was calculated based on an exchange rate of 6.6 RMB to 1US dollar and is expressed as the mean ± standard deviation.RMB is the Ren Min Bi, or the official currency of the People's Republic of China.

patients. Results of ROC curve analysis are shown in Figure 2. The cut-offvalue for total bilirubin was 218.75 $\mu$ mol/L, with a sensitivity of 70.5%, a specificity of 72.1 %, a PPV of 44.3 %, and an NPV of 88.6 % in terms of predicting whether PBD was needed. The area under the ROC curve was 0.78. Based on the current findings, preoperative TB of 218.75  $\mu$ mol/L (12.4 mg/dL) was an optimal reference point for deciding whether patients needed to undergo PBD.

### 3.3. Comparison of charge

The total charges and charges per day were shown in Table 3. The exchange rate was 6.6 RenMinBi (RMB, the official currency of the People's Republic of China) to 1 US dollar. The mean of total charges was higher in PBD group, but the mean total cost did not differ significantly between the two groups (14,270 ± 6,106 US\$ vs. 12,793 ± 8,621 US\$,  $p = 0.588$ ). Similarly, the cost per day did not differ significantly between the two groups (622 ± 231\$ vs. 719 ± 316\$,  $p = 0.331$ ).

## 4. Discussion

Currently, the clear consensus is that PBD is indicated for patients with cholangitis, hyperbilirubinemia-induced malnutrition, hepatic insufficiency, or renal insufficiency and patients undergoing preoperative anti-neoplastic therapy or PVE (11). The routine performance of PBD in other patients with pCC is still controversial. The current study focused on those patients. Surgical outcomes and hospital costs were compared for patients who underwent PBD and patients who did not, and ROC curve analysis was performed to find an optimal cut-off value for preoperative TB to indicate the need for PBD.

The current results indicated that the short-term surgical and postoperative outcomes of the group that directly underwent surgery were comparable to those of the group that underwent PBD. This finding is consistent with the results of previous studies and meta-analyses (12-14). Several studies have found that PBD increased the risk of postoperative complications and infections (15-17), but our data did not demonstrate this. In the current study, the disadvantages of PBD were a longer

operating time and longer duration of hospitalization. However, the total cost of hospitalization for patients in PBD group did not increase. Although the current study noted no advantages of PBD in terms of short-term surgical outcomes, attention must be paid to the potential advantages of PBD when treating patients with pCC. Nimura et al. noted that selective cholangiography through PTBD and/or ENBD allows precise preoperative staging of the disease (18). In addition, ERCP/ENBD can delineate the anatomy of the biliary system, determine the extent of bile duct involvement, and allow correct differentiation of malignant from benign lesions through cytology by brushings and biopsy, which are important in determining respectability and surgical management (19). These advantages cannot be ignored. Benign bile duct diseases are needed be excluded during the process of diagnosis, such as hepatolithiasis (20). Thus when the suspicion remains for pCC, the PBD should be indicated due to the reasons mentioned above. Although the mortality rate was comparable between the two groups in the current study, no death was found in PBD group. Probably because of after performing PBD, some patients were found out that the tumor was unresectable and part of patients' liver function worsened before surgery was planned. Those patients were ultimately not eligible for surgery and did not undergo surgery. In addition, patients underwent PBD possess more time to evaluate the tumor, and a small part of tumors are progressing before surgery resulting in selecting other treatment. Regarding to vascular resection and reconstruction, a Belghiti's group showed that PBD increased the percentage of resectability (21). The rate of vascular resection and reconstruction in PBD group was higher in their study, but in our study the rate was lower. In our center, as the value of resection and reconstruction of portal vein or hepatic artery (stage IV, AJCC 7<sup>th</sup> staging system) is still controversial (22), so some of those patients at the current authors' Hospital wished to undergo chemotherapy rather than surgery for financial reasons. In addition, staging was more precise in the PBD group resulting in more patients with stage IV cancer were detected and ruled out in this study. This could explain the lower rate of vascular resection and reconstruction in the current study.

Among patients with obstructive jaundice, PBD is the best way to reduce the bilirubin level to reverse cholestasis-associated liver dysfunction and impaired hepatic regeneration (23). However, there are no guidelines or indications regarding the level of bilirubin that warrants a patient undergoing PBD. A ROC curve was used in the current study to find the cut-off value for TB to indicate PBD. The classifier result should be a real value, so we excluded the patients underwent bad prognosis (death or heavy complications caused hospital stay over 30 days), and the remaining patients all had a good prognosis, and the cut-off value for TB in those patients can be regarded as a correct/real value. The cut-off value for preoperative TB was 218.75  $\mu\text{mol/L}$  (12.4 mg/dL) based on the current findings. Su et al. reported that preoperative PTBD is advisable for pCC with severe jaundice (> 10 mg/dL) (24). The cut-off value for TB in the current study was very close to the value reported by Su et al. A subgroup of patients with a TB level over 218.75  $\mu\text{mol/L}$  was also analyzed in terms of those who underwent PBD and those that directly underwent surgery, but the outcomes for those patients were consistent with the outcomes for patients as a whole. Therefore, this cut off value of TB did not show any clinical benefit. We just emphasized that this point of value could be the best reference point to indicate the PBD based on our data. In the future, more clinical data need to be assembled and randomized controlled trials need to be conducted to resolve the controversy regarding PBD.

The current study had several limitations. First, incomplete data precluded the comparison of the two groups in terms of long-term outcomes and survival rates. Second, this study was retrospective, so selection bias potentially occurred and the study involved a small sample. Third, patient insurance differs widely among regions of China, so data on actual expenses could not be obtained. Only data on the total cost according to the hospital was available.

## 5. Conclusion

PBD has several advantages and disadvantages. In patients who did not undergo PVE and who did not have cholangitis, those that underwent PBD had comparable short-term outcomes to those that directly underwent surgery. When the diagnosis is still suspicious of pCC, PBD should be performed for the patients. The total hospital charges and charges per day were similar for the two groups. Based on our data, the optimal cut-off value for preoperative TB was 218.75  $\mu\text{mol/L}$  (12.4 mg/dL) to indicate the need for PBD in patients with pCC. These findings may offer some clues for further study. More RCTs and large-scale studies need to be conducted to resolve the controversy concerning PBD.

## References

1. Klatskin G. Adenocarcinoma of the hepatic duct at its bifurcation within the porta hepatis: An unusual tumor with distinctive clinical and pathological features. *Am J Med.* 1965; 38:241-256.
2. Ito F, Agni R, Rettammel RJ, Been MJ, Cho CS, Mahvi DM, Rikkers LF, Weber SM. Resection of hilar cholangiocarcinoma: Concomitant liver resection decreases hepatic recurrence. *Ann Surg.* 2008; 248:273-279.
3. Nagino M, Kamiya J, Uesaka K, Sano T, Yamamoto H, Hayakawa N, Kanai M, Nimura Y. Complications of hepatectomy for hilar cholangiocarcinoma. *World J Surg.* 2001; 25:1277-1283.
4. Kawasaki S, Imamura H, Kobayashi A, Noike T, Miwa S, Miyagawa S. Results of surgical resection for patients with hilar bile duct cancer: Application of extended hepatectomy after biliary drainage and hemihepatic portal vein embolization. *Ann Surg.* 2003; 238:84-92.
5. Cai Y, Cheng N, Ye H, Li F, Song P, Tang W. The current management of cholangiocarcinoma: A comparison of current guidelines. *Biosci Trends.* 2016; 10:92-102.
6. Iacono C, Ruzzenente A, Campagnaro T, Bortolasi L, Valdegamberi A, Guglielmi A. Role of preoperative biliary drainage in jaundiced patients who are candidates for pancreatoduodenectomy or hepatic resection: highlights and drawbacks. *Ann Surg.* 2013; 257:191-204.
7. Sewnath ME, Karsten TM, Prins MH, Rauws EJ, Obertop H, Gouma DJ. A meta-analysis on the efficacy of preoperative biliary drainage for tumors causing obstructive jaundice. *Ann Surg.* 2002; 236:17-27.
8. Bismuth H, Nakache R, Diamond T. Management strategies in resection for hilar cholangiocarcinoma. *Ann Surg.* 1992; 215:31-38.
9. Dindo D, Demartines N, Clavien PA. Classification of surgical complications: A new proposal with evaluation in a cohort of 6336 patients and results of a survey. *Ann Surg.* 2004; 240:205-213.
10. Japan LCSGo. General Rules for the Clinical and Pathological Study of Primary Liver Cancer. Tokyo: Kanehara, Tokyo, Japan, 2000.
11. Mansour JC, Aloia TA, Crane CH, Heimbach JK, Nagino M, Vauthey JN. Hilar cholangiocarcinoma: Expert consensus statement. *HPB (Oxford).* 2015; 17:691-699.
12. Farges O, Regimbeau JM, Fuks D, Le Treut YP, Cherqui D, Bachellier P, Mabrut JY, Adham M, Pruvot FR, Gigot JF. Multicentre European study of preoperative biliary drainage for hilar cholangiocarcinoma. *Br J Surg.* 2013; 100:274-283.
13. Liu F, Li Y, Wei Y, Li B. Preoperative biliary drainage before resection for hilar cholangiocarcinoma: Whether or not? A systematic review. *Dig Dis Sci.* 2011; 56:663-672.
14. Ribero D, Zimmiti G, Aloia TA, Shindoh J, Forchino F, Amisano M, Passot G, Ferrero A, Vauthey JN. Preoperative cholangitis and future liver remnant volume determine the risk of liver failure in patients undergoing resection for hilar cholangiocarcinoma. *J Am Coll Surg.* 2016; 223:87-97.
15. Ercolani G, Zanello M, Grazi GL, Cescon M, Ravaioli M, Del Gaudio M, Vetrone G, Cucchetti A, Brandi G, Ramacciato G, Pinna AD. Changes in the surgical approach to hilar cholangiocarcinoma during an 18-year period in a Western single center. *J Hepatobiliary*

- Pancreat Sci. 2010; 17:329-337.
16. Ferrero A, Lo Tesoriere R, Vigano L, Caggiano L, Sgotto E, Capussotti L. Preoperative biliary drainage increases infectious complications after hepatectomy for proximal bile duct tumor obstruction. *World J Surg.* 2009; 33:318-325.
  17. Hochwald SN, Burke EC, Jarnagin WR, Fong Y, Blumgart LH. Association of preoperative biliary stenting with increased postoperative infectious complications in proximal cholangiocarcinoma. *Arch Surg.* 1999; 134:261-266.
  18. Nimura Y. Preoperative biliary drainage before resection for cholangiocarcinoma (Pro). *HPB (Oxford).* 2008; 10:130-133.
  19. Alvaro D, Cannizzaro R, Labianca R, Valvo F, Farinati F, Italian Society of G, Italian Association of Hospital G, Italian Association of Medical O, Italian Association of Oncological R. Cholangiocarcinoma: A position paper by the Italian Society of Gastroenterology (SIGE), the Italian Association of Hospital Gastroenterology (AIGO), the Italian Association of Medical Oncology (AIOM) and the Italian Association of Oncological Radiotherapy (AIRO). *Dig Liver Dis.* 2010; 42:831-838.
  20. Feng X, Zheng S, Xia F, Ma K, Wang S, Bie P, Dong J. Classification and management of hepatolithiasis: A high-volume, single-center's experience. *Intractable Rare Dis Res.* 2012; 1:151-156.
  21. Belghiti J, Ogata S. Preoperative optimization of the liver for resection in patients with hilar cholangiocarcinoma. *HPB (Oxford).* 2005; 7:252-253.
  22. Miyazaki M, Yoshitomi H, Miyakawa S, *et al.* Clinical practice guidelines for the management of biliary tract cancers 2015: 2nd English edition. *J Hepatobiliary Pancreat Sci.* 2015; 22:249-273.
  23. van der Gaag NA, Kloek JJ, de Castro SM, Busch OR, van Gulik TM, Gouma DJ. Preoperative biliary drainage in patients with obstructive jaundice: History and current status. *J Gastrointest Surg.* 2009; 13:814-820.
  24. Su CH, Tsay SH, Wu CC, Shyr YM, King KL, Lee CH, Lui WY, Liu TJ, P'Eng F K. Factors influencing postoperative morbidity, mortality, and survival after resection for hilar cholangiocarcinoma. *Ann Surg.* 1996; 223:384-394.

(Received January 23, 2017; Revised May 5, 2017; Accepted May 15, 2017)

# Perfusion and drainage difference in the liver parenchyma: Regional plane in segment 6

Hayato Abe, Shintaro Yamazaki\*, Masamichi Moriguchi, Tokio Higaki, Tadatoshi Takayama

Department of Digestive Surgery, Nihon University School of Medicine, Tokyo, Japan.

## Summary

The differences between the perfusion areas of portal vein and the drainage areas of hepatic vein result in the occurrence of either ischemic or congested areas after liver resection. To elucidate which factors are related to the differences between these areas of segment (S) 6 were therefore investigated. The portal-vein-based and hepatic-vein-based regional planes of S6 were defined using the region-growing and Voronoi tessellation methods in 103 consecutive patients who undergo liver resection. Finally, factors related to the difference between the perfusion and drainage areas of S6 were identified. The S6 regional plane based on the portal was coincident with that of hepatic veins (non-difference group) in 57 patients (55.3%), but was discordant on the ventral side (S6-dominant group) in 43 patients (41.7%) and the dorsal side (S5-dominant group) in 3 patients (3.0%). The presence of a proximal branch of the first portal 6 (S6-dominant group vs. non-difference group, 72.1% vs. 17.0%,  $p < 0.001$ ) and the presence of an inferior right hepatic vein (S6-dominant group vs. non-difference group, 72.1% vs. 43.9%,  $p = 0.008$ ) suggested large S6 ventrally. The median volume difference between the perfusion area of the portal vein and drainage area of the hepatic vein in S6 was 73 mL (range: 29-189 mL). In conclusion, preoperative 3D-simulation may enhance the preciseness of anatomic liver resection.

**Keywords:** Anatomic liver resection, three-dimensional liver anatomy, regional plane

## 1. Introduction

Recent advances in three dimensional (3D)-computed tomography (CT) of the liver anatomy have revealed that the perfusion areas of the portal vein and drainage area of the hepatic vein in the same segment did not always coincident (1-3). The liver anatomy as defined by Couinaud is the widely accepted clinical anatomy which defined the hepatic veins as one of the major landmarks of each segment (4,5). The liver staining method, in which dye is injected into the tumor occupying area of the portal vein, had been accepted as an anatomic liver resection method based on the

perfusion area of portal vein (6). For precise liver resection, it is necessary to understand that there is a difference of tumor occupying area between the concepts.

The preoperative evaluation in 3D-CT is an ideal approach to understand this difference. However, few reports have so far focused on this essential issue in anatomic liver resection (7,8). We investigate which anatomic factors influenced to such differences and how much parenchymal volume was different between the perfusion areas and drainage area of the liver parenchyma.

## 2. Materials and Methods

### 2.1. Patients

Between October 2013 and September 2014, preoperative 3D reconstruction and volumetric analyses of the liver were performed in 103 consecutive patients who underwent liver resection for hepatocellular carcinoma. All patients had radically resectable

Released online in J-STAGE as advance publication May 8, 2017.

\*Address correspondence to:

Dr. Shintaro Yamazaki, Department of Digestive Surgery, Nihon University School of Medicine 30-1 Ohya-guchikami-chou, Itabashi-ku, Tokyo 173-8610, Japan.  
E-mail: yamazaki-nmed@umin.ac.jp

hepatocellular carcinomas; the tumor diameter measured within 50 mm in a single tumor and within 30 mm in multiple tumors. The operative management strategies that are used at our institution have been described elsewhere (9-12). Ethics Committee approval was obtained (protocol number: RK-170214-03).

### 2.2. Three-dimensional reconstruction protocol

Three-phase, contrast-enhanced dynamic CT scans (unenhanced and hepatic arterial [37 seconds], portal venous [60 seconds], and liver parenchymal phases [150 seconds]) were obtained using a 16- or 350-detector row scanner (Aquilion 16/ONE; Toshiba Medical Systems, Otawara, Japan). The total dose of nonionic iodinated contrast medium was 630 mgI/kg body weight of iomeprol (350 mgI/mL). Scanning was performed using a 15.0- or 53.0-helical pitch, a table feed speed of 0.75 or 0.5 mm per rotation, a slice thickness of 0.5 mm, and 120 kV on a Volume EC system (Toshiba Corporation, Mie, Japan).

To perform 3D image reconstruction and volumetric measurements, the region-growing and the Voronoi tessellation method software programs (Volume Analyzer SYNAPSE VINCENT, FUJIFILM Corporation, Tokyo, Japan) were used. The 3D liver images were created using a region-growing algorithm.

### 2.3. Assessment view and definition of the portal-vein-based and hepatic-vein-based anatomies

The assessment view in the 3D-liver was defined as follows. First, the rotation angle ( $\theta$ ) between the proximal trunk of the right hepatic vein (RHV) and the median line on the inferior vena cava (IVC) of the horizontal plane of the CT scan was defined as a vertical and frontal view (RHV frontal view) on 3D-simulation (Figure 1a). This distal side of the RHV was extracted when the main trunk of the RHV was fully exposed as long as possible in virtual liver resection. This extracted RHV line was defined as the RHV trunk line. The assessment view was fixed as this RHV trunk line was located in the most dorsal of the 3D-liver.

Next, portal-vein-based S6 was defined as the perfusion area of P6 (Figure 1b), and the cranial-dorsal side from the posterior branch was defined as S6 if there were multiple trunks of P6. The hepatic-vein-based S6 was defined as the drainage area of lateral-dorsal tributaries to the RHV in the region growing method (Figure 1c). When the inferior or middle RHV was present, the drainage area of S6 was measured. The dominance of the parenchymal volume was defined by the position relationship of the regional plane of portal-vein-based S6 to the main trunk of the RHV: the plane runs ventrally beyond the RHV (S6-dominant group); dorsally beyond the RHV (S5-dominant group) or almost equal (non-difference group).

### 2.4. Hepatic vein analysis in the 3D liver

First, the tributary pattern, thicknesses of the main trunk and second-order tributaries, angles between the IVC and RHV, and the presence of tributaries of the RHV (*i.e.*, inferior or middle RHV) were assessed. Next, the second-order large drainage veins from the right liver to the RHV (V7) and the middle hepatic vein (MHV) (V6 and V8) were assessed.

### 2.5. Portal vein analysis in the 3D liver

Regarding the portal vein, the branch type of the main portal trunk, the length of the second-order portal vein, and the distance from the main portal trunk were assessed in the 3D liver. Next, the lengths of the anterior and posterior branches, the angle between these branches, and the number of P6 branches were assessed. When there were multiple trunks of P6, the entire caudal-dorsal side from the posterior branch was defined as S6. The perfusion area of the entire caudal-ventral side of the anterior portal trunk was defined as S5. S7 or S8 was derived by subtracting S5 or S6. Standard bifurcation of the portal vein was defined as the absence of an abnormally branched right portal vein (*i.e.*, no independent posterior branch), with anterior branches or P8 arising from the left portal trunk (umbilical portion). Anatomical variations of the portal branches were evaluated for the right liver, as described by Couinaud (1,13).

The branch patterns of P6 were divided into two types (Figure 2). On the assessment view, the first branch of P6 was branched toward the proximal side of the RHV trunk line (proximal type) or branched distal side (distal type). Finally, the factors related to the dominance of the hepatic parenchymal volume in S6 were assessed.

### 2.6. Volume difference between the portal-vein-based and hepatic-vein-based anatomies in S6

The parenchymal volume of the portal-vein-based S6 was calculated according to the perfusion area of P6 (Figure 3a), while the parenchymal volume of the hepatic-vein-based S6 was defined by the drainage area of lateral-dorsal tributaries to the RHV (Figure 3b) using the Voronoi tessellation method. These volumes were calculated using the workstation (SYNAPSE VINCENT). Finally, the volume difference between the portal-vein-based and hepatic-vein-based anatomies in S6 was compared.

### 2.7. Statistical analysis

Clinical data were recorded on an Excel (Microsoft) spreadsheet and analyzed using the JMP<sup>®</sup> 9.0 statistical software package (SAS Institute Inc., Cary, NC, USA). All variables were analyzed using the Mann-Whitney

*U* test or Fisher's exact test. A *p* value of < 0.05 was considered statistically significant.

### 3. Results

#### 3.1. Anatomical characteristics

In the 103 preoperative patients (male:female ratio, 77:26, and median age, 66 years (range, 41-85 years)), the median rotation angle ( $\theta$ ) used to obtain the RHV frontal view of the RHV trunk line was 83.3 degrees (range, 56.2-97.4 degrees) (Figure 1a). On this RHV frontal view, 46 patients (44.7%) were different to the RHV trunk line on the ventral side (S6-dominant group) in 43 patients (41.7%) and the dorsal side (S5-dominant

group) in 3 patients (3.0%). In 57 patients (55.3%), the portal perfusion area agreed with the hepatic drainage area for the RHV trunk line (non-difference group). The S5-dominant segmentation was noted in only 3 patients (3.0%), and further estimation was thus not performed.

#### 3.2. Tributary pattern of the hepatic vein

There was no significant difference in the angle of the RHA trunk ( $\theta$ ) for creating the RHV trunk line (80.8 degrees [66.4-95.4] vs. 84.2 degrees [56.2-97.4], *p* = 0.177), the median thickness of the RHV (6.5 mm [2.8-11.2] vs. 6.6 mm [2.8-14.9], *p* = 0.316), and V7 (4.5 mm [2.3-7.9] vs. 4.2 mm [2.3-8.3], *p* = 0.318) (Table 1). The proportion of patients with an inferior right hepatic vein

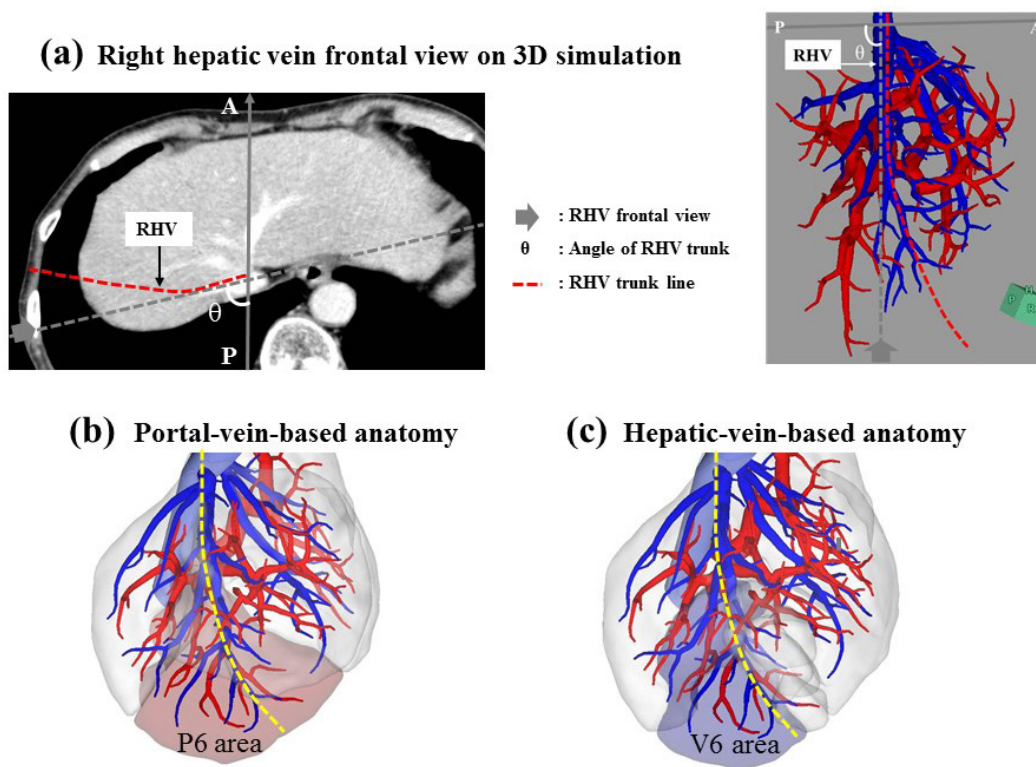


**Figure 1. Definition of each anatomy in segment 6.** (a) The frontal view was defined as the rotation angle ( $\theta$ ) between the RHV trunk and the median line on the inferior vena cava of the horizontal plane of the CT scan. The median angle ( $\theta$ ) of the basic trunk of the RHV was 83.3 degrees (range, 56.2-97.4 degrees) for all the patients. Three-dimensional simulation was always performed using the RHV frontal view. The basic line was drawn as the RHV trunk line when the RHV trunk was fully exposed as long as possible. The RHV trunk line was defined as the main trunk of the RHV fully exposed as long as possible. (b, c) The portal-vein-based segment(S) 6 and hepatic-vein-based S6 were expressed as the perfusion areas of the portal vein (P6) and drainage areas of the hepatic vein (V6), respectively, on the RHV trunk line of the 3D anatomy.

**Table 1. Anatomic characteristics and tributary pattern of the hepatic vein**

Items	All ( <i>n</i> = 103 <sup>*</sup> )	S6-dominant ( <i>n</i> = 43)	Non-difference ( <i>n</i> = 57)	<i>p</i> value <sup>**</sup>
Angle of RHV trunk ( $\theta$ ) (degree) <sup>***</sup>	83.3 (56.2-97.4)	80.8 (66.4-95.4)	84.2 (56.2-97.4)	0.177
RHV thickness (mm) <sup>***</sup>	6.5 (2.8-14.9)	6.5 (2.8-11.2)	6.6 (2.8-14.9)	0.316
V7 thickness to RHV (mm) <sup>***</sup>	4.3 (2.3-8.3)	4.5 (2.3-7.9)	4.2 (2.3-8.3)	0.318
Presence of IRHV, <i>n</i> (%)	56/103 (54.4)	31/43 (72.1)	25/57 (43.9)	0.008
V6 to MHV, <i>n</i> (%)	21/103 (20.4)	15/43 (34.9)	6/57 (10.5)	0.006
V8 to MHV, <i>n</i> (%)	48/103 (46.6)	22/43 (51.2)	26/57 (45.6)	0.687

<sup>\*</sup>Include S5-dominant patients (*n* = 3); <sup>\*\*</sup>S6-dominant vs. Non-difference; <sup>\*\*\*</sup>median (range). RHV = right hepatic vein; IRHV = inferior right hepatic vein; MHV = middle hepatic vein.

(IRHV) was significantly higher (72.1% vs. 43.9%,  $p = 0.008$ ), and the proportion of patients with V6 of the MHV tributary was higher (34.9% vs. 10.5%,  $p = 0.006$ ) in the S6-dominant group than in non-difference group. On the other hand, the presence of V8 of the MHV tributary ( $p = 0.687$ ) did not differ significantly among the groups.

### 3.3. Branch pattern of the portal vein

Standard bifurcation was found in 93 patients, trifurcation in 3 patients, and other specific branch types of the main portal trunk were found in 7 patients. There was no significant difference in the normal branch pattern of the main portal trunk (S6-dominant group vs. non-difference group, 41 patients [95.3%] vs. 50 patients [87.7%], respectively,  $p = 0.293$ ). In the 93 patients with the standard branch type, the length of the right portal trunk ( $p = 0.439$ ) and anterior branch trunk ( $p = 0.809$ ) did not differ significantly between the S6-dominant group and non-difference group (Table 2). In contrast, the

median posterior branch was significantly shorter in the S6-dominant group than in the non-difference group (15.6 [0-44.3] vs. 18.7 mm [0-47.8],  $p = 0.026$ ). The angle between the anterior and posterior trunks did not differ significantly between the S6-dominant group and non-difference group ( $p = 0.479$ ). The number of branches of P6 also did not differ significantly ( $p = 0.856$ ).

Regarding the branch patterns of the first P6, the S6-dominant group included a significantly higher proportion of the proximal type than the non-difference group (31 patients [72.1%] vs. 12 patients [27.9%]) (Figure 2). The non-difference group included a significantly higher proportion of the distal type than the S6-dominant group (10 patients [17.0%] vs. 47 patients [83.0%],  $p < 0.001$ ).

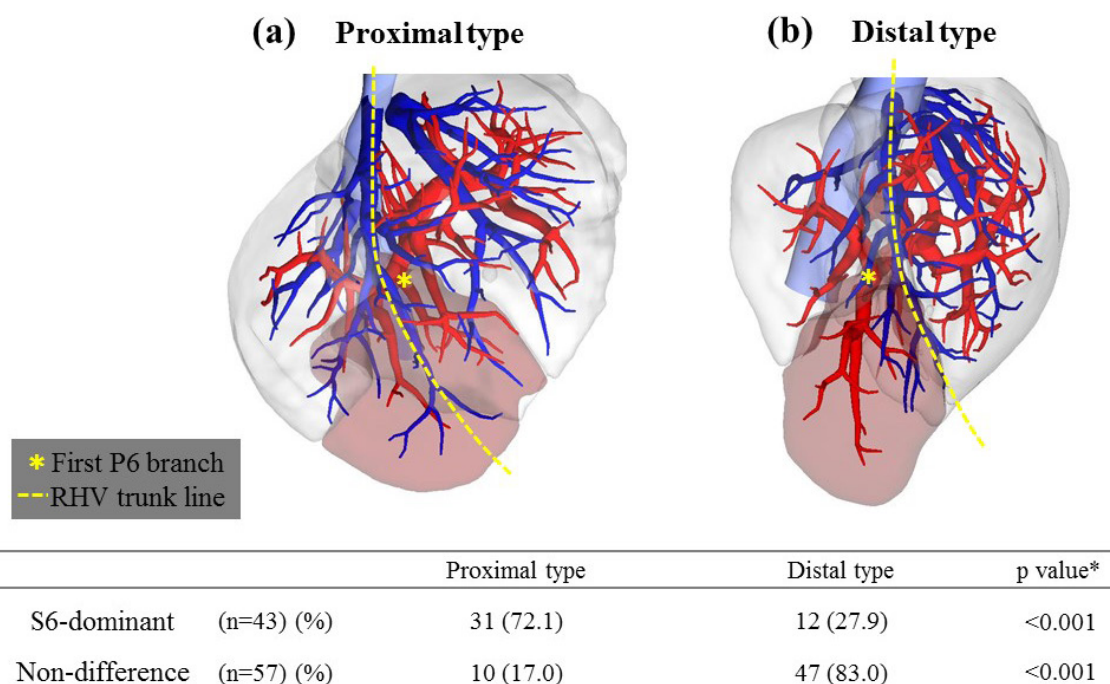
### 4. Volume analysis

According to the perfusion area of each segment, the volumes of S6 (204 [69-366] vs. 152 mL [44-287],  $p < 0.001$ ) and S7 (224 [82-561] vs. 205 mL [74-366],  $p$

**Table 2. Anatomic characteristics of the portal vein in standard bifurcation type cases (n = 93)**

Items	All (n = 93*)	S6-dominant (n = 41)	Non-difference (n = 50)	p value**
Length of right portal vein trunk (mm)	23.6 (5.4-41.9)	23.8 (5.4-41.9)	22.4 (6.5-39.4)	0.439
Length of anterior branch trunk (mm)	16.3 (0-37.5)	16.1 (0-36.4)	16.1 (0-37.5)	0.809
Length of posterior branch trunk (mm)	17.2 (0-47.8)	15.6 (0-44.3)	18.7 (0-47.8)	0.026
Angle between anterior and posterior trunk (degrees)	71.4 (41.2-106.3)	71.6 (46.8-106.3)	71.4 (41.2-100.6)	0.479
Number of portal veins in segment 6	1 (1-3)	1 (1-3)	1 (1-3)	0.856

Data are expressed as the medians (range). \*Include S5-dominant patients (n = 2); \*\*S6-dominant vs. Non-difference.



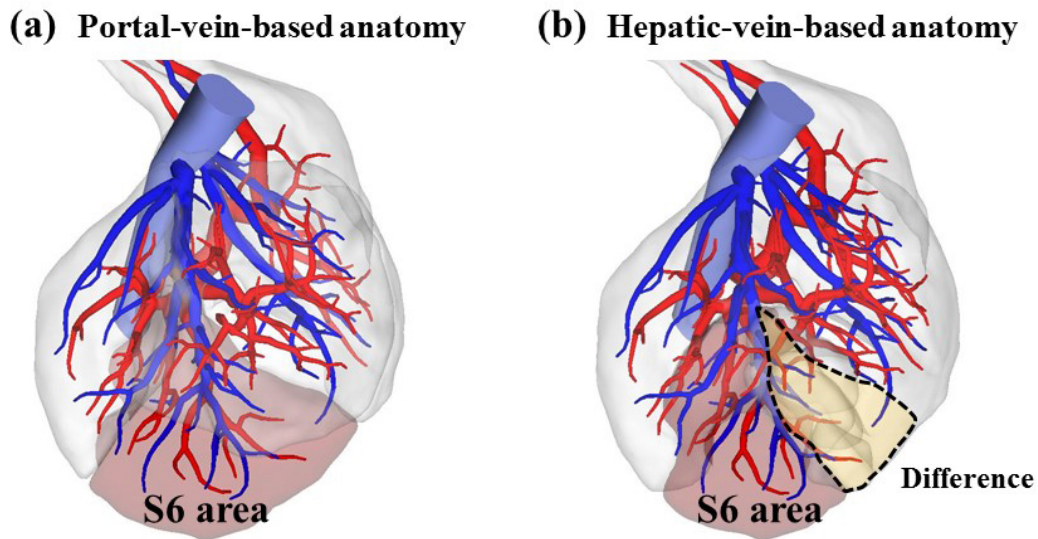
\* Fisher's exact test.

**Figure 2. Branch pattern of the first portal vein in segment 6.** (a) In the branch patterns of first P6, the S6-dominant group included a significantly higher proportion of the proximal type than the non-difference group on the RHV trunk line. (b) In contrast, the non-difference group included a significantly higher proportion of the distal type.

**Table 3. Volume analysis of each segment in the right liver**

Segment	All (n = 103 <sup>*</sup> )	S6-dominant (n = 43)	Non-difference (n = 57)	p value <sup>**</sup>
S5 (mL)	115 (33-360)	106 (33-312)	115 (39-360)	0.328
S6 (mL)	164 (44-366)	204 (69-366)	152 (44-287)	< 0.001
S7 (mL)	215 (74-561)	224 (82-561)	205 (74-366)	0.037
S8 (mL)	202 (43-536)	198 (45-536)	208 (43-464)	0.834

Data are expressed as the medians (range). <sup>\*</sup>Include S5-dominant patients (n = 3); <sup>\*\*</sup>S6-dominant vs. Non-difference.



	Portal-vein-based	Hepatic-vein-based	Volume difference	p value <sup>*</sup>
Parenchymal volume (mL)	164 (44-366)	142 (34-287)	73 (29-189)	<0.001

Figures represent median (range). <sup>\*</sup> Portal-vein-based vs. Hepatic-vein-based.

**Figure 3. Volume difference in segment 6.** (a, b) The portal-vein-based S6 was significantly larger than that derived from the hepatic-vein-based liver anatomy. The volume difference between the two groups was 73 mL [29-189 ml] in S6.

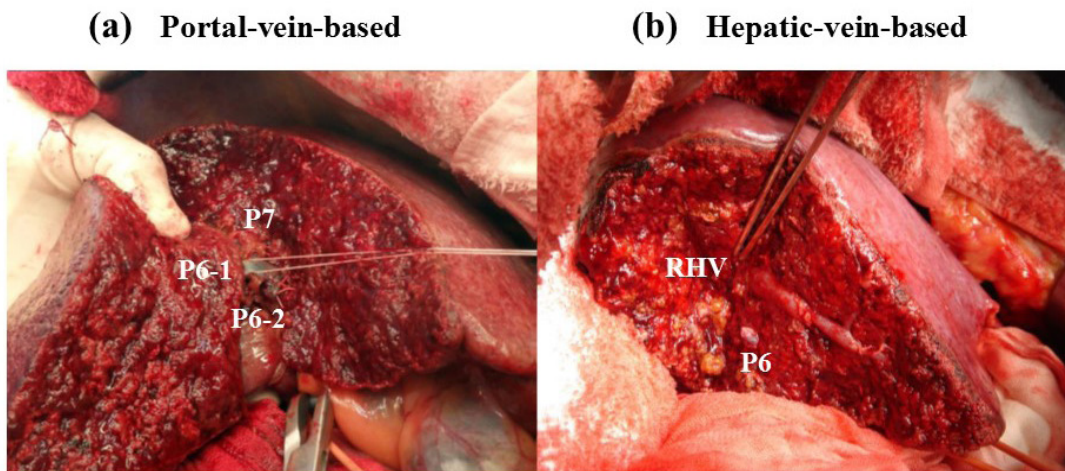


**Figure 4. Liver transection based on each anatomy.** (a) The portal-vein-based liver transection was performed. Two P6 branches were detected using dye injected into each branch of P6. Each P6 branch was divided at the root and P7 was preserved. No thick branch of RHV was visualized. (b) The hepatic-vein-based liver transection was performed in proximal branch type P6. The full length of RHV in S6 was exposed, while root of P6 was not visualized.

= 0.037) were significantly larger in the S6-dominant group than in the non-difference group (Table 3). However, there was no significant difference in S5 and S8 between the two groups. The median volume of the portal-vein-based anatomy of S6 (Figure 3a) was 164 mL (44-366 mL), while the median volume of the hepatic-vein-based anatomy of S6 (Figure 3b) was 142 mL (34-287 mL;  $p < 0.001$ ). The median volume difference in S6 between the two groups was 73 mL (29-189 mL) (Figure 3).

#### 5. Liver transection in each model

In the clinical technique, the portal-vein-based liver transections were performed using dye injected into two branch of P6 and the hepatic-vein-based liver transection was performed in proximal branch type of P6 (Figure 4a). In the portal-vein-based transection, each P6 branch was divided at the root and P7 was preserved. No thick branch of RHV was visualized at the transection site. The full length of RHV in S6 was exposed in the hepatic-vein-based transection. Thus, the root of P6 was not visualized because of proximal branch type of P6 (Figure 4b).

#### 4. Discussion

This study showed that 41.7% of the segment planes in S6 did not match with the portal-vein-based and hepatic-vein-based 3D anatomies. The proximal branch type of P6 (72.1%) and the presence of the IRHV (72.1%) were conclusive factors for S6-dominant segmentation.

Several studies have mentioned the anatomical difference between the perfusion area of portal vein and drainage area of hepatic vein (1,2,8). However, objective rules for assessing this difference have not yet been established. The RHV frontal view in the present study can classify the branch pattern of P6 into the proximal or distal. In particular, the all proximal branch of P6 perfused the ventral side of the RHV, which is thought to correspond to S5 in the hepatic-vein-based anatomy. To understand these anatomic characteristics enables to perform more precise anatomic liver resection (e.g.; anatomic resection in less than subsegment). This novel rule might also apply to the other segmental planes in the liver parenchyma.

Transection of the liver parenchyma along with the major hepatic vein is considered to be one of the gold-standard methods for anatomic liver resection (6,7). However, present study revealed that the 41.7% was failed to remove entire perfusion area in S6 when the patients was performed based on the hepatic-vein-based anatomy. In contrast, the parenchymal staining method which established by Makuuchi is one of an anatomic liver resection. The dye is injected into the portal vein to determine the region that should be resected.

This procedure can be contributed to resect potential metastases *via* the portal vein in the tumor-occupying segment (14-16). Therefore, in the presence of portal vein tumor thrombus, the portal-vein-based liver transection is a prefer procedure to avoid intrahepatic recurrence (9).

The S6-dominant group has two unique features on 3D. First, 72.1% of the patients had one or more IRHV. Second, 72.1% of the patients had a proximal branch of P6, which was supported by the result of a shorter posterior branch of the portal trunk. These findings reflect a large drainage area in the liver parenchyma as well as a wide perfusion area in the S6-dominant group. Therefore, the parenchymal volume in S6 was significantly larger in the S6-dominant group than that in the non-difference group.

The preoperative liver volume measurements based on 3D anatomy imaging have been shown to agree with the actual volume of the liver resected at operation (17-19). The median volume difference between the portal-vein-based and hepatic-vein-based anatomies in S6 was 73 mL. We believe this volume difference is large because the median parenchymal volume of S6 was 164 mL. Therefore, almost half of the liver volume was discordant between the portal-vein-based and hepatic-vein-based anatomies.

Few studies have thus far identified the factors accounting for the anatomical features between the portal and hepatic veins at liver surgery. The present study emphasized the priority of portal-vein-based anatomic liver resection when precise resection is required such as portal vein thrombus, intra sub segmental metastasis and smaller anatomic resection which depend on the each portal vein branch. We believe that taking this anatomic concept into careful consideration before operation may increase the patient's benefits in liver resection.

#### References

1. Kakazu T, Makuuchi M, Kawasaki S, Miyagawa S, Nakazawa Y, Kubota T, Takayama T, Kosuge T. Reconstruction of the middle hepatic vein tributary during right anterior segmentectomy. *Surgery*. 1995; 117:238-240.
2. Hashimoto T, Sugawara Y, Kishi Y, Akamatsu N, Matsui Y, Kokudo N, Makuuchi M. Reconstruction of the middle hepatic vein tributary in a right lateral sector graft. *Liver Transpl*. 2005; 11:309-313.
3. Mise Y, Hasegawa K, Satou S, Aoki T, Beck Y, Sugawara Y, Makuuchi M, Kokudo N. Venous reconstruction based on virtual liver resection to avoid congestion in the liver remnant. *Br J Surg*. 2011; 98:1742-1751.
4. Couinaud C. *Surgical anatomy of the liver* revised (Pers, ed.). Paris, France, 1989.
5. Couinaud C. Liver anatomy: Portal (and suprahepatic) or biliary segmentation. *Dig Surg*. 1999; 16:459-467.
6. Makuuchi M, Hasegawa H, Yamazaki S. Ultrasonically guided subsegmentectomy. *Surg Gynecol Obstet*. 1985; 161:346-350.

7. Shindoh J, Mise Y, Satou S, Sugawara Y, Kokudo N. The intersegmental plane of the liver is not always flat--tricks for anatomical liver resection. *Ann Surg.* 2010; 251:917-922.
8. Sato F, Igami T, Ebata T, Yokoyama Y, Sugawara G, Mizuno T, Nagino M. A study of the right intersectional plane (right portal scissura) of the liver based on virtual left hepatic trisectionectomy. *World J Surg.* 2014; 38:3181-3185.
9. Yamazaki S, Takayama T. Surgical treatment of hepatocellular carcinoma: Evidence-based outcomes. *World J Gastroenterol.* 2008; 14:685-692.
10. Hayashi Y, Takayama T, Yamazaki S, Moriguchi M, Ohkubo T, Nakayama H, Higaki T. Validation of perioperative steroids administration in liver resection: A randomized controlled trial. *Ann Surg.* 2011; 253:50-55.
11. Yamazaki S, Takayama T, Kimura Y, Moriguchi M, Higaki T, Nakayama H, Fujii M, Makuuchi M. Transfusion criteria for fresh frozen plasma in liver resection: A 3 + 3 cohort expansion study. *Arch Surg.* 2011; 146:1293-1299.
12. Yamazaki S, Takayama T, Moriguchi M, Mitsuka Y, Okada S, Midorikawa Y, Nakayama H, Higaki T. Criteria for drain removal following liver resection. *Br J Surg.* 2012; 99:1584-1590.
13. Mise Y, Satou S, Shindoh J, Conrad C, Aoki T, Hasegawa K, Sugawara Y, Kokudo N. Three-dimensional volumetry in 107 normal livers reveals clinically relevant intersegment variation in size. *HPB (Oxford).* 2014; 16:439-447.
14. Takayama T, Makuuchi M, Watanabe K, Kosuge T, Takayasu K, Yamazaki S, Hasegawa H. A new method for mapping hepatic subsegment: Counterstaining identification technique. *Surgery.* 1991; 109:226-229.
15. Makuuchi M, Hashikura Y, Kawasaki S, Tan D, Kosuge T, Takayama T. Personal experience of right anterior segmentectomy (segments V and VIII) for hepatic malignancies. *Surgery.* 1993; 114:52-58.
16. Torzilli G, Procopio F, Cimino M, Del Fabbro D, Palmisano A, Donadon M, Montorsi M. Anatomical segmental and subsegmental resection of the liver for hepatocellular carcinoma: A new approach by means of ultrasound-guided vessel compression. *Ann Surg.* 2010; 251:229-235.
17. Yamanaka J, Saito S, Fujimoto J. Impact of preoperative planning using virtual segmental volumetry on liver resection for hepatocellular carcinoma. *World J Surg.* 2007; 31:1249-1255.
18. Li YC, Hu Y, Zhang MM, Jin XQ, Fan X, Pu CL, Guo CB, Kang Q, Dai XK, Deng YH. Usage of 64-detector-row spiral computed tomography volumetry in preoperative volume prediction in living donor liver transplantation in children. *Pediatr Surg Int.* 2011; 27:445-449.
19. Takamoto T, Hashimoto T, Ogata S, Inoue K, Maruyama Y, Miyazaki A, Makuuchi M. Planning of anatomical liver segmentectomy and subsegmentectomy with 3-dimensional simulation software. *Am J Surg.* 2013; 206:530-538.

(Received March 13, 2017; Revised April 12, 2017; Accepted April 13, 2017)

# Index of convexity: A novel method for assessing liver functional reserve using technetium-99m-galactosyl human serum albumin liver scintigraphy

Takafumi Sato<sup>1</sup>, Junichi Arita<sup>2</sup>, Yosuke Inoue<sup>1</sup>, Rintaro Koga<sup>1</sup>, Yu Takahashi<sup>1</sup>, Akio Saiura<sup>1,\*</sup>

<sup>1</sup> Department of Gastroenterological Surgery, Cancer Institute Hospital of the Japanese Foundation for Cancer Research, Tokyo, Japan;

<sup>2</sup> Hepato-Biliary-Pancreatic Division, Department of Surgery, The University of Tokyo, Tokyo, Japan.

## Summary

Preoperative evaluation of liver functional reserve is important in hepatobiliary surgery. Although the indocyanine green retention rate at 15 minutes (ICG-R15) is the gold standard for this purpose, a new method without technical complexity would be preferable. We assessed the usefulness of the previously established index of convexity (IOC). In total, 159 consecutive patients who underwent both technetium-99m-galactosyl human serum albumin (<sup>99m</sup>Tc-GSA) scintigraphy and the ICG-R15 were included. Correlation coefficients between indices from <sup>99m</sup>Tc-GSA scintigraphy and blood examinations including ICG-R15 were evaluated, and a conversion formula from the IOC to the ICG-R15 was established. The IOC was calculated as  $[L(15) \times 2 - L(3) - L(27)] / [L(27) - L(3)]$ , where L(t) indicates the radiation counts within the whole liver at t minutes after <sup>99m</sup>Tc-GSA injection. The IOC showed a significantly stronger correlation with the ICG-R15 ( $r = -0.532, p < 0.001$ ) than the index of blood clearance (HH15) and the receptor index (LHL15). A formula for estimating ICG-R15 from IOC was "ICG-R15 =  $-31.0 \times \text{IOC} + 30.1$ ". In conclusion, the IOC is a better index for evaluating preoperative liver functional reserve than the conventional indices. A formula for estimating ICG-R15 from the IOC will be useful.

**Keywords:** Preoperative assessment, liver function, hepatectomy, GSA scintigraphy

## 1. Introduction

Preoperative evaluation of liver functional reserve is important to predict severe complication after hepatectomy, which has been more enhanced because the indication for hepatic resection has been expanded along with the development of surgical techniques and perioperative management protocols (1-5). Among many indicators of liver functional reserve (3,4,6-13), the indocyanine green retention rate at 15 minutes (ICG-R15) is the gold standard technique (1,14,15). However, the patients should be rested for 2 to 3 hours in a horizontal

position and the pretest fasting is necessary before ICG-R15 test, which usually necessitates hospitalization of the patients. Moreover, the technique of ICG-R15 test is somewhat complex because three times of blood sampling after injecting ICG should be performed accurately with time-lag less than a few seconds. Additionally, the results can be inconclusive in patients with obstructive jaundice or congenital ICG excretory defects (16). Another auxiliary or even alternative examination for estimating the liver functional reserve is desired.

Technetium-99m diethylenetriamine-penta-acetic acid-galactosyl human serum albumin (<sup>99m</sup>Tc-GSA) scintigraphy is one of the prevalent examinations performed for evaluation of liver functional reserve (17-25). Conventional indices of <sup>99m</sup>Tc-GSA scintigraphy, namely the blood clearance index (HH15) and the receptor index (LHL15), use accumulation counts of only two time points. The index of convexity (IOC) was proposed by Miki *et al.* (26) as a novel alternative to

Released online in J-STAGE as advance publication May 8, 2017.

\*Address correspondence to:

Dr. Akio Saiura, Department of Gastroenterological Surgery, Cancer Institute Hospital of the Japanese Foundation for Cancer Research, 3-8-31 Ariake, Koto-ku, Tokyo 135-8550, Japan.

E-mail: akio.saiura@jfcrr.or.jp

HH15 and LHL15. The IOC is calculated from hepatic accumulation counts on GSA scintigraphy at three fixed time points, surrogating the convexity of the hepatic accumulation curve of GSA scintigraphy. This index was created based on data obtained in patients, most of whom (68.5%) had hepatocellular carcinoma. However, more and more patients with liver metastases from colorectal carcinoma undergone hepatic resection thanks to advent of preoperative chemotherapy. In this study, we assessed the usefulness of the IOC utilizing a patient cohort including many patients with colorectal liver metastases. In addition, we propose a new conversion formula from the IOC to the ICG-R15.

## 2. Materials and Methods

### 2.1. Patients and data collection

A total of 159 consecutive patients underwent both  $^{99m}\text{Tc}$ -GSA scintigraphy and ICG-R15 test within one month before hepatic resection from June 2011 to October 2012 at the Cancer Institute Hospital of the Japanese Foundation for Cancer Research. Two patients who were diagnosed with constitutional ICG excretory defect were excluded from the study. The  $^{99m}\text{Tc}$ -GSA scintigraphy was incorporated into the routine preoperative examination in our hospital from 2011 after private communication with the creator of this index; the index was published in the literature in 2013 (26). The IOC, ICG-R15, and other clinical data were collected from a retrospective review of the clinical records. The indices calculated from  $^{99m}\text{Tc}$ -GSA scintigraphy were HH15, LHL15, and IOC. The serum levels of total bilirubin (T-Bil), direct bilirubin, aspartate aminotransferase (AST), alanine aminotransferase (ALT), choline esterase, albumin (Alb), transthyretin (TTR), total cholesterol (T-Cho), prothrombin time-international normalized ratio (PT-INR), and platelet count (Plt) were determined after admission. Histopathological examination of the noncancerous part of the resected liver was performed to estimate liver impairment.

### 2.2. $^{99m}\text{Tc}$ -GSA scintigraphy

After intravenous injection of 3 mg of  $^{99m}\text{Tc}$ -GSA (1 ml, 185 MBq; Nihon Medi-Physics Co., Ltd., Nishinomiya, Japan), dynamic images were recorded with the patient in the supine position using a gamma camera (Infinia 3; GE Healthcare, Chicago, IL, USA) under a large field of view. Digital images were acquired at the rate of 30 seconds per frame until 30 minutes after the injection. The regions of interests (ROIs) were determined by specialized medical engineers. The radiation counts obtained from the ROIs for the whole liver and heart were recorded at each time point. The data were processed on a workstation (GENIE Xeleris, version 3.1; GE Healthcare).

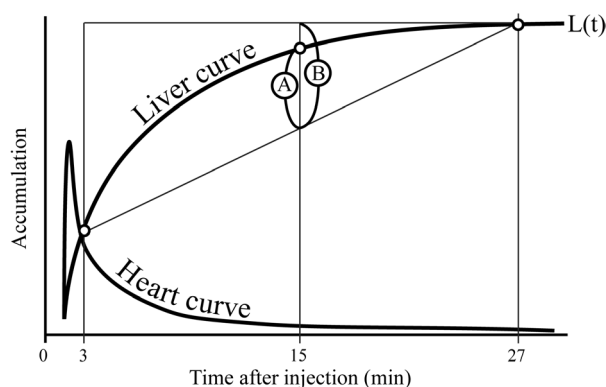


**Figure 1. Representative accumulation curves and time points for calculation of the index of convexity.** The solid line is the liver accumulation curve, and the dashed line is the heart curve. The index of convexity is the ratio of line A to B. A higher value indicates better liver function.

### 2.3. IOC

The IOC was calculated as  $[L(15) \times 2 - L(3) - L(27)] / [(L(27) - L(3))]$ , the HH15 was calculated as  $H(15) / H(3)$ , and the LHL15 was calculated as  $L(15) / [L(15) + H(15)]$ , where  $L(t)$  and  $H(t)$  indicate the radiation counts at  $t$  minutes after  $^{99m}\text{Tc}$ -GSA injection within the whole liver and whole heart, respectively. This index is a surrogate for the numerical index of the convexity of the curve of liver radiation counts until 27 minutes after injection (26). The IOC was devised using line ratio: the ratio of each distance between the midpoint of  $L(3)$  and  $L(27)$  to  $L(15)$  (Figure 1A) and the midpoint of  $L(3)$  and  $L(27)$  to  $L(27)$  (Figure 1B).

### 2.4. Statistical analysis

The correlation between the indices from  $^{99m}\text{Tc}$ -GSA scintigraphy and all other indices were analyzed using Spearman's rank correlation coefficient test as a nonparametric test. A linear model was calculated by simple and multiple regression analyses with a stepwise method using significant  $p$  values. Subanalyses comparing liver functional indices were performed after the division of the patients into the following groups: first and repeat hepatectomy groups, non-chemotherapy and chemotherapy groups, and non-cirrhosis and cirrhosis groups. The correlations among the indices were also analyzed using Spearman's rank correlation coefficient test. All statistical analyses were performed using IBM SPSS Statistics for Windows, version 23.0 (IBM Corp., Armonk, NY, USA). Statistical significance was established at  $p < 0.05$ .

## 3. Results

### 3.1. Patient characteristics

Table 1 shows the background of the patients.

**Table 1. Summary of patient characteristics**

Age (Median, range)	64 (29-84)
Sex (Male/Female)	116/43
Preoperative Chemotherapy (+/-)	51/108
Duration between ICG and GSA scintigraphy (days, mean $\pm$ SD)	10.1 $\pm$ 8.2
Times of hepatectomy (First/Repeat)	129/30
Diagnosis (n, %)	
Metastatic liver tumor	87 (54.7%)
Colorectal cancer	73 (83.9%)
Gastric cancer	5 (5.7%)
Lung cancer	3 (3.4%)
Renal cell cancer	2 (2.3%)
Breast cancer	1 (1.1%)
Lingual cancer	1 (1.1%)
Pancreatic neuroendocrine tumor	1 (1.1%)
Duodenal carcinoid	1 (1.1%)
Hepatocellular carcinoma	53 (33.3%)
Cholangiocarcinoma	17 (10.7%)
Others	2 (1.3%)
Histopathological findings of the liver (n, %)	
Normal liver	119 (74.8%)
Fatty liver	4 (2.5%)
Chronic hepatitis	10 (6.3%)
Liver cirrhosis	26 (16.4%)

SD: standard deviation, ICG: indocyanine green clearance test, GSA scintigraphy: technetium-99m-galactosyl human serum albumin liver scintigraphy.

Preoperative chemotherapy was performed in 32% and a repeat hepatectomy (*i.e.*, second time or more) was performed in 19% of all patients. 55% of all patients had liver metastasis, 33% had hepatocellular carcinoma, and 11% had cholangiocarcinoma. Among 87 patients with liver metastasis, colorectal carcinoma was the origin of the liver metastasis in 73 patients (84%). Of these 73 patients, preoperative chemotherapy was administered to 51 patients: 5-fluorouracil, leucovorin, plus oxaliplatin (FOLFOX) in 23 patients, capecitabine plus oxaliplatin (CapeOX) in 11, capecitabine in 6, 5-fluorouracil, leucovorin, plus irinotecan (FOLFIRI) in four, and other regimens in seven. Molecular target drugs were used in 31 patients: anti-vascular endothelial growth factor antibody (bevacizumab) in 18 and anti-epidermal growth factor receptor antibody (cetuximab or panitumumab) in 11.

Postoperative histopathological examination of the noncancerous part of the resected liver revealed normal liver in 119 patients, fatty liver in 4, chronic hepatitis in 10, and liver cirrhosis in 26. The cirrhosis group included patients with liver cirrhosis and chronic viral hepatitis, and the non-cirrhosis group included the remaining patients with normal and fatty liver (Table 1).

### 3.2. Correlation between the GSA scintigraphy indices and other indices

Scatter diagrams of the ICG-R15 and each index obtained from  $^{99m}\text{Tc}$ -GSA scintigraphy, namely, IOC, HH15, and LHL15, in all patients group are shown in Figure 2. Scatter diagrams of subgroups are shown in Figure 3. Table 2 shows the correlation coefficients between the indices obtained from  $^{99m}\text{Tc}$ -GSA scintigraphy and other indices. The IOC showed the

strongest correlation ( $r = -0.532$ ,  $p < 0.01$ ) to ICG-R15 compared with HH15 ( $r = 0.336$ ,  $p < 0.01$ ) and LHL15 ( $r = -0.348$ ,  $p < 0.01$ ). This trend was seen in all subgroups except the cirrhosis group. The IOC showed the strongest correlation to most of other indices (total bilirubin, direct bilirubin, choline esterase, albumin, transthyretin, and Plt). Non-chemotherapy group and cirrhosis group showed stronger correlation coefficients between IOC and ICG-R15 ( $r = -0.605$ ,  $p < 0.001$ ;  $r = -0.600$ ,  $p < 0.001$ ). In the chemotherapy group and repeat hepatectomy group, only the IOC showed a significant correlation with the ICG-R15. ICG-R15 and Plt showed stronger correlation coefficients ( $r = 0.532$ ,  $p < 0.01$ ;  $r = 0.496$ ,  $p < 0.01$ ) to the IOC followed by TTR ( $r = 0.420$ ,  $p < 0.01$ ).

### 3.3. Linear regression equation and conversion formula

Based on a simple linear regression analysis, a conversion formula estimating ICG-R15 value from the IOC value was generated: "ICG-R15 =  $-30.4 \times \text{IOC} + 29.8$ " ( $r = 0.612$ ,  $p < 0.001$ ). Among the subgroups, the first hepatectomy group showed the highest  $r$  value, and the estimation formula from the first hepatectomy group was calculated as "ICG-R15 =  $-31.0 \times \text{IOC} + 30.1$ " ( $r = 0.650$ ,  $p < 0.001$ ). A simplified diagram estimating ICG-R15 from the IOC value is shown in Figure 4.

## 4. Discussion

In this study, the IOC showed a significant correlation with the ICG-R15, which is the current gold standard test for estimating liver functional reserve. The IOC is a surrogate for the curve convexity of continual hepatic radiation counts during 30 minutes following

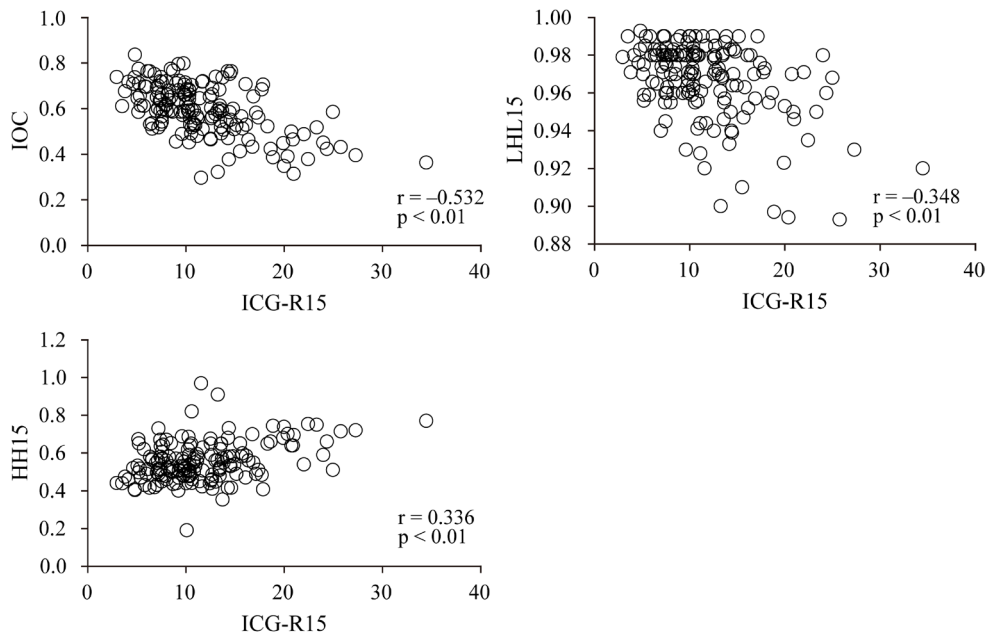


**Figure 2.** Scatter diagrams of the ICG-R15 and the indices of  $^{99m}\text{Tc}$ -GSA scintigraphy. ICG-R15: indocyanine green retention rate at 15 min, GSA: galactosyl human serum albumin.

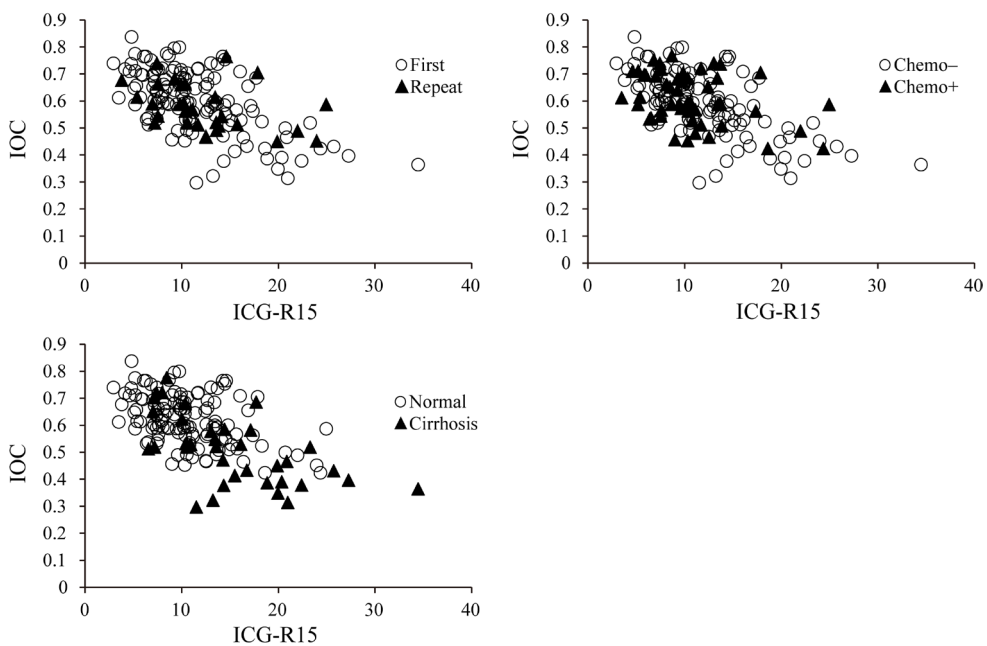


**Figure 3.** Scatter diagrams of the ICG-R15 and IOC for each subgroup. ICG-R15: indocyanine green retention rate at 15 min, IOC: index of convexity, First: first hepatectomy, Repeat: repeat hepatectomy, Chemo: preoperative chemotherapy, Normal: normal liver in noncancerous area of the liver, Cirrhosis: liver cirrhosis in noncancerous area of the liver.

the injection (26), of which the calculation is so complicated. This novel index uses only three hepatic radiation counts at 3, 15, and 27 minutes after injection, respectively. A larger IOC value indicates that  $^{99m}\text{Tc}$ -GSA accumulates in the liver more rapidly and the curve of the radiation counts reaches to a plateau faster, meaning higher hepatic capacity of uptake.

The correlation coefficients between ICG-R15 and the IOC were significantly stronger than the conventional indices of HH15 and LHL15. The calculation of the IOC incorporates three radiation counts at different time

points, while that of HH15 incorporates two counts. The IOC utilizes more information obtained from the scintigraphy than HH15, thus may be superior to HH15. The calculation of LHL15 incorporates a hepatic radiation count and a heart radiation count only at single time point of 15 minutes, respectively, so that IOC may be superior to LHL15 from the similar viewpoint. Furthermore, both HH15 and LHL15 use radiation counts from the heart, of which the ROI usually includes not only the heart but also the liver because the two organs are tightly adjacent. This inaccuracy of measuring

**Table 2. Correlation coefficients between the indices obtained from GSA scintigraphy and blood tests**

Items	All Patients (n = 159)						Non-chemotherapy, First hepatectomy, and Non-cirrhosis Group (n = 58)					
	IOC	p	HH15	p	LHL15	p	IOC	p	HH15	p	LHL15	p
ICG-R15	-0.532	††	0.336	††	-0.348	††	-0.430	††	-	n.s.	-	n.s.
T-Bil	-0.249	†	-	n.s.	-	n.s.	-	n.s.	-	n.s.	-	n.s.
D-Bil	-0.363	††	0.271	†	-	n.s.	-0.418	†	-	n.s.	-	n.s.
Cho-E	0.292	†	-0.287	†	0.185	*	-	n.s.	-	n.s.	-	n.s.
Alb	0.232	†	-0.210	†	0.209	†	-	n.s.	-	n.s.	-	n.s.
TTR	0.420	††	-0.371	††	0.178	*	0.391	†	-	n.s.	-	n.s.
Plt	0.496	††	-0.374	††	0.250	†	0.351	†	-	n.s.	-	n.s.
<hr/>												
Non-chemotherapy Group (n = 108)						Chemotherapy Group (n = 51)						
ICG-R15	-0.605	††	0.429	††	-0.392	††	-0.327	*	-	n.s.	-	n.s.
T-Bil	-0.243	*	-	n.s.	-	n.s.	-	n.s.	-	n.s.	-	n.s.
D-Bil	-0.390	††	0.312	†	-	n.s.	-	n.s.	-	n.s.	-	n.s.
Cho-E	0.339	†	-0.365	††	0.255	*	-	n.s.	-	n.s.	-	n.s.
Alb	0.245	*	-0.230	*	0.250	†	-	n.s.	-	n.s.	-	n.s.
TTR	0.472	††	-0.428	††	0.270	†	-	n.s.	-	n.s.	-	n.s.
Plt	0.507	††	-0.424	††	0.294	†	0.448	††	-	n.s.	-	n.s.
<hr/>												
First Hepatectomy Group (n = 129)						Repeat Hepatectomy Group (n = 30)						
ICG-R15	-0.544	††	0.352	††	-0.375	††	-0.477	†	-	n.s.	-	n.s.
T-Bil	-0.244	†	-	n.s.	-	n.s.	-	n.s.	-	n.s.	-	n.s.
D-Bil	-0.372	††	0.255	†	-	n.s.	-0.388	*	-	n.s.	-	n.s.
Cho-E	0.343	††	-0.350	††	0.218	*	-	n.s.	-	n.s.	-	n.s.
Alb	0.265	†	-0.273	†	0.216	*	-	n.s.	-	n.s.	-	n.s.
TTR	0.440	††	-0.428	††	0.268	†	-	n.s.	-	n.s.	-	n.s.
Plt	0.492	††	-0.370	††	0.242	†	0.390	*	-	n.s.	-	n.s.
<hr/>												
Non-cirrhosis group (n = 123)						Cirrhosis Group (n = 36)						
ICG-R15	-0.390	††	-	n.s.	-0.178	*	-0.600	††	0.440	†	-0.630	††
T-Bil	-0.234	†	-	n.s.	-	n.s.	-	n.s.	-	n.s.	-	n.s.
D-Bil	-0.291	†	-	n.s.	-	n.s.	-	n.s.	-	n.s.	-	n.s.
Cho-E	-	n.s.	-	n.s.	-	n.s.	0.360	*	-0.390	*	0.471	†
Alb	0.191	*	-	n.s.	-	n.s.	-	n.s.	-	n.s.	-	n.s.
TTR	0.339	††	-0.229	*	-	n.s.	-	n.s.	-	n.s.	0.397	*
Plt	0.412	††	-0.268	†	-	n.s.	0.509	†	-0.374	*	0.474	†

IOC: index of convexity, ICG-R15: indocyanine green retention rate at 15 minutes, T-Bil: total bilirubin, D-Bil: direct bilirubin, Cho-E: choline esterase, Alb: albumin, TTR: transthyretin, Plt: platelet count, \*: p < 0.05, †: p < 0.01, ††: p < 0.001, n.s.: not significant.

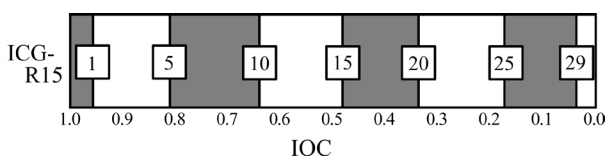


**Figure 4. Simplified diagram of conversion formula from IOC to ICG-R15 in the first hepatectomy group.** IOC: index of convexity, ICG-R15: indocyanine green retention rate at 15 min.

of the radiation count may cause the difference. Another possible reason for the difference would be difference of the mechanism. The IOC focuses on the change of the rate of material uptake, while the HH15 indicates clearance rate of the material from the blood pool, and the LHL15 indicates the proportion of hepatic uptake to all injected material at one time point.

In the present study, the most common cause

for hepatectomy was liver metastasis (54%), and preoperative chemotherapy was performed in as many as 59% of these patients. The IOC was initially devised based on the data from the patients of whom 69% had hepatocellular carcinoma and thus had impaired liver (26). Nonetheless, the IOC values were well correlated with ICG-R15 values; the IOC can be applied to the patients with various kinds of disease. In our result, in spite of the small cohort with only 36 patients, the correlation coefficient between IOC and ICG-R15 in cirrhosis group was stronger than most other subgroups, which is consistent with the previous report. On the other hand, chemotherapy group showed the lowest correlation value. This trend may be because various regimens of chemotherapy were performed according to the each cause and medical history, and perhaps because small sample size. Further analysis utilizing a large number of patients undergoing chemotherapy is

necessary.

The correlation coefficients were worse in the repeat hepatectomy group than in the first hepatectomy group. A possible cause for this is the deformity of the liver shape after the preceding hepatectomy; setting of ROI during  $^{99m}\text{Tc}$ -GSA scintigraphy may be difficult in some cases. The ROI setting should be confirmed if the IOC value showed discrepancy with expected one in the patients who had undergone hepatectomy.

In the chemotherapy group, the correlation coefficients were unsatisfactory. Sinusoidal obstructive syndrome (SOS) and chemotherapy-associated steatohepatitis (CASH) are well-known side effects of chemotherapy affecting liver functional reserve (27-29). SOS is characterized by obstruction of a central vein within a sinusoid, and CASH is caused by a metabolic disorder. The IOC indicates the rate of the material uptake and its alteration, while the ICG-R15 indicates the clearance of the material from the blood pool, deeply influenced by the velocity of portal venous flow. This difference of mechanisms may be the key for explaining this discrepancy and, perhaps, either of the two examinations may be superior to the other in patients undergoing chemotherapy. This should be further confirmed utilizing data including postoperative complication.

We created a conversion formula for estimating the ICG-R15, which so far is the gold standard for estimating liver functional reserve. Because the liver functional reserve is so complicated that no one can precisely define this term, the liver surgeons should decide surgical indication and plan for hepatic resection referring to not only ICG-R15 but also other indices. A conversion formula from the IOC value to the ICG-R15 value may be useful in comparison to ICG-R15 value. Moreover, in patients with congenital ICG excretory defect or those with portosystemic shunt, this formula may be more enhanced in estimating the liver functional reserve.

In conclusion, the IOC is superior to the conventional index obtained from  $^{99m}\text{Tc}$ -GSA scintigraphy in terms of evaluating liver functional reserve. A conversion formula from the IOC to ICG-R15 is proposed for further utility in preoperative patient management.

### Acknowledgements

We are grateful to Dr. Kenji Miki from the Department of Gastrointestinal Surgery of JR Tokyo General Hospital for his presentation of the research data and explanation of the concept and calculation method of the index of convexity before publication of his report.

### References

1. Wakiya T, Kudo D, Toyoki Y, Ishido K, Kimura N, Narumi S, Kijima H, Hakamada K. Evaluation of the usefulness of the indocyanine green clearance test for

- chemotherapy-associated liver injury in patients with colorectal cancer liver metastasis. *Ann Surg Oncol*. 2014; 21:167-172.
2. Eguchi S, Takatsuki M, Soyama A, Hidaka M, Nakao K, Shirasaka T, Yamamoto M, Tachikawa N, Gatanaga H, Kugiyama Y, Yatsuhashi H, Ichida T, Kokudo N. Analysis of the hepatic functional reserve, portal hypertension, and prognosis of patients with human immunodeficiency virus/hepatitis C virus coinfection through contaminated blood products in Japan. *Transplant Proc*. 2014; 46:736-738.
3. Imura S, Shimada M, Utsunomiya T. Recent advances in estimating hepatic functional reserve in patients with chronic liver damage. *Hepato Res*. 2015; 45:10-19.
4. Hoekstra LT, de Graaf W, Nibourg GA, Heger M, Bennink RJ, Stieger B, van Gulik TM. Physiological and biochemical basis of clinical liver function tests: A review. *Ann Surg*. 2013; 257:27-36.
5. Seyama Y, Kokudo N. Assessment of liver function for safe hepatic resection. *Hepato Res*. 2009; 39:107-116.
6. Nanashima A, Abo T, Arai J, Matsumoto H, Kudo T, Nagayasu T. Functional liver reserve parameters predictive for posthepatectomy complications. *J Surg Res*. 2013; 185:127-135.
7. Fung J, Poon RT, Yu WC, Chan SC, Chan AC, Chok KS, Cheung TT, Seto WK, Lo CM, Lai CL, Yuen MF. Use of liver stiffness measurement for liver resection surgery: Correlation with indocyanine green clearance testing and post-operative outcome. *PLoS One*. 2013; 8:e72306.
8. Cao Y, Wang H, Johnson TD, Pan C, Hussain H, Balter JM, Normolle D, Ben-Josef E, Ten Haken RK, Lawrence TS, Feng M. Prediction of liver function by using magnetic resonance-based portal venous perfusion imaging. *Int J Radiat Oncol Biol Phys*. 2013; 85:258-263.
9. Yoshida M, Shiraishi S, Sakaguchi F, Utsunomiya D, Tashiro K, Tomiguchi S, Okabe H, Beppu T, Baba H, Yamashita Y. Fused  $^{99m}\text{Tc}$ -GSA SPECT/CT imaging for the preoperative evaluation of postoperative liver function: Can the liver uptake index predict postoperative hepatic functional reserve? *Jpn J Radiol*. 2012; 30:255-262.
10. Sourbron S, Sommer WH, Reiser MF, Zech CJ. Combined quantification of liver perfusion and function with dynamic gadoteric acid-enhanced MR imaging. *Radiology*. 2012; 263:874-883.
11. de Graaf W, van Lienden KP, Dinant S, Roelofs JJ, Busch OR, Gouma DJ, Bennink RJ, van Gulik TM. Assessment of future remnant liver function using hepatobiliary scintigraphy in patients undergoing major liver resection. *J Gastrointest Surg*. 2010; 14:369-378.
12. de Graaf W, Bennink RJ, Vetelainen R, van Gulik TM. Nuclear imaging techniques for the assessment of hepatic function in liver surgery and transplantation. *J Nucl Med*. 2010; 51:742-752.
13. Kubota K, Makuuchi M, Kusaka K, Kobayashi T, Miki K, Hasegawa K, Harihara Y, Takayama T. Measurement of liver volume and hepatic functional reserve as a guide to decision-making in resectional surgery for hepatic tumors. *Hepatology*. 1997; 26:1176-1181.
14. Derpapas MK, Contis J, Fragulidis GP, Lykoudis PM, Polymeneas G, Ntourakis S, Voros D. Correlation of the ICG test with risk factors and postoperative outcomes following hepatic resection. *J BUON*. 2013; 18:703-707.
15. Takamoto T, Hashimoto T, Sano K, Maruyama Y,

- Inoue K, Ogata S, Takemura T, Kokudo N, Makuuchi M. Recovery of liver function after the cessation of preoperative chemotherapy for colorectal liver metastasis. *Ann Surg Oncol*. 2010; 17:2747-2755.
16. Kadono J, Kumemura H, Nishida S, Nakamura N, Gejima K, Nakajo M, Tsuchimochi S, Matsumoto J, Hamada N, Sakata R. <sup>99m</sup>Tc-DTPA-galactosyl-human-serum-albumin liver scintigraphy for evaluating hepatic functional reserve before hepatectomy in a patient with indocyanine green excretory defect: Report of a case. *Surg Today*. 2006; 36:481-484.
  17. Nanashima A, Tobinaga S, Abo T, Sumida Y, Araki M, Hayashi H, Sakamoto I, Kudo T, Takeshita H, Hidaka S, Sawai T, Hatano K, Nagayasu T. Relationship of hepatic functional parameters with changes of functional liver volume using technetium-99m galactosyl serum albumin scintigraphy in patients undergoing preoperative portal vein embolization: A follow-up report. *J Surg Res*. 2010; 164:e235-242.
  18. Kaibori M, Ha-Kawa SK, Maehara M, Ishizaki M, Matsui K, Sawada S, Kwon AH. Usefulness of Tc-99m-GSA scintigraphy for liver surgery. *Ann Nucl Med*. 2011; 25:593-602.
  19. de Graaf W, Vetelainen RL, de Bruin K, van Vliet AK, van Gulik TM, Bennink RJ. <sup>99m</sup>Tc-GSA scintigraphy with SPECT for assessment of hepatic function and functional volume during liver regeneration in a rat model of partial hepatectomy. *J Nucl Med*. 2008; 49:122-128.
  20. Kwon AH, Matsui Y, Kaibori M, Ha-Kawa SK. Preoperative regional maximal removal rate of technetium-99m-galactosyl human serum albumin (GSA-Rmax) is useful for judging the safety of hepatic resection. *Surgery*. 2006; 140:379-386.
  21. Miki K, Kubota K, Inoue Y, Vera DR, Makuuchi M. Receptor measurements via Tc-GSA kinetic modeling are proportional to functional hepatocellular mass. *J Nucl Med*. 2001; 42:733-737.
  22. Mitsumori A, Nagaya I, Kimoto S, Akaki S, Togami I, Takeda Y, Joja I, Hiraki Y. Preoperative evaluation of hepatic functional reserve following hepatectomy by technetium-99m galactosyl human serum albumin liver scintigraphy and computed tomography. *Eur J Nucl Med*. 1998; 25:1377-1382.
  23. Kwon A, Ha-Kawa SK, Uetsuji S, Inoue T, Matsui Y, Kamiyama Y. Preoperative determination of the surgical procedure for hepatectomy using technetium-99m-galactosyl human serum albumin (<sup>99m</sup>Tc-GSA) liver scintigraphy. *Hepatology*. 1997; 25:426-429.
  24. Ha-Kawa SK, Tanaka Y, Hasebe S, Kuniyasu Y, Koizumi K, Ishii Y, Yamamoto K, Kashiwagi T, Ito A, Kudo M, Ikekubo K, Tsuda T, Murase K. Compartmental analysis of asialoglycoprotein receptor scintigraphy for quantitative measurement of liver function: A multicentre study. *Eur J Nucl Med*. 1997; 24:130-137.
  25. Kwon AH, Ha-Kawa SK, Uetsuji S, Kamiyama Y, Tanaka Y. Use of technetium 99m diethylenetriamine-pentaacetic acid-galactosyl-human serum albumin liver scintigraphy in the evaluation of preoperative and postoperative hepatic functional reserve for hepatectomy. *Surgery*. 1995; 117:429-434.
  26. Miki K, Matsui Y, Teruya M, Kaminishi M, Kokudo N. Index of convexity: A novel liver function index using Tc-GSA scintigraphy. *World J Gastroenterol*. 2013; 19:92-96.
  27. Morris-Stiff G, Tan YM, Vauthey JN. Hepatic complications following preoperative chemotherapy with oxaliplatin or irinotecan for hepatic colorectal metastases. *Eur J Surg Oncol*. 2008; 34:609-614.
  28. Ryan P, Nanji S, Pollett A, Moore M, Moulton CA, Gallinger S, Guindi M. Chemotherapy-induced liver injury in metastatic colorectal cancer: Semiquantitative histologic analysis of 334 resected liver specimens shows that vascular injury but not steatohepatitis is associated with preoperative chemotherapy. *Am J Surg Pathol*. 2010; 34:784-791.
  29. Zorzi D, Laurent A, Pawlik TM, Lauwers GY, Vauthey JN, Abdalla EK. Chemotherapy-associated hepatotoxicity and surgery for colorectal liver metastases. *Br J Surg*. 2007; 94:274-286.
- (Received January 19, 2017; Revised march 17, 2017; Accepted April 2, 2017)

## Clinical correspondence to hepatocellular carcinoma-related lesions with atypical radiological pattern

Tokio Higaki<sup>1</sup>, Yutaka Midorikawa<sup>1,\*</sup>, Yosuke Nakashima<sup>1</sup>, Hisashi Nakayama<sup>1</sup>, Shunichi Matsuoka<sup>2</sup>, Mitsuhiro Moriyama<sup>2</sup>, Masahiko Sugitani<sup>3</sup>, Tadatoshi Takayama<sup>1</sup>

<sup>1</sup>Department of Digestive Surgery, Nihon University School of Medicine, Tokyo, Japan;

<sup>2</sup>Department of Gastroenterology and Hepatology, Nihon University School of Medicine, Tokyo, Japan;

<sup>3</sup>Department of Pathology, Nihon University School of Medicine, Tokyo, Japan.

### Summary

In patients at risk of hepatocarcinogenesis, tumors are frequently detected with atypical radiological patterns related to hepatocellular carcinoma (HCC) on imaging studies. Despite their high potential for malignancy, whether to resect such lesions immediately is controversial. Based on histological findings, patients with non-enhanced tumors or enhanced tumors without washout were divided into two groups: those with tumors that should be treated containing well, moderately, and poorly differentiated HCC (Group 1), and those that can be observed containing early HCC, hepatocellular adenoma, focal nodular hyperplasia, dysplastic nodules, and regenerative nodules (Group 2), and we elucidated the clinical correspondence to these tumors. Seventy-two patients had a single tumor with atypical radiological pattern: 39 patients had HCC (Group 1), while 33 patients had benign tumors or early HCC (Group 2). Among nine baseline variables, serum  $\alpha$ -fetoprotein (AFP) level in Group 1 (median, 13.2 ng/mL; range, 0.6-5881.6) was significantly higher than that in Group 2 (5.6 ng/mL; 0.8-86.3,  $P = 0.003$ ). The cut-off value of AFP was 36.4 ng/mL for prediction of Group 1, and the median overall and recurrence-free survival periods of 23 patients in the high-AFP ( $\geq 36.4$  ng/mL) group (5.3 years; 95%CI, 2.1 – N.A. and 1.6 years; 0.5-2.2) were significantly shorter than those of the 49 patients in the low-AFP ( $< 36.4$ ) group (7.5 years; 7.5 – N.A.,  $P = 0.047$ , and 2.8 years; 1.9-3.3,  $P = 0.001$ ). Taken together, HCC-related tumors with an atypical radiological pattern could be observed unless serum AFP level is elevated.

**Keywords:**  $\alpha$ -fetoprotein, atypical radiological pattern, benign liver tumor, hepatocellular carcinoma

### 1. Introduction

Diagnosis of hepatocellular carcinoma (HCC) is defined by early enhancement in the arterial phase and washout in the portal phase on imaging studies, including computed tomography (CT) and magnetic resonance imaging (MRI) (1). On the other hand, non-enhanced lesions in the arterial phase or hypervascular

nodules without washout in the portal phase are found during the follow-up period in patients with high risk of hepatocarcinogenesis (2-4). The frequency of diagnosis of such nodules has increased since gadoteric acid-enhanced MRI has become clinically available (5-7).

Tumors associated with HCC with an atypical radiological pattern are considered as "dysplastic nodules" or "early HCC", and are known to have substantial malignant potential (1,8-10). In contrast, some of these tumors may be poorly differentiated HCC, and grow rapidly during observation. As these lesions are often small and it is difficult to perform a biopsy to confirm malignancy, whether such nodules should be treated immediately is controversial (11-13).

Due to the better prognosis after treatment for such lesions with atypical radiological patterns, some authors

Released online in J-STAGE as advance publication June 18, 2017.

\*Address correspondence to:

Dr. Yutaka Midorikawa, Department of Digestive Surgery, Nihon University School of Medicine, 30-1 Oyaguchikami-machi, Itabashi-ku, Tokyo 173-8610, Japan.

E-mail: mido-tky@umin.ac.jp

have suggested extensive treatment including ablation for non-enhanced tumors (9,14,15). On the other hand, we reported previously that non-enhanced lesions and enhanced lesions without washout coexisting with HCC should be considered as risk factors for new lesions in the remnant liver, and not target lesions for treatment (16). Furthermore, it is not necessary to treat hypovascular tumors associated with HCC immediately after diagnosis due to the long lead time and the substantial risk of developing classical HCC in the remnant liver (17,18).

In this study, we investigated the risk of malignancy of tumors with atypical radiological patterns on imaging studies and clarified what types of such nodules associated with HCC should be treated immediately.

## 2. Materials and Methods

### 2.1. Patients

Patients undergoing liver resection for malignant tumors at Nihon University Itabashi Hospital during the period from 2006 to 2014 were included in this study. Among these patients, those diagnosed as having a single non-enhanced tumor or a hypervascular tumor without washout associated with HCC were analyzed.

### 2.2. Diagnosis

Nodules that are hypervascular in arterial phase but become hypovascular in portal phase on contrast CT and/or MRI are defined as classical HCC. On the other hand, other nodules that show hypovascularity in arterial phase and are distinguishable from cysts or hemangiomas are defined as non-enhanced lesions (1).

All patients underwent preoperative multiphase contrast-enhanced CT with/without gadoxetate disodium-enhanced MRI, as described previously (16). Briefly, a four-channel multidetector CT scanner was used. After precontrast CT scans, two sets of contrast-enhanced CT scans were performed, with one during the arterial phase and the other during the portal phase. The standard protocol for contrast-enhanced CT required 120-150 mL of nonionic intravenous contrast material (370 mg/mL) administered by a power injector at a rate of 3 mL/s, with a delay of 35 seconds for the arterial phase and 65 seconds for the portal phase. MRI was performed using gadoxetate disodium administered intravenously at a rate of 2 mL/s, with delay times for the arterial and portal phases of 20 and 60 seconds, respectively.

### 2.3. Pathology

Pathological evaluations of resected specimens were performed by two pathologists with more than 10 years of experience in the field of liver pathology as follows (19-22):

I) HCC: well-vascularized tumors with wide trabeculae (> 3 cells), prominent acinar pattern, small cell changes, cytological atypia, mitotic activity, vascular invasion, absence of Kupffer cells, and loss of the reticulin network

II) Early HCC: characterized by intratumoral portal tracts, the presence of stromal invasion, increased cell density, and structural atypia.

III) Hepatocellular adenoma: benign hepatocytes arranged in mildly thickened cell plates, with a preserved reticulin network and thin-walled arteries.

IV) Regenerative nodule: local proliferation of hepatocytes surrounded by fibrous septa, and hemosiderin deposition is fairly common.

V) Dysplastic nodule: regenerative nodule containing atypical cells without definite histological features of malignancy.

VI) Focal nodular hyperplasia: presence of ductular reaction with varied intensity at the junction of the fibrous septa with the hepatocellular component.

Based on the pathological findings, non-enhanced tumors or hypervascular tumors without washout were divided into two groups; tumors that should be treated immediately including well, moderately, and poorly differentiated HCC (Group 1) and those that could be followed up by observation consisting of early HCC, hepatocellular adenoma, focal nodular hyperplasia, dysplastic nodule, regenerative nodules, and other benign tumors (Group 2).

### 2.4. Statistical analysis

Variables in each of the groups were analyzed using Fisher's exact test and the Mann-Whitney *U* test. Prognostic factors among the nine parameters (Table 1) for classification for treatment (Group 1) or observation (Group 2) were identified with the logistic regression model. The predictive ability of variables for classification into Group 1 and Group 2 was assessed by receiver operating characteristic (ROC) curve analysis and the corresponding area under the curve (AUC). The optimal cut-off value was set as the value maximizing the sum of sensitivity and specificity. Survival curves were generated using the Kaplan-Meier method and compared using the log-rank test. In all analyses,  $P < 0.05$  was taken to indicate statistical significance.

## 3. Results

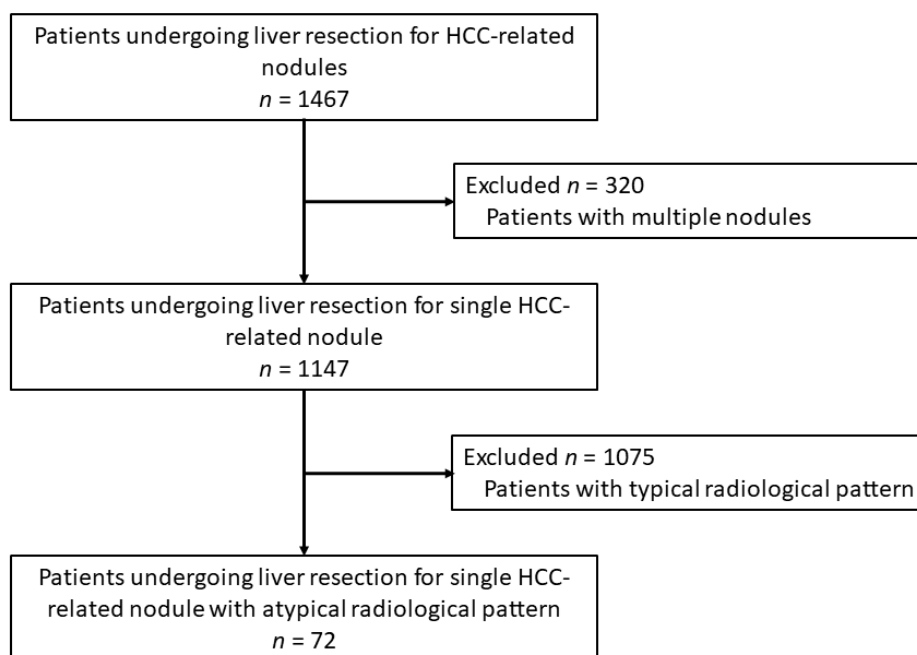
### 3.1. Patients

Among the total of 1467 patients that underwent curative liver resection under a diagnosis of HCC, 1147 were diagnosed as having a single tumor. Overall, 72 patients underwent liver resection for a tumor with atypical radiological patterns (Figure 1). These patients included 45 (72.0%) men and the median age was 70

**Table 1. Patient characteristics**

Variables	Group 1 (n = 39)	Group 2 (n = 33)	P value
Age, yr	70 (41-82)	68 (30-81)	0.088
Male, n (%)	27 (69.2)	18 (54.5)	0.290
Non-enhanced tumor, n (%)	16 (41.0)	23 (69.6)	0.015
Hepatitis, HB/HC/nBnC	5 / 25 / 9	4 / 20 / 9	0.919
Liver, LC/CH/NL	22 / 15 / 2	7 / 11 / 5	0.357
Size, mm	20 (9-40)	17 (8-32)	0.056
AFP, ng/mL	13.2 (0.6-5881)	5.6 (0.8-86.3)	0.003
DCP, mAU/mL	26 (10-915)	21 (1-18142)*	0.263
Repeated liver resection, n (%)	7 (17.9)	2 (6.0)	0.128

\*One patient with high DCP level took warfarin before surgery. HB, hepatitis B virus; HC, hepatitis C virus; LC, liver cirrhosis; CH, chronic hepatitis; NL, normal liver; AFP, alpha-fetoprotein; DCP, Des-gamma carboxy prothrombin.

**Figure 1. Flow diagram of patient recruitment.**

years (range, 30-82 years) (Table 1).

### 3.2. Pathology

Based on the results of histological examination of the resected specimens, 14 patients had well-differentiated, 21 moderately differentiated, and four poorly differentiated HCCs (Group 1, 39 (54.1%) patients). On the other hand, 24 patients were given a diagnosis of early HCC, one with hepatocellular adenoma, two with dysplastic nodules, two with regenerative nodules, and four with focal nodular hyperplasia (Group 2, 33 (45.8%) patients). The median tumor size was 1.8 cm (range, 0.8-4.0 cm). Among the 72 patients, 39 (54.1%) had liver cirrhosis, 26 (36.1%) had chronic hepatitis, and seven (9.7%) had normal livers.

### 3.3. Risks of hepatocellular carcinoma

By univariate analysis, serum  $\alpha$ -fetoprotein (AFP) level

was significantly higher in Group 1 (median, 13.2 ng/mL; range, 0.6-5881.6) than in Group 2 (5.6 ng/mL; 0.8-86.3,  $P = 0.003$ ). Patients with hypervascular tumors without washout were significantly more frequent in Group 1 (69.7% vs. 30.3%,  $P = 0.015$ ). On the other hand, the logistic regression model indicated that serum AFP level was the only independent factor for Group 1 (odds ratio, 0.98; 95%CI, 0.96-0.99,  $P = 0.011$ ), and hypervascular nodules without washout tended to be more frequent in Group 1 ( $P = 0.065$ ) (Table 2).

### 3.4. Cut-off value of $\alpha$ -fetoprotein level

The AUC of the ROC was 0.56 ( $P = 0.003$ ) for AFP in relation to the need for treatment of tumors with an atypical radiological pattern. The calculated cut-off value for AFP was 36.4 ng/mL, with sensitivity of 41.0%, specificity of 84.8%, positive predictive value of 76.1%, and negative predictive value of 54.9% for prediction of malignancy (Figure 2).

**Table 2. Uni- and multivariate analysis**

Variables	Univariate Analysis		Multivariate Analysis*	
	OR (95%CI)	P value	OR (95%CI)	P value
Age	70 (41-82)	0.290	68 (30-81)	0.359
Gender	27 (69.2)	0.088	18 (54.5)	0.731
Vascularity	16 (41.0)	0.015	23 (69.6)	0.065
Hepatitis	5 / 25 / 9	0.919	4 / 20 / 9	0.693
Liver**	22 / 15 / 2	0.357	7 / 11 / 5	0.885
Size	20 (9-40)	0.056	17 (8-32)	0.094
AFP	13.2 (0.6-5881)	0.003	5.6 (0.8-86.3)	0.014
DCP	26 (10-915)	0.263	21 (1-18142)*	0.172
Repeated liver resection	7 (17.9)	0.128	2 (6.0)	0.129

\*Logistic regression model. \*\* Diagnosis by imaging studies containing liver cirrhosis, chronic hepatitis, and normal liver. AFP,  $\alpha$ -fetoprotein; DCP, Des-gamma carboxy prothrombin.

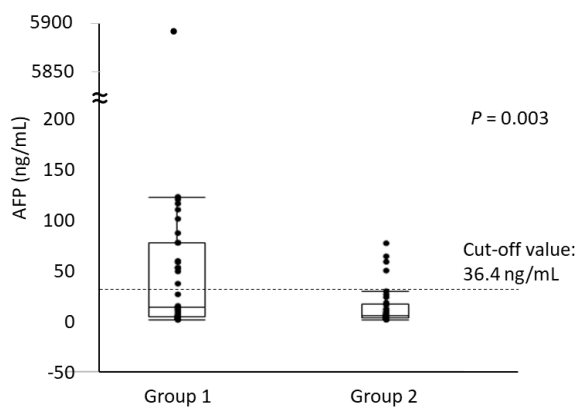


**Figure 2. Distribution of serum AFP level and tumor pathology as shown by box plots.** There was a significant correlation between AFP and pathology ( $P = 0.003$ ).

### 3.5. Survival

We defined patients with AFP level  $\geq 36.4$  ng/mL as the high-AFP group and those with AFP level  $< 36.4$  ng/mL as low-AFP group, and compared survival rates between the patients in these groups.

After a median follow-up of 3.9 years (range, 0.6-9.0 years), 14 (63.6%) and 21 (42.0%) patients had recurrence in the high- and low-AFP groups, respectively. A total of 33 patients (94.2%) had recurrence in the remnant liver, and recurrence occurred in distant sites in two patients (5.7%). There were no significant differences in recurrence site ( $P = 0.152$ ) or treatments for recurrent HCC ( $P = 0.749$ ) between the two groups.

The median overall and recurrence-free survival periods were 5.3 (95% CI, 2.1 to N.A.) years and 1.6 (0.5-2.2) years in the high-AFP group and 7.5 years (95% CI, 7.5 to N.A.,  $P = 0.047$ ) and 2.8 years (1.9-3.3,  $P = 0.001$ ) in the low-AFP group, respectively. The 5-year overall survival rates were 61.7% and 76.8%, and the recurrence-free survival rates at the end of 5 years were 0% and 57.2% in the two groups, respectively (Figure 3).

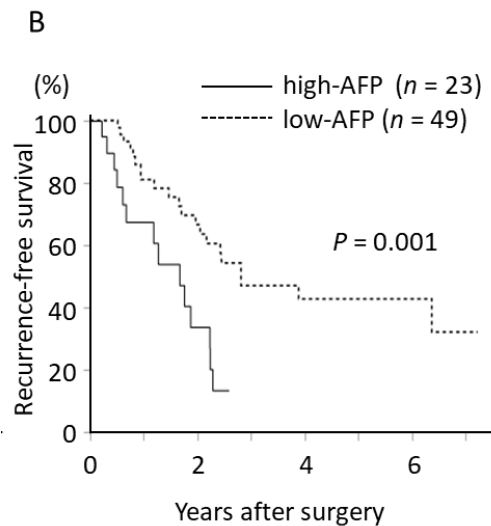
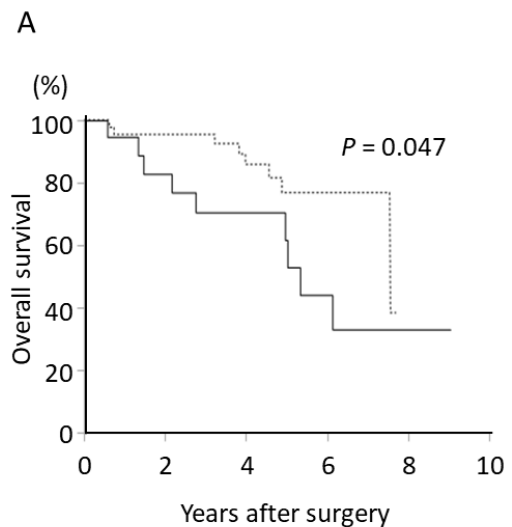


**Figure 3. Survival outcomes after liver resection.** There were significant differences between the two groups in both overall (A) and recurrence-free (B) survival rates for patients after liver resection.

### 4. Discussion

We found that tumors associated with HCC with an atypical radiological pattern have a high risk of

malignancy if serum AFP level is high, especially in patients with non-enhanced nodules at arterial phase.

Through the development of carcinogenesis, HCC gains vascularity and washout at the portal phase (2,23), and non-enhanced and hypervascular nodules without washout could be precancerous lesions, including early HCC (8,10). Nearly half of such tumors that were suspected to be HCC could have been placed under observation in this series. With improvements in diagnostic modalities, including gadoxetic acid-enhanced MRI and contrast ultrasound, more lesions that are not definitively HCC are discovered (5-7).

Whether non-enhanced nodules should be treated immediately after diagnosis remains controversial. Treatment of these marginal lesions with high malignant potential is inconclusive, as some authors have suggested that these lesions should be strictly monitored or ablated (14). On the other hand, a study using a statistical model to estimate the long-term survival benefit of radiofrequency ablation of high-grade dysplastic nodules indicated no additional time benefit compared to regular follow-up and timely treatment (24).

In our previous report, survival rates from diagnosis of hypovascular liver tumors were similar between patients that underwent liver resection immediately and those treated after vascularization (18). Furthermore, the tumors associated with HCC with atypical radiological pattern that coexisted with classical HCC were not necessarily removed, because new classical HCC lesions, which should be treated immediately, often appear prior to the malignant transformation of non-enhanced lesions or hypervascular tumors without washout due to multicentric hepatocarcinogenesis (16,17).

These findings were attributed to the fact that treatment of early HCC does not contribute to patient survivals due to the long lead time from early to classical HCC (25). That is, the survival benefit of patients undergoing liver resection for early HCC is too marginal to justify the procedure. Therefore, similar to the premalignant lesions such as hepatocellular adenoma or dysplastic nodules which are not necessary to be treated immediately, it was appropriate for early HCC to be classified into Group 2 in this study.

Serum AFP level was the only independent factor and hypervascular nodules without washout tended to be HCC compared with non-enhanced tumors in this study. We decided a cut-off value of AFP based on the AUC of the ROC, and the survival periods of patients in the high-AFP group were significantly shorter than those in the low-AFP group. Therefore, patients with HCC-related tumors with atypical radiological pattern and high serum AFP level should be candidates for treatment rather than observation.

The approach for tumors with an atypical radiological pattern depends on the clinical features of the nodules. Non-enhanced nodules > 2 cm in diameter had high malignant potential (26), and 41-62% of HCC

smaller than 2 cm showed an atypical radiological pattern (1,10). In contrast, the majority of nodules in the cirrhotic liver < 1 cm are benign (8). On the other hand, our data showed that high serum AFP level was the only independent factor for malignancy and the tumor size was not significantly larger in tumors of Group 1 compared to Group 2, and these clinical features tended to be dominant in patients with hypervascular nodules without washout. In addition, the sensitivity according to the cut-off value of serum AFP in this study is not so high and therefore, vascularity and tumor size as well as AFP level should be taken into account in decision-making regarding resection for such tumors.

In conclusion, non-enhanced nodules or enhanced tumors without washout associated with HCC could be observed unless serum AFP levels are not elevated. In particular, large hypervascular tumors without washout should be followed-up carefully because of the high potential for malignancy.

### Acknowledgements

This work was mainly supported by a Grant-in-Aid for Scientific Research (C) 15K10152 (Y.M.) from the Ministry of Education, Culture, Sports, Science and Technology (MEXT), Japan.

### References

1. Bolondi L, Gaiani S, Celli N, Golfieri R, Grigioni WF, Leoni S, Venturi AM, Piscaglia F. Characterization of small nodules in cirrhosis by assessment of vascularity: The problem of hypovascular hepatocellular carcinoma. *Hepatology*. 2005; 42:27-34.
2. Matsui O, Kobayashi S, Sanada J, Kouda W, Ryu Y, Kozaka K, Kitao A, Nakamura K, Gabata T. Hepatocellular nodules in liver cirrhosis: Hemodynamic evaluation (angiography-assisted CT) with special reference to multi-step hepatocarcinogenesis. *Abdom Imaging*. 2011; 36:264-272.
3. Rao PN. Nodule in Liver: Investigations, Differential Diagnosis and Follow-up. *J Clin Exp Hepatol*. 2014; 4:S57-62.
4. Takayasu K, Arii S, Sakamoto M, Matsuyama Y, Kudo M, Ichida T, Nakashima O, Matsui O, Izumi N, Ku Y, Kokudo N, Makuuchi M; Liver Cancer Study Group of Japan. Clinical implication of hypovascular hepatocellular carcinoma studied in 4,474 patients with solitary tumour equal or less than 3 cm. *Liver Int*. 2013; 33:762-770.
5. Ichikawa S, Ichikawa T, Motosugi U, Sano K, Morisaka H, Enomoto N, Matsuda M, Fujii H, Araki T. Presence of a hypovascular hepatic nodule showing hypointensity on hepatocyte-phase image is a risk factor for hypervascular hepatocellular carcinoma. *J Magn Reson Imaging*. 2014; 39:293-297.
6. Maruyama H, Takahashi M, Ishibashi H, Yoshikawa M, Yokosuka O. Contrast-enhanced ultrasound for characterisation of hepatic lesions appearing non-hypervascular on CT in chronic liver diseases. *Br J Radiol*. 2012; 85:351-357.

7. Matsuda M, Ichikawa T, Amemiya H, Maki A, Watanabe M, Kawaida H, Kono H, Sano K, Motosugi U, Fujii H. Preoperative gadoteric Acid-enhanced MRI and simultaneous treatment of early hepatocellular carcinoma prolonged recurrence-free survival of progressed hepatocellular carcinoma patients after hepatic resection. *HPB Surg.* 2014; 2014:641685.
8. Bruix J, Sherman M, American Association for the Study of Liver D. Management of hepatocellular carcinoma: An update. *Hepatology.* 2011; 53:1020-1022.
9. Takayama T, Makuuchi M, Hirohashi S, Sakamoto M, Yamamoto J, Shimada K, Kosuge T, Okada S, Takayasu K, Yamasaki S. Early hepatocellular carcinoma as an entity with a high rate of surgical cure. *Hepatology.* 1998; 28:1241-1246.
10. Yoon SH, Lee JM, So YH, Hong SH, Kim SJ, Han JK, Choi BI. Multiphasic MDCT enhancement pattern of hepatocellular carcinoma smaller than 3 cm in diameter: Tumor size and cellular differentiation. *AJR Am J Roentgenol.* 2009; 193:W482-489.
11. Borzio M, Fargion S, Borzio F, Fracanzani AL, Croce AM, Stroffolini T, Oldani S, Cotichini R, Roncalli M. Impact of large regenerative, low grade and high grade dysplastic nodules in hepatocellular carcinoma development. *J Hepatol.* 2003; 39:208-214.
12. Kobayashi M, Ikeda K, Hosaka T, Sezaki H, Someya T, Akuta N, Suzuki F, Suzuki Y, Saitoh S, Arase Y, Kumada H. Dysplastic nodules frequently develop into hepatocellular carcinoma in patients with chronic viral hepatitis and cirrhosis. *Cancer.* 2006; 106:636-647.
13. Sato T, Kondo F, Ebara M, *et al.* Natural history of large regenerative nodules and dysplastic nodules in liver cirrhosis: 28-year follow-up study. *Hepatol Int.* 2015; 9:330-336.
14. Roncalli M, Borzio M, Di Tommaso L. Hepatocellular dysplastic nodules. *Ann Ital Chir.* 2008; 79:81-89.
15. Yamamoto M, Takasaki K, Otsubo T, Katsuragawa H, Katagiri S, Yoshitoshi K, Ariizumi S, Saito A, Nakano M. Favorable surgical outcomes in patients with early hepatocellular carcinoma. *Ann Surg.* 2004; 239:395-399.
16. Ebisawa K, Midorikawa Y, Higaki T, Nakayama H, Tsuji S, Nishimaki H, Haradome H, Abe O, Sugitani M, Moriyama M, Takayama T. Natural history of nonenhancing lesions incidentally detected during the diagnosis of hepatocellular carcinoma. *Surgery.* 2016; 160:654-660.
17. Midorikawa Y, Takayama T, Higaki T, Nakayama H, Yamamoto M, Ariizumi S, Shimada K, Kokudo N, Tsuji S, Tsuchiya K, Kurosaki M, Izumi N. Early hepatocellular carcinoma as a signaling lesion for subsequent malignancy. *Jpn J Clin Oncol.* 2016; 46:1102-1107.
18. Midorikawa Y, Takayama T, Nara S, Hashimoto T, Omichi K, Ebisawa K, Higaki T, Tsuji S, Sakamoto H, Shimada K, Makuuchi M. No Need of Immediate Treatment for Hypovascular Tumors Associated with Hepatocellular Carcinoma. *World J Surg.* 2016; 40:2460-2465.
19. Ward J, Robinson PJ. How to detect hepatocellular carcinoma in cirrhosis. *Eur Radiol.* 2002; 12:2258-2272.
20. Dhingra S, Fiel MI. Update on the new classification of hepatic adenomas: Clinical, molecular, and pathologic characteristics. *Arch Pathol Lab Med.* 2014; 138:1090-1097.
21. Makhlof HR, Abdul-Al HM, Goodman ZD. Diagnosis of focal nodular hyperplasia of the liver by needle biopsy. *Hum Pathol.* 2005; 36:1210-1216.
22. Schlageter M, Terracciano LM, D'Angelo S, Sorrentino P. Histopathology of hepatocellular carcinoma. *World J Gastroenterol.* 2014; 20:15955-15964.
23. Oikawa T, Ojima H, Yamasaki S, Takayama T, Hirohashi S, Sakamoto M. Multistep and multicentric development of hepatocellular carcinoma: Histological analysis of 980 resected nodules. *J Hepatol.* 2005; 42:225-229.
24. Cho YK, Wook Chung J, Kim Y, Je Cho H, Hyun Yang S. Radiofrequency ablation of high-grade dysplastic nodules. *Hepatology.* 2011; 54:2005-2011.
25. Midorikawa Y, Takayama T, Shimada K, Nakayama H, Higaki T, Moriguchi M, Nara S, Tsuji S, Tanaka M. Marginal survival benefit in the treatment of early hepatocellular carcinoma. *J Hepatol.* 2013; 58:306-311.
26. Yu JS, Chung JJ, Kim JH, Kim KW. Large (> or = 2 cm) non-hypervascular nodules depicted on MRI in the cirrhotic liver: Fate and implications. *Clin Radiol.* 2008; 63:1121-1130.

(Received May 10, 2017; Revised June 7, 2017; Accepted June 9, 2017)

# Sustained release vancomycin-coated titanium alloy using a novel electrostatic dry powder coating technique may be a potential strategy to reduce implant-related infection

Jing Han<sup>1,§</sup>, Yi Yang<sup>1,§</sup>, Junren Lu<sup>1,§</sup>, Chenzhong Wang<sup>1</sup>, Youtao Xie<sup>2</sup>, Xuebin Zheng<sup>2</sup>, Zhenjun Yao<sup>1</sup>, Chi Zhang<sup>1,\*</sup>

<sup>1</sup>Department of Orthopaedic surgery, Zhongshan Hospital of Fudan University, Shanghai, China;

<sup>2</sup>Key Laboratory of Inorganic Coating Materials, Chinese Academy of Sciences, Shanghai, China.

## Summary

In order to tackle the implant-related infection, a novel way was developed in this study to coat vancomycin particles mixed with controlled release coating materials onto the surface of titanium alloy by using an electrostatic dry powder coating technique. To characterize this sustained release antibacterial coating, surface morphology, *in vitro* and *in vivo* drug release were sequentially evaluated. *In vitro* cytotoxicity was tested by Cell Counting Kit-8 (CCK-8) assay and cytological changes were observed by inverted microscope. The antibacterial properties against MRSA, including a bacterial growth inhibition assay and a colony-counting test by spread plate method were performed. Results indicated that the vancomycin-coated sample was biocompatible for Human osteoblast cell line MG-63 and displayed effective antibacterial ability against MRSA. The coating film was revealed uniform by scanning electron microscopy. Both the *in vitro* and *in vivo* drug release kinetics showed an initially high release rate, followed by an extended period of sustained drug release over 7 days. These results suggest that with good biocompatibility and antibacterial ability, the sustained release antibacterial coating of titanium alloy using our novel electrostatic dry powder coating process may provide a promising candidate for the treatment of orthopedic implant-related infection.

**Keywords:** Implant-related infection, antibacterial coating, drug delivery system, electrostatic coating, surface modification

## 1. Introduction

With the increasing incidence of trauma, joint degeneration and bone tumor, more and more implants are applied in orthopedic surgeries, playing a critical role in improving the stability and rebuilding the anatomical structure of bone and joint. However, the treatment of implant-related infections still remains a huge challenge for orthopedic surgeons. Incidence of postoperative

infection after arthroplasty or closed fracture fixation ranges from 0.3 to 3% (1-4) and reaches nearly 30% in open fracture. The consequences for patients, with no doubt, are tremendous including prolonged hospitalization with pain and immobilization, revision surgery and long-term antibiotic therapy, and the huge costs during the entire treatment (5,6). The conventional treatment for implant-associated infections is limited to systemic administration of antibiotics, which is usually difficult to achieve the required local delivery of medicine and ineffective once the bacteria biofilm on the surface of implant is formed. Fortunately, the application of local drug delivery system (LDDS) in orthopedics, like modification of the titanium surface or antibiotics delivery coating of implants, which can effectively raise the antibiotic concentrations around bones and reduce the risk of toxicity from large systemic administration, has brought us a new way to tackle this problem (7). Though

Released online in J-STAGE as advance publication May 26, 2017.

<sup>§</sup>These authors contributed equally to this work.

\*Address correspondence to:

Dr. Chi Zhang, Department of Orthopaedic surgery, Zhongshan Hospital of Fudan University, 180 Fenglin Road, Xuhui District, Shanghai 200032, China.

E-mail: drzhang.chi@aliyun.com

great progress has been made, there still remain some technical difficulties like limited antimicrobial spectrum, short maintenance of effective antibiotic concentration due to the burst release of loaded drugs, relatively complicated and high energy consuming coating process *etc.*

In this study, we developed a novel way to coat vancomycin particles mixed with controlled release coating materials onto the surface of titanium alloy by using an electrostatic dry powder coating technology, which had formerly been applied for pharmaceutical usage (8). The surface morphology, *in vitro* antibacterial properties, biocompatibility and drug releasing kinetics of the vancomycin-coated titanium alloy were evaluated.

## 2. Materials and Methods

### 2.1. Preparation process of vancomycin-coated titanium alloy

#### 2.1.1. Preparation of titanium alloy

Plain titanium alloy discs (Ti6Al4V) were custom made by Shanghai Institute of Ceramics, Chinese Academy of Sciences, 6 mm in diameter and 2 mm in height (Figure 1A). Before the coating process, the matrix surface is cleaned by 1 mol/L hydrochloric acid, methanol, 70% ethanol and ultrasonic vibration of distilled water, each for 10 min, and then air-dried.

#### 2.1.2. Preparation of coating materials

Eudragit RS and Eudragit RL (Evonik Degussa Corporation, Germany), as sustained release control agents, are copolymers derived from esters of acrylic and methacrylic acid usually used for sustained release coating of pharmaceutical dosage forms. Triethyl citrate (TEC), as a liquid plasticizer, was purchased from Caledon Laboratories Ltd. (Ontario, Canada). Talc was purchased from Mallinckrodt Baker Inc (Canada). Vancomycin were provided (Zhejiang Medicine Co, Ltd Xinchang Pharmaceutical factory, China) as antibiotics.

Particle size reduction of Eudragit RL, Eudragit RS, talc and vancomycin were conducted separately by a jet mill, prior to use. Particle size of the powder was confirmed by a Particle Size Distribution Analyzer (TSI Corporation, Model 3603, Shoreview, MN, USA). The particle size at 50% of total weight fraction was used as average particle size. The average particle size of Eudragit RL, Eudragit RS, talc and vancomycin was 18.4  $\mu\text{m}$ , 16.5  $\mu\text{m}$ , 28.9  $\mu\text{m}$ , and 29.0  $\mu\text{m}$  respectively.

#### 2.1.3. Electrostatic powder coating process

The powder coating process was conducted in a laboratory scale electrostatic dry powder pan coater system comprising of a heating oven, a liquid spray

nozzle and an electrostatic spray gun (Figure 1C). The titanium alloy discs were suspended inside the oven and preheated at a certain temperature (30-60°C) for 10 min before the coating started. The liquid plasticizer (TEC) was regulated by a liquid metering pump (Fluid Metering Inc., USA) and sprayed onto the titanium surface through a liquid atomizing nozzle at a rate of 0.3 g/min (Table 1). Afterwards, the coating particles were sprayed by an electrostatic spray gun (Nordson Corporation, USA). After spraying the powder, the titanium alloy discs were further cured for 4-8 h to allow film formation. In order to achieve the sustained release effect of the drug, the antibiotics coating materials and polymer coating materials were coated onto the surface of the titanium alloy discs by a plurality of sets of spray. It sprayed a mixture of antibiotics and polymer materials for the first layer then sprayed the sustained release polymer materials for the second layer (Table 1). This step was repeated for several times. By improving the thickness and strength of the coating film, it achieved the effect of the drug release. The average weight gained after coating was up to 16%. The coated samples were then air dried for 3 days at 37°C (Figure 1B).

### 2.2. Surface characterization

The surface morphology of the coated sample at curing temperature 60°C and curing time (4, 8 h) were examined by scanning electron microscopy (SEM). The samples were sputter coated with gold for 120 s under argon atmosphere using EMITECH K550 sputter coater (Emitech Ltd, Ashford, UK), and then were observed with a scanning electron microscope (S-2600 N Hitachi, Ontario, Canada).

### 2.3. *In vitro* drug release

Release of vancomycin from coated samples was investigated in a PBS buffer (pH 7.4). The coated surfaces were immersed in 10 mL of PBS and incubated at 37°C with an orbital shaker at 70 rpm. The PBS was replaced fresh by the addition of the same volume at 4, 24, 48, 72, 120, 170 h. PBS samples (10  $\mu\text{L}$ ) were collected at a predetermined time (1, 4, 24, 48, 72, 120, 170 h) and then diluted 20 times. The content of vancomycin in the supernatant was measured with LC-MS/MS. The LC-MS/MS system consists of an AB Sciex Qtrap 5500 (AB SCIEX, USA) with a Waters Acquity UPLC (Waters Corporation, USA). The instrument conditions are shown in Table 2. The cumulative amount of vancomycin released from the samples was plotted against time.

### 2.4. Antibacterial tests of vancomycin-coated sample

#### 2.4.1. Bacterial zone of inhibition test (ZOL)

To check for the antibacterial potency of the vancomycin-

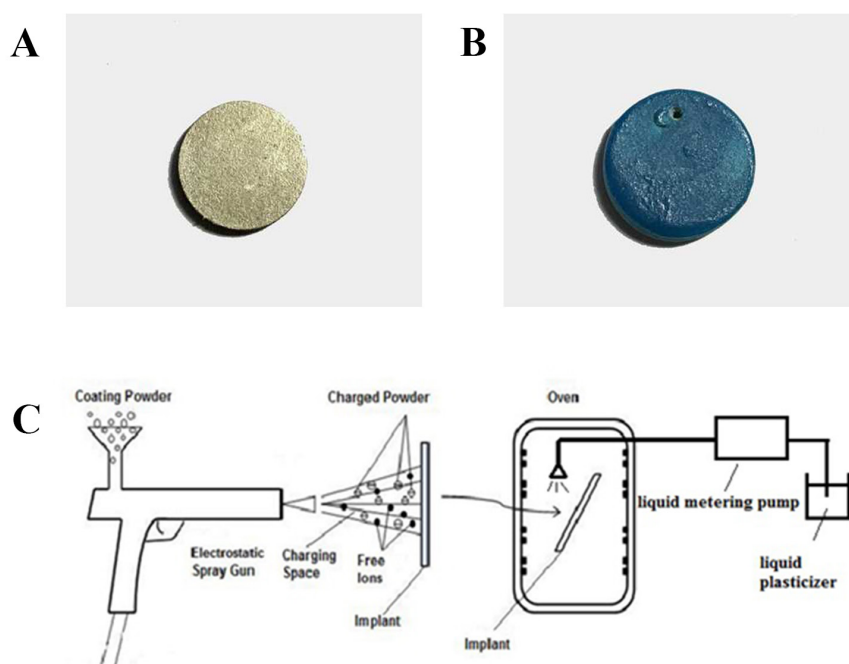


**Figure 1. The appearance and coating process of the titanium alloy sample. (A), Uncoated sample; (B), Vancomycin-coated samples; (C), The electrostatic powder coating process.**

**Table 1. Compositions and processing condition of coating**

Antibiotics coating materials	65% Eudragit RS/Eudragit RL (2:1) + 35% Vancomycin
Sustained release coating materials	80% Eudragit RS/Eudragit RL (2:1) + 19.9% Talc + 0.1% TiO <sub>2</sub>
Plasticizer	TEC
Temperature (°C)	60
Curing time (h)	4 to 8
Air flow rate (SCFH)	2.5
Atomizing pressure (psi)	54
Carrier air pressure (psi)	54
Voltage of spray gun (KV)	50

**Table 2. The LC-MS/MS conditions**

Column	Waters CORTECS UPLC, 2.1 × 50 mm, 1.6 μm 0.4 mL/min		
Flow rate	45°C		
Column temperature	10 μL		
Injection volume	Water (0.1%FA, A), acetonitrile (0.1%FA, B)		
Mobile phase	Time (min)	%A	%B
Gradient	1. Initial	99.0	1.0
	2. 1.50	85.0	15.0
	3. 1.60	5.0	95.0
	4. 2.60	5.0	95.0
	5. 2.70	99.0	1.0
The MS/MS conditions	Analyte: Vancomycin		
	Precursor ion: 724.5		
	Product ion: 144.1		
	DP (Volts): 100		
	EP (Volts): 10		
	CE (Volts): 20		
	CXP (Volts): 13		
Ion source	ESI		
Curtain Gas, Ion Source Gas 1, Ion Source Gas 2	45.0 psi		
Temperature	550°C		
Ion Spray Voltage	5500V		

coated sample, bacterial growth inhibition assay was performed. MRSA as the experimental bacteria, was offered by the Microbiology Laboratory of Zhongshan Hospital Affiliated to Fudan University. The bacterial

suspension was diluted to 10<sup>7</sup> CFU/mL and inoculated on an agar plate. Then the sterile coated sample was put gently on the MRSA spreaded agar plate and incubated at 36.5°C. Without replacing the coated sample, the

MRSA spreaded agar plate was replaced every three days and the zone of inhibition was measured. The uncoated sample was treated with the same methods.

#### 2.4.2. Colony-counting test by spread plate method

MRSA offered by the Microbiology Laboratory of Zhongshan Hospital Affiliated to Fudan University was incubated in a sterile Brain Heart Infusion broth (BHI) for 24 h. The concentration of MRSA was then adjusted to  $10^7$  CFU/mL and 100  $\mu$ L of the suspension was added onto the surface of a coated sample. The sample surface was then covered by a plastic film to maintain the humidity above 90%, and incubated at 36.5°C for 48 h. After that, the sample was collected, washed with 2 mL of NS to remove loosely adherent cells on both sample surface and plastic film, and placed on a sterile plate. 100  $\mu$ L of the suspension was then plated onto the agar plates and incubated at 36.5°C for another 48h. Mean numbers of colony-forming units (CFU) were quantified as a measure of antibacterial activity for each sample. The uncoated samples were treated with the same methods and served as a control.

#### 2.5. In vitro biocompatibility evaluation

##### 2.5.1. Cell cultivation

Human osteoblast cell line (MG-63, Cells Resource Center, Shanghai Institutes of Biological Science, Shanghai, China) was used for study. The MG-63 cells were cultured in the dulbecco's modified eagle medium (DMEM; Gibco, Invitrogen, Inc, USA) with 10% fetal bovine serum (FBS; Gibco, Invitrogen, Inc, USA), 1% antimicrobial of penicillin-streptomycin (Antibiotic-Antimycotic; Gibco, Invitrogen, Inc, USA) at 37°C in a humidified atmosphere of 5% CO<sub>2</sub>. The DMEM was refreshed every 3 days during cell culturing. Confluent cells were harvested after trypsinization (0.25% trypsin, EDTA) and then placed in 96-well plates with the cell density of  $1.0 \times 10^4$  cell/mL, prepared for further experiments.

##### 2.5.2. Preparation of the leaching solution

The coated samples, with uncoated samples serving as a control were separately put in a centrifuge tube and completely soaked in a-MEM medium supplemented with 10% FBS. Then the centrifuge tubes were placed onto an automatic shaking bed with an appropriate speed and swing trace, allowing a full contact between the sample and culture medium. The culture supernatant of both coated and uncoated samples were filtered at predetermined times (2, 5, 8 days) as the leaching solution and stored at 4°C for further use.

##### 2.5.3. Cytotoxicity evaluation with the CCK-8 assay

#### and the inverted microscope

The leaching solution collected at 2, 5, 8 days were separately added to a 96-well plate where the prepared MG-63 cells were seeded in advance. The CCK-8 (Cell Counting Kit-8) assay was then tested to evaluate the cells proliferation at predetermined times (12 h, 24 h, 3 d, 6 d, 8 d) and the cytological changes of MG-63 was also observed by the inverted microscope. At each time point, 1 mL medium was added to each well with 100  $\mu$ L CCK-8 reagent. After a 4 h incubation at 37°C, the optical density was read as 450 nm using an automated plate reader (ELX800, Bio-Tek, USA).

#### 2.6. In vivo drug release in animal studies

The 10-week-old male SD rats (Shanghai Sippr-BK laboratory animal Co. Ltd, Animal license No. 2013-0016) were kept in cages with individual filtered aeration and fed with a standard diet with water ad libitum. Before implantation, the animals were anesthetized by intraperitoneal injection of 10% chloral hydrate (0.3 mL/100 g). The back of the mice, which was chosen as the implantation site, was shaved and sterilized with 70% ethanol. Then, the coated sample was buried subcutaneously and the wound was closed by simple interrupted wound sutures. The venous bloods from the tails were collected at different time points after surgery and centrifugated to plasma, frozen at -20°C. Plasma samples (20  $\mu$ L) were collected and added 100  $\mu$ L 8% HClO<sub>4</sub> as the protein precipitation agent, and then centrifugated under 20,000g for 10 min. Since the accumulative amount of released drug can't be achieved because of the metabolic processes of drugs in rats, the concentration of vancomycin at different time points in the supernatant was then measured instead with LC-MS/MS. The instrument and testing conditions were the same as the *in vitro* drug release part (Table 2). All animal experiments were done in accordance with the regulations and with the approval from Laboratory Animal Ethics Committee of Zhongshan Hospital Affiliated to Fudan University.

#### 2.7. Statistical analysis

Data were presented as the mean  $\pm$  standard deviation from at least three independent experiments and each experiment was performed twice. Statistical analyses were performed using a one-way analysis of variance (ANOVA).  $p < 0.05$  was considered significant.

### 3. Results

#### 3.1. Surface morphology of vancomycin-coated sample

Figure 2 (A, B) shows SEM images (1.8 k $\times$ ) of the surface of coated sample after different curing times.

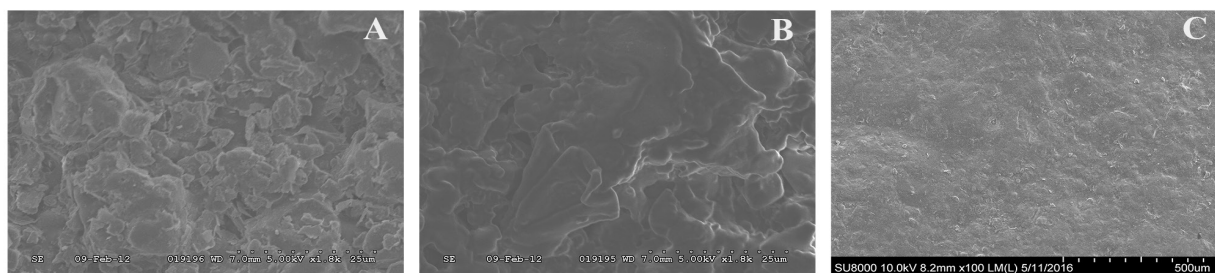


**Figure 2. SEM micrographs of vancomycin-coated sample surface curing at 60°C for different time intervals. (A),** After 4 h, the film was partly formed and the boundaries between particles were still obvious. **(B),** After 8 h, the boundaries became smaller and the film was relatively uniform. **(C),** SEM image (100×) shows the overall surface morphology of the coating and its compact granular structure of different sizes from 10 to 30 µm.

The film was partly formed after the sample was cured for 4 h and the boundaries between particles were still obvious (Figure 2A). After being cured for 8 h, the boundaries became smaller and the film was relatively uniform (Figure 2B). Another SEM image (100×) shows the overall surface morphology of the coating and its compact granular structure of different sizes from 10 µm to 30 µm (Figure 2C).

### 3.2. *In vitro* and *in vivo* drug release kinetics of vancomycin

*In vitro* drug release from vancomycin-coated samples was observed and the average cumulative amount of drug at 1, 4, 24, 48, 72, 120 and 170 h was  $47.077 \pm 3.943$ ,  $78.167 \pm 21.915$ ,  $178.301 \pm 70.127$ ,  $228.992 \pm 93.012$ ,  $274.898 \pm 113.220$ ,  $302.003 \pm 131.446$ , and  $312.084 \pm 137.919$  µg respectively. The data were then plotted against time and as is presented in the drug release profile (Figure 3A), the vancomycin-coated samples show a sustained release over 7 days, followed by the elution of 80% of the drug within the first 72 h and the antibiotic release rate gradually declines over time.

During the *in vivo* experiment, all animals tolerated the surgery without death, local infection or other complications. The average vancomycin concentration was measured to be  $86.940 \pm 22.775$ ,  $269.780 \pm 58.983$ ,  $512.440 \pm 45.349$ ,  $534.160 \pm 93.924$ ,  $401.000 \pm 113.225$ ,  $197.100 \pm 125.807$ ,  $72.300 \pm 32.604$ ,  $34.740 \pm 15.099$ ,  $18.020 \pm 7.986$ ,  $14.660 \pm 7.545$ ,  $11.600 \pm 6.280$ , and  $10.000 \pm 4.288$  µg/L at 0.5, 1, 2, 3, 6, 24, 50, 72, 97, 120, 148, and 168 h respectively using LC-MS/MS and then plotted against time (Figure 3B). As is presented in the drug release profile (C-T), the drug concentration was detected at 0.5 h after the implantation of the vancomycin-coated sample and increased rapidly until reaching the peak at 2 h, and then followed by a sustained slow release. The drug concentration could be still detected seven days after the surgery.

### 3.3. Analysis of *in vitro* antibacterial ability

The antibacterial property of the coated sample can

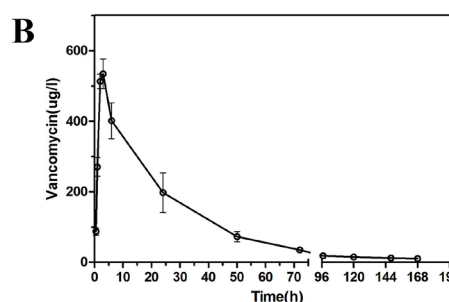
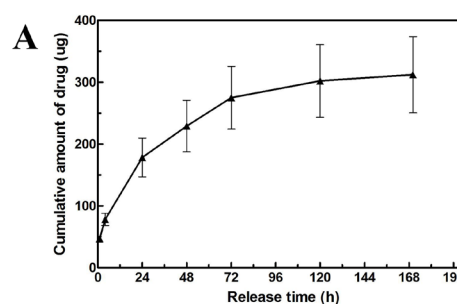


**Figure 3. *In vitro* and *in vivo* drug release profile from vancomycin-coated samples. (A),** *In vitro* drug release from vancomycin-coated samples were observed and the average cumulative amount of drug at 1, 4, 24, 48, 72, 120, and 170 h were recorded respectively and plotted against time. **(B),** During the *in vivo* experiment, the average vancomycin concentration was measured at 0.5, 1, 2, 3, 6, 24, 50, 72, 97, 120, 148, and 168 h respectively using LC-MS/MS and then plotted against time (C-T profile).

be directly visualized through the image of bacterial inhibition zone after 3 days incubation (Figure 4A). Bacterial zone of inhibition depends on the amount of released vancomycin and directly proportionate to the amount of eradicated bacteria. The average diameter of inhibition zone at 3, 6, 9, 12, 15, and 18 d were  $16.48 \pm 2.74$ ,  $10.98 \pm 1.14$ ,  $6.12 \pm 1.47$ ,  $4.15 \pm 1.19$ ,  $2.55 \pm 1.15$ ,  $0.30 \pm 0.27$  mm and then plotted against time. As is presented in Figure 4C, the zone of inhibition showed the highest diameter on the third day. Then with the incubation time prolonged, the size of the antibacterial inhibition zone gradually decreased and became nearly undetectable after 18 days. As was expected, the

uncoated sample did not generate the zone of inhibition under the same conditions (Figure 4B).

The MRSA adhesion was examined by the spread plate method, with the number of viable bacteria expressed relative to that of bacteria grown on uncoated Ti6Al4V. As is showed in Figure 4D, the uncoated sample had no effect on MRSA adhesion after 48 h and abundant bacteria had grown all over the plate. However,

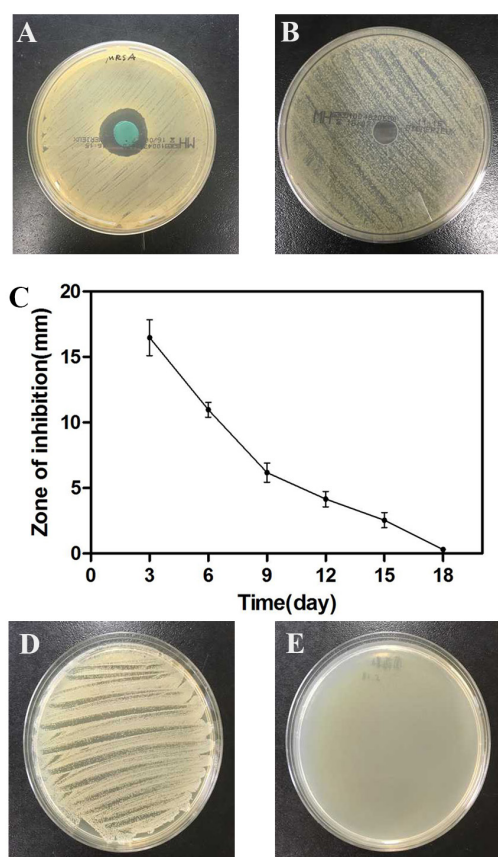


**Figure 4. Antibacterial tests of vancomycin-coated samples.** (A), Bacterial zone of inhibition was shown by the amount of released vancomycin from coated sample and directly proportional to the amount of eradicated bacteria. (B), The uncoated sample did not generate the zone of inhibition under the same conditions. (C), The ZOI diameters of coated samples at different times were measured and plotted against time. (D), In the colony-counting test by spread plate method, the uncoated sample showed no effect on MRSA adhesion after 48 h and abundant bacteria had grown all over the plate. (E), No bacterial colony was observed on the coated sample.

no bacterial colony was observed on the coated sample (Figure 4E), indicating that the vancomycin-coated Ti6Al4V has an effective antibacterial ability against MRSA.

### 3.4. Cytotoxicity test and cytological changes of MG-63

The cyto-compatibility of coated and uncoated samples were evaluated with the CCK-8 assay using MG-63 as a model. The OD of MG-63 cells in coated and uncoated groups at different times as measured by after the CCK-8 assay were presented in Table 3, and then plotted against time (Figure 5A-C), suggesting the proliferation behaviors of MG-63 cells grown in the leaching solution (2, 5, 8 days) of both coated and uncoated samples. A twofold increase in absorbance from day 1 to day 3 was recorded, which indicated cell viability with both coated and uncoated samples. Both numbers then decreased after that. The proliferation behaviors of MG-63 cells in both coated and uncoated groups were very similar to each other in every measurement point and no significant statistical differences of OD were found between two groups ( $p > 0.05$ ).

The cells in both groups were clustered, confluent, multi-layered, mature, clearly fusiform with increased volume, showed similar distribution, well spreading and cell-cell contact by inverted microscope after a 3 days cultivation (Figure 5D), indicating that the vancomycin-coated Ti6Al4V presented no obvious cytotoxicity.

## 4. Discussion

The implant-related infection, which often leads to prolonged patient pain, functional losses and causes huge treatment costs, is a catastrophic complication of orthopedic surgery. In the past forty years, a new method of local drug delivery system (LDDS) has been developed based on a series of original inorganic materials and organic-polymers with fine biocompatibility. Compared with traditional systemic drug delivery, it can directly raise the local antibiotic concentration, allow greater control over toxicity of dose and reduce the risk of promoting antibiotic resistance.

A series of challenges are involved when it comes to the developing process of the antibacterial coating

**Table 3. OD of MG-63 cells in coated and uncoated groups at different times with the CCK-8 assay**

Items	Vancomycin-coated group			Uncoated group		
	2 days LS*	5 days LS	8 days LS	2 days LS	5 days LS	8 days LS
0.5 day	0.489 ± 0.048	0.573 ± 0.049	0.555 ± 0.038	0.448 ± 0.020	0.472 ± 0.043	0.455 ± 0.038
1 day	0.517 ± 0.076	0.567 ± 0.024	0.547 ± 0.072	0.474 ± 0.058	0.496 ± 0.051	0.481 ± 0.026
3 days	1.174 ± 0.211	1.168 ± 0.216	1.140 ± 0.156	1.140 ± 0.302	1.057 ± 0.194	1.123 ± 0.093
6 days	1.076 ± 0.237	0.822 ± 0.107	0.721 ± 0.138	1.090 ± 0.106	0.771 ± 0.166	0.743 ± 0.200
8 days	0.479 ± 0.036	0.609 ± 0.105	0.427 ± 0.041	0.465 ± 0.085	0.499 ± 0.118	0.497 ± 0.081

\*LS, leaching solution.

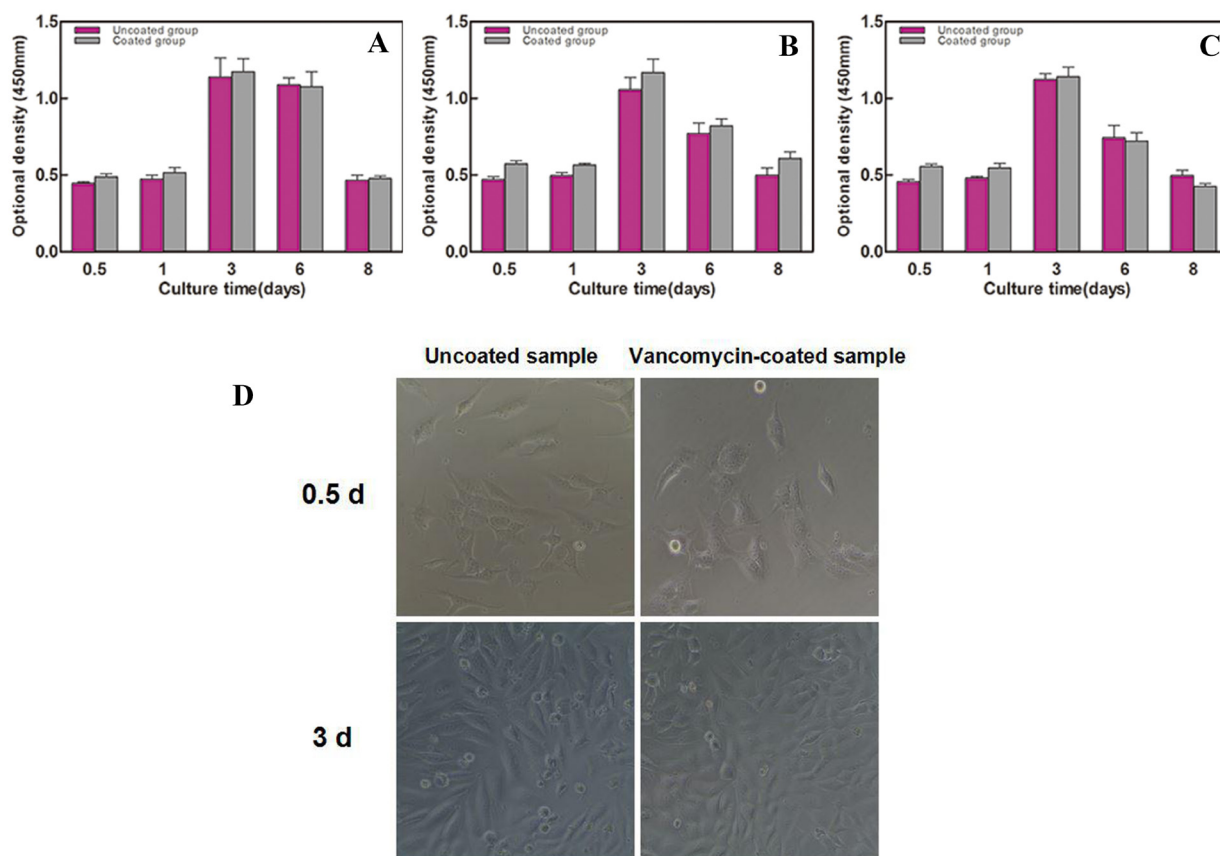


**Figure 5. Proliferation behaviors of MG-63 cells.** The OD of MG-63 cells in (A), 2 days, (B), 5 days, (C), 8 days leaching solution of coated and uncoated groups as measured by after the CCK-8 assay were plotted against time. (D), Morphological changes of MG-63 cells cultured in 5 days leaching solution of coated and uncoated sample for 0.5 d and 3 d were observed by inverted microscopy.

for metals. For example, the antibiotics usually would no longer stay active when experiencing dramatic changes of the environmental temperature or their own physicochemical properties. Also, an effective binding pathway or interface between antibacterial agents and the implants remains to be found. Furthermore, the whole coating process of the antibacterial coating should be carried out on an environmental and economical base.

To overcome those challenges, efforts have been made throughout the world. In some researches, the titanium alloy was simply immersed in antibacterial solution and then dried for subsequent use, which is effective and easy to operate. But the relatively long processing time, less drug loading, burst release of drug and short maintenance time limit the application of this method. It is also reported that huge progress has been made in antibacterial property and osteointegration of titanium alloy through nanoscale surface patterning methods (9-11) or subsequently in conjunction with some antibacterial ions like silver ion (12,13). Nevertheless, disadvantages still exist in many aspects of this surface modification method such as the narrow antibacterial spectrum and inadequate maintenance of effective antibiotic concentration.

Additionally, it should be cautioned that the dendritic cells and macrophages activated by nanotechnologies can also lead to unintended inflammation which is definitely harmful (14). Meanwhile, the mechanical property of titanium nanocoatings is also a concern since damages may occur during surgical implantation. Some other researchers tried to modify the implant's surface by grafting bioactive molecules like protein or polypeptide, together with antibacterial agents onto them (15,16). It's not yet well accepted because of the unstable antibacterial properties after a multiple organic processing and the harsh requirements for preservation.

The trends toward "green" manufacturing and cost effectiveness have further spurred development of solvent-free coating techniques in both pharmaceutical and medical products. Some coating processes like hot-melting coating (17), compression coating (18,19) and dry powder coating (20,21) have been investigated and widely used within the paint and automobile industries.

In the last few years, a low-temperature electrostatic dry powder coating process has been developed and successfully applied to make a sustained release coating of tablets (8). On the basis of that, we made a series of preliminary experiments, and first applied this electrostatic dry powder coating technology to

coat vancomycin particles mixed with control release coating materials onto the surface of titanium alloy. Different from the traditional dry powder coating technology, it forms an electrical field created by an electrostatic charging gun and grounded substrate to direct the charged powder flow and assist charged powder particle deposition. Also the repulsive force among the charged particles can cause a better distribution of deposited particles so that a more uniform coating film is achieved. Massive production can be done and no complicated physicochemical treatment is needed during the coating process. Besides, certain amount of liquid plasticizer is sprayed onto the surface of the implants through a liquid atomizing nozzle before the coating process, which greatly increases the surface electrical conductivity and reduces the transition temperature ( $T_g$ ) of the coating polymers, thus facilitating the coalescence of charged polymeric particles into film and ensuring the whole coating process is done at a relatively low temperature (30-60°C). Since the vancomycin powder, usually mixed with bone cement, is commonly taken as an effective antibiotic in a LDDS, it can tolerate the high temperature (70-100°C) during the polymerizing process of PMMA and is absolutely applicable for the antibacterial coating of titanium alloy. Also, due to the solvent-free and low-temperature coating process, there will be no effect on the physicochemical property of coating particles and no acid metabolites degraded by polymers.

An ideal drug delivery system, especially an antibacterial coating in orthopedics, should be first biocompatible and exhibit initially high release rates (*i.e.* burst release) to counter increased infection risk immediately following surgery, followed by an extended period of sustained drug release conforming to therapeutic efficacious dose to prevent latent infection (22). The *in vitro* biocompatibilities of coated and uncoated samples were evaluated with the CCK-8 assay using MG-63 as a model. The cytological changes and proliferation behaviors of viable MG-63 cells showed that both coated and uncoated group had almost the same cells growth trend ( $p > 0.05$ ) (Figure 5A). From our results, we also found that the number of viable cells was slightly higher in coated group than uncoated group for the most of time. We hypothesized that maybe it was the relatively high concentration of metal ions in uncoated group that inhibited the cell growth. In contrast, the leaching solution of vancomycin-coated group might not only provide a relatively sterile environment for cells, but also slow down the release of toxic metal ions from the implant itself. Further study is needed to determine the exact causes. Therefore, the data suggested that the vancomycin-coated Ti6Al4V had no inhibitory effect on the proliferation of MG-63 cells than uncoated one and proved its good biocompatibility.

As is presented in the *in vitro* drug release profile

(Figure 3A), the vancomycin-coated sample shows an elution of 80% of the drug within the first 72 h, then followed by a sustained release over 7 days and the antibiotic release rate gradually declines over time, which directly indicates its property of *in vitro* sustained drug release. On the other hand, after the vancomycin-coated sample was buried inside the rats and went through the process of drug absorption, distribution and metabolism, the drug concentration was detected at 0.5 h and increased rapidly until reaching the peak at 2 h, and then followed by a sustained slow release (Figure 3B), which in another way indicates its property of *in vivo* sustained drug release. Therefore, from the point of drug release kinetics, the sustained release vancomycin-coated sample using a novel electrostatic dry powder coating process meets the conditions required for an ideal orthopedic implant.

The *in vitro* antibacterial property of the vancomycin-coated sample can be directly visualized through the bacterial inhibition zone and the colony-counting tests. As is presented in Figure 4C, the zone of inhibition showed the highest diameter at the third day. Then with the incubation time prolonged, the size of the antibacterial inhibition zone gradually decreased and became undetectable after 18 days. This result also supported the drug release profiles (Figure 3). It could be found that the existence time of bacterial inhibition zone (18 d) lagged behind the time of *in vitro* drug release (7 d). That was because the viscosity of agar is much greater than the PBS solution, which might hinder the drug release and extend the release time. During the colony-counting test, no bacterial colony was observed on coated sample (Figure 4E), indicating that the vancomycin-coated Ti6Al4V has effective antibacterial ability of MRSA.

## 5. Conclusion

In this study, a sustained release antibacterial coating of titanium alloy was produced by using a novel electrostatic dry powder coating process. This coating technique overcomes the limitations associated with some traditional coating techniques and offers many advantages like good antibacterial ability, ideal sustained drug release, low energy consuming and processing temperature, being environmental-friendly and economical, no complicated physicochemical treatment required, no acid metabolites degraded by polymers and availability for massive production. The clinical feasibility of this method awaits the results of further studies.

In conclusion, with good biocompatibility and antibacterial ability, the sustained release antibacterial coating of titanium alloy using a novel electrostatic dry powder coating process will provide a promising candidate for the treatment of orthopedic implant-related infections.

## Acknowledgements

This work was supported by Shanghai Municipal Health and Planning Commission Fund (grant no. 201440391). We thank Dr. Jesse Zhu and Dr. Yingliang Ma from Department of Chemical and Biochemical Engineering, University of Western Ontario, Canada for providing us with constant technical support during the coating process.

## References

1. Phillips JE, Crane TP, Noy M, Elliott TS, Grimer RJ. The incidence of deep prosthetic infections in a specialist orthopaedic hospital: A 15-year prospective survey. *J Bone Joint Surg Br.* 2006; 88:943-948.
2. Pulido L, Ghanem E, Joshi A, Purtill JJ, Parvizi J. Periprosthetic joint infection: The incidence, timing, and predisposing factors. *Clin Orthop Relat Res.* 2008; 466:1710-1715.
3. Jämsen E, Varonen M, Huhtala H, Lehto MU, Lumio J, Kontinen YT, Moilanen T. Incidence of prosthetic joint infections after primary knee arthroplasty. *J Arthroplasty.* 2010; 25:87-92.
4. Parvizi J, Saleh KJ, Ragland PS, Pour AE, Mont MA. Efficacy of antibiotic-impregnated cement in total hip replacement. *Acta Orthop.* 2008; 79:335-341.
5. Parvizi J, Adeli B, Zmistowski B, Restrepo C, Greenwald AS. Management of periprosthetic joint infection: The current knowledge: AAOS exhibit selection. *J Bone Joint Surg Am.* 2012; 94:e104.
6. Poultsides LA, Liaropoulos LL, Malizos KN. The socioeconomic impact of musculoskeletal infections. *J Bone Joint Surg Am.* 2010; 92:e13.
7. Klemm K. Gentamicin-PMMA-beads in treating bone and soft tissue infections (author's transl). *Zentralbl Chir.* 1979; 104:934-942. (Article in German)
8. Qiao M, Luo Y, Zhang L, Ma Y, Stephenson TS, Zhu J. Sustained release coating of tablets with Eudragit® RS/RL using a novel electrostatic dry powder coating process. *Int J Pharm.* 2010; 399:37-43.
9. Liu X, Chu PK, Ding C. Surface modification of titanium, titanium alloys, and related materials for biomedical applications. *Mater Sci Eng R.* 2004; 47:49-121.
10. Giavaresi G, Ambrosio L, Battiston GA, Casellato U, Gerbasì R, Finia M, Aldini NN, Martini L, Rimondini L, Giardino R. Histomorphometric, ultrastructural and microhardness evaluation of the osseointegration of a nanostructured titanium oxide coating by metal-organic chemical vapour deposition: An *in vivo* study. *Biomaterials.* 2004; 25:5583-5591.
11. Casaletto MP, Ingo GM, Kaciulis S, Mattogno G, Pandolfi L, Scavia G. Surface studies of *in vitro* biocompatibility of titanium oxide coatings. *Appl Surf Sci.* 2001; 172:167-177.
12. Rimondini L, Rondelli G, Quirici N. *In vitro* corrosion characterization and cell proliferation on surface-modified Ti. *Materialwiss Werkst.* 2003; 33:716-719.
13. Xue W, Liu X, Zheng X, Ding C. *In vivo* evaluation of plasma-sprayed titanium coating after alkali modification. *Biomaterials.* 2005; 26:3029-3037.
14. Gallo PM, Gallucci S. The dendritic cell response to classic, emerging, and homeostatic danger signals. Implications for autoimmunity. *Front Immunol.* 2013; 4:138.
15. Chua PH, Neoh KG, Kang ET, Wang W. Surface functionalization of titanium with hyaluronic acid/chitosan polyelectrolyte multilayers and RGD for promoting osteoblast functions and inhibiting bacterial adhesion. *Biomaterials.* 2008; 29:1412-1421.
16. Oya K, Tanaka Y, Saito H, Kurashima K, Nogi K, Tsutsumi H, Tsutsumi Y, Doi H, Nomura N, Hanawa T. Calcification by MC3T3-E1 cells on RGD peptide immobilized on titanium through electrodeposited PEG. *Biomaterials.* 2009; 30:1281-1286.
17. Achanta AS, Adusumilli PS, James KW, Rhodes CT. Development of Hot Melt Coating Methods. *Drug Dev Ind Pharm.* 1997; 23:441-449.
18. Ozeki Y, Watanabe Y, Inoue S, Danjo K. Evaluation of the compression characteristics and physical properties of the newly invented one-step dry-coated tablets. *Int J Pharm.* 2003; 267:69-78.
19. Kim CJ. Drug release from compressed hydrophilic POLYOX-WSR tablets. *J Pharm Sci.* 1995; 84:303-306.
20. Cerea M, Zheng W, Young CR, McGinity JW. A novel powder coating process for attaining taste masking and moisture protective films applied to tablets. *Int J Pharm.* 2004; 279:127-139.
21. Pearnchob N, Bodmeier R. Coating of pellets with micronized ethylcellulose particles by a dry powder coating technique. *Int J Pharm.* 2003; 268:1-11.
22. Zhang X, Wyss UP, Pichora D, Goosen MF. Biodegradable controlled antibiotic release devices for osteomyelitis: Optimization of release properties. *J Pharm Pharmacol.* 1994; 46:718-724.

(Received March 12, 2017; Revised May 10, 2017; Accepted May 19, 2017)

# Comparative transcriptomic analysis identifies reprogramming and differentiation genes differentially expressed in UiPSCs and ESCs

Liang Shi<sup>1,2,§</sup>, Yazhou Cui<sup>2,§</sup>, Xiaoyan Zhou<sup>2</sup>, Jing Luan<sup>2</sup>, Linli Wang<sup>3</sup>, Jinxiang Han<sup>2,\*</sup>

<sup>1</sup>School of Medicine and Life Sciences, University of Jinan-Shandong Academy of Medical Sciences, Ji'nan, Shandong, China;

<sup>2</sup>Key Laboratory for Rare Disease Research of Shandong Province, Key Laboratory for Biotech Drugs of the Ministry of Health, Shandong Medical Biotechnological Center, Shandong Academy of Medical Sciences, Ji'nan, Shandong, China;

<sup>3</sup>Guangzhou Biocare Institute of Cancer, Guangzhou, China.

## Summary

Embryonic stem cells (ESCs) technology has garnered worldwide attention for its therapeutic applications *in vivo*. Researchers have previously shown that non-viral induced pluripotent stem cells (iPSCs) can be generated from urine. As a potential alternative, Urinary iPSCs (UiPSCs) are highly similar to embryonic stem cells (ESCs) in many aspects such as morphology, expression of pluripotency markers and the capacity to develop into three germ layers *in vitro* and *in vivo*. However, the degree of gene expression similarity between iPSCs and ESCs has not been completely elucidated. In the present study, we performed a comparative study on the gene expression profile between UiPSCs and ESCs using microarray technology, and identified 19 differentially expressed genes. Furthermore, four genes associated with reprogramming and differentiation including neuronatin (*NNAT*), piwi-like RNA-mediated gene silencing 2 (*PIWIL2*), early growth response 1 (*EGR1*) and TATA-box binding protein associated factor 9b (*TAF9B*) were validated by quantitative real-time PCR (qRT-PCR) assays. Our results indicate that compared with ESCs, UiPSCs demonstrated a different pathway in reprogramming and differentiation preference from ESCs, and can be used as a potential tool in disease modeling, drug discovery and regenerative medicine.

**Keywords:** Urinary iPSCs, embryonic stem cells, transcriptome

## 1. Introduction

The advent of human induced pluripotent stem cells (iPSCs) in 2007 (1,2), has ushered in an era of considerable excitement about the prospects of using these cells to develop new opportunities for healthcare, from their potential for regenerative medicine to their use as tools for studying the cellular basis of many diseases and the discovery of new drugs. In recent years, research on iPSCs technologies in mice and humans has progressed greatly. Human iPSCs can be generated

from multiple donor sources, such as neural cells (3), hepatocytes (4), and amniocytes (5). Generation of urinary iPSCs (UiPSCs) may be a better choice since the isolation of urinary cells is simple, and safely, affordably, and frequently obtained (6,7). This approach has been widely used for modeling disorders and offering proof of principle for basic biological research and clinical applications (8,9). Previous methods used to derive iPSCs are not "footprint-free" and random integration may alter the transcriptional signature, a serious obstacle to comprehensive transcriptional analysis. Recently different integration-free methods have been used to reprogram these cells, which greatly improve the prospects for iPSCs applications (10). Although human iPSCs are shown to mimic ESCs, global transcriptional comparison of human ESCs and iPSCs derived from other sources has revealed some significant differences. Several studies have identified as many as 1267 to 3947 genes with varying levels of deviation (11,12). Nevertheless, previous study suggests that UiPSCs are "nearly identical" to ESCs,

Released online in J-STAGE as advance publication May 20, 2017.

<sup>§</sup>These authors contributed equally to this work.

**\*\*Address correspondence to:**

Dr. Jinxiang Han, Key Laboratory for Rare Disease Research of Shandong Province, Key Laboratory for Biotech Drugs of the Ministry of Health, Shandong Medical Biotechnological Center, Shandong Academy of Medical Sciences, Ji'nan, Shandong 250062, China.

E-mail: jxhan9888@aliyun.com

but it remains unclear whether the small percentage of genes that are differentially expressed between iPSCs and ESCs is biologically significant.

In this study, we investigated the differences in gene expression profiles of UiPSCs and ESCs, and identified a set of differentially expressed genes for the first time. After bioinformatic analysis, four genes related to reprogramming and differentiation were further validated by qRT-PCR. The results of the present study extended our understanding of the transcriptional profiles in ESCs and UiPSCs and highlighted that the substantial gene expression differences between these cell populations can be helpful to direct the utility of UiPSCs in the future.

## 2. Materials and Methods

### 2.1. Cell origin and culturing

The experimental procedures were approved by the ethics committee of Shandong Medical Biotechnological Center. Human ESCs were derived from discarded human embryos and co-cultured with Guangzhou Biocare Cancer Institute (GBCI). UiPSCs were generated from urine using an integration-free reprogramming method provided by Guangzhou Institutes of Biomedicine and Health. All the above cells were maintained in defined medium BioCISO (Biocare Biotech., Ltd., Guangzhou, China) on matrigel (Corning, New York, USA). The culture medium was changed daily and cells were passaged with 0.5mM EDTA (Gibco, Carlsbad, CA, USA) when the culture grew confluent.

### 2.2. Bioinformatic analysis

Genome-wide expression profiling analysis was performed using Affymetrix GeneChip Human Transcriptome Array 2.0 between ESCs and UiPSCs according to the manufacturer's instructions. CEL-files of the raw data uploaded to the website of Gene Cloud of Biotechnology Information (GCBI Platform, Shanghai, China) ([www.gcbi.com.cn](http://www.gcbi.com.cn)) for further data mining, including differences in mRNA profiles, and other bioinformatic analysis. We selected the differentially expressed mRNAs based on the *P*-value, *Q*-value and at least a 2-fold change. To determine the interactions among differentially expressed genes, gene co-expression networks were built according to the normalized signal intensity of specific expressed genes. In a network analysis, degree is the most important measure of an mRNA centrality within a network. A higher degree of a gene indicates that it plays a more important role in the signaling network. A GO analysis was applied to analyze the main functions of the differentially expressed mRNAs (13). Pathway analysis of differentially expressed genes was performed based on the Kyoto encyclopedia of genes and genomes (KEGG) (14).

**Table 1. Targeted gene sequences of the primers used for qRT-PCR**

Gene	Sequences 5'-3'
<i>TAF9B</i>	Forward, GGATGACGAGTGGCTGGATA Reverse, GCCAGTCTCACATCATCTGC
<i>NNAT</i>	Forward, ACCGCATTCTGATCTGGACA Reverse, ACCCTCCTTCTCAACTGTG
<i>PIWIL2</i>	Forward, TTGTGGACAGCCTGAAGCTA Reverse, CCATCAGACACTCCATCAGC
<i>EGR1</i>	Forward, CCACCAGTACTCCTCTGT Reverse, GAACCCTCCTCTCCTATGGC
<i>ACTIN</i>	Forward, CCCAGAGCAAGAGAGG Reverse, GTCCAGACGCAGGATG

### 2.3. qRT-PCR

Alteration of targeted genes at the mRNA level was confirmed by qRT-PCR analysis. Total RNA was extracted using Trizol reagent (Gibco, Carlsbad, CA, USA) and the purified total RNA was used for cDNA synthesis with a first-strand cDNA synthesis kit (Toyobo, Osaka, Japan). After the reverse transcription reaction, cDNA was used as the template for qRT-PCR of *NNAT*, *EGR1*, *PIWIL2*, and *TAF9B*. The sequences of the primers used are listed in Table 1. qRT-PCR was performed (LightCycler 480 thermocycler, Roche Applied Science, Mannheim, Germany) using a SYBR Green qPCR Kit (Toyobo, Osaka, Japan). *ACTIN* was used as an internal control to determine the relative expression of target mRNA. All reactions were performed in triplicate.

### 2.4. Statistical analysis

Data are shown as the mean  $\pm$  S.D., and student's *t*-test (two-tailed) was used to determine the statistical significance of quantitative data. *P* < 0.05 was considered to be statistically significant.

## 3. Results

### 3.1. Bioinformatic analysis of microarray data between ESCs and UiPSCs

To identify differentially expressed genes between the ESCs and the UiPSCs, we selected the differentially expressed mRNAs according to the *P*-value and *Q*-value by using the GCBI platform. *P*-values < 0.01 and *Q* < 0.01 were considered significant. The list of significant genes was further filtered using fold change (FC) > 2 (Table 2). Although the hierarchical clustering analysis showed that UiPSCs were similar to ESCs in expression levels, there were still 19 mRNAs with the largest differences in each of the two cell populations (Figure 1A). Of these, 5 showed higher expression in UiPSCs than in ESCs, and 14 were more highly expressed in ESCs than in UiPSCs. To further evaluate

**Table 2. The 19 differentially expressed genes**

Gene Symbol	Gene Description	Fold Change	Gene Feature
<i>TAF9B</i>	TAF9B RNA polymerase II, TATA box binding protein (TBP)-associated factor, 31kDa	9.64011	Up
<i>CLC</i>	Charcot-Leyden crystal protein	9.120564	Down
<i>NNAT</i>	Neuronatin , transcript variant 1	5.586741	Down
<i>CCDC152</i>	Coiled-coil domain containing 152	4.242718	Up
<i>LGALS14</i>	Lectin, galactoside-binding, soluble, 14, transcript variant 1, mRNA	4.231168	Down
<i>SERPINB9</i>	Serpin peptidase inhibitor, clade B (ovalbumin), member 9	3.28019	Down
<i>ZNF676</i>	Zinc finger protein 676	2.949182	Down
<i>CAPN6</i>	Calpain 6	2.870614	Down
<i>ZNF208</i>	Zinc finger protein 208	2.797106	Down
<i>LUZP2</i>	Leucine zipper protein 2, transcript variant 1, mRNA	2.564051	Down
<i>PIWIL2</i>	Piwi-like RNA-mediated gene silencing 2, transcript variant 1	2.45924	Down
<i>GRPR</i>	Gastrin-releasing peptide receptor	2.356274	Down
<i>GSTT1</i>	Glutathione S-transferase theta 1	2.309566	Up
<i>LCP1</i>	Lymphocyte cytosolic protein 1 (L-plastin)	2.250113	Down
<i>ZNF248</i>	Zinc finger protein 248, transcript variant 1	2.223748	Up
<i>SDR42E1</i>	Short chain dehydrogenase/reductase family 42E, member 1	2.216083	Up
<i>ZNF729</i>	Zinc finger protein 729	2.074822	Down
<i>EGR1</i>	Early growth response 1	2.042328	Down
<i>AASS</i>	Amino adipate-semialdehyde synthase, nuclear gene encoding mitochondrial protein	2.004129	Down

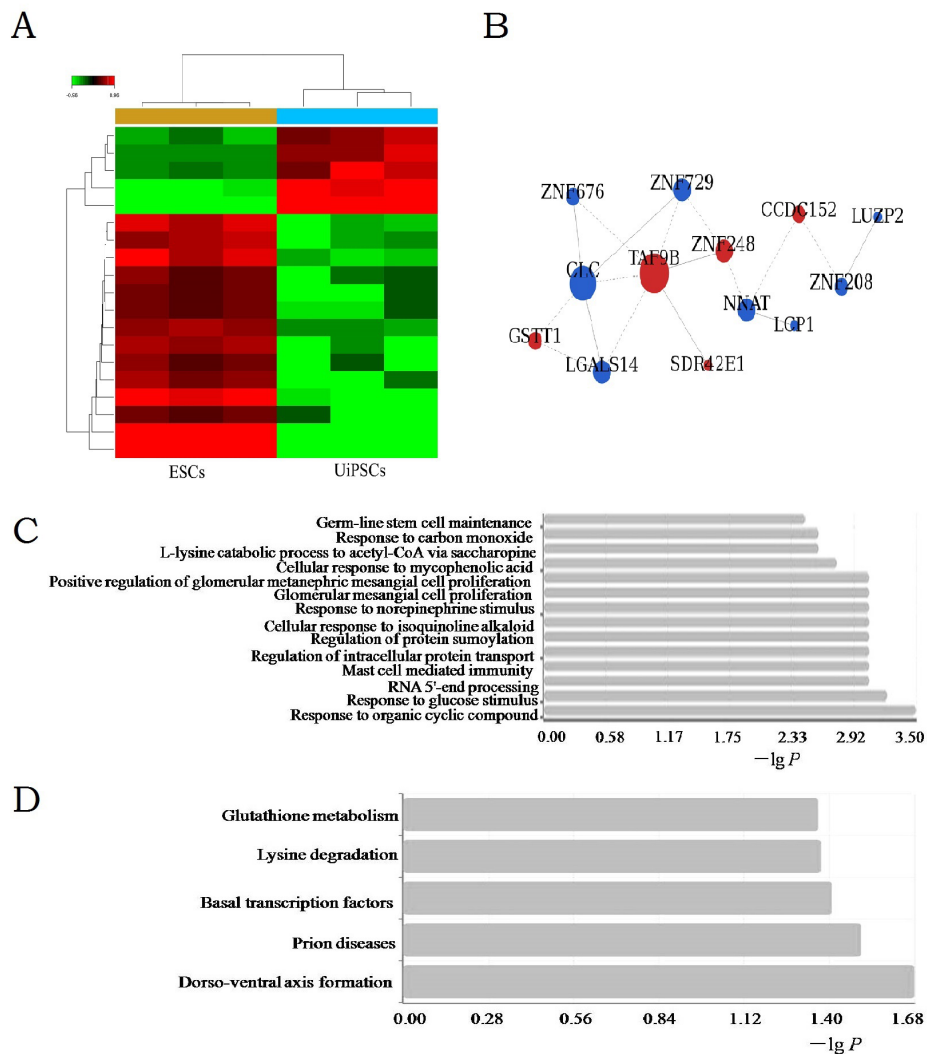


**Figure 1. Comparative transcriptomic analysis between ESCs and UiPSCs. (A)** Hierarchical clustering analysis of the differentially expressed genes in ESCs and UiPSCs. Red color indicates upregulated genes and green color indicates downregulated genes. **(B)** Gene co-expression network analysis based on the differentially expressed genes. The red circles represent upregulated genes, and blue circles represent downregulated genes. The size of the circle represents the degree value. **(C)** Histogram of changed GO analysis based on the differentially expressed genes. **(D)** Histogram of signaling pathways based on the differentially expressed genes.

the interactions among the differentially expressed genes and to locate core regulatory genes in the network, we constructed a gene co-expression network by GCBI. The higher degree of a gene indicated that it was regulating or being regulated by a greater number of genes, implying it had a more important role in the signaling network. A  $P$  value  $< 0.05$  was considered statistically significant. As shown in Figure 1B, *TAF9B* was identified as the core regulatory node with the highest degree. By using the GCBI platform, significantly altered cell functions were generated. We focused on GOs with a  $P$  value of  $< 0.05$  and a FDR of  $< 0.05$  (top 14 affected cell functions are listed in Figure 1C). High-enrichment GOs of biological processes included the organic cyclic compound response, glucose stimulus response, glomerular mesangial cell proliferation, positive regulation of glomerular metanephric mesangial cell proliferation, and germline stem cell maintenance. Among these differentially expressed genes, *PIWIL2* participated in germ-line stem cell maintenance, and *EGR1* is involved in glomerular mesangial cell proliferation. Pathway analyses were used to determine the significantly enriched pathways of the differentially expressed genes. As shown in Figure 1D, significant signaling pathways between ESCs and UiPSCs groups included dorso-ventral axis formation, prion diseases, basal transcription factors, lysine degradation, and glutathione metabolism.

### 3.2. Validation of differently expressed genes by qRT-PCR

In order to validate differential mRNA expression patterns, 4 selected genes, related to reprogramming and differentiation, were analyzed by qRT-PCR. *NNAT*, *PIWIL2*, *EGR1* were found to be more highly expressed in ESCs, and *TAF9B* was found to be more highly expressed in UiPSCs (Figure 2), which is consistent with our findings using the microarray platform.

UiPSCs are shown to mimic human ESCs (15,16), the degree of molecular similarity between UiPSCs derived from urine by transcriptional reprogramming and those of embryo-derived human ESCs has not been completely elucidated. In this study, we performed a comparison of gene expression profiling between the UiPSCs and ESCs. Our data suggest that, although the global transcriptional profiles of human ESCs and UiPSCs were globally similar, small but significant differences indeed exist. A total of 19 differentially expressed genes were identified and 4 genes (*TAF9B*, *NNAT*, *EGR1*, *PIWIL2*) were further validated.

Among down-regulated genes in UiPSCs, *NNAT*, *EGR1* have been demonstrated to be involved in generation and maintenance of stem cell properties as negative regulators (17,18). Teichroeb *et al.* found that *NNAT* was consistently silenced in iPSCs compared with its isogenic ESCs, and suppression of *NNAT* could

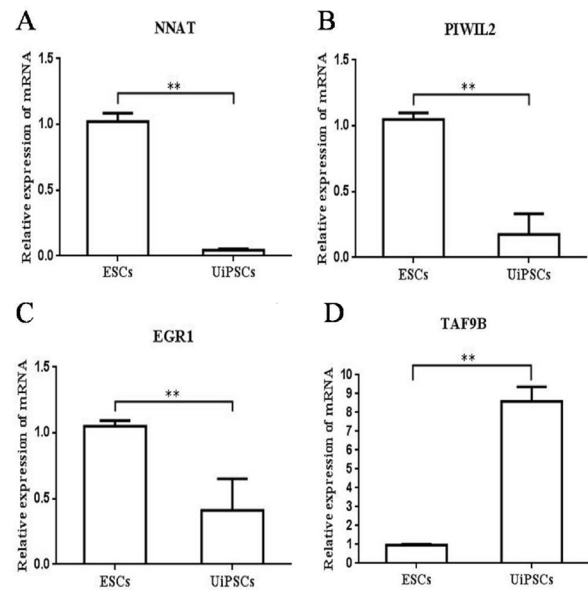


**Figure 2. qRT-PCR analysis of 4 selected mRNAs expression. (A) *NNAT*. (B) *PIWIL2*. (C) *EGR1*. (D) *TAF9B*.** Bars are shown as the mean  $\pm$  S.D. \*\* $p < 0.01$  vs. group ESCs.

be used as a biomarker for successful reprogramming (17). *EGR1* is a zinc-finger pro-differentiation factor that plays an important role in the regulation of differentiation and development in several contexts (19). Recently, Worringer *et al.* suggested that *EGR1* might be a barrier to reprogramming of *let-7*, and inhibition *EGR1* mRNA by RNA-binding protein (RBP) LIN-41 could promote reprogramming (18).

PIWI proteins have been found to play essential and conserved roles in germline stem cell maintenance, and are expressed in ESCs at higher levels (20). Moreover, a recent study reported that PIWI proteins are dispensable for reprogramming of mouse fibroblasts into iPSCs (21). Therefore, combining the above facts with our findings, it is reasonable to deduce that UiPSCs may be dependent on a different gene background to maintain stem cell properties from ESCs. According to current evidence, UiPSCs seem to be far more transcriptionally similar to iPSCs derived from other sources than ESCs.

Interestingly, in this study, we also found that a neuron differentiation regulator *TAF9B* as a top candidate gene increases in UiPSCs more than in ESCs (more than 9 fold). Previous studies reported that *TAF9B* was dispensable for global gene expression and pluripotency of murine ESCs, but *TAF9B* was required for the efficient *in vitro* differentiation of murine ESCs into motor neurons (22). Moreover, it has been shown that epithelial-like cells from human urine can be reprogrammed into UiPSCs, and even directly into human neural progenitor cells (23,24). Therefore, our result may indicate that the level of *TAF9B* in UiPSCs would account for its preference towards neuron differentiation. Compared with ESCs and even other iPSCs, UiPSCs may be able to be induced into neurons

more easily.

In conclusion, our above results further revealed that UiPSCs and ESCs had different gene expression profiles, in particular in stem cells properties maintenance mechanisms. The high basic level of *TAF9B* may partly account for the potential of UiPSCs in neuron differentiation. The molecular differences between UiPSCs and ESCs described here should drive intense efforts in the future aimed at uncovering UiPSCs as a potential tool for disease modeling, drug discovery and regenerative medicine.

### Acknowledgements

This study was supported by The Innovation Project of Shandong Academy of Medical Sciences & the Key Projects in the National Science & Technology Pillar Program during the Twelfth Five-year Plan Period (2013BAI07B00).

### References

1. Takahashi K, Tanabe K, Ohnuki M, Narita M, Ichisaka T, Tomoda K, Yamanaka S. Induction of pluripotent stem cells from adult human fibroblasts by defined factors. *Cell*. 2007; 131:861-872.
2. Yu J, Vodyanik MA, Smuga-Otto K, Antosiewicz-Bourget J, Frane JL, Tian S, Nie J, Jonsdottir GA, Ruotti V, Stewart R, Slukvin II, Thomson JA. Induced pluripotent stem cell lines derived from human somatic cells. *Science*. 2007; 318:1917-1920.
3. Kim JB, Greber B, Arauzo-Bravo MJ, Meyer J, Park KI, Zaehres H, Scholer HR. Direct reprogramming of human neural stem cells by *OCT4*. *Nature*. 2009; 461:649-643.
4. Liu H, Ye Z, Kim Y, Sharkis S, Jang YY. Generation of endoderm-derived human induced pluripotent stem cells from primary hepatocytes. *Hepatology*. 2010; 51:1810-1819.
5. Ruiz S, Brennand K, Panopoulos AD, Herreras A, Gage FH, Izpisua-Belmonte JC. High-efficient generation of induced pluripotent stem cells from human astrocytes. *PLoS One*. 2010; 5:e15526.
6. Zhou T, Benda C, Duzinger S, *et al.* Generation of induced pluripotent stem cells from urine. *J Am Soc Nephrol*. 2011; 22:1221-1228.
7. Xue Y, Cai X, Wang L, Liao B, Zhang H, Shan Y, Chen Q, Zhou T, Li X, Hou J, Chen S, Luo R, Qin D, Pei D, Pan G. Generating a non-integrating human induced pluripotent stem cell bank from urine-derived cells. *PLoS One*. 2013; 8:e70573.
8. Zhang SZ, Li HF, Ma LX, Qian WJ, Wang ZF, Wu ZY. Urine-derived induced pluripotent stem cells as a modeling tool for paroxysmal kinesigenic dyskinesia. *Biol Open*. 2015; 4:1744-1752.
9. Hildebrand L, Rossbach B, Kühnen P, Gossen M, Kurtz A, Reinke P, Seemann P, Stachelscheid H. Generation of integration free induced pluripotent stem cells from fibrodysplasia ossificans progressiva (FOP) patients from urine samples. *Stem Cell Res*. 2016; 16:54-58.
10. Seo BJ, Hong YJ, Do JT. Cellular reprogramming using protein and cell-penetrating peptides. *Int J Mol Sci*. 2017; 18. pii:E552.
11. Chin MH, Mason MJ, Xie W, *et al.* Induced pluripotent stem cells and embryonic stem cells are distinguished by gene expression signatures. *Cell Stem Cell*. 2009; 5:111-123.
12. Marchetto MC, Yeo GW, Kainohana O, Marsala M, Gage FH, Muotri AR. Transcriptional signature and memory retention of human-induced pluripotent stem cells. *PLoS One*. 2009; 4:e7076.
13. Ashburner M, Ball CA, Blake JA, *et al.* Gene ontology: Tool for the unification of biology. The Gene Ontology Consortium. *Nat Genet*. 2000; 25:25-29.
14. Kanehisa M, Goto S, Kawashima S, Okuno Y, Hattori M. The KEGG resource for deciphering the genome. *Nucleic Acids Res*. 2004; 32:D277-280.
15. Drozd AM, Walczak MP, Piaskowski S, Stoczynska-Fidelus E, Rieske P, Grzela DP. Generation of human iPSCs from cells of fibroblastic and epithelial origin by means of the oriP/EBNA-1 episomal reprogramming system. *Stem Cell Res Ther*. 2015; 6:122.
16. Zhou T, Benda C, Duzinger S, *et al.* Generation of human induced pluripotent stem cells from urine samples. *Nat Protoc*. 2012; 7:2080-2089.
17. Teichroeb JH, Betts DH, Vaziri H. Suppression of the imprinted gene *NNAT* and X-chromosome gene activation in isogenic human iPS cells. *PLoS One*. 2011; 6:e23436.
18. Worringer KA, Rand A, Hayashi Y, Sami S, Takahashi K, Tanabe K, Narita M, Srivastava D, Yamanaka S. The *let-7/LIN-41* pathway regulates reprogramming to human induced pluripotent stem cells by controlling expression of prodifferentiation genes. *Cell Stem Cell*. 2014; 14:40-52.
19. de Klerk N, Saroj SD, Wassing GM, Maudsdotter L, Jonsson AB. The host cell transcription factor *EGR1* is induced by bacteria through the EGFR-ERK1/2 pathway. *Front Cell Infect Microbiol*. 2017; 7:16.
20. Juliano C, Wang J, Lin H. Uniting germline and stem cells: The function of piwi proteins and the piRNA pathway in diverse organisms. *Annu Rev Genet*. 2011; 45:447-469.
21. Cheng EC, Kang D, Wang Z, Lin H. Piwi proteins are dispensable for mouse somatic development and reprogramming of fibroblasts into pluripotent stem cells. *PLoS One*. 2014; 9:e97821.
22. Herrera FJ, Yamaguchi T, Roelink H, Tjian R. Core promoter factor *TAF9B* regulates neuronal gene expression. *Elife*. 2014; 3:e02559.
23. Wang L, Wang L, Huang W, Su H, Xue Y, Su Z, Liao B, Wang H, Bao X, Qin D, He J, Wu W, So KF, Pan G, Pei D. Generation of integration-free neural progenitor cells from cells in human urine. *Nat Methods*. 2013; 10:84-89.
24. Wang L, Li X, Huang W, Zhou T, Wang H, Lin A, Hutchins AP, Su Z, Chen Q, Pei D, Pan G. TGF $\beta$  signaling regulates the choice between pluripotent and neural fates during reprogramming of human urine derived cells. *Sci Rep*. 2016; 6:22484.

(Received March 30, 2017; Accepted May 12, 2017)

# Once malaria is eliminated, more attention should be paid to imported malaria: Data from five years of surveillance in the City of Yiwu in eastern China

Xuanjun Dong<sup>1,§</sup>, Jie Yang<sup>1,§</sup>, Lianqin Lou<sup>2</sup>, Liebo Zhu<sup>1</sup>, Xiayan Feng<sup>1</sup>, Linong Yao<sup>3,\*</sup>

<sup>1</sup> Yiwu Center for Disease Control and Prevention, Yiwu, Zhejiang, China;

<sup>2</sup> Yiwu Central Hospital, Yiwu, Zhejiang, China;

<sup>3</sup> Zhejiang Provincial Center for Disease Control and Prevention, Hangzhou, Zhejiang, China.

## Summary

This study reviewed and analyzed data on malaria cases in Yiwu from 2012 to 2016 via a web-based system for managing and reporting information on infectious diseases. A total of 161 cases were diagnosed (77.02% due to *Plasmodium falciparum*, 18.01% due to *P. vivax*, 4.35% due to *P. ovale*, and 0.62% due to *P. malariae*). One case was imported from Yunnan Province in China and the others were imported from overseas. The ratio of male to female patients was 7.47:1. The average age was 36.34 years (SD: 9.63). Most cases (87.58%) were imported from 1 of 30 countries in Africa. As malaria is gradually being eliminated in China, the main task at this stage has transitioned to the prevention and control of cases of imported malaria. Particular attention should be paid to malaria cases from Africa.

**Keywords:** Malaria, imported, China

## 1. Introduction

Malaria is a debilitating parasitic disease. According to the Roll Back Malaria (RBM) Partnership, each year approximately 860,000 people (89% in the African region, followed by 6% in the Eastern Mediterranean region, and 5% in the South-East Asia region), mainly children and women, succumb to the disease. Despite successful elimination programs, a resurgence of malaria has occurred in Eastern Europe, Jamaica, the Bahamas (1,2), and the Korean peninsula (3,4). The City of Yiwu had been an area of China with a high rate of malaria transmission, with a morbidity of 2,830/10,000 in 1957. Due to large-scale surveys and anti-malaria campaigns, the incidence of malaria dropped sharply below 1/10,000 after 1977, and the last autochthonous case was reported in June 2008. With the growth of international trade and travel, migrants have accounted for most cases

of imported malaria in Yiwu. Given the high rate of transmission and the susceptibility of the population, effective strategies are required to prevent re-introduction and re-establishment of the disease in Yiwu.

The current study reviewed and analyzed data on malaria cases in Yiwu from 2012 to 2016 via a web-based system for managing and reporting information on infectious diseases. Cases must be differentiated into autochthonous and imported cases in line with the "1-3-7" strategy (which refers to reporting suspected cases of malaria within 1 day, investigating and confirming the diagnosis within 3 days, and investigating the focus and responding to prevent further transmission within 7 days) launched in 2012 (5). Clinically diagnosed cases, laboratory confirmed cases, autochthonous cases, and imported cases were all included in this study. Population data were obtained from the Bureau of Statistics of Yiwu. Spatial cluster analysis was performed to test whether the malaria cases were randomly distributed spatially; if not, any identified spatial clusters of disease were examined for statistical significance. Statistics were described using the software Excel version 2010.

From 2012 to 2016, a total of 161 cases of malaria were reported in Yiwu, and the annual average incidence was 13.05/10,000 during this time. There were 22 cases in 2012, 34 in 2013, 29 in 2014, 30 in 2015, and 46 in

Released online in J-STAGE as advance publication June 18, 2017.

<sup>§</sup>These authors contributed equally to this work.

\*Address correspondence to:

Dr. Linong Yao, Zhejiang Provincial Center for Disease Control and Prevention, Hangzhou, Zhejiang, China.

E-mail: ylinong@163.com

2016. As a result of proper treatment, no deaths occurred. The ratio of male to female patients was 7.47:1, and the average age was  $36.34 \pm 9.63$  years. All of the cases were imported from abroad, except for one imported from Yunnan Province. More than half of the patients were foreigners (55.90%). Most patients were in the service industry (83.85%) or migrant workers (11.18%) and lived on Choucheng Street (55.76%) or Jiangdong Street (24.22%) (Table 1). More than three quarters (77.02%) of the cases were due to *P. falciparum*, 29 cases (18.01%) were due to *P. vivax*, 7 cases (4.35%) were due to *P. ovale*, and 1 case (0.62%) was due to *P. malariae* (Table 2). Five cases of *P. vivax* and 1 case of *P. ovale* recurred. Twenty-five cases (15.53%) were imported in August. The seasonal distribution of cases did not differ significantly throughout the year. Most cases (87.58%) were imported from 1 of 30 countries in Africa, and the three leading countries were Ghana, Nigeria, and Angola. Sixteen cases were from South Asia, and 10 of those were from India (Table 3). The time interval from onset to diagnosis was 0-47 days, with a median of 3 days. Most cases (79.5%) were diagnosed 5 days after

onset. One hundred and fourteen cases of malaria were diagnosed at primary care facilities. Eighty-one patients had previously had malaria.

This study revealed substantial changes in the epidemiological characteristics of malaria reported in Yiwu from 2012 to 2016. Yiwu faces an increasing incidence of malaria imported by migrants returning from Africa and South Asia, and an epidemic may occur if no efforts are made to prevent these outbreaks. The international flow of people has led to a large number of cases of imported malaria. The "1-3-7" strategy for elimination of malaria should be followed and all of the indicators and timeframes must be observed to promptly diagnosis and treat the increasing number of cases of imported malaria in Yiwu. Potential reservoirs must be eliminated and outbreaks due to imported pathogens must be prevented. The government should continue to emphasize the elimination of malaria and ensure efforts are funded. Effective mechanisms of multisectoral cooperation and coordination should be enhanced. Capacity should also be improved with a focus on surveillance, urgent responses, diagnosis, and treatment. Moreover, studies by and cooperation among universities, research institutes, and government agencies should be fostered and enhanced as malaria is being eliminated.

**Table 1. Characteristics of patients with imported malaria in Yiwu from**

Characteristics	Cases	Proportion (%)
Gender		
Male	142	88.20
Female	19	11.80
Nationality		
Chinese	71	44.10
Foreigner	90	55.90
Occupation		
Service industry	135	83.85
Migrant worker	18	11.18
Other	8	4.97
Present address		
Choucheng Street	93	57.76
Jiangdong Street	39	24.22
Beiyuan Street	7	4.35
Other	22	13.67
Total	161	100.00

**Acknowledgements**

The authors wish to thank all of the staff members at the Yiwu CDC. This study was supported by the Zhejiang Provincial Health Department (Grant No. 2015ZHB016) and the Yiwu Science and Technology Bureau Program (Grant No. 14-3-06).

**References**

1. WHO. World Malaria Report 2009. Geneva: World Health Organization; 2009. [http://www.who.int/malaria/world\\_malaria\\_report\\_2009/mal2009\\_rep\\_chap5\\_0040](http://www.who.int/malaria/world_malaria_report_2009/mal2009_rep_chap5_0040).

**Table 2. Classification of imported malaria in Yiwu from 2012-2016**

Type	2012	2013	2014	2015	2016	Total	Proportion (%)
<i>P. falciparum</i>	17	21	21	25	40	124	77.02
<i>Plasmodium vivax</i>	5	11	6	3	4	29	18.01
<i>P. ovale</i>	0	2	1	2	2	7	4.35
<i>P. malariae</i>	0	0	1	0	0	1	0.62
Total	22	34	29	30	46	161	100

**Table 3. Origin of imported malaria in Yiwu from 2012-2016**

Type	Africa	South Asia	Southeast Asia	Oceania	China	Total
<i>P. falciparum</i>	123	0	0	0	1	124
<i>P. vivax</i>	10	16	2	1	0	29
<i>P. ovale</i>	7	0	0	0	0	7
<i>P. malariae</i>	1	0	0	0	0	1
Total	141	16	2	1	1	161
Proportion (%)	87.58	9.94	1.24	0.62	0.62	100

- pdf?ua=1*. (Accessed May 12, 2017).
2. Webster-Kerr K, Peter Figueroa J, Weir PL, Lewis-Bell K, Baker E, Horner-Bryce J, Lewis-Fuller E, Bullock Ducasse M, Carter KH, Campbell-Forrester S. Success in controlling a major outbreak of malaria because of *Plasmodium falciparum* in Jamaica. *Trop Med Int Health*. 2011; 16:298-306.
  3. Kho WG, Jang JY, Hong ST, Lee HW, Lee WJ, Lee JS. Border malaria characters of re-emerging *Plasmodium vivax* in the Republic of Korea. *Korean J Parasitol*. 1999; 37:71-76.
  4. Global Health Science Group. Eliminating malaria in the Republic of Korea, Country briefing; 2015. <https://globalhealthsciences.ucsf.edu/sites/globalhealthsciences.ucsf.edu/files/pub/rokorea-2015-final.pdf>. (Accessed May 12, 2017).
  5. Cao J, Sturrock HJ, Cotter C, Zhou S, Zhou H, Liu Y, Tang L, Gosling RD, Feachem RG, Gao Q. Communicating and monitoring surveillance and response activities for malaria elimination: China's "1-3-7" strategy. *PLoS Med*. 2014; 11:e1001642.

(Received May 17, 2017; Revised June 12, 2017; Accepted June 14, 2017)

## Potential proteins targeted by let-7f-5p in HeLa cells

Yu Wang<sup>1,2</sup>, Xiujuan Chen<sup>1</sup>, Yi Zhang<sup>2</sup>, Jiandong Song<sup>1,2,\*</sup>

<sup>1</sup>Department of Gynecology and Obstetrics, Inner Mongolia Medical University affiliated Hospital, Hohhot, China;

<sup>2</sup>The Laboratory of AB Sciex Company, Beijing, China.

**Summary** MicroRNAs are a class of small, endogenous, non-coding RNAs mediating posttranscriptional gene silencing. The current authors hypothesized that let-7f-5p is likely involved in cell invasion and proliferation by regulating the expression of target genes. The current study combined let-7f-5p with iTRAQ to assess its effect on gene expression in HeLa cells. Results indicated that 164 proteins were expressed at different levels in HeLa cells overexpressing let-7f-5p and negative controls and that 172 proteins were expressed at different levels in let-7f-5p-silenced HeLa cells and negative controls. Results indicated that let-7f-5p may suppress insulin-like growth factor 2 mRNA binding protein 1 (IGF2BP1) in HeLa cells.

**Keywords:** Proteomic analysis, let-7f-5p, IGF2BP1, HeLa cells

MicroRNAs (miRNAs) are a class of endogenous, non-protein coding RNAs that are small (approximately 22 nucleotides in length) and highly conserved. MiRNAs have a widespread impact on regulation of gene expression and evolution and are thought to affect over 50% of all human genes (1). let-7 miRNA was originally identified in *Caenorhabditis elegans* (*C. elegans*) as a regulator of developmental timing and cell proliferation (2). The let-7 family is a particularly interesting example as one of the few families that are also conserved in *Drosophila* and *C. elegans*. In humans, the let-7 family consists of 9 mature let-7 miRNAs encoded by 12 different genomic loci, some of which are clustered together.

let-7f, which is a member of the let-7 family, is located at 9q22.3. More importantly, let-7f is a novel regulator in human endocervical cells and is involved in the induction of immune tolerance (3). let-7f was found to play an important role in cell growth, migration, invasion, and angiogenesis in tumors (4). The aim of the current study was to investigate the relationship between let-7f-5p and the genes it potentially targets at the protein level *in vitro*.

Five thousand and fifty-two proteins were identified from 31,666 peptides at a minimum confidence level of 95%. Results identified 164 proteins that were expressed at significantly different levels in HeLa cells overexpressing let-7f-5p, including 59 proteins that were up-regulated (1.5-fold,  $p < 0.5$ ) and 105 proteins that were down-regulated (1.5-fold,  $p < 0.5$ ). One hundred and seventy-two proteins were identified in let-7f-5p-inhibited HeLa cells, including 44 proteins that were up-regulated (1.5-fold,  $p < 0.5$ ) and 128 proteins that were down-regulated (1.5-fold,  $p < 0.5$ ). Expression of IGF2BP1, vimentin, Keratin, and Protein FAM decreased while expression of Integrin $\alpha$ 1 increased in HeLa cells overexpressing let-7f-5p. In let-7f-5p-silenced HeLa cells, expression of IGF2BP1 and Integrin  $\alpha$ 1 increased while expression of vimentin and T-complex protein decreased. KEGG analysis revealed that 4 biological pathways including arrhythmogenic right ventricular cardiomyopathy, pyrimidine metabolism, RNA degradation, and the pentose phosphate pathway differed significantly in HeLa cells overexpressing let-7f-5p and that three pathways including glycolysis, alanine, aspartate and glutamate metabolism, and the spliceosome pathway differed significantly in let-7f-5p-silenced HeLa cells.

Study data revealed that let-7f-5p overexpression dramatically suppressed *IGF2BP1* and *vimentin*, thus possibly regulating cell migration and invasion *in vitro*. Moreover, let-7f-5p inhibitors significantly upregulated the expression of IGF2BP1 (Table 1). Vimentin and keratin are markers of cell proliferation and invasion,

Released online in J-STAGE as advance publication April 17, 2017.

\*Address correspondence to:

Dr. Jiandong Song, Department of Gynecology and Obstetrics, Inner Mongolia Medical University affiliated hospital, 1 Tongdao North Street, Hohhot, China.

E-mail: 425echo@163.com

Table 1. Proteins expressed at different levels in HeLa cells transfected with a let-7f mimic and an inhibitor

Gene symbol	Protein	Molecular function	Let-7f mimic/control -fold change	P value	Let-7f inhibitor/control -fold change	P value
<i>RPS4X</i>	ribosomal protein S4, X-linked	poly(A) RNA binding	2.188	0.026	0.433	0.008
<i>ADARBI</i>	adenosine deaminase, RNA-specific, B1	RNA binding	1.722	0.020	1.600	0.014
<i>MAN2A1</i>	mannosidase, alpha, class 2A, member 1	carbohydrate binding	2.188	0.035	1.675	0.046
<i>BZW1</i>	basic leucine zipper and W2 domains 1	poly(A) RNA binding	0.525	0.018	0.515	0.010
<i>CCDC6</i>	coiled-coil domain containing 6	SH3 domain binding	0.555	0.037	0.377	0.031
<i>HNRNPU</i>	heterogeneous nuclear ribonucleoprotein U	ATP binding	3.020	0.026	2.443	0.004
<i>HIST1H4A</i>	histone cluster 1, H4a	poly(A) RNA binding	0.074	0.010	2.109	0.004
<i>IGF2BP1</i>	insulin like growth factor 2 mRNA binding protein 1	mRNA binding	0.525	0.020	2.858	0.009
<i>ITGAI</i>	integrin subunit alpha 1	collagen binding	2.291	0.039	2.630	0.042
<i>ITSN2</i>	intersectin 2	SH3 /SH2 adaptor activity	0.308	0.018	0.608	0.040
<i>NFRKB</i>	nuclear factor related to kappaB binding protein	protease binding	0.575	0.019	0.083	0.037
<i>PLEC</i>	plectin	poly(A) RNA binding	0.631	0.030	0.145	0.000
<i>VAC14</i>	Vac14 homolog	protein binding	0.096	0.036	0.013	0.019
<i>RMND1</i>	required for meiotic nuclear division 1 homolog	protein binding	0.305	0.004	5.598	0.025
<i>RPLA</i>	ribosome 5-phosphate isomerase A	protein binding	0.305	0.031	0.156	0.018
<i>DDBI</i>	damage-specific DNA binding protein 1	DNA binding	1.629	0.048	0.525	0.041
<i>PRKDC</i>	protein kinase, DNA activated, catalytic polypeptide	DNA-dependent protein kinase activity	1.977	0.000	3.698	0.000
<i>ESRP2</i>	epithelial splicing regulatory protein 2	mRNA binding	0.011	0.019	0.011	0.019
<i>CSE1L</i>	CSE1 chromosome segregation 1-like	nuclear export signal receptor activity	2.070	0.030	0.525	0.047
<i>FKBP15</i>	FK506 binding protein 15	ATP binding	0.157	0.018	0.631	0.039
<i>HSP90AA1</i>	heat shock protein 90kDa alpha family class A member 1	ATP binding	2.421	0.017	0.535	0.011
<i>KNTC1</i>	kinetochore associated 1	protein binding	2.270	0.049	3.281	0.015
<i>MED16</i>	mediator complex subunit 16	protein binding	0.095	0.037	0.179	0.080
<i>MYH9</i>	myosin, heavy chain 9, non-muscle	ATP binding	0.394	0.000	0.127	0.000
<i>NOA1</i>	nitric oxide associated 1	GTP binding	1.542	0.040	1.675	0.042
<i>SRRM2</i>	serine/arginine repetitive matrix 2	poly(A) RNA binding	0.592	0.000	0.331	0.016
<i>RIOK1</i>	RIO kinase 1	protein binding	0.104	0.018	31.333	0.049
<i>TOX4</i>	TOX high mobility group box family member 4	protein binding	0.142	0.003	0.265	0.003
<i>VIM</i>	vimentin	protein binding	0.619	0.020	0.334	0.002
<i>ZNF784</i>	zinc finger protein 784	DNA binding	0.104	0.018	0.104	0.019

and let-7f-5p mimics decreased the levels of vimentin and keratin protein.

IGF2 mRNA binding protein 1 is a member of the RNA-binding IGF2BP protein family, and 3 members of that family are found in mammals (IGF2BP1/2/3) (5). To the extent known, *IGF2BP1* is exclusively expressed during embryogenesis but is synthesized *de novo* in a broad variety of malignancies (6). The overexpression of *IGF2BP1* not only enhances the velocity of cell motility but also promotes the directionality of migration (7). A high level of *IGF2BP1* expression enhances the migratory and invasive potential of cells and promotes their proliferation (8). *IGF2BP* family members are essential for the migration of neural crest cells and the central regulation of the properties of stem cells within the LIN28/Let-7 networks (9,10). In the current study, expression of IGF2BP1 decreased while expression of Integrin $\alpha$ 1 increased in HeLa cells overexpressing let-7f-5p. In let-7f-5p-silenced HeLa cells, expression of IGF2BP1 and Integrin $\alpha$ 1 increased.

#### Acknowledgements

The study was supported by the National Natural Science Foundation of China (81560260), the Inner Mongolia Natural Science Foundation of China (2014MS0346, 2015MS08125, 2016MS(LH)0813), the MERCK CREAT Project (2014), the Chinese Medical Association fund (16020260642), and the Doctorial Fund of Inner Mongolia Medical University Hospital (2016).

#### References

- Huntzinger E, Izaurralde E. Gene silencing by microRNAs: Contributions of translational repression and mRNA decay. *Nat Rev Genet.* 2011; 12:99-110.
- Reinhart BJ, Slack FJ, Basson M, Pasquinelli AE, Bettinger JC, Rougvie AE, Horvitz HR, Ruvkun G. The 21-nucleotide let-7 RNA regulates developmental timing in *Caenorhabditis elegans*. *Nature.* 2000; 403:901-906.
- Sathe A, Patgaonkar MS, Bashir T, Reddy KV. MicroRNA let-7f: A novel regulator of innate immune response in human endocervical cells. *Am J Reprod Immunol.* 2014; 71:137-153.
- Liang S, He L, Zhao X, Miao Y, Gu Y, Guo C, Xue Z, Dou W, Hu F, Wu K, Nie Y, Fan D. MicroRNA let-7f inhibits tumor invasion and metastasis by targeting MYH9 in human gastric cancer. *PLoS One.* 2011; 6:e18409.
- Yisraeli JK. VICKZ proteins: A multi-talented family of regulatory RNA-binding proteins. *Biol Cell.* 2005; 97:87-96.
- Yaniv K, Yisraeli JK. The involvement of a conserved family of RNA binding proteins in embryonic development and carcinogenesis. *Gene.* 2002; 287:49-54.
- Stohr N, Kohn M, Lederer M, Glass M, Reinke C, Singer RH, Huttelmaier S. IGF2BP1 promotes cell migration by regulating MK5 and PTEN signaling. *Genes Dev.* 2012; 26:176-189.
- Gutschner T, Hammerle M, Pazaitis N, *et al.* Insulin-like growth factor 2 mRNA-binding protein 1 (IGF2BP1) is an important protumorigenic factor in hepatocellular carcinoma. *Hepatology.* 2014; 59:1900-1911.
- Farina KL, Huttelmaier S, Musunuru K, Darnell R, Singer RH. Two ZBP1 KH domains facilitate beta-actin mRNA localization, granule formation, and cytoskeletal attachment. *J Cell Biol.* 2003; 160:77-87.
- Nishino J, Kim S, Zhu Y, Zhu H, Morrison SJ. A network of heterochronic genes including *Imp1* regulates temporal changes in stem cell properties. *ELife.* 2013; 2:e00924.

(Received March 12, 2017; Accepted March 28, 2017)

### Guide for Authors

#### 1. Scope of Articles

BioScience Trends is an international peer-reviewed journal. BioScience Trends devotes to publishing the latest and most exciting advances in scientific research. Articles cover fields of life science such as biochemistry, molecular biology, clinical research, public health, medical care system, and social science in order to encourage cooperation and exchange among scientists and clinical researchers.

#### 2. Submission Types

**Original Articles** should be well-documented, novel, and significant to the field as a whole. An Original Article should be arranged into the following sections: Title page, Abstract, Introduction, Materials and Methods, Results, Discussion, Acknowledgments, and References. Original articles should not exceed 5,000 words in length (excluding references) and should be limited to a maximum of 50 references. Articles may contain a maximum of 10 figures and/or tables.

**Brief Reports** definitively documenting either experimental results or informative clinical observations will be considered for publication in this category. Brief Reports are not intended for publication of incomplete or preliminary findings. Brief Reports should not exceed 3,000 words in length (excluding references) and should be limited to a maximum of 4 figures and/or tables and 30 references. A Brief Report contains the same sections as an Original Article, but the Results and Discussion sections should be combined.

**Reviews** should present a full and up-to-date account of recent developments within an area of research. Normally, reviews should not exceed 8,000 words in length (excluding references) and should be limited to a maximum of 100 references. Mini reviews are also accepted.

**Policy Forum** articles discuss research and policy issues in areas related to life science such as public health, the medical care system, and social science and may address governmental issues at district, national, and international levels of discourse. Policy Forum articles should not exceed 2,000 words in length (excluding references).

**Case Reports** should be detailed reports of the symptoms, signs, diagnosis, treatment, and follow-up of an individual patient. Case reports may contain a demographic profile of the patient but usually describe an unusual or novel occurrence. Unreported or unusual

side effects or adverse interactions involving medications will also be considered. Case Reports should not exceed 3,000 words in length (excluding references).

**News** articles should report the latest events in health sciences and medical research from around the world. News should not exceed 500 words in length.

**Letters** should present considered opinions in response to articles published in BioScience Trends in the last 6 months or issues of general interest. Letters should not exceed 800 words in length and may contain a maximum of 10 references.

#### 3. Editorial Policies

**Ethics:** BioScience Trends requires that authors of reports of investigations in humans or animals indicate that those studies were formally approved by a relevant ethics committee or review board.

**Conflict of Interest:** All authors are required to disclose any actual or potential conflict of interest including financial interests or relationships with other people or organizations that might raise questions of bias in the work reported. If no conflict of interest exists for each author, please state "There is no conflict of interest to disclose".

**Submission Declaration:** When a manuscript is considered for submission to BioScience Trends, the authors should confirm that 1) no part of this manuscript is currently under consideration for publication elsewhere; 2) this manuscript does not contain the same information in whole or in part as manuscripts that have been published, accepted, or are under review elsewhere, except in the form of an abstract, a letter to the editor, or part of a published lecture or academic thesis; 3) authorization for publication has been obtained from the authors' employer or institution; and 4) all contributing authors have agreed to submit this manuscript.

**Cover Letter:** The manuscript must be accompanied by a cover letter signed by the corresponding author on behalf of all authors. The letter should indicate the basic findings of the work and their significance. The letter should also include a statement affirming that all authors concur with the submission and that the material submitted for publication has not been published previously or is not under consideration for publication elsewhere. The cover letter should be submitted in PDF format. For example of Cover Letter, please visit <http://www.biosciencetrends.com/downcentre.php> (Download Centre).

**Copyright:** A signed JOURNAL PUBLISHING AGREEMENT (JPA) form must be provided by post, fax, or as a scanned file before acceptance of the article. Only forms with a hand-written signature are accepted. This copyright will ensure the widest possible dissemination of information. A form facilitating transfer of copyright can be downloaded by clicking the

appropriate link and can be returned to the e-mail address or fax number noted on the form (Please visit [Download Centre](#)). Please note that your manuscript will not proceed to the next step in publication until the JPA Form is received. In addition, if excerpts from other copyrighted works are included, the author(s) must obtain written permission from the copyright owners and credit the source(s) in the article.

**Suggested Reviewers:** A list of up to 3 reviewers who are qualified to assess the scientific merit of the study is welcomed. Reviewer information including names, affiliations, addresses, and e-mail should be provided at the same time the manuscript is submitted online. Please do not suggest reviewers with known conflicts of interest, including participants or anyone with a stake in the proposed research; anyone from the same institution; former students, advisors, or research collaborators (within the last three years); or close personal contacts. Please note that the Editor-in-Chief may accept one or more of the proposed reviewers or may request a review by other qualified persons.

**Language Editing:** Manuscripts prepared by authors whose native language is not English should have their work proofread by a native English speaker before submission. If not, this might delay the publication of your manuscript in BioScience Trends.

The Editing Support Organization can provide English proofreading, Japanese-English translation, and Chinese-English translation services to authors who want to publish in BioScience Trends and need assistance before submitting a manuscript. Authors can visit this organization directly at <http://www.iacmhr.com/iac-eso/support.php?lang=en>. IAC-ESO was established to facilitate manuscript preparation by researchers whose native language is not English and to help edit works intended for international academic journals.

#### 4. Manuscript Preparation

Manuscripts should be written in clear, grammatically correct English and submitted as a Microsoft Word file in a single-column format. Manuscripts must be paginated and typed in 12-point Times New Roman font with 24-point line spacing. Please do not embed figures in the text. Abbreviations should be used as little as possible and should be explained at first mention unless the term is a well-known abbreviation (e.g. DNA). Single words should not be abbreviated.

**Title Page:** The title page must include 1) the title of the paper (Please note the title should be short, informative, and contain the major key words); 2) full name(s) and affiliation(s) of the author(s), 3) abbreviated names of the author(s), 4) full name, mailing address, telephone/fax numbers, and e-mail address of the corresponding author; and 5) conflicts of interest (if you have an actual or potential conflict of interest to disclose, it must be included as a footnote on the title page of the manuscript; if no conflict of

interest exists for each author, please state "There is no conflict of interest to disclose"). Please visit [Download Centre](#) and refer to the title page of the manuscript sample.

**Abstract:** The abstract should briefly state the purpose of the study, methods, main findings, and conclusions. For article types including Original Article, Brief Report, Review, Policy Forum, and Case Report, a one-paragraph abstract consisting of no more than 250 words must be included in the manuscript. For News and Letters, a brief summary of main content in 150 words or fewer should be included in the manuscript. Abbreviations must be kept to a minimum and non-standard abbreviations explained in brackets at first mention. References should be avoided in the abstract. Key words or phrases that do not occur in the title should be included in the Abstract page.

**Introduction:** The introduction should be a concise statement of the basis for the study and its scientific context.

**Materials and Methods:** The description should be brief but with sufficient detail to enable others to reproduce the experiments. Procedures that have been published previously should not be described in detail but appropriate references should simply be cited. Only new and significant modifications of previously published procedures require complete description. Names of products and manufacturers with their locations (city and state/country) should be given and sources of animals and cell lines should always be indicated. All clinical investigations must have been conducted in accordance with Declaration of Helsinki principles. All human and animal studies must have been approved by the appropriate institutional review board(s) and a specific declaration of approval must be made within this section.

**Results:** The description of the experimental results should be succinct but in sufficient detail to allow the experiments to be analyzed and interpreted by an independent reader. If necessary, subheadings may be used for an orderly presentation. All figures and tables must be referred to in the text.

**Discussion:** The data should be interpreted concisely without repeating material already presented in the Results section. Speculation is permissible, but it must be well-founded, and discussion of the wider implications of the findings is encouraged. Conclusions derived from the study should be included in this section.

**Acknowledgments:** All funding sources should be credited in the Acknowledgments section. In addition, people who contributed to the work but who do not meet the criteria for authors should be listed along with their contributions.

**References:** References should be numbered in the order in which they appear in the text. Citing of unpublished results, personal communications, conference abstracts, and theses in the reference list is not recommended but these sources may be mentioned in the text. In the reference list,

cite the names of all authors when there are fifteen or fewer authors; if there are sixteen or more authors, list the first three followed by *et al.* Names of journals should be abbreviated in the style used in PubMed. Authors are responsible for the accuracy of the references. Examples are given below:

*Example 1* (Sample journal reference): Inagaki Y, Tang W, Zhang L, Du GH, Xu WF, Kokudo N. Novel aminopeptidase N (APN/CD13) inhibitor 24F can suppress invasion of hepatocellular carcinoma cells as well as angiogenesis. *Biosci Trends*. 2010; 4:56-60.

*Example 2* (Sample journal reference with more than 15 authors): Darby S, Hill D, Auvinen A, *et al.* Radon in homes and risk of lung cancer: Collaborative analysis of individual data from 13 European case-control studies. *BMJ*. 2005; 330:223.

*Example 3* (Sample book reference): Shalev AY. Post-traumatic stress disorder: diagnosis, history and life course. In: Post-traumatic Stress Disorder, Diagnosis, Management and Treatment (Nutt DJ, Davidson JR, Zohar J, eds.). Martin Dunitz, London, UK, 2000; pp. 1-15.

*Example 4* (Sample web page reference): Ministry of Health, Labour and Welfare of Japan. Dietary reference intakes for Japanese. <http://www.mhlw.go.jp/houdou/2004/11/h1122-2a.html> (accessed June 14, 2010).

**Tables:** All tables should be prepared in Microsoft Word or Excel and should be arranged at the end of the manuscript after the References section. Please note that tables should not be image format. All tables should have a concise title and should be numbered consecutively with Arabic numerals. If necessary, additional information should be given below the table.

**Figure Legend:** The figure legend should be typed on a separate page of the main manuscript and should include a short title and explanation. The legend should be concise but comprehensive and should be understood without referring to the text. Symbols used in figures must be explained.

**Figure Preparation:** All figures should be clear and cited in numerical order in the text. Figures must fit a one- or two-column format on the journal page: 8.3 cm (3.3 in.) wide for a single column, 17.3 cm (6.8 in.) wide for a double column; maximum height: 24.0 cm (9.5 in.). Please make sure that the symbols and numbers appeared in the figures should be clear. Please make sure that artwork files are in an acceptable format (TIFF or JPEG) at minimum resolution (600 dpi for illustrations, graphs, and annotated artwork, and 300 dpi for micrographs and photographs). Please provide all figures as separate files. Please note that low-resolution images are one of the leading causes of article resubmission and schedule delays. All color figures will be reproduced in full color in the online edition of the journal at no cost to authors.

**Units and Symbols:** Units and symbols

conforming to the International System of Units (SI) should be used for physicochemical quantities. Solidus notation (*e.g.* mg/kg, mg/mL, mol/mm<sup>2</sup>/min) should be used. Please refer to the SI Guide [www.bipm.org/en/si/](http://www.bipm.org/en/si/) for standard units.

**Supplemental data:** Supplemental data might be useful for supporting and enhancing your scientific research and BioScience Trends accepts the submission of these materials which will be only published online alongside the electronic version of your article. Supplemental files (figures, tables, and other text materials) should be prepared according to the above guidelines, numbered in Arabic numerals (*e.g.*, Figure S1, Figure S2, and Table S1, Table S2) and referred to in the text. All figures and tables should have titles and legends. All figure legends, tables and supplemental text materials should be placed at the end of the paper. Please note all of these supplemental data should be provided at the time of initial submission and note that the editors reserve the right to limit the size and length of Supplemental Data.

## 5. Submission Checklist

The Submission Checklist will be useful during the final checking of a manuscript prior to sending it to BioScience Trends for review. Please visit [Download Centre](#) and download the Submission Checklist file.

## 6. Online Submission

Manuscripts should be submitted to BioScience Trends online at <http://www.biosciencetrends.com>. The manuscript file should be smaller than 5 MB in size. If for any reason you are unable to submit a file online, please contact the Editorial Office by e-mail at [office@biosciencetrends.com](mailto:office@biosciencetrends.com).

## 7. Accepted Manuscripts

**Proofs:** Galley proofs in PDF format will be sent to the corresponding author via e-mail. Corrections must be returned to the editor ([proof-editing@biosciencetrends.com](mailto:proof-editing@biosciencetrends.com)) within 3 working days.

**Offprints:** Authors will be provided with electronic offprints of their article. Paper offprints can be ordered at prices quoted on the order form that accompanies the proofs.

**Page Charge:** Page charges will be levied on all manuscripts accepted for publication in BioScience Trends (\$140 per page for black white pages; \$340 per page for color pages). Under exceptional circumstances, the author(s) may apply to the editorial office for a waiver of the publication charges at the time of submission.

(Revised February 2013)

## Editorial and Head Office:

Pearl City Koishikawa 603  
2-4-5 Kasuga, Bunkyo-ku  
Tokyo 112-0003 Japan  
Tel: +81-3-5840-8764  
Fax: +81-3-5840-8765  
E-mail: [office@biosciencetrends.com](mailto:office@biosciencetrends.com)

### JOURNAL PUBLISHING AGREEMENT (JPA)

---

**Manuscript No.:**

**Title:**

**Corresponding Author:**

---

The International Advancement Center for Medicine & Health Research Co., Ltd. (IACMHR Co., Ltd.) is pleased to accept the above article for publication in BioScience Trends. The International Research and Cooperation Association for Bio & Socio-Sciences Advancement (IRCA-BSSA) reserves all rights to the published article. Your written acceptance of this JOURNAL PUBLISHING AGREEMENT is required before the article can be published. Please read this form carefully and sign it if you agree to its terms. The signed JOURNAL PUBLISHING AGREEMENT should be sent to the BioScience Trends office (Pearl City Koishikawa 603, 2-4-5 Kasuga, Bunkyo-ku, Tokyo 112-0003, Japan; E-mail: [office@biosciencetrends.com](mailto:office@biosciencetrends.com); Tel: +81-3-5840-8764; Fax: +81-3-5840-8765).

#### 1. Authorship Criteria

As the corresponding author, I certify on behalf of all of the authors that:

- 1) The article is an original work and does not involve fraud, fabrication, or plagiarism.
- 2) The article has not been published previously and is not currently under consideration for publication elsewhere. If accepted by BioScience Trends, the article will not be submitted for publication to any other journal.
- 3) The article contains no libelous or other unlawful statements and does not contain any materials that infringes upon individual privacy or proprietary rights or any statutory copyright.
- 4) I have obtained written permission from copyright owners for any excerpts from copyrighted works that are included and have credited the sources in my article.
- 5) All authors have made significant contributions to the study including the conception and design of this work, the analysis of the data, and the writing of the manuscript.
- 6) All authors have reviewed this manuscript and take responsibility for its content and approve its publication.
- 7) I have informed all of the authors of the terms of this publishing agreement and I am signing on their behalf as their agent.

#### 2. Copyright Transfer Agreement

I hereby assign and transfer to IACMHR Co., Ltd. all exclusive rights of copyright ownership to the above work in the journal BioScience Trends, including but not limited to the right 1) to publish, republish, derivate, distribute, transmit, sell, and otherwise use the work and other related material worldwide, in whole or in part, in all languages, in electronic, printed, or any other forms of media now known or hereafter developed and the right 2) to authorize or license third parties to do any of the above.

I understand that these exclusive rights will become the property of IACMHR Co., Ltd., from the date the article is accepted for publication in the journal BioScience Trends. I also understand that IACMHR Co., Ltd. as a copyright owner has sole authority to license and permit reproductions of the article.

I understand that except for copyright, other proprietary rights related to the Work (e.g. patent or other rights to any process or procedure) shall be retained by the authors. To reproduce any text, figures, tables, or illustrations from this Work in future works of their own, the authors must obtain written permission from IACMHR Co., Ltd.; such permission cannot be unreasonably withheld by IACMHR Co., Ltd.

#### 3. Conflict of Interest Disclosure

I confirm that all funding sources supporting the work and all institutions or people who contributed to the work but who do not meet the criteria for authors are acknowledged. I also confirm that all commercial affiliations, stock ownership, equity interests, or patent-licensing arrangements that could be considered to pose a financial conflict of interest in connection with the article have been disclosed.

---

**Corresponding Author's Name (Signature):**

**Date:**



